DYNAMICS OF INTENSE MULTI-DAY WET SPELLS OVER WEST AFRICA

BY

ILORI, OLUWASEUN WILSON

B.Tech, M.Tech (MCS/09/7304)

A Thesis of the Doctoral Research Programme of the West African Climate Systems, under the West African Science Service Center on Climate Change and Adapted Land Use, in the Department of Meteorology and Climate Science submitted to the School of Postgraduate Studies in partial fulfillment of the requirements for the award of the Degree of Doctor of Philosophy in Meteorology and Climate Science of The Federal University of Technology, Akure, Nigeria

MAY, 202025

DECLARATION

I hereby declare that this Thesis was written by me and is a correct record of my own research work. It has not been presented in any previous application for any degree of this or any other University. All citations and sources of information are clearly acknowledged by means of references.

Candidate's Name: **ILORI, OLUWASEUN WILSON**

Signature: ………………………………… Date: ……………….

CERTIFICATION

We certify that this thesis entitled "Dynamics of Intense Multi-day Wet Spells Over West Africa" is the outcome of the research carried out by ILORI, Oluwaseun Wilson under the West African Science Service Centre on Climate Change and Adapted Land-Use Doctorate Research Programme in West African Climate Systems (WASCAL DRP-WACS) in the Department of Meteorology and Climate, The Federal University of Technology, Akure.

Major Supervisor's Name: **PROF. Z. DEBO ADEYEWA**

Signature: …………………………………………... Date: …………………………….

Co-Supervisor's Name: **PROF. (DR.) ANDREAS H. FINK**

Signature: …………………………………………... Date: …………………………….

ACKNOWLEDGEMENTS

This research was primarily funded by the German Federal Ministry of Education and Research (BMBF) through the West African Science Service Centre on Climate Change and Adapted Land Use (WASCAL) Graduate Research Programme in West African Climate Systems (GRP-WACS), hosted at the Federal University of Technology Akure (FUTA), Nigeria.

I am deeply grateful to my major supervisor, Prof. Z. Debo Adeyewa, and my co-supervisor, Prof. (Dr.) Andreas H. Fink, for their unwavering encouragement, constructive criticism, insightful suggestions, and invaluable guidance throughout the course of this research.

My sincere thanks go to Dr. Marlon Maranan of the Institute of Meteorology and Climate Research at Karlsruhe Institute of Technology (IMK-KIT), Germany, for his immeasurable technical and scientific support from the beginning to the completion of this work.

I also wish to thank Prof. I. A. Balogun and Prof. A. Oluleye for their helpful comments, and Prof. V. O. Ajayi for his technical support and outstanding mentorship.

The rain gauge data used in this research were provided by IMK-KIT. I gratefully acknowledge the high-performance computing resources (bwUniCluster 2.0 and bwUniCluster 3.0) made available by the Karlsruhe Institute of Technology, Germany.

Special thanks to my wonderful and ever-encouraging parent, Chief (Mr.) Ilori J. O., and to every member of my family for their continuous moral support and understanding. I am especially thankful to my dear wife for her enduring patience and encouragement throughout this journey.

DEDICATION

This thesis is dedicated to the Almighty God – the source of knowledge, understanding, and wisdom – whose grace made the successful completion of this research possible. It is also dedicated to all taxpayers whose contributions support research and development efforts in developing countries.

ABSTRACT

Intense multi-day wet spells, characterized by prolonged heavy rainfall, significantly influence West Africa's hydroclimate, driving flood risks and shaping socio-economic vulnerabilities. However, their dynamics remain poorly understood due to observational data limitations, methodological inconsistencies, and the complex interplay of atmospheric processes. The study defines intense 3-day and 5-day wet spells as rainfall accumulations exceeding the 90th percentile, with specific wet-day criteria and addresses critical gaps in understanding their characteristics by investigating the drivers, and future changes of intense 3-day and 5-day wet spells over West Africa from 1982–2020 to enhance climate resilience and disaster preparedness.

Utilizing a novel high-resolution gridded rainfall dataset (KASS-D), developed from 239 quality-controlled rain gauge stations (1982–2020) via SPHEREMAP interpolation, the research evaluates rainfall variability across the Guinea Coast, Savannah, and Sahel. KASS-D outperforms global datasets (GPCC, CHIRPS, IMERG) in capturing daily rainfall, onset/cessation periods, and extreme events, with lower root-mean-square error and higher probability of detection, making it a robust tool for hydrometeorological analyses in data-sparse regions and was selected as the standard for characterizing wet spells.

Spatial analyses reveal a latitudinal gradient, with the Guinea Coast and Cameroon Highlands exhibiting the highest frequencies and intensities. Temporal trends indicate a post-2000 increase in large-scale, longer-duration wet spells, contributing significantly to annual rainfall (20% in the Sahel, 16% for 3-day and 14% for 5-day spells in the Savannah, 9% in the Guinea Coast). A composite analysis of wet and dry spells reveals a dipole-like atmospheric structure influencing multi-day rainfall events. Wet spells are preceded by easterly anomalies, with a weakened AEJ and strengthened TEJ that enhance deep convection, while dry spells involve offshore moisture export and suppressed vertical development due to deeper moisture depth. Intense 3- and 5-day wet spells is associated with high total column water vapor and strong low-level moisture flux

convergence fueled by Atlantic and Gulf of Guinea moisture advection, dual cyclonic systems over the Atlantic and Sahel maintained by Southern Hemisphere anticyclonic flow. Their lifecycle involves vertically coupled dynamics with strong low-level southwesterlies and upper-level easterlies during initiation and peak phases, while the decay phase involves weakened inflows and reduced humidity. Multi-day wet spells significantly increase flood risks in West Africa, especially in the Sahel and Guinea Coast. Their predictability via atmospheric signals like SHL dynamics and AEWs can enhance early warnings.

Adjusted observation datasets using climate change signal obtained from the ensemble mean of 23 NEX-GDDP-CMIP6 models under SSP2-4.5 and SSP5-8.5 scenarios, suggest intensified wet spell frequency and magnitude, particularly under SSP5-8.5, with increases exceeding 15% in coastal zones and the Niger Delta. Frequency trends show annual rises of 0.02–0.29 events/year in the Savannah and Sahel, signaling a shift toward a wetter, more extreme hydroclimate. These changes heighten risks to agriculture, urban infrastructure, and water management, necessitating adaptive strategies.

The findings underscore the critical role of wet spells in flood risks, particularly in the Sahel and Guinea Coast, where prolonged rainfall amplifies socio-economic impacts. The predictability of atmospheric precursors offers opportunities to enhance early warning systems, with lead times of 3–5 days. Recommendations include expanding gauge networks, integrating KASS-D into forecasting platforms, and fostering regional cooperation for transboundary flood management. By informing flood risk models, community preparedness, and climate services, this research provides actionable insights for policymakers to develop anticipatory disaster risk reduction mechanisms, strengthening resilience in West Africa's climate-vulnerable communities.

TABLE OF CONTENTS

LIST OF TABLES

LIST OF FIGURES

LIST OF EQUATIONS

LIST OF ABBREVATIONS

AEJ	African Eater Jet
AEW	African Easterly Waves
BID	Bias in Detection
CAPE	Convective Available Potential Energy
CCD	Cold Cloud Duration
CHIRPS	Climate Hazards Group InfraRed Precipitation
CIN	Convective Inhibition
CMIP	Coupled Model Intercomparison Project
CMIP6	Coupled Model Intercomparison Project Phase 6
CORDEX	Coordinated Regional Downscaling Experiment
EnsMean	Ensemble Mean
EVT	Extreme Value Theory
GCM	Global Climate Model
GPCC	Global Precipitation Climatology Center
GTS	Global Telecommunication System
HSS	Heidke skill score
IMERG	Integrated Multi-satellite Retrieval for Global Precipitation Measurement

IPCC	Intergovernmental Panel on Climate Change
IPCC	Intergovernmental Panel on Climate Change
ITD	Inter-Tropical Discontinuity
JJAS	June-September
KASS-D	Karlsruhe African Surface Station
LLJ	Low level Jet
MAE	Mean Absolute Bias
MAE	Mean absolute error
MCS	Mesoscale Convective System
ME	Mean error
MFC	Moisture Flux Convergence
MFD	Moisture Flux Divergence
NEX-GDDP-CMIP6	NASA Earth Exchange Global Daily Downscale Project Coupled Model Intercomparison Project Phase 6
OLR	Outgoing Longwave Radiation
PD	Probability bias
POD	Probability of Detection
POFA	Probability of False Alarm
POT	Peak Over Threshold

Q-Q	Quantile-Quantile
r	Pearson correlation coefficient
RCM	Regional Climate Model
RMSE	Root-mean-square error
SHL	Saharan Heat Low
SSA	Sub Saharan Africa
SSP	Shared Socio-economic Pathway
SSP2-4.5	Share Socio-economic Pathway for $4.5Wm^{-2}$ radiative forcing
SSP5-8.5	Share Socio-economic Pathway for $8.5Wm^{-2}$ radiative forcing
TCWV	Total Column Vertically-Integral Water Vapor
TEJ	Tropical Easterly Jet
TIR	Thermal Infrared
VIDMF	Vertical Integral of Divergence of Moisture Flux
VIEWV	Vertical Integral of Eastward Water Vapor
VINWV	Vertical Integral of Northward Water Vapor
WAM	West African Monsoon

CHAPTER ONE

INTRODUCTION

1.1 BACKGROUND OF THE STUDY

Rainfall is a critical component of the climate system, influencing regional climate variability and change worldwide. Over West Africa, rainfall exhibits substantial spatial and temporal heterogeneity, driven by complex atmospheric dynamics and large-scale circulation patterns. The West African region has experienced significant rainfall variability, ranging from severe droughts in the 1970s and 1980s to an increasing frequency of extreme rainfall events and devastating floods in recent decades (Nicholson, 2013; Panthou *et al*., 2014; Elagib *et al*., 2021). The intensification of extreme rainfall projected under future climate scenarios (Kendon *et al*., 2019; Finney *et al*., 2020; Onyutha, 2020) underscores the need for a deeper understanding of rainfall extremes, particularly multi-day wet spells. These are critical drivers of flooding and other socio-economic impacts in the region.

Flooding, whether caused by prolonged multi-day wet spells or intense short-duration rainfall, has become a major climate hazard across West Africa, leading to loss of lives, destruction of infrastructure, and disruption of livelihoods (Di Baldassarre *et al*., 2010). For instance, the reported catastrophic 2022 floods in Nigeria by the Nigerian Meteorological Agency (NiMet) and the World Food Programme (WFP-UN) affected over 3.48 million people, submerged more than 63,700 hectares of farmland and resulted in significant casualties. Similarly, Gambia experienced severe flooding in the same year that affected over 109,000 urban residents while the Ouagadougou flood of 2009, with over 260 mm of rainfall in 24 hours, caused extensive damage, displacing more than 180,000 people and destroying key infrastructure that include the city’s main hospital (Lafore *et* *al*., 2017). The vulnerability of West African countries to extreme rainfall events is exacerbated by limited adaptive capacity, limited financial resources, and technological gaps (Sylla *et al*., 2016). Given these challenges, understanding the frequency, intensity, and duration of multi-day wet spells is critical for developing effective disaster risk reduction strategies and improving climate resilience while informing sustainable development planning in West Africa.

Studying extreme rainfall events over West Africa requires high-quality and long-term in-situ datasets. However, the scarcity of reliable in-situ rainfall observations has been a major limitation that compelled researchers to rely on alternative datasets that include satellite-derived products, reanalysis datasets and climate model simulations (Gbode *et al*., 2022; Odoulami & Akinsanola, 2018; Froidurot & Diedhiou, 2017; Cretat *et al*., 2015). Despite their widespread use, these datasets exhibit varying degrees of uncertainty and biases due to the sparse network of rain gauge stations used to create them (Maranan *et al*., 2020; Gosset *et al*., 2018; Casse *et al*., 2015). Climate models, although invaluable for understanding historical and future rainfall changes have not been able to accurately simulate the complex regional rainfall patterns of West Africa (Ilori and Ajayi 2020; Biasutti, 2013; Monerie *et al*., 2012; Afiesimama *et al*., 2006). Consequently, in-situ station data remains the most reliable source for analyzing extreme rainfall events, and this study leverages long-term observations from 256 rain gauge stations to investigate the characteristics of multi-day wet spells over West Africa.

West African rainfall is primarily governed by the dynamics of West African Monsoon (WAM). This is a system characterized by seasonal wind reversals primarily driven by land-sea temperature gradient (Sylla *et al*., 2010). The WAM exhibits pronounced intra-seasonal variability that are marked by alternating wet and dry spells, which significantly influence convective activity and precipitation patterns. Key atmospheric features influencing rainfall variability include African easterly waves (AEWs) and two major tropospheric jets: the African easterly jet (AEJ) at approximately 700 hPa and the tropical easterly jet (TEJ) at around 200 hPa. Several studies have examined interannual WAM variability, highlighting distinct atmospheric circulation anomalies between wet and dry years (Nicholson & Grist, 2001; Jenkins *et al*., 2005; Sylla *et al*., 2010). For instance, Sylla *et al*. (2010) reported that dry years are typically associated with weaker AEW activity in combination to a southward-displaced AEJ, and a weakened TEJ. Akinsanola & Zhou (2020) confirmed that wet years exhibit a weaker AEJ and a stronger TEJ. However, despite extensive research on interannual variability of WAM, relatively few studies have explored its intra-seasonal characteristics during intense multi-day wet spells. This gap in knowledge is crucial, as short-term variations in rainfall can have profound implications for flood forecasting, agricultural productivity, and water resource management in West Africa.

Climate change is increasingly altering rainfall patterns and amplifying the frequency and intensity of extreme weather events, including heatwaves, droughts, and floods (Trenberth, 2018; IPCC, 2023). West Africa has already witnessed significant warming, with global mean temperatures rising by approximately 0.25°C per decade since the 1970s (IPCC, 2023; Robinson *et al*., 2021). This warming trend has been linked to an increase in rainfall extremes with studies like Bobde *et al*., 2024 and Sawadogo *et al*., 2024 reported the likely occurrence of very wet years five times more than historical period and 30% increase in rainfall amount under SSP5-8.5 in the future, respectively. This further emphasize the need to understand evolving rainfall dynamics in a changing climate.

Historically, rainfall variability over West Africa has been influenced by large-scale ocean-atmosphere interactions, such as the pacific decadal oscillation and Atlantic multidecadal variability that modulates monsoon strength and rainfall trends (Zhang & Zhou, 2011; IPCC, 2013). While a drying trend was observed from 1951 to 2012, recent evidence suggests a partial recovery of rainfall in the Sahel that is attributed to both natural variability and anthropogenic greenhouse gas emissions (Dong & Sutton, 2015; Biasutti, 2013; Sanogo *et al*., 2015). However, future projections from the Coupled Model Intercomparison Project Phase 6 (CMIP6) indicate that extreme rainfall events will intensify with prolonged dry spells which is expected to heightened hydro-climatic extremes (Dosio *et al*., 2021).

The Coupled Model Intercomparison Project (CMIP) under the World Climate Research Programme (WCRP) has substantially increased the knowledge of climate change and variability due to regular improvements in spatial resolution and parameterization of different physical processes (Simpkins, 2017; Eyring *et al*., 2016). Studies such as Diba *et al*., 2022 and Monerie *et al*., (2020) have used older versions of the CMIP GCM in West Africa to examine observed and projected changes in mean and extreme rainfall under different climate scenarios. However, like other climate models, uncertainties exist from the biases in these models despite the robust projections over West Africa, which limits their reliability in creating climate adaptation strategies (Diba *et al*., 2022). Comparative studies of CMIP5 and CMIP6 models reported that CMIP6 gives improved simulation of rainfall over West Africa, with reduced bias and enhanced representation of extreme events, though regional variations persist. Compared to the previous phases of the CMIP, the latest phase (CMIP6) gives the opportunity for an improved understanding of historical and future climates owing to improvements in deep convective schemes, contributions of aerosols to the formation of clouds and cloud microphysics (Eyring *et al*., 2016). These methods are reported to have reduced biases in simulating rainfall characteristics (Dioha *et al*., 2024). Like previous phases of CMIP and other coarse climate models, CMIP6 may produce globally accurate projections that are locally biased due to its coarse resolution. Despite its improvement compared to older phases, this means that they may not agree with observed statistical characteristics at local scales. The coarse resolutions in CMIP6 poorly resolves some sub-scales systems over complex domain of West Africa (Ilori and Balogun 2021; Afiesimama 2006). This led to the creation of a very high-resolution GCM known as the NASA Earth Exchange Global Daily Downscale Project (NEX-GDDP-CMIP6; Thrasher *et al*., 2022), which is expected and has been shown to better reproduce local climate conditions and provide more robust information about climate change (Sawadogo *et al*., 2024; Dioha *et al*., 2024) at the local scale.

Given the increasing urbanization and growing population across West Africa, the socio-economic risks associated with changing rainfall characteristics are expected to escalate in the coming decades. Understanding the dynamics of intense multi-day wet spells is crucial for improving climate resilience, guiding infrastructure development, and informing early warning systems. This study seeks to address existing gaps by systematically documenting the frequency, intensity, and duration of multi-day wet spells across West Africa, leveraging high-resolution observational datasets. The findings will contribute to a more comprehensive understanding of extreme rainfall variability in the region, with implications for flood risk management, agricultural planning, and climate adaptation strategies.

1.2 STATEMENT OF PROBLEM

Rainfall over West Africa is predominantly driven by mesoscale convective systems (MCSs), which are widely acknowledged as the most significant contributors to precipitation in the region (Fink *et al*., 2017). These organized clusters of convective storms account for a substantial proportion of rainfall during the monsoon season. On daily timescales, the modulation of MCS activity has been closely associated with African Easterly Waves (AEWs), especially within the Sahelian belt where AEWs serve as synoptic-scale precursors for convective development (Fink

& Reiner, 2003). While the link between AEWs and daily-scale convective activity has been the subject of considerable scientific attention, our understanding of the processes governing the persistence and organization of rainfall over multiple days referred to as multi-day wet spells remains comparatively limited. Yet, it is these prolonged rainfall events that have demonstrated some of the most severe socio-economic impacts across sub-Saharan Africa in recent years, that include widespread flooding, displacement of people, crop losses, and infrastructure damage (Paeth *et al*., 2011; Panthou *et al*., 2014; Lafore *et al*., 2017; Dos Santos *et al*., 2019).

Unlike short-lived convective events, multi-day wet spells reflect more complex atmospheric dynamics and potentially involve larger-scale and more persistent meteorological drivers. One such driver is the formation of slow-moving or quasi-stationary cyclonic low-level vortices, whose genesis and evolution are still poorly understood (Fink *et al*., 2006; Knippertz *et al*., 2017). Also, potential causes have been linked, to tropical-extratropical interactions via extratropical trough systems that not only influence the intensity of the Saharan Heat Low (SHL, Lavaysse *et al*., 2010) but also strengthen moisture transport deep into the Sahel (Knippertz and Martin 2005). However, such interactions remain inadequately quantified, and their temporal and spatial patterns across the West African domain are not well documented.

Despite increasing recognition of the devastating impacts of multi-day wet spells, particularly in the context of a warming climate and expanding urban populations. There is still no comprehensive or systematic climatological framework that characterizes the occurrence, intensity and dynamical drivers of such events in West Africa. Most existing studies have focused on seasonal or daily variability of rainfall that overlook intermediate timescales which are critical for understanding cumulative hydrological impacts. This gap in knowledge represents a significant barrier to improving early warning systems, flood forecasting capabilities and regional climate adaptation strategies. Furthermore, the absence of a unified definition or diagnostic criteria for identifying multi-day wet spells complicates inter-study comparisons and hinders the development of robust risk assessment frameworks.

Hence, the need to undertake a systematic investigation into the frequency, intensity, duration, and underlying drivers of intense multi-day wet spells across West Africa. This will not only help to identify the key dynamical mechanisms but also provide critical insights for improving predictive capabilities and informing climate resilience policies. Bridging this knowledge gap is particularly timely, given the projected intensification of extreme rainfall events under future climate scenarios and the increasing vulnerability of West African societies to hydro-meteorological hazards.

1.3 RESEARCH QUESTIONS AND HYPOTHESIS

This research study will be guided by the following research questions and corresponding hypotheses, structured to systematically explore the nature, drivers, and implications of intense multi-day wet spells across West Africa.

The research questions are:

i. What are the spatial and temporal characteristics of intense multi-day wet spells across different climatic zones of West Africa?

ii. Which mesoscale and synoptic-scale atmospheric processes govern the initiation, organization, and persistence of intense multi-day wet spells in the region?

iii. How are the frequency, intensity, and contribution of intense multi-day wet spells to annual rainfall amount would have changed under different future climate scenarios if the current rainfall matches projected distribution?

iv. What are the implications of improved understanding of multi-day wet spells for early warning systems, flood risk forecasting, and climate resilience planning in West Africa?

v. What are the implications of improved understanding of multi-day wet spells for early warning systems, flood risk forecasting, and climate resilience planning in West Africa*?*

The corresponding hypothesis for each research question is as follows:

i. Intense multi-day wet spells display statistically significant spatial and temporal variability across West Africa, with evidence of increasing frequency and intensity in the Sahel and Sudanian zones over recent decades.

ii. The initiation and persistence of intense multi-day wet spells are primarily modulated by the interaction of MCSs, particularly squall lines, AEWs, and quasi-stationary low-level vortices, which create favorable dynamical and thermodynamical conditions for sustained convection.

iii. Intrusions of extratropical troughs and associated Rossby wave breaking events enhance low-level moisture convergence and vertical instability, thereby reinforcing the persistence and spatial extent of multi-day wet spells across the Sahelian belt.

iv. Under future climate scenarios (e.g., SSP2-4.5 and SSP5-8.5), the frequency and intensity of intense multi-day wet spells in West Africa will increase, driven by enhanced atmospheric moisture content and modified large-scale circulation patterns associated with global warming.

v. Integrating the spatio-temporal and dynamical characteristics of intense wet spells into early warning and risk modelling frameworks will significantly enhance the accuracy of flood forecasts and provide robust scientific input for climate adaptation and resilience strategies in vulnerable communities.

1.4 AIM AND OBJECTIVES

1.4.1 Aim

The aim of this study is to investigate the characteristics, occurrence patterns, and underlying drivers of intense multi-day wet spells in West Africa, with a view to improving understanding, prediction, and disaster preparedness in the context of a changing climate.

1.4.2 Objectives

The specific objectives are to:

i. perform comprehensive quality control on in-situ rainfall data and interpolate it to a regular grid over West Africa to ensure reliable detection of intense wet spells,

ii. examine the spatial and temporal occurrence, frequency, and intensity of multi-day wet spells across different West African climate zones,

iii. investigate the mesoscale, synoptic, and thermodynamic drivers that influence the initiation and persistence of intense wet spells,

iv. assess changes in the characteristics of intense multi-day wet spells based on the assumption that current rainfall reflects future projected distributions under different SSP scenarios, and

v. examine the implications of intense multi-day wet spells for flood risks and early warning systems, with a view to informing climate resilience and disaster preparedness strategies.

1.5 SCOPE AND LIMITATIONS OF THE STUDY

This section outlines the scope and limitations of the study on the *"Dynamics of Intense Multi-Day Wet Spells Over West Africa"*. The scope defines the geographical, temporal, and methodological boundaries of the research, while the limitations address constraints and challenges that may affect the findings.

1.5.1 Scope of the Study

The study focuses on understanding the characteristics, drivers, and potential future changes of intense multi-day wet spells in West Africa, with an emphasis on enhancing climate resilience and disaster preparedness. The scope is delineated as follows:

(1) Geographical Coverage:

- (i) The research covers the West African region, specifically analyzing rainfall patterns across three climatic zones: the Guinea Coast, Savannah, and Sahel.
- (ii) The study domain for data interpolation is constrained to areas east of 3°W due to poor spatial distribution of rain gauge stations west of this longitude (Section 3.1, Figure 3.1).
- (iii) Key locations, such as Ouagadougou, Jos, Parakou, and Port Harcourt, are used for detailed analyses to represent diverse climatic and topographic conditions.

(2) Temporal Scope:

- (i) The analysis spans the period from 1982 to 2020 for observational data (e.g., KASS-D, GPCC, CHIRPS), with IMERG data limited to 2001–2020 due to its shorter record (Section 5.1.1).

(ii) Future projections are assessed using CMIP6 NEX-GDDP models under SSP2-4.5 and SSP5-8.5 scenarios, assuming current rainfall distributions reflect future projections up to 2011 for adjusted datasets (Section 4.5).

(3) Methodological Scope:

(i) The study employs a high-resolution, gauge-based dataset (KASS-D) developed from 239 quality-controlled rain gauge stations, interpolated using the SPHEREMAP technique (Section 5.1.1).

(ii) Intense multi-day wet spells are defined as 3-day or 5-day rainfall accumulations exceeding the 90th percentile threshold, with specific criteria for wet days (≥ 1 mm) and consecutive dry days (Section 5.1.2).

(iii) Atmospheric drivers are investigated using composite and lead-lag analyses, focusing on mesoscale convective systems (MCSs), African Easterly Waves (AEWs), and thermodynamic factors like total column water vapor (TCWV) and convective available potential energy (CAPE) (Section 5.1.3).

(iv) Future changes are evaluated using the ensemble mean (EnsMean) of 23 NEX-GDDP-CMIP6 models, focusing on frequency, intensity, and spatial extent of wet spells (Section 5.1.4).

(4) Objectives and Applications:

(i) The research addresses five objectives: quality control and interpolation of rainfall data, spatial and temporal analysis of wet spells, investigation of atmospheric drivers, assessment of future changes under climate scenarios and the implications of intense multi-day wet spells for flood risks and early warning systems and preparedness strategies (Section 1.4.2).

(ii) Findings are intended to inform early warning systems, flood risk management, and climate adaptation strategies, particularly for agriculture, water management, and urban infrastructure (Section 5.2).

1.5.2 Limitations of the Study

The study acknowledges several constraints that may influence the interpretation and generalizability of its findings, primarily due to data availability, methodological choices, and regional challenges:

(2) Sparse Observational Network:

(i) The analysis is limited by the uneven distribution of rain gauge stations, particularly west of 3°W, which restricts the spatial coverage of the KASS-D dataset and potentially introduces interpolation biases in data-sparse regions (Section 5.2).

(ii) Areas with more than four gauging stations per 1° grid cell exhibit reduced accuracy in capturing localized rainfall extremes, affecting the reliability of wet spell detection in those regions (Section 5.1.1).

(iii) Rain gauge data remain sparse and unevenly distributed across the region, particularly in parts of the Sahel and mountainous or conflict-prone zones. This scarcity introduces spatial sampling bias and may impact the accuracy of the interpolated rainfall fields.

(3) Data Temporal Constraints:

(i) The shorter temporal coverage of IMERG (2001–2020) compared to KASS-D, GPCC, and CHIRPS (1982–2020) limits its use in long-term trend analyses, particularly for assessing decadal variability (Section 4.5).

(ii) The assumption that current (1982-2011) rainfall distributions reflect future (2071-2100) projections for adjusted datasets may oversimplify climate change impacts, as it does not account for non-linear changes beyond this period (Section 5.1.4).

(4) Inherent Biases in Satellite and Reanalysis Products**:**

(i) While gridded datasets like CHIRPS, GPCC, and IMERG help fill spatial gaps, they exhibit known systematic biases, particularly over regions with low gauge density or complex terrain. For instance, CHIRPS underestimates localised convective rainfall, and IMERG's short record length (2001–2020) limits its suitability for long-term trend analysis (Funk et al., 2015; Katsekpor et al., 2024).

(5) Methodological Limitations:

(i) The SPHEREMAP interpolation technique, while effective, may smooth out microscale rainfall variations, potentially underestimating extreme events in complex terrains like the Jos Plateau or Cameroon Highlands (Section 5.1.1).

(ii) The 90th percentile threshold for defining intense wet spells is sensitive to dataset resolution and station density, leading to inter-dataset discrepancies (e.g., GPCC overestimating upper quantiles, CHIRPS underestimating lower quantiles) (Section 5.1.2).

(iii) The use of EnsMean from NEX-GDDP-CMIP6 models reduces individual model biases but may obscure model-specific uncertainties, particularly in simulating sub-scale systems like MCSs (Section 5.1.4).

(6) Methodological Simplifications in Extreme Value Analysis:

(i) The use of block maxima and peak-over-threshold approaches in extreme value theory assumes stationarity and may not fully capture non-linear trends or shifting baselines under changing climate regimes. Also, sample sizes in certain zones or periods may be insufficient to robustly estimate return levels.

(7) Regional and Atmospheric Complexity:

(ii) The study's focus on mesoscale and synoptic drivers (e.g., AEWs, MCSs) may not fully capture tropical-extratropical interactions or other large-scale influences (e.g., Atlantic multidecadal variability) due to limited analysis of these processes (Section 5.1.3).

(iii) The complex topography and coastal dynamics of West Africa (e.g., Niger Delta, Dahomey Gap) introduce variability that is challenging to resolve with the current observational and modelling frameworks (Section 4.5.2).

(8) Applicability Constraints:

(i) The findings are primarily applicable to regions with adequate station coverage, limiting their direct use in sparsely monitored areas without additional validation (Section 5.2).

(iv) The study's recommendations for early warning systems and forecasting tools assume institutional capacity for implementation, which may be constrained by financial and technological gaps in West African countries (Section 5.2).

(9) Climate Scenario Assumptions:

(i) The reliance on SSP2-4.5 and SSP5-8.5 scenarios may not fully represent the range of possible future climate pathways, particularly low-emission scenarios (e.g., SSP1-2.6), limiting the scope of adaptation strategies (Section 5.1.4).

(ii) The assumption that current rainfall matches future distributions simplifies the dynamic interplay of climate variables, potentially underestimating future variability (Section 5.1.4).

(10) Challenges in Climate Model Representation:

(i) The high resolution CMIP6 models (GCMs) used for projection often struggle to simulate the complex West African monsoon system, including important phenomena like AEWs, the AEJ, and MCS dynamics. This necessitated bias correction and downscaling to improve reliability, but residual uncertainties remain in the projections (Sylla et al., 2020; Thrasher et al., 2022).

The availability of high-resolution downscaled projections limited the future analyses to 2001–2100, and some variables (e.g., atmospheric circulation fields) were not consistently available across all GCMs, restricting the depth of future driver diagnostics.

1.6 JUSTIFICATION

Over decades, almost all countries in West Africa have been struck by floods of unprecedented magnitude. This flood has been associated with heavy rainfall over a short period or sequence of rainfall events known as multi-day wet spells in addition to land use and land cover changes and global warming (Panthou *et al*., 2014). Many casualties have been recorded, millions of people have been displaced, properties and crops land have been damaged and many infrastructural facilities have been destroyed (Dos Santos *et al*., 2019; Baldassarre *et al*., 2010; Sighomnou *et al*., 2013; Levinson and Lawrimore, 2008). Hence, it is important to study the dynamical component and evolution of these multi-day wet spells to adequately forecast the occurrence of flood and build stronger climate resilience and adaptation strategies against future climate change. This will help in achieving Sustainable Development Goals (SDGs) number 2 and 13 namely: zero hunger and climate action, respectively.

CHAPTER TWO

LITERATURE REVIEW

2.1 THE WEST AFRICAN MONSOON

This chapter provides a comprehensive review of past studies on West African monsoon, its controlling mechanisms, as well as rainfall variability and intense events and climate modelling.

The West African Monsoon (WAM) is a seasonal climatic system that significantly influences rainfall across the Sahel region, playing a vital role in sustaining vegetation and biomass production (Nicholson, 2013; Herrmann *et al*., 2005). The monsoon is most active between July and August during which it delivers approximately 80% of the region's annual precipitation (Biasutti *et al*., 2008; Nicholson, 2009, Fink and Reiner 2007). The onset of the WAM is primarily driven by the formation of a low-pressure system over the Sahara, commonly referred to as the Saharan Heat Low (SHL). This phenomenon occurs during the boreal summer and marks a transition from the dry, northeasterly Harmattan winds that originate in the Sahara to the humid south-to-southwesterly winds that transport moisture into the continent from the Equatorial Atlantic (Thorncroft *et al*., 2011; Figure 2.1)

Historically, the WAM was perceived as a classic example of tropical rainfall associated with the Intertropical Convergence Zone (ITCZ), where local thermal instability and low-level convergence drive heavy precipitation (Griffiths, 1972). However, Nicholson (2013) highlights that this understanding was largely based on the Hadley circulation model and is more applicable to oceanic environments. Recent studies over West Africa indicate that the region of low-level wind convergence and the primary rain belt are separated by several hundred kilometers, challenging earlier interpretations of monsoonal dynamics (Nicholson, 2009).

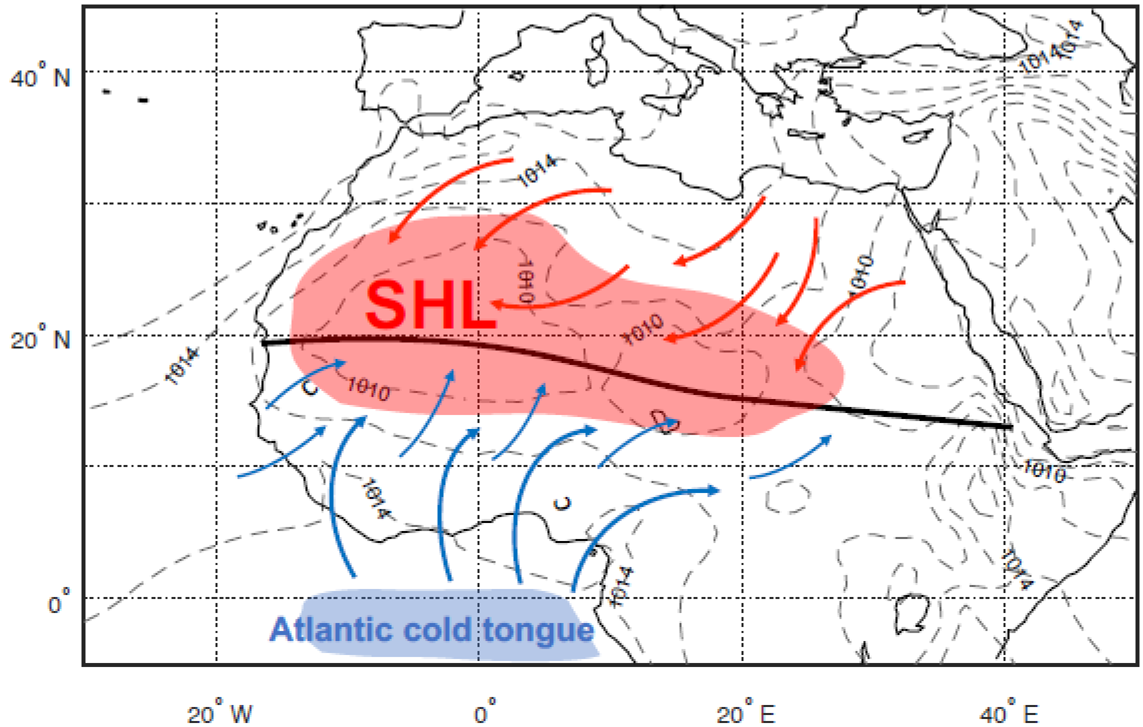

Figure 2.1: Mean Sea level pressure (broken contour lines) and surface winds for the period 1900–2010 during July-September depicted with blue arrows representing moisture-laden winds originating from the equatorial Atlantic and flowing toward the Sahel region

NOTE: Red arrows denote the dry Harmattan winds blowing from the Sahara region. These wind systems converge at the Intertropical Convergence Zone (ITCZ) and also referred to as the Inter-Tropical Discontinuity (ITD; highlighted in thick black line). The Sahara Heat Low (SHL) is marked in red while the Atlantic cold tongue is indicated in blue. This analysis is derived from ERA-20C reanalysis data (Poli *et al*., 2016).

The seasonal rainfall associated with the WAM, which peaks around 10°N latitude is modulated by the northward migration of the maximum solar insolation during the boreal spring and summer (Sultan and Janicot, 2000; Thorncroft *et al*., 2011). The progressive warming of the Sahara and the intensification of the SHL in conjunction with the development of the Atlantic cold tongue, contribute to a sharp land-ocean temperature and surface pressure gradient (Figure. 2.1). This gradient reinforces the primary monsoonal wind patterns over West Africa by facilitating the influx of moist air from the Atlantic (Lavaysse *et al*., 2010; Thorncroft *et al*., 2011).

The WAM circulation system is further characterized by two distinct meridional overturning cells: one shallow and other deep, as well as two critical jet streams namely the African Easterly Jet (AEJ) and the Tropical Easterly Jet (TEJ) (Figure. 2.2). The shallow meridional circulation is closely linked to the SHL and is associated with dry convection contrasts across the region (Thorncroft and Blackburn, 1999; Zhang *et al*., 2008; Thorncroft *et al*., 2011). In contrast, the deep overturning circulation is situated equatorward, aligning with the rain belt and driven by deep moist convection (Nicholson and Grist, 2003; Thorncroft *et al*., 2011).

The AEJ, forming at an altitude of approximately 600–700 hPa, develops in response to temperature and moisture gradients between the Sahara and the Atlantic Ocean (Cook, 1999; Nicholson and Grist, 2003). It is sustained by dry convection to the north over the Sahara and deep moist convection to the south (Cook, 1999; Thorncroft and Blackburn, 1999; Zhang *et al*., 2008). Positioned south of the AEJ at around 200 hPa is the TEJ that originates from the Asian monsoon system and plays a role in enhancing divergence over West Africa, particularly poleward of the jet stream (Grist and Nicholson, 2001). The rain belt is characterized by a deep column of moist air that is situated between these two jet streams and is closely associated with the deep meridional overturning circulation (Nicholson and Grist, 2003; Nicholson, 2009).

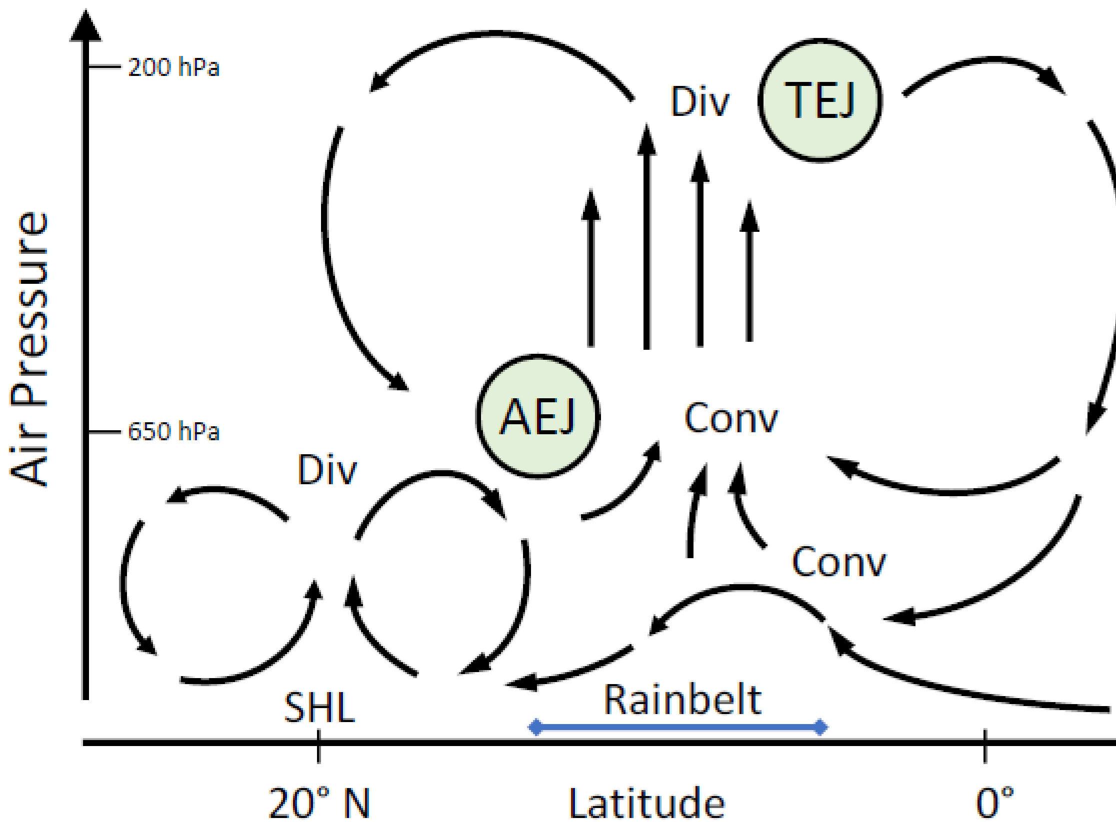

Figure 2.2: Schematic illustration of the dynamics of the West African Monsoon, featuring key components such as the SHL, the shallow overturning circulation, the rain belt, the deep overturning circulation, the TEJ, and the AEJ**.**

NOTE: This representation is from Berntell (2023) and adapted from Nicholson (2013).

2.1.1 Components of West African Monsoon

A critical aspect of the West African monsoon system involves several interconnected components that include the Inter-Tropical Discontinuity (ITD), the African Easterly Jet (AEJ), the Tropical Easterly Jet (TEJ), and African Easterly Waves (AEWs). Additionally, the subtropical high-pressure systems in both hemispheres known as St. Helena in the Southern Hemisphere and Azores in the Northern Hemisphere also play a significant role. Other factors include the depth of the monsoon layer, the presence of deep convective systems, as well as the types and distribution of vegetation cover and soil types. These components interact in a highly complex manner to influence precipitation patterns and the overall weather conditions across West Africa.

2.1.2 The Inter-tropical Discontinuity

The Intertropical Discontinuity (ITD) represents a convergence zone where two distinct air masses meet: the warm, moisture-laden southwesterly monsoon winds from the tropical Atlantic Ocean and the cool, dry northeasterly winds originating from the Sahara. This interaction forms a quasi-stationary west-east moisture-temperature boundary over West Africa (Lélé and Lamb, 2010). The seasonal oscillation of the ITD plays a crucial role in modulating rainfall across the West Africa, as its northward and southward migration influence precipitation patterns (Sultan and Janicot, 2000; Redelsperger *et al*., 2002). The latitudinal migration of the ITD follows the seasonal movement of maximum solar insolation by maintaining relative consistency from year to year despite significant variations in the positioning of rain belts (Lebel and Ali, 2009). During the boreal summer, the ITD advances northward, reaching its farthest extent at approximately 22°N in August (Lebel and Ali, 2009). This stability in ITD positioning, despite the variability in rain belt locations highlights its predictable seasonal cycle.

West Africa has been classified into different weather zones (A, B, C1, C2, and D) based on the surface position of the ITD (Adejokun, 1966; Hamilton and Archbold, 1945). As the ITD shifts northward or southward, distinct weather regimes emerge across these zones. While convergence and uplift occur along the ITD, deep convective systems do not typically develop directly at this boundary due to the shallow monsoon layer and the presence of mid-tropospheric subsidence. The depth of the moist monsoonal layer increases sharply south of the ITD at an approximate rate of 1 km per degree latitude (Lélé and Lamb, 2010). For deep convection to be initiated, the monsoon flow must reach a depth of at least 1–2 km that results in the cloudiness and peak rainfall occurring 300–500 km south of the ITD, where the moisture layer is more developed (Nicholson, 2009; Lélé and Lamb, 2010). Ultimately, the seasonal variability of the ITD together with changes in the regional wind patterns reflects the evolving state of the West African Monsoon (WAM).

2.1.3 African Easterly Jet

The African Easterly Jet (AEJ) has been the subject of extensive study due to its critical role in the formation of African Easterly Waves (AEWs) due to its inherent instability. The AEJ develops because of a strong moisture and meridional temperature gradient between the Sahara Desert to the north and the Atlantic Ocean to the south. This thermal contrast generates maximum wind speeds at mid-tropospheric levels, typically around 600 hPa, with zonal wind velocities reaching approximately 15 ms^{-1} (Chen, 2005). The temperature gradient is most pronounced between June and August, while the AEJ reaches its peak intensity in May and June preceding the onset of Sahelian rainfall.

Chen (2005) suggests that the Saharan High plays a fundamental role in the formation of the AEJ, as the jet is located along its periphery. This aligns with previous findings that highlight the temperature influence of gradient on jet formation. Additionally, moisture processes contribute to the AEJ's meridional extent and intensification, as noted by Cornforth *et al*. (2009). The AEJ is maintained by both deep and shallow meridional circulations linked to the West African Monsoon (WAM) with the local Hadley circulation supporting the deep component and the Saharan Heat Low (SHL) sustaining the shallow component (Cook, 1999). The SHL's influence is particularly significant during the pre- and post-monsoon periods, whereas boundary layer processes become dominant during the peak monsoon season (Kalapureddy, 2010).

An alternative explanation for the maintenance of the AEJ is proposed by Chen (2005), who attributes it to Coriolis acceleration associated with divergent northerly winds in the mid-troposphere over the Chad-Sudan region. The instability characteristics of the AEJ were first analyzed by Burpee (1972), who demonstrated that the jet satisfies the conditions for combined barotropic-baroclinic instability. Consequently, this instability has long been considered a key factor in the development of AEWs over West Africa. However, more recent studies argue that while AEJ instability is a necessary condition for wave formation, it is not sufficient on its own (Hsieh and Cook, 2005). The AEJ is also susceptible to convective heating-induced instability, as evidenced by the reversal of the potential vorticity gradient near the jet stream (Hsieh and Cook, 2005).

Nicholson and Grist (2001) analyzed the mean characteristics of the AEJ across its eastern and western sectors. The jet reaches its maximum strength in May and June, with core wind speeds averaging 12 m s^{-1} in the western sector (10°W–10°E) and 10 m s^{-1} in the eastern sector (10°E–30°E). During the Sahelian phase of the monsoon in boreal summer, these wind speeds decrease by approximately 2 m s^{-1}. However, in some years, the monthly mean wind speed of the AEJ core can reach up to 16 m s^{-1}. Notably, the western core tends to be more pronounced in wetter years, whereas the eastern core is more dominant in drier years, indicating a strong interannual variability in AEJ intensity.

2.1.4 Tropical Easterly Jet

The Tropical Easterly Jet (TEJ) is a significant component of the global atmospheric circulation, situated in the upper troposphere at altitudes corresponding to 150–200 hPa. The jet typically forms around 5°N latitude, with core wind speeds reaching approximately 40 m s^{-1}. The TEJ arises due to the strong meridional temperature gradient between the Himalayan Plateau and the Indian Ocean, and it is primarily maintained by tropical divergent circulations associated with both the east-west Walker circulation and the north-south Hadley circulation (Chen and Van Loon, 1987). The jet emerges off the eastern coast of China, extends westward over India and the Middle East, and gradually weakens as it crosses the Horn of Africa. It appears to dissipate near the Sudan region of West Africa (~20°E); however, this location is better understood as a jet exit and entrance region rather than a true dissipation point. During the boreal summer, the TEJ has a mean wind speed of approximately 18 m s^{-1} over the eastern Sahel (Nicholson and Grist, 2001). Although it is commonly described as a boreal summer feature, the TEJ remains active between January and March when it shifts to the Southern Hemisphere, with its core positioned around 5–10°S (Nicholson and Grist, 2001).

Unlike the African Easterly Jet (AEJ), the TEJ over West Africa demonstrates minimal latitudinal variability from year to year. However, its wind speed and east-west extent fluctuate significantly (Grist and Nicholson, 2001; Nicholson, 2008; Lélé and Lamb, 2010). The interannual variability of the TEJ has been widely studied, with evidence linking a stronger TEJ to wetter conditions and a weaker TEJ to drier conditions in several regions, including the Sahel (Hulme and Tosdevin, 1989; Nicholson, 2008), western equatorial Africa (Nicholson and Dezfuli, 2013; Dezfuli and

Nicholson, 2011), Ethiopia (Segele *et al*., 2009), and India (Pattanaik and Satyan, 2000). Additionally, the TEJ has been correlated with cyclone activity in the Bay of Bengal, with stronger TEJ phases linked to fewer cyclones and weaker TEJ phases associated with increased cyclone frequency (Srinivasa *et al*., 2004). The TEJ is also recognized as a key factor in shaping West Africa's mean climate (Flohn, 1964; Webster and Fasullo, 2003). Its connection to rainfall variability is primarily attributed to upper-level divergence near the jet core, which enhances atmospheric instability and precipitation (Nicholson, 2013). This effect is particularly noticeable during wet years in the Sahel, where a stronger TEJ not only contributes to higher rainfall totals but also to the intensification of the regional rain belt (Nicholson, 2009).

2.1.5 Mesoscale Convective System

A Mesoscale Convective System (MCS) refers to a highly organized cluster of convective clouds, typically aligned in a north-south orientation and moving east to west. These systems are characterized by heavy rainfall, strong gusty winds, and thunderstorms (Fink and Reiner, 2003). The MCSs play a crucial role in the West African climate, contributing over 70% of the total rainfall in the region, with their influence reaching nearly 95% in the Sahelian belt (Omotosho, 1985). The diurnal cycle of convection in the Sahel is largely influenced by the westward propagation of MCSs. In West Africa, MCSs are commonly initiated by intense daytime heating and orographic effects, which provide the necessary instability for convective development (Rowell *et al*., 1995). Once formed, these storms migrate westward, and as they move away from their source regions, the timing of peak precipitation shifts progressively later in the day (Thorncroft, et al., 2011). The formation of MCSs over West Africa begins with the development of multiple cumulonimbus clouds in specific areas that are favorable for convection. These clouds intensify, organize into linear structures, and subsequently propagate westward as a cohesive system. Studies by Fortune (1980) and Peters and Tetzlaff (1988) indicate that Sahelian MCSs typically move at average speeds of 14–17 m s^{-1}. Additional research by Fink *et al*. (2006) suggests that MCS propagation speeds can vary significantly, with median values ranging from 3 to 19 m s^{-1}, depending on the intensity metrics applied.

2.2 MONSOON FLOW AND MOISTURE DYNAMICS IN WEST AFRICA

The West African monsoon flow is primarily driven by thermodynamic contrasts between the Sahara Desert and the equatorial Atlantic Ocean during the summer months (Nicholson, 2013). According to Thorncroft *et al*. (2011), Peyrillé *et al*. (2007), and Nicholson (2013), the simultaneous development of the Atlantic cold tongue (a region of cool equatorial waters presents between boreal spring & summer and the SHL) leads to the establishment of a southwesterly monsoonal flow that transports moisture inland. The northward extent of this flow is restricted by the cyclonic circulation around the SHL that plays a critical role in regulating the penetration depth of the monsoon as reported by Peyrillé and Lafore, 2007.

Understanding the balance between rainfall, evapotranspiration, atmospheric moisture content, and vertically integrated moisture flux convergence (VIMFC) is essential for assessing the atmospheric water budget in the West Africa. Fontaine *et al*. (2003) demonstrated that the intraseasonal variability of both the WAM and ITD can be analyzed through differences between evaporation and precipitation (P-E). However, the low-level southwesterly monsoon flow is not the sole contributor of moisture to West Africa. Fontaine *et al*. (2003) estimated that approximately 75% of the moisture entering the WAM region between 1000 and 300 hPa during July–September originates not only from the south but also from the north and east. This indicate that moisture sources such as the Mediterranean, East Africa, and the Indian Ocean also influence monsoon strength.

Additional studies have further highlighted the complexity of West African moisture transport. Long *et al*. (2000) noted that easterly flow dominates the regional water vapor flux while Gong and Eltahir (1996) estimated that about 27% of the rainfall-producing moisture in West Africa originates from local land surface evaporation. This underscores the critical role of soil moisture and biospheric feedbacks in modulating regional climate patterns. Similarly, Meynadier *et al*. (2010a) established a strong correlation between precipitation variability and VIMFC, emphasizing that rainfall anomalies in the region are typically preceded by anomalous moisture flux convergence, followed by moisture flux divergence and shifts in evapotranspiration patterns.

At a monthly timescale, the evolution of moisture flux convergence (MFC) exhibits a strong correlation with rainfall, indicating that atmospheric moisture availability is a major control on precipitation during the rainy season. Under dry conditions, moisture divergence prevails, causing the land surface to act as a net source of atmospheric moisture. Hagos and Cook (2007) observed that from mid-May onward, boundary layer moisture supply surpasses divergence, leading to a net increase in atmospheric moisture content and subsequent condensational heating in the lower troposphere. This process generates inertial instability, which promotes the establishment of the primary Sahelian rain belt by late June. As the meridional convergence zone shifts further inland, condensation and precipitation along the coastline decrease accordingly.

Using a hybrid dataset combining satellite observations and numerical weather prediction analyses, Meynadier *et al*. (2010b) further emphasized the significant role of moisture flux convergence in determining rainfall distribution across different regional scales. Their findings indicate that variability of moisture flux is strongly influenced by precipitation trends across multiple timescales that ranges from daily to seasonal and even interannual fluctuations.

2.3 FACTORS INFLUENCING SUMMER MONSOON RAINFALL VARIABILITY IN WEST AFRICA

Rainfall patterns across West Africa are influenced by multiple factors, including the WAM system, sea surface temperatures (SSTs), land use changes, and atmospheric aerosols. The land-sea thermal gradient, which arises from monsoonal systems play a particularly significant role in shaping West Africa rainfall patterns (Odekunle *et al*., 2005). The complex interplay of these climatic drivers accounts for the spatial and temporal variability in rainfall across different zones and subregions within West Africa (Abiodun *et al*., 2008). Consequently, a comprehensive understanding of these factors is essential for improving the predictability and projection of rainfall variability in the region.

The relationship between rainfall and large-scale atmospheric circulations has been extensively examined in previous studies. Historical changes in rainfall have been attributed to variations in large-scale tropospheric features, including the AEJ, low-level westerly monsoon flow, and Saharan Heat Low dynamics, all of which influence the latitudinal migration of the ITD (Nicholson and Grist, 2001; Grist, 2002; Nicholson and Grist, 2003; Sultan *et al*., 2003). Sylla *et al*. (2010) linked the northward shift and weakening of the AEJ between June and August to the onset and progression of the monsoon rain belt. Their findings also indicate that the intensification of the TEJ coincides with this northward displacement. In drier years, the TEJ weakens while the AEJ strengthens and shifts southward. This leads to a reduction in African Easterly Wave (AEW) activity with a pattern previously reported by Omotosho (2007), who observed a stronger AEJ during dry years compared to wetter years.

The impact of air-sea interactions on coastal rainfall has also been examined. Leduc-Leballeur *et al*. (2013) found that consecutive wind bursts from the Saint Helena Anticyclone can induce significant and lasting changes in atmospheric circulation over the northern Gulf of Guinea, influencing coastal precipitation patterns. Similarly, Vizy (2002) investigated the effect of Gulf of Guinea sea surface temperature anomalies (SSTAs) on the WAM and observed that warmer SSTAs increased evaporation, enhancing lower tropospheric moisture content and rainfall along the Guinean coast. However, this also led to reduced rainfall over the southern Sahel, because of the enhanced subsidence in the lower troposphere and a southward shift in monsoonal circulation (Flaounas *et al*., 2012).

The positioning and intensity of both the AEJ and TEJ have been strongly linked to drought and wet conditions in West Africa. Jenkins *et al*. (2005) associated Sahelian droughts with a southward displacement of the AEJ, while wetter-than-average conditions were linked to a stronger TEJ. Nicholson (2008) further emphasized that both jets play a crucial role in determining regional rainfall variability, with similar conclusions drawn by Grist (2002) and Nicholson *et al*. (2007), who connected drought periods to changes in AEW activity.

African Easterly Waves (AEWs), which develop between the AEJ and TEJ, contribute to the maintenance of Mesoscale Convective Systems (MCSs) in the tropics (Hsieh and Cook, 2008). According to Lebel *et al*. (2003), rainfall in the Sahel is more strongly associated with AEWs and large-scale MCSs than with localized thunderstorms. Given that approximately 80% of West Africa's annual rainfall originates from the West African Summer Monsoon (WASM), any disruption to these systems, particularly the TEJ, AEJ, and low-level westerly flow can significantly contribute to dry or wet anomalies across the region. Figure 2.3 shows the schematic illustration all these features in January (dry season) and July (wet season)

On a multi-day timescale, analysis of zonal wind variability by Basse *et al*. (2021) and Osei *et al*. (2022) show that the monsoonal flux is significantly stronger over the Northern Sahel and the

Guinea Coast region during wet spells compared to dry spells. This enhancement in monsoon strength is associated with a weaker and northward-shifted AEJ during wet periods, whereas dry spells are characterized by a stronger AEJ positioned further south. The observed strengthening of the monsoon flow during wet spells aligns with an intensification of the SHL. Vertical velocity analysis further reveals that deep convection is more intense during wet spells, as indicated by a stronger southern updraft core compared to dry periods. In the upper troposphere, the TEJ also exhibits greater intensity during wet spells while it weakens during dry periods (Basse *et al*. 2021).

Additionally, the activity of AEWs and relative humidity levels are both higher during wet spells that suggest monsoonal fluxes transport sufficient moisture to sustain enhanced convective activity. This interplay between monsoon strength, atmospheric moisture content, and wave activity plays a crucial role in determining the intensity and duration of wet and dry periods across West Africa.

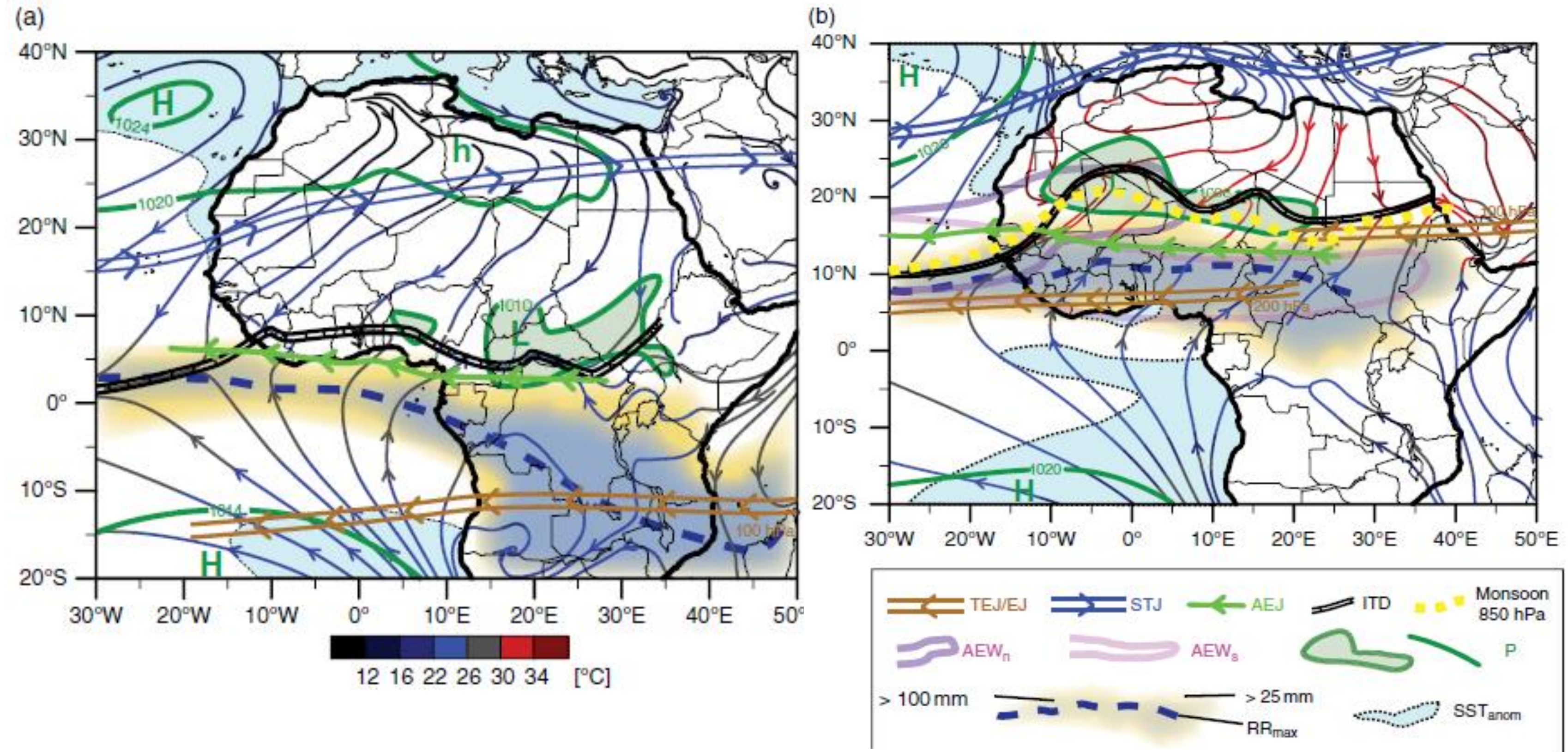

Figure 2.3: Schematic illustration of the atmospheric and oceanic features that influence the weather and climate of West Africa during (a) January and (b) July.

NOTE: Key elements depicted include the positions of the ITD, the monsoon trough and upper-level air streams such as AEJ, TEJ, and the Subtropical Jet (STJ). Surface winds are color-coded based on 2-meter air temperature (refer to the color bar). The tropical rain belt is shown with the maximum axes of rainfall (RRmax). Additionally, the propagation zones for northerly and southerly AEW vortices (AEWn and AEWs, respectively) are indicated. (source: Diop *et al.***,** 2017)

2.4 INFLUENCE OF SEA SURFACE TEMPERATURE AND LARGE -SCALE CLIMATE VARIABILITY ON WEST AFRICAN RAINFALL

A significant portion of WAM rainfall variability is driven by slowly evolving climate components, particularly sea surface temperatures (SSTs). Early studies on the relationship between Sahelian rainfall and SST variability were motivated by the region's historical droughts. Lamb (1978) initially proposed links between rainfall fluctuations and SST anomalies in the equatorial and subtropical Atlantic, while Folland *et al*. (1986) emphasized the role of inter-hemispheric SST gradients. Despite ongoing debate, one widely accepted conclusion is that SST variations across the global oceans play a crucial role in modulating WAM rainfall patterns (Giannini *et al*., 2003; Biasutti *et al*., 2008). However, uncertainties remain regarding ENSO's impact on WAM rainfall and relative influence of different ocean basins and the Mediterranean, and the ability of climate models to accurately simulate rainfall trends (Nicholson, 2013).

Among the dominant interannual drivers, tropical Atlantic variability is considered the primary mode of influence (Carton *et al*., 1996). Several studies using different methodologies have consistently shown that positive SST anomalies in the Atlantic (Atlantic Niños) create a dipole rainfall pattern, with increased precipitation along the Guinean coast and reduced rainfall in the Sahel (Horel *et al*., 1986; Wagner and da Silva, 1994; Fontaine and Janicot, 1996; Ward, 1998). Atmospheric General Circulation Models (AGCMs) suggest that this dipole effect arises from a weakening of the sea-level pressure gradient between ocean and land, which in turn limits ITCZ displacement, resulting in enhanced coastal rainfall and suppressed Sahelian precipitation. Similarly, warming in the tropical Pacific has been associated with higher rainfall over the Gulf of Guinea but drier conditions in the Sahel (Ward, 1998; Camberlin *et al*., 2001; Rowell, 2001; Joly *et al*., 2007). Within the African Monsoon Multidisciplinary Analysis (AMMA) framework, experiments assessing WAM sensitivity to Pacific SST anomalies between 1979 and 2002 confirmed that positive SST anomalies in the Pacific negatively impact Sahel rainfall (Mohino *et al*., 2011).

The Indian Ocean also influences Sahelian rainfall at both interannual and decadal timescales. Biasutti *et al*. (2008) identified a negative correlation between Indian Ocean SSTs and Sahel precipitation, a relationship confirmed in both observational data and coupled global climate models (CGCMs). Bader and Latif (2011) attributed the 1983 drought in the western Sahel to positive SST anomalies in the Indian Ocean, possibly persisting from the 1982/83 El Niño event. However, except for extreme cases like 1983, Indian Ocean SST anomalies at interannual timescales tend to be weaker compared to those in other ocean basins that may reduce their apparent influence on Sahelian rainfall.

Further research has examined how simultaneous SST anomalies across multiple basins interact to shape regional rainfall trends. Palmer and Räisänen (2002) analyzed AGCM responses to individual ocean basin SST anomalies, confirming that while Indian Ocean warming slightly enhances rainfall over the western Sahel, concurrent SST anomalies in the Atlantic and Pacific are more strongly linked to Sahelian drought (Folland *et al*., 1986). Fontaine *et al*. (2011a) found that positive SST differences between the Indian Ocean and the eastern Mediterranean coincide with synchronized rainfall deficits across the entire Sudan-Sahel region. Additionally, Rowell (2001) suggested that Indian Ocean influences act through changes in large-scale SST gradients between the western Pacific and the Indian Ocean, triggering stationary equatorial Rossby wave responses that induce subsidence over the Sahel, thereby suppressing rainfall.

More recently, both empirical and numerical studies have strengthened the case for Mediterranean SST anomalies influencing WAM rainfall (Jung *et al*., 2006; Fontaine *et al*., 2011b; Polo *et al*., 2011). The mechanisms driving northward monsoon migration have been explored in depth by Peyrillé *et al*. (2007) and Peyrillé and Lafore (2007). Fontaine *et al*. (2010) provided evidence that warm Mediterranean SST anomalies are associated with an intensified WAM that leads to a stronger low-level moisture advection and enhanced ascending motion over West Africa. Their study also identified a link between western Mediterranean SST anomalies and deep convection over the Gulf of Guinea just as eastern Mediterranean SST anomalies primarily influence atmospheric circulation over North Africa. Further analysis by Gaetani *et al*. (2010) at sub-seasonal timescales found that Sahelian rainfall anomalies are most pronounced during July–August when the monsoon circulation is fully developed inland. During this period, the effect of moisture transport from the Mediterranean peaks and maximizing its impact on rainfall variability in the Sahel.

2.5 COMPARISON OF RAINFALL PRODUCTS OVER SUB-SAHARAN AFRICA

Rainfall is a critical climatic variable that significantly impacts the livelihoods of millions in Sub-Saharan Africa (SSA), where over 95% of agriculture depends on rainfed systems (Le Coz & van de Giesen, 2020). Given the region's vulnerability to climate variability, droughts, and extreme weather events, accurate rainfall data is essential for climate monitoring, water resource management, and disaster preparedness. However, measuring and predicting rainfall in SSA is particularly challenging due to high spatial and temporal variability, a sparse rain gauge network, and inconsistent satellite and model-based estimates.

Several rainfall estimation techniques have been developed to address these challenges, categorized into gauge-based, satellite-based, and reanalysis products. Each method has strengths and limitations, necessitating a comparative assessment to determine their suitability for different applications such as hydrological modelling, drought monitoring, and climate studies. The study by Le Coz and van de Giesen (2020) provides a comprehensive review of rainfall datasets used in SSA, highlighting their accuracy, biases, and potential application.

2.5.1 Rainfall Products and their Challenges

Rainfall products in SSA can be classified into three main categories:

i. Gauge-Based Products: These datasets rely on ground-based rain gauge measurements, offering high accuracy in areas with dense station networks. However, SSA has limited coverage of weather stations, with many regions falling below World Meteorological Organization (WMO) standards (Le Coz & van de Giesen, 2020). This limitation affects data reliability, especially in remote and conflict-prone areas.

ii. Satellite-Based Products: Satellite rainfall estimates provide widespread spatial coverage, particularly useful in data-scarce regions. They rely on infrared (IR) or microwave (MW) sensors to infer precipitation from cloud-top temperature or atmospheric moisture content. While satellite products such as Climate Hazards Group Infrared Precipitation with Stations (CHIRPS), Tropical Application of Meteorology using Satellite (TAMSAT), and TRMM Multi-satellite Precipitation Analysis (TMPA) have proven useful, they often require bias correction using gauge data (Funk *et al*., 2015). Additionally, convective rainfall which dominates SSA can be difficult to capture accurately with satellite methods alone (Maidment *et al*., 2013).

iii. Reanalysis Products: Reanalysis datasets integrate observational data with climate models to reconstruct historical weather conditions. Products such as ERA-5 and MERRA-2 are widely used in climate studies, but their performance in SSA is hindered by limited ground truth data for calibration (Sun *et al*., 2018). Furthermore, these models often struggle to represent localized convective rainfall systems accurately.

Each of these rainfall datasets exhibits spatial and temporal biases, making it essential to assess their performance across different climatic zones in SSA.

2.5.2 Intercomparison of Rainfall Products

Several studies have evaluated the performance of different rainfall products over SSA (Adeyewa and Nakamura, 2003; Adeyewa, 2005; Ageet *et al*., 2022; Ilori and Balogun, 2021; Maranna *et al*., 2020; Sun *et al*., 2018; Maidment *et al*., 2013). Sun *et al*. (2018) found significant discrepancies among global rainfall datasets, particularly in northern Africa. Regionally focused products such as ARC2, RFE2, and TAMSAT, which are calibrated for SSA conditions, tend to outperform global datasets in the region.

Research has also emphasized the importance of choosing rainfall products based on their intended application. Maidment *et al*. (2017) highlighted that drought monitoring requires datasets capable of capturing small precipitation amounts while hydrological models need datasets with long-term consistency to ensure reliable simulations. However, Funk & Verdin (2003) noted that satellite-derived rainfall estimates generally outperform reanalysis models in capturing daily precipitation patterns in the tropics.

Despite improvements in satellite retrieval methods, the rainfall products still require validation with ground observations. The International Precipitation Working Group (IPWG) maintains a database of publicly available rainfall datasets but large-scale validation efforts in SSA remain limited (Le Coz & van de Giesen, 2020).

2.5.3 Key Factors Influencing Rainfall Estimation in SSA

Several climatic and methodological challenges influence rainfall estimate in SSA:

i. Sea Surface Temperature Variability: SST anomalies in the Atlantic, Pacific, and Indian Oceans influence monsoonal and convective rainfall in SSA. Giannini *et al*. (2003) found that warming in the tropical Atlantic and Pacific is linked to Sahelian droughts, while ENSO variability affects rainfall patterns along the Guinea coast (Nicholson, 2013).

ii. African Easterly Jet and Tropical Easterly Jet: The strength and positioning of these tropospheric jets play a crucial role in rainfall distribution. Nicholson & Grist (2001) showed that a stronger AEJ shifts convection southward, reducing rainfall in the Sahel, whereas a stronger TEJ enhances monsoon circulation, increasing precipitation.

iii. Convective Storms and Localized Variability: Rainfall in SSA is highly localized, often generated by convective systems that develop and dissipate rapidly. This small-scale variability is difficult for global climate models and satellite sensors to capture accurately, leading to estimation biases (Maidment *et al*., 2013).

2.5.4 Criteria for Selecting Rainfall Datasets

Given the strengths and weaknesses of each dataset, different products are recommended based on specific applications:

i. For hydrology and water resource management: CHIRPS and TAMSAT are suitable due to their high-resolution, gauge-calibrated estimates.

ii. For drought monitoring: ARC2 and RFE2 are preferable, as they capture small precipitation amounts more accurately.

iii. For climate research and trend analysis: Reanalysis datasets like ERA-5 and MERRA-2 offer long-term consistency for detecting climatic shifts.

iv. For flood prediction and extreme rainfall events: Near-real-time datasets such as TMPA and GSMaP provide high temporal resolution.

While no single dataset is universally superior, integrating multiple rainfall products using satellite, gauge, and model-based estimates can enhance the accuracy of precipitation assessments. Gauge-based data is often the most reliable, its sparse coverage necessitates the use of satellite and reanalysis datasets. However, these alternative methods come with inherent biases that require validation with ground observations to improve accuracy.

2.6 COUPLED MODEL INTER-COMPARISON PROJECT (CMIP5 AND CMIP6)

The Coupled Model Intercomparison Project (CMIP) has been a cornerstone of climate science, by providing a framework for evaluating and improving global climate models (GCMs) and generating projections of future climate change. CMIP5 that supported the Intergovernmental Panel on Climate Change (IPCC) Fifth Assessment Report (AR5) marked a significant milestone in climate modelling. However, the latest phase of CMIP (CMIP6), has introduced a more detailed and comprehensive experimental framework that incorporate higher spatial resolution and improved parameterization schemes of physical processes in addition to an expanded set of climate scenarios. These advancements have improved the ability to simulate regional climate dynamics, feedback mechanisms, and extreme events.

One of the most notable advancements in CMIP6 is the increased complexity and resolution of climate models. CMIP5 models that is state-of-the-art at their time, operated at relatively coarse spatial resolutions, typically ranging from 100 to 200 kilometres for atmospheric components (Taylor *et al*., 2012). This limited their ability to resolve regional-scale processes and extreme events like tropical cyclones and localized precipitation patterns. In contrast, CMIP6 models benefit from enhanced computational power that enable the model to run at higher spatial resolutions, with some models achieving grid spacings of 25 to 50 kilometers (Eyring *et al*., 2016). This improvement allows for better representation of small-scale and sub-scale phenomena that include localized convection, cloud formation, and effect of topography. These are critical for accurate regional climate projections.

Also, CMIP6 models incorporate more comprehensive Earth system components. While CMIP5 models primarily focused on physical climate processes, CMIP6 further includes advanced representations of biogeochemical cycles, dynamic vegetation, and interactive ice sheets (Eyring *et al*., 2016). For example, many CMIP6 models now include coupled carbon-climate feedback that enable a more realistic simulation of the interactions between terrestrial and atmospheric CO2 concentrations and oceanic carbon sinks. These advancements provide a more holistic understanding of the Earth system and its responses to anthropogenic forcing.

The experimental design of CMIP6 represents a significant evolution from CMIP5 in the development of future scenarios. CMIP5 relied on Representative Concentration Pathways (RCPs) that were defined by their radiative forcing levels (e.g., RCP2.6, RCP4.5, RCP8.5) by the end of the 21st century (Moss *et al*., 2010). While RCPs were useful for exploring a range of climate outcomes, they did not explicitly account for socioeconomic factors driving emissions. Hence, CMIP6 address this limitation by introducing Shared Socioeconomic Pathways (SSPs). This combines radiative forcing targets with narratives about societal development, energy use, and land-use change (O'Neill *et al*., 2016). Notable differences between RCPs and SSPs include:

i. SSP1-1.9, a new scenario in CMIP6 that aligns with efforts to limit warming to 1.5°C by providing a reference for stringent mitigation strategies.

ii. SSP5-8.5 represent a high-emission, fossil fuel-driven trajectory that replaces RCP8.5 as the worst-case scenario. Though recent research suggests it may be less probable than initially assumed (Hausfather & Peters, 2020).

This integration allows for a more distinct exploration of climate mitigation and adaptation strategies in addition to their interactions with socioeconomic trajectories.

In addition to the SSP scenarios, CMIP6 includes a broader suite of experiments under the Diagnostic, Evaluation, and Characterization of Klima (DECK) framework and numerous Model Intercomparison Projects (MIPs). These MIPs focus on specific scientific questions, such as aerosol-cloud interactions, stratospheric processes, and climate extremes that provide more deeper insights into key uncertainties and feedback mechanisms (Eyring *et al*., 2016). This expanded experimental design enhances the capability of CMIP6 for addressing interdisciplinary research questions and informing policy decisions.

CMIP6 has established a significant stride in improving the simulation of historical climate and projecting future changes. For example, CMIP6 models exhibit better skill in replicating observed atmospheric circulation patterns, ocean heat uptake, and regional precipitation trends when compared to CMIP5 (IPCC, 2021). They also show improved simulation of climate variability modes like the El Niño–Southern Oscillation (ENSO) and the North Atlantic Oscillation (NAO), that are critical for understanding regional climate impacts. In addition, CMIP6 models provide more robust projections of extreme events like heatwaves, heavy precipitation, and tropical cyclones due to their higher resolution and improved physics (Seneviratne *et al*., 2021).

However, CMIP6 has its own challenges. One notable issue is the wider spread in equilibrium climate sensitivity (ECS; i.e., biases) estimates among models with some CMIP6 models exhibiting higher ECS values than their CMIP5 counterparts (Zelinka *et al*., 2020). This increased spread raises questions about the representation of key feedback processes, such as cloud-aerosol interactions and atmospheric convection that underscores the need for continued model evaluation and refinement. Additionally, the enhanced complexity of CMIP6 models places greater demands on computational resources and data storage, creating challenges for researchers and institutions with limited computational and storage infrastructures (Balaji *et al*., 2018).

The advancements in CMIP6 have profound implications for climate science and policy. By providing more detailed and comprehensive projections, CMIP6 supports the AR6 and offers critical insights into the impacts of climate change on ecosystems, water resources, and human societies (IPCC, 2021). The integration of SSPs allows policymakers to explore the consequences of different development pathways by identify strategies for achieving climate targets, such as those outlined in the Paris Agreement (O'Neill *et al*., 2016).

Nevertheless, the increased complexity and uncertainties in CMIP6 indicate the importance of interdisciplinary collaboration and continued investment in climate modelling. Addressing these challenges will require advances in observational data that are limited in the SSA, process-level understanding, and computational techniques (Eyring *et al*., 2019). As the scientific community moves toward future phases of CMIP, CMIP7 particularly, the lessons learned from CMIP5 and CMIP6 will be invaluable for guiding model development and ensuring that climate projections remain robust and actionable.

2.7 SHARED SOCIOECONOMIC PATHWAYS (SSPS)

The latest generation of climate scenarios developed for CMIP6 and utilized in the IPCC Sixth AR6 are based on the SSPs (IPCC 2021). These SSP-based scenarios represent the most complex set of future projections developed to date, spanning a wide range of possible futures from strong mitigation efforts to unrestricted emissions growth. Among them, the most ambitious scenario was specifically designed to align with the Paris Agreement's goal of limiting global temperature rise to well below 2°C, while striving to remain under 1.5°C above pre-industrial levels. Unlike previous climate scenario frameworks, the SSPs integrate socioeconomic trajectories with climate forcing pathways, offering a more comprehensive assessment of potential future climate conditions (Riahi *et al*., 2017).

Five distinct SSP narratives were developed, each reflecting a unique trajectory of global societal evolution (Riahi *et al*. 2017). SSP1, labelled "Sustainability: taking the green road" represents a future where the world gradually transitions toward sustainable development, prioritizing inclusive economic growth, environmental conservation, and resource efficient consumption. This pathway envisions reduced inequality, strong global cooperation, and technological advancements that are aimed at achieving low-carbon energy and sustainable land-use practices. SSP2, known as "middle of the road" depicts a future where global socioeconomic trends continue largely along historical trajectories. Some regions achieve sustainable development, while others struggle with persistent inequality and environmental degradation. Progress toward international climate goals is gradual but inconsistent.

In contrast, SSP3, "Regional rivalry: a rocky road" portrays a world marked by rising nationalism, trade conflicts together with regional competition. Countries prioritize short-term economic and security interests over global cooperation. This scenario leads to high levels of inequality, slow technological progress with limited investments in climate mitigation that exacerbate environmental degradation and increasing the vulnerability of low-income nations. SSP4, "Inequality: a road divided" envisions a future with high economic and political stratification, where a technologically advanced global elite thrives and lower-income societies experience stagnant development and reduced access to resources. This results in low adaptation capacity for the most vulnerable regions/nations despite the availability of high-tech climate solutions in wealthier parts of the world.

Finally, SSP5, “Fossil-fuelled development: taking the highway,” describes a high-growth, market-driven world that prioritizes economic expansion and rapid technological innovation but relying heavily on fossil fuel resources to meet soaring energy demands. While this scenario fosters strong investments in education, health, and infrastructure, it also leads to high GHG emissions, and making climate mitigation challenging. Environmental management focuses primarily on localized pollution control with limited global efforts to curb climate change.

Each SSP corresponds to a set of greenhouse gas emissions and land-use projections that define a baseline trajectory for climate change. These pathways are further combined with an updated version of the RCPs that describe radiative forcing levels (measured in watts per square meter, W/m^2) expected by the end of the century. The SSP-RCP framework allows superimposition of climate policy choices on each socioeconomic pathway while simulating the potential impact of different mitigation efforts. The new set of radiative forcing targets ranges from SSP1-1.9 W/m^2, that indicate a stringent mitigation scenario compatible with the 1.5°C Paris Agreement goal to SSP5-8.5 W/m^2 that denote a high emission, fossil-fuel-intensive scenario associated with severe climate warming.

Not all SSP-RCP combinations are physically or politically viable, as some require levels of mitigation that are incompatible with the underlying socioeconomic conditions. For example, a low-emission scenario (SSP1-1.9), which necessitates rapid decarbonization, would not align with SSP5, a world highly dependent on fossil fuels. Conversely, high-emission pathways such as SSP3-7.0 or SSP5-8.5 depict futures where global cooperation on climate policy is weak or non-existent, leading to continued reliance on carbon-intensive energy sources.

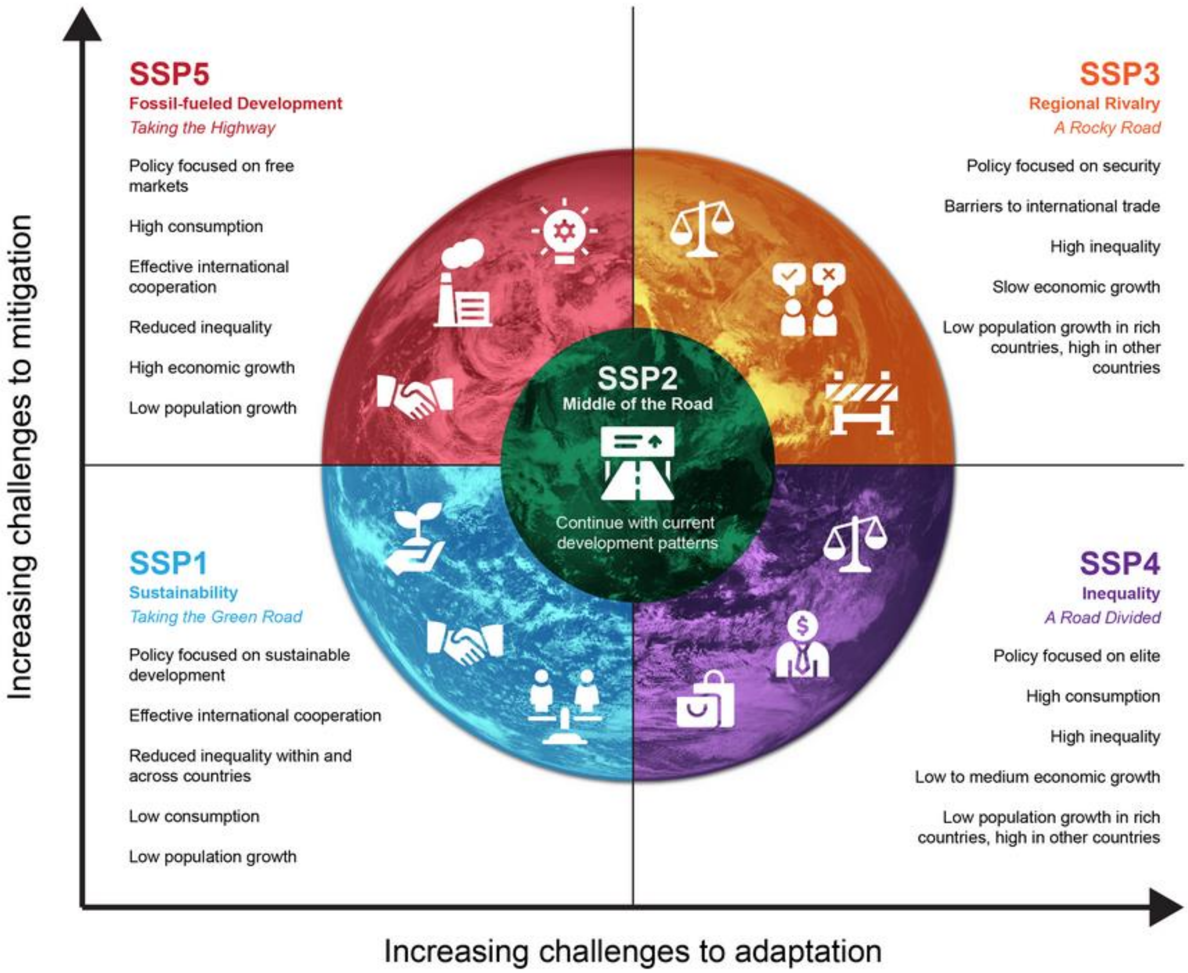

Figure 2.4: All Five Shared Socioeconomic Pathways and the associated challenges to mitigation and adaptation (Carbon Brief 2018)

2.8 CLIMATE MODELLING IN WEST AFRICA AND ITS CHALLENGES

The simulation and prediction of climate variability at regional and local scales remain a significant challenge for climate scientists. The complexity of climate systems arises from intricate interactions between physical processes operating across multiple spatial and temporal scales. These interactions involve the atmosphere, ocean, land, and cryosphere, as well as anthropogenic influences that further modify climate patterns at local scale. Among the most challenging regions to simulate are monsoon-dominated areas such as West Africa because variability in atmospheric circulation, land surface feedbacks, and oceanic conditions drive significant fluctuations in rainfall. Understanding, modelling, and predicting monsoonal behaviour requires an integrated approach that accounts for the dynamic interactions among these components.

GCMs have long served as fundamental tools for studying global climate patterns and their response to external forcings. Because climate systems are governed by physical laws, GCMs can effectively simulate large-scale atmospheric and oceanic circulations, enabling researchers to examine global climate variability and climate change projections. The assessment reports of the Intergovernmental Panel on Climate Change (IPCC 2007, 2013) have relied heavily on GCMs to provide critical insights into future climate scenarios and policy recommendations. However, over West Africa, the use of GCMs has been met with notable challenges, particularly in accurately representing the WAM and its response to global warming. Several studies have used GCMs to investigate the influence of large-scale climatic drivers on West African rainfall variability. For example, Giannini *et al*. (2003) employed an Atmosphere-Ocean General Circulation Model (AOGCM) to explore the links between Sahelian drought and sea surface temperature (SST) anomalies. While such studies have been instrumental in identifying large-scale teleconnections, the coarse spatial resolution of GCMs limits their ability to capture regional and local climate processes (Sylla *et al*., 2010a).

A major drawback of GCMs is their inability to adequately simulate key atmospheric features that regulate West African climate. The AEJ, AEWs, and TEJ are essential components of the WAM system, but they are often poorly represented in GCM simulations (Sylla *et al*., 2009). Moreover, critical land-atmosphere interactions, such as the effects of vegetation cover, soil moisture variations, topography, and dust emissions, are either oversimplified or omitted in GCMs. These deficiencies hinder the accuracy of climate predictions related to monsoon onset, rainfall intensity, and extreme weather events in the region. Given these limitations, researchers have turned to RCMs as an alternative approach to improve the representation of West African climate dynamics.

RCMs provide a higher-resolution framework that allows for a more detailed representation of local climate processes. By dynamically downscaling GCM outputs, RCMs enable the incorporation of finer-scale atmospheric and land surface interactions by offering a more accurate depiction of monsoonal variability. In recent years, the application of RCMs has significantly improved the understanding of WAM dynamics and their interactions with land processes (Afiesimama *et al*., 2006; Pal *et al*., 2007; Diallo *et al*., 2012). Studies using RCMs have provided critical insights into the mechanisms driving WAM variability. For instance, Vizy and Cook (2002) analysed the response of the WAM to oceanic heating patterns, while Jenkins *et al*. (2005) and Sylla *et al*. (2010b) investigated the dominant drivers of Sahelian droughts under both present and future climate conditions. Other researches have examined the impact of land surface changes on regional climate. Abiodun *et al*. (2008) assessed the influence of deforestation and desertification on rainfall variability, while Moufouma-Okia and Rowell (2010) explored how soil moisture initialization affects WAM simulations. The collective findings from these studies demonstrate that RCMs add substantial value to climate modelling by refining the representation of key monsoonal features and improving rainfall projections.

Model evaluation efforts have consistently shown that RCMs outperform their parent GCMs in capturing regional-scale climatic phenomena. The ability of RCMs to better resolve convective systems, land-atmosphere feedbacks, and orographic influences has enhanced confidence in their use for climate risk assessments and early warning systems. Despite these advancements, several challenges persist in the application of RCMs over West Africa. A primary concern is the limited availability of high-quality observational data, which is necessary for model validation and bias correction. Additionally, the computational demands of high-resolution climate simulations present a barrier to widespread implementation particularly in resource-limited regions. Recognizing these challenges, the climate research community has initiated coordinated efforts to improve climate modelling capabilities in West Africa.

Several initiatives have been established to enhance climate simulation and data availability in the region. The West African Monsoon Modelling and Evaluation (WAMME) project (Druyan *et al*., 2010), the African Monsoon Multidisciplinary Analysis (AMMA) (Hourdin *et al*., 2010), and the ensemble-based Precipitations and Their Impacts (ENSEMBLES) project (Paeth *et al*., 2011) have facilitated collaboration among climate scientists to improve monsoon modeling. More recently, the COordinated Regional Downscaling Experiment for Africa (CORDEX-Africa) has implemented ten RCMs over the continent to support climate risk assessment and decision-making (Giorgi *et al*., 2009; Jones *et al*., 2003). Studies have demonstrated that CORDEX models effectively simulate seasonal and annual precipitation cycles in West Africa (Nikulin *et al*., 2012; Hernández-Díaz *et al*., 2013). Given that CORDEX models offer improvements in spatial resolution and process representation over CMIP5 and CMIP6 GCMs, exist is another high spatial resolution and statistically downscaled CMIP6 model name NASA Earth Exchange Global Daily Downscale Projections (NEX-GDDP-CMIP6, Thrasher *et al*., 2022). NEX-GDDP-CMIP6 expected to better reproduce local climate conditions and give robust information about climate change (Sawadogo *et al*., 2024; Dioha *et al*., 2024) at local scale.

2.9 EXTREME EVENTS IDENTIFICATION METHOD

Identification of extreme climate and weather events, such as heatwaves, floods, and droughts is critical for mitigating their impacts on ecosystems, economies and human lives. Various methods have been developed to address this challenge and each with its strengths and limitations. Statistical methods such as Extreme Value Theory (EVT) are widely used due to their simplicity and interpretability. EVT focuses on modelling rare events through approaches like the Block Maxima method that fits a Generalized Extreme Value (GEV) distribution to annual maxima and the Peak Over Threshold (POT) method which uses the Generalized Pareto Distribution (GPD) to model exceedances above a predefined threshold (Coles, 2001; Sanogo *et al*., 2021). Indices-based approaches, such as those developed by the Expert Team on Climate Change Detection and Indices (ETCCDI; Alexander *et al*., 2011) provide standardized metrics like the number of hot days (TX90p) or heavy precipitation days (R95p) that enabling consistent monitoring of extreme events across regions (Zhang *et al*., 2011).

POT method is a widely used statistical approach for identifying extreme climate and weather events, particularly for analysing rare and high-impact phenomena such as heavy rainfall, floods, and extreme temperatures. Unlike the Block Maxima method that focuses on the maximum values within fixed time intervals, the POT method examines all values that exceed a predefined threshold making it more efficient in capturing extreme events that occur irregularly. This method is based on the GPD that models the exceedances above the threshold by providing a flexible framework for estimating the probability and magnitude of extreme events (Smith, 1989). One of the key advantages of the POT method is its ability to utilize more data points as it considers all exceedances rather than just the single maximum value per block, thereby improving the statistical robustness of the analysis (Coles, 2001). However, the choice of threshold is critical; if set too low, the method may include non-extreme events that may lead to biased estimates while a threshold set too high may result in insufficient data for reliable modelling (Pickands, 1975). To address this, various threshold selection techniques such as the Mean Residual Life plot and parameter stability plots have been developed to ensure an appropriate balance between bias and variance (Davison & Smith, 1990). The POT method has been successfully applied in numerous studies, such as estimating extreme rainfall for flood risk assessment and analysing heatwaves for climate impact studies (Katz *et al*., 2002; Beguería and Vicente-Serrano, 2013; Sanogo *et al*., 2021). Despite its strengths, the POT method faces challenges that include the need for independence between exceedances and the potential influence of climate non-stationarity on threshold selection and parameter estimation (Milly *et al*., 2008).

With the rise of big data and computational advancements, machine learning (ML) techniques have become increasingly popular for identifying extreme weather and climate events. Supervised learning algorithms like Support Vector Machines (SVM), Random Forests and Neural Networks have been employed to classify extreme events based on labelled data. For example, SVM has been used to detect tropical cyclones in satellite imagery and Random Forests have been applied to predict extreme rainfall events by analysing atmospheric variables (Knaff *et al*., 2010; Gagne *et al*., 2014). Unsupervised learning techniques such as clustering and anomaly detection are valuable for identifying extreme events without labelled data. Self-Organizing Maps (SOM) have also been used to cluster atmospheric patterns associated with extreme precipitation and anomaly detection methods like Isolation Forests can identify unusual patterns in climate data (Hewitson & Crane, 2002; Liu *et al*., 2008). Deep learning models like Convolutional Neural Networks (CNN) and Recurrent Neural Networks (RNN) have shown promise in detecting extreme weather events. CNNs have been used to identify tropical cyclones and atmospheric rivers in satellite imagery, while RNNs, especially Long Short-Term Memory (LSTM) networks, are effective for modelling time-series data and predicting extreme temperatures and precipitation (Racah *et al*., 2017; Shi *et al*., 2015).

CHAPTER THREE

DATA AND METHODOLOGY

3.1 STUDY AREA

The study focuses on West Africa that broadly lies between longitude 20°W and 20°E and latitude 0°and 20°N as shown in Figure 3.1. However, because of the spatial distribution of available rainfall gauging stations with 80% data record from 1982-2020, intense multi-day events were identified and their characteristics was studied over the blue rectangular box in Figure 3.1(a & b) (longitude 2.5°W - 15°E and latitude 0°and 16°N) region. This region covers Nigeria, Benin, Togo, much of Ghana and Burkina Faso, and parts of southern Niger based on the availability of station data in Karlsruhe African Surface Station Database (KASS-D; Simeon *et al*., 2022 and Vogel *et al*., 2018). The topography in West Africa ranges from coastal lowlands to over 2000 m above mean sea level at the Cameroon Line Mountains, reaching more than 4000 m at the volcano of Mount Cameroon and influencing rainfall distribution (Omotosho and Abiodun, 2007). West Africa is divided into three climatic zones: Guinea Coast (4°–8°N, 20°W–20°E), Savannah (8°–11°N, 20°W–20°E) and Sahel (11°–16°N, 20°W–20°E) based on ecosystems, climate, and land use/land-cover (Omotosho and Abiodun 2007; Abiodun *et al*., 2013). Rainfall is affected by the ITD, which shifts from 22°N in August to 6°N in January/February (Nicholson, 2013). From May to October, the Guinea Coast experiences bimodal rainfall with a little dry season in August, while the Savannah and Sahel have a unimodal pattern peaking in August. Annual rainfall ranges from 1200 mm to 1500 mm at the Guinea Coast, dropping to less than 900 mm in the Sahel (Diallo *et al*., 2016). Variability in rainfall can impact the region's economy and agriculture, making this study crucial for climate change risk management (Sultan *et al*., 2019).

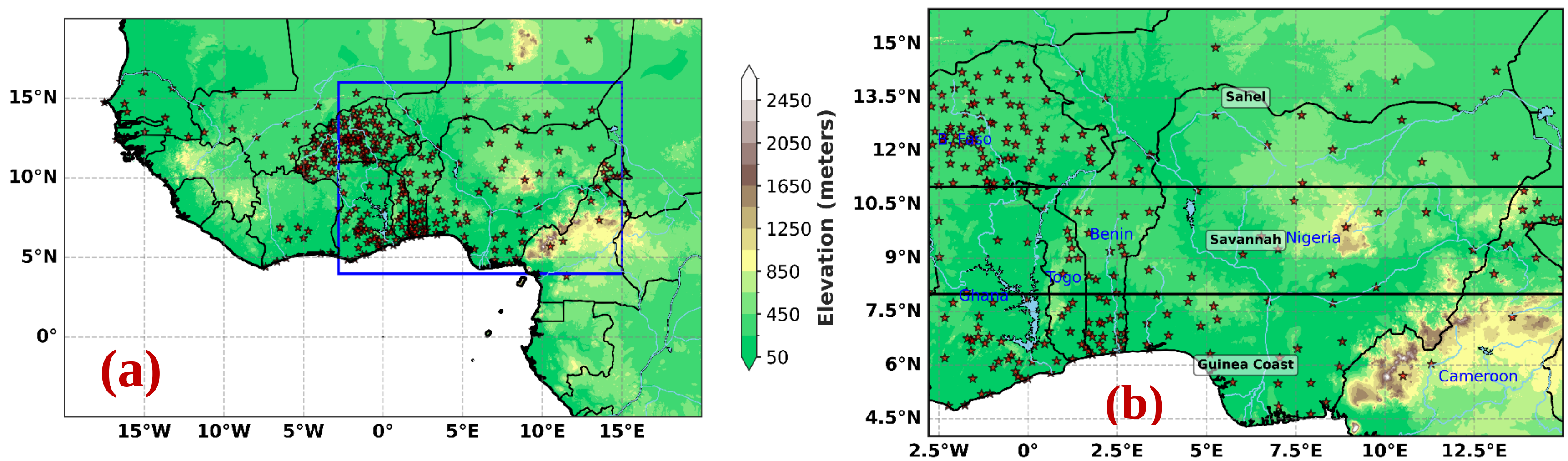

Figure 3.1: The study area map of West Africa (a) with the blue rectangular box showing location of the rain gauge stations and domain used for SPHEREMAP interpolation (b) due to poor spatial distribution of gauging stations west of 3°W.

NOTE: The colour shading shows the elevation from Global Land One-km Base Elevation Project (GLOBE; Hastings *et al*., 1999)

3.2 DATA

3.2.1 Rain Gauge Data and Quality Control Within KASS-D

Despite advancements in satellite rainfall estimation, these products suffer from biases, especially for extreme rainfall events (Ageet *et al*., 2022; Ilori and Balogun, 2021; Adeyewa and Nakamura, 2003). Thus, whenever available, direct station measurements are preferred. In West Africa, meteorological station networks are sparse, and many stations are not reporting to the Global Telecommunication System (GTS). To overcome the data paucity to a great extent, daily rainfall data from KASS-D (Ageet *et al*., 2022; Vogel *et al*., 2018) was used for this study, providing consistent long-term daily rainfall data from 239 stations with at least 80% data coverage from 1982 to 2020. This period includes the novel droughts of the 1980s and the wetter decades of the 1990s and 2000s. Figure 3.1 shows the station spatial distribution.

Rainfall's high spatial and temporal variability complicates automated quality control. Fiebrich and Crawford (2001) established a global range (0–1825 mm) for 1-day accumulated precipitation, which all the selected KASS-D data satisfied. Thereafter, we used two quality control steps: timestamp consistency (Beck *et al*., 2019) and outlier detection through techniques like “letter-value plot” analysis and accumulation curves. All the 239 stations with over 80% data availability used in this study passed this quality control check.

3.2.2 Gridded Reanalysis and Satellite Rainfall Products

Consolidating on the results from existing literature (Gbode *et al*., 2022; Odoulami and Akinsanola, 2017) over West Africa, three additional gridded rainfall products were added to KASS-D to increase the robustness of the analysis and results. Global Precipitation Climatology Center (GPCC) version 2022 that is available at 1° resolution (Schamm *et al*., 2015; Becker *et al*. 2013); Climate Hazards Group InfraRed Precipitation with Station data version 2 (CHIRPS v2;

CHIRPS hereinafter), a 0.25° horizontal resolution of merged satellite and rain gauge precipitation estimate available from 1981 to near-present (Funk *et al*., 2015) and Integrated Multi-satellite Retrieval for Global Precipitation Measurement (IMERG) for Global Precipitation Measurement (GPM) version 07 dataset (IMERG hereinafter; Huffman *et al*., 2020).

GPCC data provides 1° resolution global daily rainfall amount over the land-surface on a rectilinear grid with temporal resolution ranging from January 1982 to near-real-time (NRT). GPCC rainfall data are based on rainfall measurements provided by national meteorological and hydrological services, global and regional data collections as well as World Meteorological organization (WMO) GTS data base. All these irregular spaced rainfall measurements are interpolated to regular grid using modified SPHEREMAP interpolation method described by Becker *et al*., 2013 and Schamm *et al*., 2014.

According to Funk *et al*. 2015, CHIRPS, a dataset with quasi-global coverage offers rainfall estimates on a daily, five-day (pentad), and monthly basis. It is constructed from a global monthly precipitation climatology (CHPclim), thermal infrared (TIR) cold cloud duration (CCD), and daily and monthly rain gauge (RG) data. TIR CCD dataset at a consistent temperature threshold of 235 K, are locally calibrated using TMPA 3B42 five-day precipitation data. These five-day estimates are then multiplied by their corresponding CHPclim estimates to generate Climate Hazard Infrared Precipitation (CHIRP). CHIRP is then combined with RG data to create CHIRPS at five-day and monthly intervals. The five-day rainfall estimates in CHIRPS is further broken down into daily CHIRPS rainfall amount using daily CCD data. TRMM 3B42 improves the accuracy of CHIRPS through bias correction, improved detection of rainfall events, and better temporal consistency, especially in regions with sparse rain gauge coverage like West Africa. CHIRPS calibration process helps in reducing errors associated with satellite-based infrared (IR) precipitation estimates and ensuring a more reliable rainfall dataset for climate monitoring. However, with these improvements, CHIRPS has known limitations when applied to areas with complex topography and microclimates like West Africa. It has the tendency to underestimate orographic rainfall and may inadequately capture localized convective storms that are common in tropical and semi-arid regions because of its reliance on cloud-top temperature. These can lead to biases in highland areas and the Sahel region of West Africa.

IMERG gives global surface precipitation rate estimates at 0.1° every 30 minutes, with three Runs for different latency needs. This latest version reprocesses the entire record of over 20 years from the TRMM and GPM projects uniformly. Huffman *et al*. (2020) provides extensive details about IMERG. Tan *et al*. (2022) explain the main differences between IMERG-V06 and IMERG-V07 and demonstrate the improvements in the latest version. A notable problem with IMERG V06 was the satellite-only precipitation estimates being too high, especially in the TRMM era, which was fixed. Moreover, IMERG's Kalman filter was changed to enhance the distribution of precipitation rate estimates and reduce the discrepancies caused by using various types of sensors. Other modifications in V07 are a change in the motion vector source to fix the issues in the precipitation movement near mountains (orography adjustment), an improved infrared precipitation algorithm, a revision of the precipitation phase parametrization for better consistency, and a new attempt to apply climatological gauge adjustment to the near-real-time Runs

Despite the limitation associated with satellite and reanalysis rainfall products, GPCC, CHIRPS and IMERG have been used as observation datasets to evaluate climate models (Bobde *et al*., 2024; Maranan *et al*., 2020; Gosset *et al*., 2018; Casse *et al*., 2015; Roc *et al*., 2010) to study different aspects of rainfall over West Africa (Rauch *et al*., 2025) and they give reliable results. Compared to IMERG that offers global coverage and higher temporal resolution (30 minutes), CHIRPS outmatch in long-term historical consistency (1981- near time) but may lack real-time accuracy shown by IMERG. Also, Precipitation Estimation from Remotely Sensed Information using Artificial Neural Networks (PERSIANN) for example, relies more heavily on satellite algorithms, making it less reliable in areas with limited ground validation like West Africa. ERA5 (Hersbach *et al*., 2020) rainfall reanalysis product provides comprehensive global data but may smooth out extreme events due to its model-based approach. CHIRPS and IMERG integration of station data coupled with very high spatial resolution improves the accuracy in estimating rainfall at local scale (Katsekpor *et al*., 2024).

3.2.3 Gridded Surface and Upper-Level Reanalysis Data

To investigate environmental factors responsible for the evolution and sustenance of intense multiday wet spells, Vertically Integrated Divergence of Moisture Flux (VIDMF), Total Column Vertically-Integral Water Vapor (TCWV), Convective Available Potential Energy (CAPE), Convective Inhibition (CIN), Vertical Integral of Eastward Water Vapor (VIEWV) and Vertical Integral of Northward Water Vapor (VINWV) variable from ERA5 (Hersbach *et al*., 2020) were used to investigate dynamical configuration associated with intense multi-day wet spells. VIDMF depicts the net transport of moisture through the column of air extending from the surface of the earth to the top of the atmosphere. Positive (Negative) values of VIDMF indicate moisture diverging (converging) that shows whether atmospheric motions act to decrease for divergence (increase for convergence) the vertical integral of moisture. TCWV refers to the total amount of water vapor present in a vertical column of air from the surface to the top of the atmosphere. TCWV provides information on the total amount of water vapor while VIDMF provides information on the movement of moisture into or out of a region. VIEWV (VINWV) represent the horizontal rate of flow of air mass in the eastward (northward) direction for a column of air extending from the surface of the earth to the top of the atmosphere. Positive values of VIEWV and VINWV depicts flux from west to east and south to north, respectively. These two variables can be used to investigate atmospheric energy budget. CAPE gives an indication of atmospheric stability or instability that can be used to examine the potential for the development of convection that can lead to heavy rainfall and severe weather. Lager positive values of CAPE are indicated that an air parcel would be warmer that its environment, meaning very buoyant in the thunderstorm environments. CAPE with values higher than 1000 Jkg-1 is considered suitable for rainfall development while value greater than 5000 Jkg-1 is associated with extreme events. CIN measures the amount of energy required for the initiation of convection. A very high value of CIN shows that moist deep convection is unlikely to occur even if CAPE-shear or CAPE are large. A CIN value greater than 200 Jkg-1 is considered a high value.

In addition, zonal wind (u-wind), meridional wind (v-wind), vertical velocity (omega), divergence of wind, specific humidity and relative vorticity variables at 27 pressure levels (1000 – 100 hPa) were used in this study. All these variables were used to assess the atmospheric configuration for the evolution and sustenance of intense multi-day wet spells over West Africa.

3.2.4 Climate Model Data

In this study, after rigid evaluation and the results shown in chapter 4, we used the ensemble mean (hereafter EnsMean) of daily rainfall simulated by 23 NEX-GDDP-CMIP6 models to examine the impact of global warming on the projected characteristics of rainfall and its extremes in West Africa and its sub-regions. The ensemble mean approach adopted enhances climate projections by reducing biases, improving accuracy, and enabling probabilistic forecasting. By averaging multiple models, it mitigates individual model errors, yielding more reliable long-term projections (Weigel *et al*., 2010). This method outperforms individual models by leveraging collective strengths while minimizing structural uncertainties. Studies have shown that multi-model EnsMean offer superior performance, with added values achievable through optimized weighting, making them essential for climate research and policy planning (Weigel *et al*., 2010).

The NEX-GDDP-CMIP6 dataset offers global climate scenarios that have been downscaled from GCM runs conducted as part of the CMIP6 experiments (Eyring *et al*. 2016). These scenarios are generated using two of the four primary GHG emission scenarios, known as shared socioeconomic pathways (SSPs; Meinshausen *et al*., 2020) that was developed to support the IPCC's Sixth Assessment Report (AR6). The dataset includes downscaled projections from ScenarioMIP model runs (Tebaldi *et al*., 2021). It is designed to provide bias-corrected climate projections at high resolution that is crucial for analyzing the impacts of climate change on small-scale processes that require fine-scale climate details and local topography. To overcome the identified limitations and biases in native CMIP6 models, the bias-correction spatial disaggregation (BCSD; Wood *et al*., 2002) method was used to create the NEX-GDDP-CMIP6 dataset (Thrasher *et al*., 2012). This is a statistically downscaling algorithm designed to address the limitations in GCM outputs. It compares GCMS with climate observations over a common period and then adjusting future projections based on the information derived to be more consistent with historical climate records. This process ensures that the projections are more realistic for specific spatial domains. Additionally, the BCSD method uses detailed observational datasets to interpolate GCM outputs onto higher-resolution grids to produce more accurate spatial detail (Thrasher *et al*., 2022) compared to native CMIP6.

Like CMIP6, NEX-GDDP-CMIP6 has five shared socioeconomic pathway (SSP) scenarios representing different trajectories of GHG concentrations in the atmosphere and socioeconomic developments (see Eyring *et al*., 2016). Two of these five SSPs were used in this study, namely, SSP245 and SSP585, which are regarded as inequality and fossil-fuelled development, respectively. The selection of SSP2-4.5 and SSP5-8.5 provides a balanced assessment of impacts of climate change that captures both realistic and worst-case scenarios. SSP2-4.5 represent stabilization of emissions that aligned with current policy trends, thereby, making it useful for moderate climate impact assessments. SSP5-8.5, a fossil fuel-intensive pathway, serves as an upper bound for investigating climate extreme risks such as flooding and droughts. These two climate scenarios are useful in climate change risk-based decision-making by helping policymakers to plan adaptation and infrastructure resilience. Other SSPs, such as SSP1-2.6 and SSP3-7.0, can be regarded as either too optimistic or highly uncertain. Hence, using SSP2-4.5 and SSP5-8.5 enables robust climate projections, informing mitigation strategies and disaster preparedness across these selected realistic emission trajectories.

NEX-GDDP-CMIP6 datasets used in this study covers both historical (1981-2014) and future periods (2071 - 2100). This is like what was defined in the IPCC sixth assessment report (IPCC 2023). The historical period was used to evaluate the performance of each NEX-GDDP-CMIP6 and EnsMean datasets in replicating rainfall, whereas the future period is used to examine the projected changes in annual extreme rainfall characteristics across the study region. A list of all the model outputs used to compute the EnsMean can be found in Table 3.1.

3.3 METHODOLOGY

The main characteristics of intense or extreme events are frequency, duration, intensity, severity and spatial extent. In a preliminary analysis we performed using irregularly spaced KASS-D rainfall data, we observed the need to interpolate the daily rainfall data of 239 stations from KASS-D to regular grid of 1° latitude by 1° longitude because of inability of unstructured KASS-D to adequately capture spatial extent of an intense multi-day wet spells. For an example, an intense multi-day wet spell identified using unstructured KASS-D dataset show 35 stations having 3-day and 5-day accumulated rainfall amount exceeding a particular threshold clustered around a region. These stations fall within 4 to 6 grid cells in 1° by 1° resolution. This showed the need to interpolate irregular spaced KASS-D dataset to regular and common grid of 1° by 1° as GPCC.

3.3.1 Interpolation and Regridding Method

After all the rainfall gauging stations selected from the KASS-D database exhibited 80% data coverage in the study period and passed the quality control check, they were interpolated to a 1° by 1° regular grid size using SPHEREMAP (Willmott *et al*., 1985) interpolation method. SPHEREMAP is the original method that adapts Shepard's inverse distance weighting (Shepard, 1968) to spherical coordinates, which is a variation of the Inverse Distance Weighting (IDW) scheme mentioned earlier. As it is with IDW, interpolation weights decrease as the distance between the grid center (i.e., grid node) and meteorological station increases. Moreover, the interpolation accounts for the clustering of stations, i.e., the available number of gauging stations and the distance between them, so the weights of stations that are close together were lowered to avoid overemphasizing these stations' data. Detailed information can be obtained from Willmott *et al*. (1985) and Becker *et al*. (2013). This interpolation method has been used by Nguyen-Xuan *et al*. (2016) and Thiemig *et al*. (2021). GPCC modified this interpolation method for regions in the world with dense data coverage but at the same time relaxing it to SPHEREMAP method in data-sparse areas, like West Africa.

In the application of the SPHEREMAP interpolation method, the relative rainfall anomaly defined as the ratio of daily rainfall to the corresponding monthly total was used instead of the absolute anomaly of daily values. After the interpolation, the resulting gridded relative anomalies were multiplied by the gridded monthly totals to derive the final gridded daily rainfall amounts. This procedure is known as Climatology Aided Interpolation (CAI; Willmott and Robeson, 1995, Schamm *et al*., 2014) and is currently used by GPCC (Becker *et al*., 2013). It has the advantage of adding climatological data to increase the precision of spatial detail while still producing a daily product (Parmentier *et al*., 2015). In the configuration of the SPHEREMAP used in this study, at a particular grid node, the minimum and maximum number of neighboring stations required to interpolate station measurements to a regular grid are 4 and 10, respectively. The grid cell size is 1.0° while the grid nodes/points are the same as that of GPCC. Weighting method used by Willmott *et al*. (1985) was retained and used as described by Shepard (1968) to determine the initial search radius to locate the nearest stations.

3.3.2 Evaluation of Interpolated KASS-D and Climate Model Data

The performance of SPHEREMAP configuration used was compared with the spatial distribution of the test dataset provided by GPCC for a year (1988). For wet days only with at least daily rainfall amount of 1.0 mm, Quantile-Quantile (Q-Q) plots was used to compare the distribution of wet days in GPCC, CHIRPS, and IMERG to interpolated KASS-D at selected pixels based on the number of stations within KASS-D grid cells by using the combination of axes alphabet and number labelling.

Furthermore, CHIRPS and IMERG datasets were remapped to a common grid of 1° by 1° to match that of GPCC and interpolated KASS-D using the first-order conservative regridding method of Jones (1999). Furthermore, for both interpolated KASS-D and climate model (individual model and EnsMean) datasets, dichotomous metrics (Ageet *et al*. 2021; Wilks 2011; Ebert 2007), namely; the Heidke skill score (HSS), bias in detection (BID), probability of false alarm (POFA), and probability of detection (POD), were used to examine the tendency of all these datasets to accurately replicate rainy days using a daily rainfall amount of 1.0 mm as the threshold and contingency table in Table 3.1. In computing the dichotomous metrics using Table 3.1 at a daily timescale and for each dataset, a hit (H) occurs if both GPCC and the dataset being evaluated have daily rainfall amount higher than 1.0 mm threshold. Similarly, a False (F) alarm occurred when dataset being evaluated have daily rainfall amount greater than 1.0 mm but GPCC has less than 1.0 mm. In addition to the dichotomous metrics, the mean error (ME), mean absolute error (MAE), root-mean-square error (RMSE) correlation (*r*), and probability of bias (PB) were used to assess accuracy of each dataset in simulating rainfall amount using the hit subset at a daily time scale. Equations 3.1 - 3.9 and Table 3.2 provides detailed information about all these metrics. The same evaluation metrics was also computed between interpolated KASS-D and direct rainfall measurement average over the three climatic zones.

$$HSS = \frac{2(HR - FM)}{(H + M)(M + R) + (H + F)(F + R)} \tag{3.1}$$

$$BID = \frac{H + F}{H + M} \tag{3.2}$$

$$POFA = \frac{F}{H + F} \tag{3.3}$$

$$POD = \frac{H}{H + M} \tag{3.4}$$

$$ME = \frac{1}{n}\sum_{i}^{n} M_i - O_i \tag{3.5}$$

$$MAE = \frac{1}{n}\sum_{i}^{n} |M_i - O_i| \tag{3.6}$$

$$RMSE = \sqrt{\frac{i}{n}\sum_{i}^{n}(M_i - O_i)^2} \tag{3.7}$$

$$r = \frac{\sum_i^n (O_i - \bar{O}_i)\ \sum_i^n (M_i - \bar{M}_i)}{\sqrt{\sum_i^n (O_i - \bar{O}_i)^2}\ \sqrt{\sum_i^n (M_i - \bar{M}_i)^2}} \tag{3.8}$$

$$PB = \frac{\frac{1}{n}\sum_i^n (M_i - O_i)}{\bar{O}} \times 100 \tag{3.9}$$

where O_i, M_i, $\bar{O}_{i,}$ and $\bar{M}_i$ represent the observed total rainfall, total rainfall being evaluated, observed mean total rainfall, and mean total rainfall being evaluated, respectively.

Table 3.1: **Contingency table used for comparing rainy days in the CHIRPS observations and the NEX-GDDP-CMIP6 simulated daily rainfall. A day is considered a wet day if the daily rainfall amount is greater than 1.0 mm.**

	GPCC ≥ 1.0 mm	**GPCC < 1.0 mm**
Dataset being evaluated ≥ 1.0 mm	Hit (H)	False Alarm (F)
Dataset being evaluated < 1.0 mm	Miss (M)	Correct Rejection (R)

Table 3.2: Description and range [possible best score] of each statistic used in evaluating each dataset in replicating (for interpolated KASS-D) or simulating (for climate models) rainy days and their rainfall amount.

Metrics [unit]	Range [best possible score]	Description
HSS	-∞ to 1 [1]	Examine the skill of the GCMs compared to random chance
BID	-∞ to +∞ [1]	Assess the tendency of GCMs to overestimate or underestimate the frequency of rainy day
POFA	0 to 1 [0]	Gives the proportion of rainy days in the GCM that were not in observation
POD	0 to 1 [1]	Measured the ability of the GCMs to correctly identify rainy days
ME [mm]	-∞ to +∞ [0]	Measures the error (bias) and its direction
MAE [mm]	0 to +∞ [0]	Measures the error (bias) irrespective of the direction
RMSE [mm]	0 to +∞ [0]	Measures the error of the GCMs while assigning more weight to outliers
r	-1 to 1 [1]	Examines the covariance of the observation with that of the GCMs
PB [%]	-∞ to +∞ [0]	Assesses the likelihood of the GCMs to underestimate or overestimate rain rates relative to the mean of the observation

3.3.3 Intense Multi-Day Wet Spell Definition and Identification

A wet spell is a consecutive period of days with daily rainfall greater than or equal to a threshold. In this study, we define wet days as having at least 1.0 mm of rainfall and focus on intense 3-day and 5-day events for each grid cell after assessing local features associated with wet and dry spells. This threshold was chosen to conform with the threshold used to defined wet days in ETCCDI extreme indices calculation (Alexander *et al*., 2019; Froidurot and Diedhiou, 2017). To identify these 3-day and 5-day intense events, we apply the following conditions:

i. 3-day intense events: A 3-day rolling accumulation with at least two wet days.

ii. 5-day intense events: A 5-day rolling accumulation with at least three wet days and no consecutive two dry days.

Thereafter, a spatially varying threshold of the 90th percentile rainfall amount for 3-day and 5-day accumulation periods from 1982 to 2020 (KASS-D, GPCC, CHIRPS) and 2001 to 2020 (IMERG; because of its shorter period of availability) was computed. Intense wet spells are defined as days when the accumulation exceeds the 90th percentile values for 3-day and 5-day periods at each grid point in each dataset and the last day of the wet spell is used as the timestamp.

Mathematically:

Let $R_t(x, y)$ denote the daily rainfall amount at time t and spatial location (x, y). A wet day is defined as any day for which:

$$R_t(x, y) \geq R_{min}$$

where $R_{min} = 1.0\ mm$ is the wet day threshold. The binary wet day indicator function is defined as:

$$W_t(x,y) = \begin{cases} 1, & if\ R_t(x,y) \geq R_{min} \\ 0, & otherwise \end{cases} \tag{3.10}$$

To identify periods of sustained wet conditions, defined is n-day rolling rainfall accumulation as:

$$A_t^{(n)}(x,y) = \sum_{i=t}^{t+n-1} R_i(x,y) \tag{3.11}$$

Where $n \in \{3, 5\}$.

A 3-day event is classified for a given window [*t*, *t + 1*, *t+2*] if:

$$\sum_{i=t}^{t+2} W_i(x,y) \geq 2 \tag{3.12}$$

Similarly, a 5-day event in the interval [*t*, *t+4*] is considered intense if the following two conditions are jointly satisfied:

$$\left(\sum_{i=t}^{t+4} W_i \geq 3\right) AND\ (W_i + W_{i+1} \geq 1\ \forall i \in \{t, t+1, t+1, t+3, t+4\}) \tag{3.13}$$

ensuring that the window contains at least three wet days and no consecutive dry days.

To select intense 3-day and 5-day wet spells, a spatially varying threshold is computed based on the 90th percentile of historical *n-day* accumulations during the baseline reference periods: 1982–2020 for KASS-D, GPCC, and CHIRPS datasets, IMERG (2001 - 2020) and EnsMean (2071 - 2100)

Let $Q_{90}^{(n)}(x,y)$ denote the 90th percentile of $A_t^{(n)}(x,y)$ over the respective baseline periods:

$$Q_{90}^{(n)}(x,y) = P_{90}\left(A_t^{(n)}(x,y)\right) \tag{3.14}$$

A multi-day wet spell is thus defined as intense extreme when the rolling accumulation exceeds the 90th percentile threshold:

$$A_t^{(n)}(x,y) \; > \; Q_{90}^{(n)}(x,y) \tag{3.15}$$

3.3.4 Intense Multi-Day Wet Spell Characteristics and Trend Analysis

This study focuses on the frequency, exceedance, and spatial coverage of intense multi-day wet spells. For frequency, number of days per month when 3-day and 5-day accumulation amounts exceed their 90th percentile at each 1° x 1° grid point was counted, averaging these counts over the Guinea Coast (4°–8°N), Savannah (8°–11°N), and Sahel (11°–15°N) to provide a seasonal representation (Roxy *et al*., 2017; Rantan and Venugopal, 2013). Monthly counts of intense multi-day wet spells were aggregated into annual totals. The spatial coverage (size) of intense events was assessed by counting grid cells exceeding the threshold on a given day and classifying them as small (1-9 cells), mid-size (10-20 cells), or large (>20 cells). Exceedance amount (intensity) was then computed as the difference between the 90th percentile value and the actual accumulation.

The average size of intense 3-day and 5-day events in a year was then computed using equation 3:16:

$$Average\ size = \frac{T_{gc}}{Total\ Number\ of\ Events\ in\ a\ Year} \tag{3.16}$$

where T_{gc} is the annual aggregate of number of grid cells per event having a 3-day/5-day accumulation amount greater than 90th percentile value. In addition, the annual maximum size of intense 3-day and 5-day events that occurred in each year was also identified and subjected to analysis.

Frequency, average and maximum size, and various sizes of 3-day and 5-day intense wet spells for the historical period were subjected to trend analysis. These mentioned characteristics for the future periods were also subjected to spatiotemporal and trend analyses relative to the historical mean in the long-term periods under SSP2-4.5 and SSP5-8.5. for these NEX-GDDP-CMIP6 dataset, at every grid point over West Africa and average over the climatic zones, a non-parametric Mann-Kendall (MK; Mann, 1945; Kendall, 1975; Taylor (2001); Wang *et al*., 2005) trend test was applied to examine the presence of statistically significant trends in the characteristics of intense multi-day wet spells at annual time scale. The MK test is useful for identifying monotonic trends in climate data because it does not depend on the distribution of the data, and it is less sensitive to outliers and non-normality. This makes it particularly useful for analysing rainfall extremes. This was test performed at a 0.05 significance level that corresponds to a 95% confidence level. The significance of the trend is determined by calculating the Kendall's tau correlation coefficient. This measures the strength and direction of the trend with the test statistic computed based on the number of concordant and discordant pairs in the time series. To ensure robustness in the result, the variance of test statistic is adjusted for tied ranks. To determine the statistical significance, the standardized Z-score of the MK test was then compared against the critical value from the standard normal distribution. Thereafter, if the absolute value of Z exceeds the critical threshold (± 1.96 at $\alpha = 0.05$), the trend is regarded statistically significant. Also, we estimate Sen's slope (Sen, 1968) to determine the magnitude and direction of detected trends while the 95% confidence intervals were calculated using a rank-based method.

3.3.5 Composite Analysis

Climatological description of all the variables for both vertically integrated and upper levels during the summer monsoon (July-August-September) was examined. Thereafter, all the 3-day and 5-day intense multi-day wet spells identified using the conditions highlighted in section 3.4 were subjected to composite analysis. Composite analysis was used to assess how the large-scale features vary for the two intense multi-day wet spells. Composite analysis has the advantages over individual event studies because compositing emphasizes commonly occurring features for all the multi-day intense events identified while smoothing out more random fluctuations. Composite analysis is also better than correlation because it allows the study of non-linearity. This was done for a day before (lead), during and a day after (lag) the intense multi-day events to investigate the time evolution and sustenance of all environmental factors of these events. For a 3-day intense events in particular, a composite analysis is performed for lead and lag days, i.e., a day prior (3T - 1) to two days after (3T + 2) the end of 3-day intense events (3T3). This is also true for 5-day intense events, a day prior (5T - 1) to a day (5T + 1) after the end (5T5) of 5-day intense events. Thereafter, a typical 3-day and 5-day intense events was further investigated.

3.3.6 Impact of Warming Climate on the Occurrence and Characteristics of Intense Multi Day Wet Spells Under Different Shared Socio-Economic Pathway

To assess impact of warming climate on the characteristics of intense multi-day wet spells, a hypothetical question was developed: "what will change in the characteristics of intense multi-day wet spells in the current time if the rainfall distribution of current times would attain the distribution of the projected future state?". To answer this question, Q-Q mapping was used to project rainfall from the KASS-D, GPCC and CHIRPS observation datasets into the long-term future (2071-2100) under SSP2-4.5 and SSP5-8.5 adopting the approach of Chapman *et al*. (2023) and Fontolan *et al*. (2019). This method compares daily rainfall amounts from the observation with the corresponding estimates from the climate models. Although it is expected that the adjusted observations do not represent true daily values compared to the observations, it has been argued that the adjusted observation change in daily rainfall and extremes may still be robust (Fowler *et al*. 2010, Chapman *et al*. 2023). Under this assumption, multiplicative factor calculated as future climate change was applied to the rainfall amount from the observations:

$$\beta_{observed\,projection} = \beta_{observed\,historical} \times \beta_{pc} \tag{3.19}$$

where β represents daily rainfall estimate and β_{pc} is the change in the corresponding daily rainfall from the EnsMean, defined as

$$\beta_{pc} = \frac{\beta_{climate\,model\,future}}{\beta_{climate\,model\,historical}} \tag{3.20}$$

CHAPTER FOUR

RESULTS AND DISCUSSION

4.1 COMPARISON BETWEEN STATION, INTERPOLATED AND SATELLITE RAINFALL PRODUCTS

This section presents and discusses the result of the evaluation between in-situ, interpolated and other rainfall datasets used in this study. This includes KASS-D (239-gauge stations, SPHEREMAP-interpolated to 1°x1°), GPCC (gauge-based, 1°), CHIRPS (satellite-gauge blend, 0.25°, regridded to 1°), and IMERG (satellite-gauge blend, 0.1°, regridded to 1°, 2001–2020). See Section 3.2 for details on data sources, interpolation, and limitations, including CHIRPS's underestimation of orographic rainfall and IMERG's limited temporal coverage. The purpose of this evaluation and comparison study is to quantify the performance of the interpolated KASS-D against direct rainfall measurements and other rainfall products. This was done at daily, seasonal and annual time scales averaged over the whole blue rectangular box [longitude 2.5°W - 15°E and latitude 0°and 16°N; Figure 3:1 (a & b)] that depicts interpolation domain due to KASS-D station availability, the three climatic zones and at selected pixels based on the number of stations within KASS-D grid cells by using the combination of axes alphabet and number labelling.

Daily Rainfall and Statistical Evaluation

Rainfall is a critical climatic parameter for assessing climate change and variability, especially in West Africa, where it exhibits a complex and heterogeneous structure across various spatio-temporal scales. This heterogenous nature of rainfall is one of the major sources of biases in satellite or gauge-based rainfall products in addition to sparse network of rain-gauge observation (Ilori and Balogun 2021; Ageet *et al.*, 2022). The weakness of these alternative rainfall products in capturing the spatio-temporal variation in rainfall necessitate the continuous evaluation of any rainfall products before its application in extreme events study (Ilori and Balogun, 2021).

Figures 4.1 and 4.2 compare the time-series of daily rainfall of direct gauge measurements (hereafter referred to as in-situ), interpolated rainfall data from KASS-D (hereafter, KASS-D) and GPCC from January to December of 1983 and 2012 for four selected stations (Ouagadougou, Jos, Parakou and Port Harcourt) respectively. These stations are in the Sahel, highland area, inland of Guinea Coast and the far coastal edge. Compared to the rain-gauge-based dataset (GPCC) and direct measurements, KASS-D captures day-to-day variations in rainfall over the four stations, albeit with instances of overestimation and underestimation on different dates.

In 1983 in particular, KASS-D estimated a maximum daily rainfall of less than 60 mm in Ouagadougou towards the end of July, whereas the gauge measurement (in situ) recorded around 75 mm. In contrast, GPCC recorded 40 mm around mid-August. However, in Parakou, KASS-D estimated a higher daily rainfall amount of approximately 85 mm, surpassing GPCC's 70 mm and the in-situ measurement. At the Jos and Port Harcourt stations, the in-situ measurements showed higher maximum daily rainfall amounts in 1983 compared to KASS-D and GPCC. Similar patterns of underestimation and overestimation were observed in both 1983 and 2012 across all datasets and stations.

Despite these discrepancies, the datasets showed consistency in capturing the onset (rainfall amount greater than 0) and cessation of rainfall (amount less than 0) for each station. For example, in Jos, all datasets recorded the onset of consistent rainfall in April. Additionally, all datasets captured rainfall throughout 2012 over Port Harcourt, highlighting their agreement on broader rainfall patterns. Spatial distribution of daily rainfall amount at 1° by 1° resolution for KASS-D and GPCC on 2018-09-09 (Figure 4.3) and 2009-09-02 (Figure 4.4) underscores the importance of sufficient number rain-gauge per grid cells to create rainfall dataset. On 2018-09-09, due to the higher number of underlying gauging stations, larger areas experienced higher rainfall amounts especially, over Nigeria compared to GPCC. On 2009-09-02 on the other hand, the higher amount of 225 mm recorded in Burkina Faso by GPCC is reduced in KASS-D (Figure 4.4). This can be associated with the higher number of underlying gauging stations in KASS-D used to interpolate rainfall for this grid cell and the distance between them to the grid node.

Figure 4.5 shows Q-Q diagrams comparing daily precipitation values between interpolated KASS-D (x-axis) and GPCC (blue curve), IMERG-V7 (green curve), and CHIRPS (red curve) datasets. The Q-Q plots are examples for nine different pixels with varying numbers of stations within the pixel in KASS-D (Figure 3.2a). Points above the diagonal line indicate overestimation, while points below indicate underestimation compared to KASS-D. CHIRPS consistently overestimates lower quantile values and underestimates upper quantile values. GPCC generally has higher values in the upper quantiles and is in close agreement with KASS-D in the lower quantiles. However, in grid cell ‘5I[0]’ without gauging stations, GPCC and IMERG show similar distributions close to KASS-D because IMERG is calibrated with GPCC. In the upper quantile, IMERG's higher quantile values are closer to that of KASS-D but less than GPCC's values in most pixels.

To further verify the SPHEREMAP configuration used, Figure 4.6 compares wet days' rainfall amounts from interpolated KASS-D to the arithmetic mean of stations within the same pixel using Q-Q plots, except for pixel ‘5I’ (without stations) replaced by pixel ‘3F’. In pixels with 1-4 gauging stations, the arithmetic mean closely aligns with the ideal line, indicating values close to KASS-D. Underestimation occurred in pixels with more than four stations compared to KASS-D, likely due to SPHEREMAP weighting method, influence of neighboring stations and station with extremely low values, resulting in lower quantiles. SPHEREMAP performs similarly to the arithmetic mean in pixels with fewer stations. Similar comparisons of GPCC, CHIRPS, and IMERG to interpolated observation data have been reported by Ageet *et al*. (2022) and Sanogo *et al*. (2022), they noted underestimation and overestimation of upper and lower quantile values, respectively, by CHIRPS in different parts of Africa.

The differences in the wet day's rainfall amount between KASS-D, GPCC, and the arithmetic of stations can be linked to the difference in the number of gauging stations per pixel used during interpolation, the percentage of available data, different QC method, the distance of each gauging station to the grid nodes that determined their weight and/or the search radius used. Also, CHIRPS and IMERG are gauge-satellite blended data sets, whereas KASS-D and GPCC are gauge only.

Averaged over the whole domain, Guinea Coast, Savannah and the Sahel climatic zones used for the interpolation, KASS-D revealed good agreement with gauge based only GPCC for either wet days only or both wet and dry days (Figures 4.7 & 4.8). For wet days only, the highest RMSE and bias value recorded between KASS-D and GPCC occurred in the Guinea Coast while the lowest occurred in the Sahel (Figure 4.7). Likewise, very similar results were also obtained in all the climatic zones for both wet and dry days (Figure 4.8). Furthermore, the capability of all the datasets to accurately reproduce rainy days as in-situ (gauge measurement) is shown in Table 4.1. KASS-D has the highest POD (probability of detection) values that range between 0.59 and 0.42 and lowest POFA (probability of false alarm) values between 0.28 and 0.13 across the three climatic zones. This POD value is higher than HSS in all the climatic zones. However, the POD of GPCC is lower than KASS-D values but higher than CHIRPS in all the climatic zones. CHIRPS have the highest POFA in all climatic zones. These show that KASS-D replicate wet days with higher degree of accuracy compared to GPCC and CHIRPS. This can be attributed to underlying number of gauging stations used compared to GPCC and the algorithm used in creating CHIRPS dataset which combine global monthly precipitation climatology, thermal infrared cold cloud duration, and daily and monthly rain gauge data. For the daily rainfall amount, low correlation value (*r*) depicts low level of agreement between direct gauge measurement and each of the other rainfall products (KASS-D, GPCC and CHIRPS). In all the climatic zones, KASS-D consistently show higher correlation value compared to GPCC and CHIRP. KASS-D, GPCC and CHIRPS underestimate daily rainfall amount in all the climatic zones as depicted by negative ME values. This is further confirmed by RMSE higher rainfall amount on the order between 20.09 - 19.59 for KASS-D, 22.64 - 21.16 for GPCC and 20.08 – 19.95 for CHIRPS. However, KASS-D consistently outperformed other rainfall products in replicating rainfall amounts and detecting rainy days overestimated by different evaluation metrics.

Seasonal and Inter-Annual Variation

On a seasonal scale, KASS-D replicates the northward variation of mean seasonal rainfall as shown by gauge measurements with highest monthly rainfall amount over the coastal region of Guinea Coast and Niger-Delta region (Figure 4.9). KASS-D further captures the highest seasonal rainfall in the peak of monsoon season (June-July-August) as seen in the in-situ dataset.

Figures 4.10 and 4.11 depict Standardized Rainfall Anomaly Index (SRAI) used to examine the ability of KASS-D to replicate interannual variation of rainfall over the entire domain and the three climatic zones used for the interpolation. Negative and Positive values of SRAI indicate dry and wet years, respectively. In all the climatic zones, in-situ shows the occurrence of more dry years in the 1980s and early 1990s and consistent more wet years between 2006 and 2020. This observed pattern was well captured by KASS-D and GPCC compared to CHIRPS and IMERG

SRAI has been used to investigate the influence of El Nino-Southern Oscillation (ENSO) on the rainfall variability over West Africa (Nicholson and Kim, 1997; Moron and Ward, 1998).

Nicholson and Kim (1997) reports that influence of ENSO on West African rainfall variability is minimal while Moron and Ward 1998 noted that ENSO tends to reduce rainfall in the Sahelian part of West Africa. Over the Guinea Coast in Figure 4.10, in-situ datasets show the occurrence of many dry years within the 1980s decade and early 1990s followed by the quasi- wet and dry years from late 1990s to 2005.

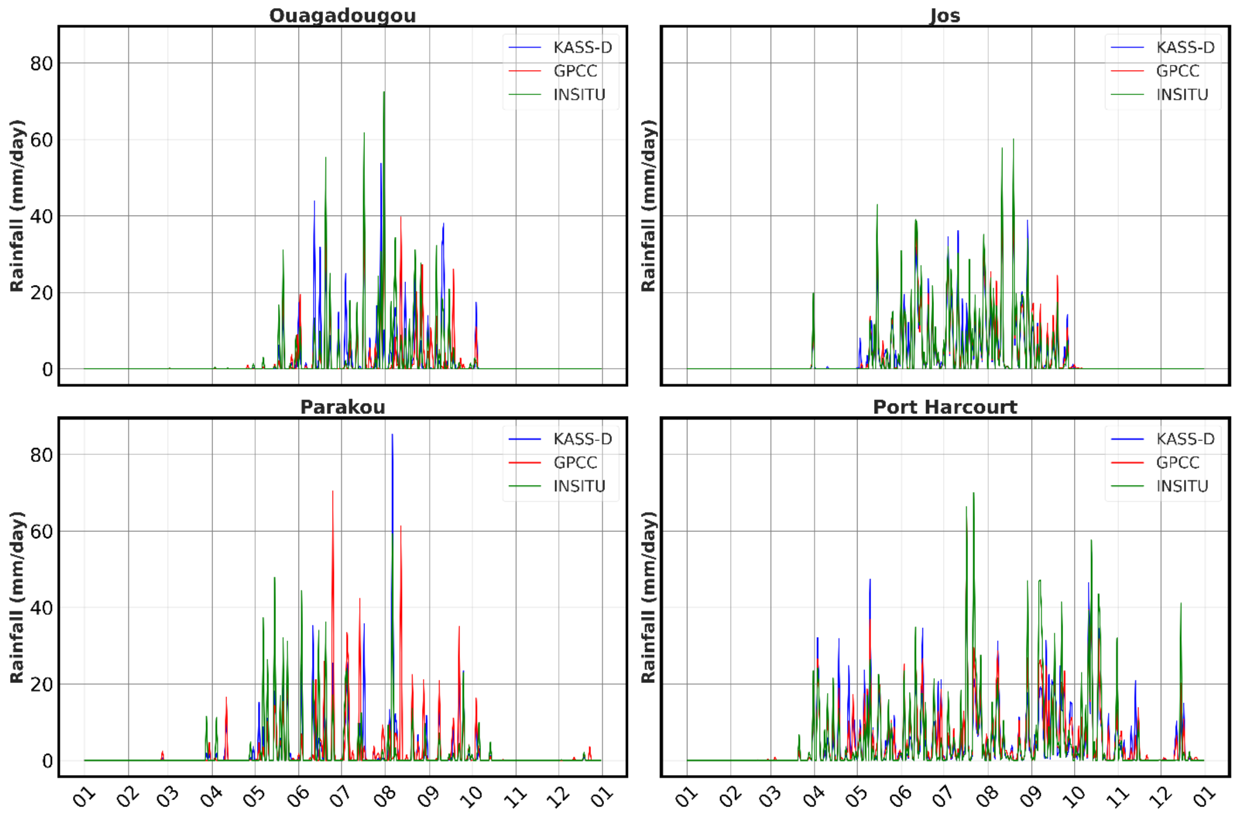

Figure 4.1: 1983 January-December time-series of daily rainfall from direct gauge measurement (in situ; green color line), GPCC and interpolated KASS-D for four selected stations, namely; Ouagadougou, Jos, Parakou and Port Harcourt.

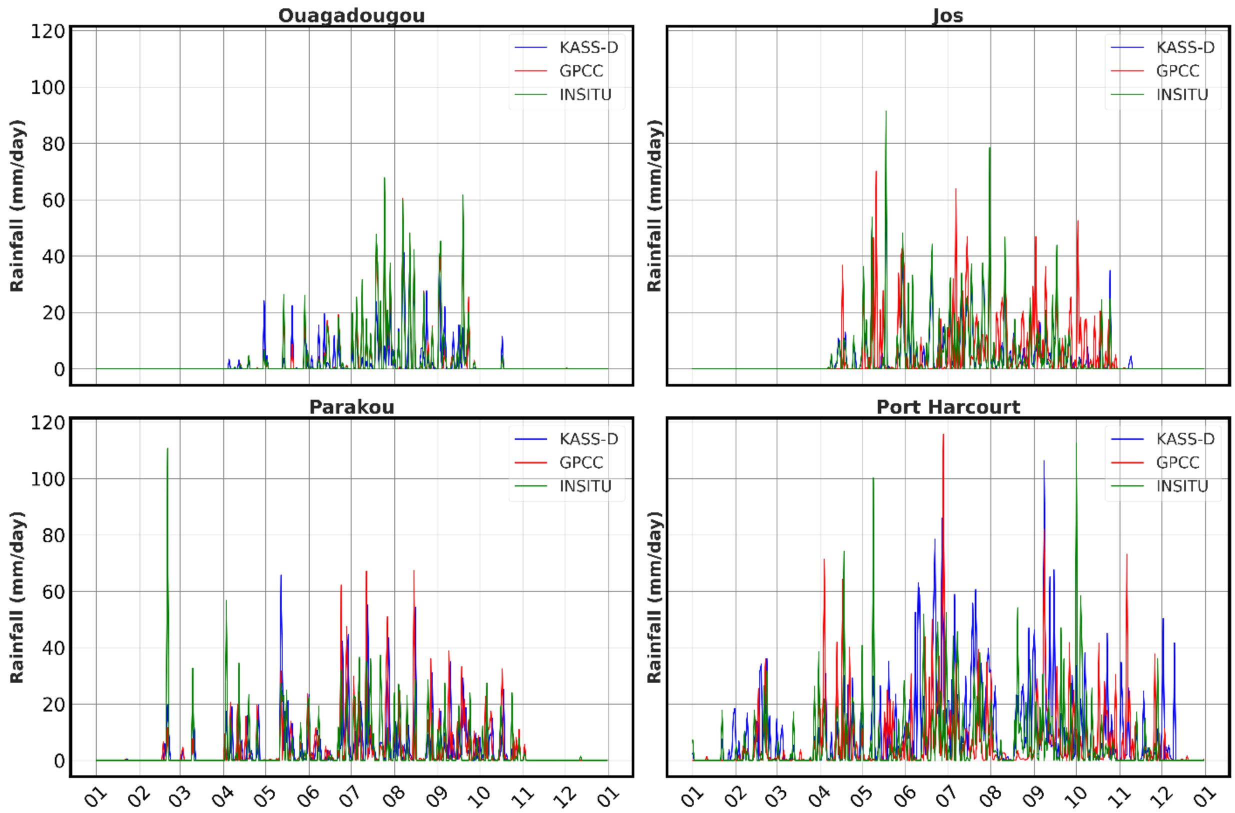

Figure 4.2: 2012 January-December time-series of daily rainfall from direct gauge measurement (in situ; green color line), GPCC and interpolated KASS-D for four selected stations, namely; Ouagadougou, Jos, Parakou and Port Harcourt.

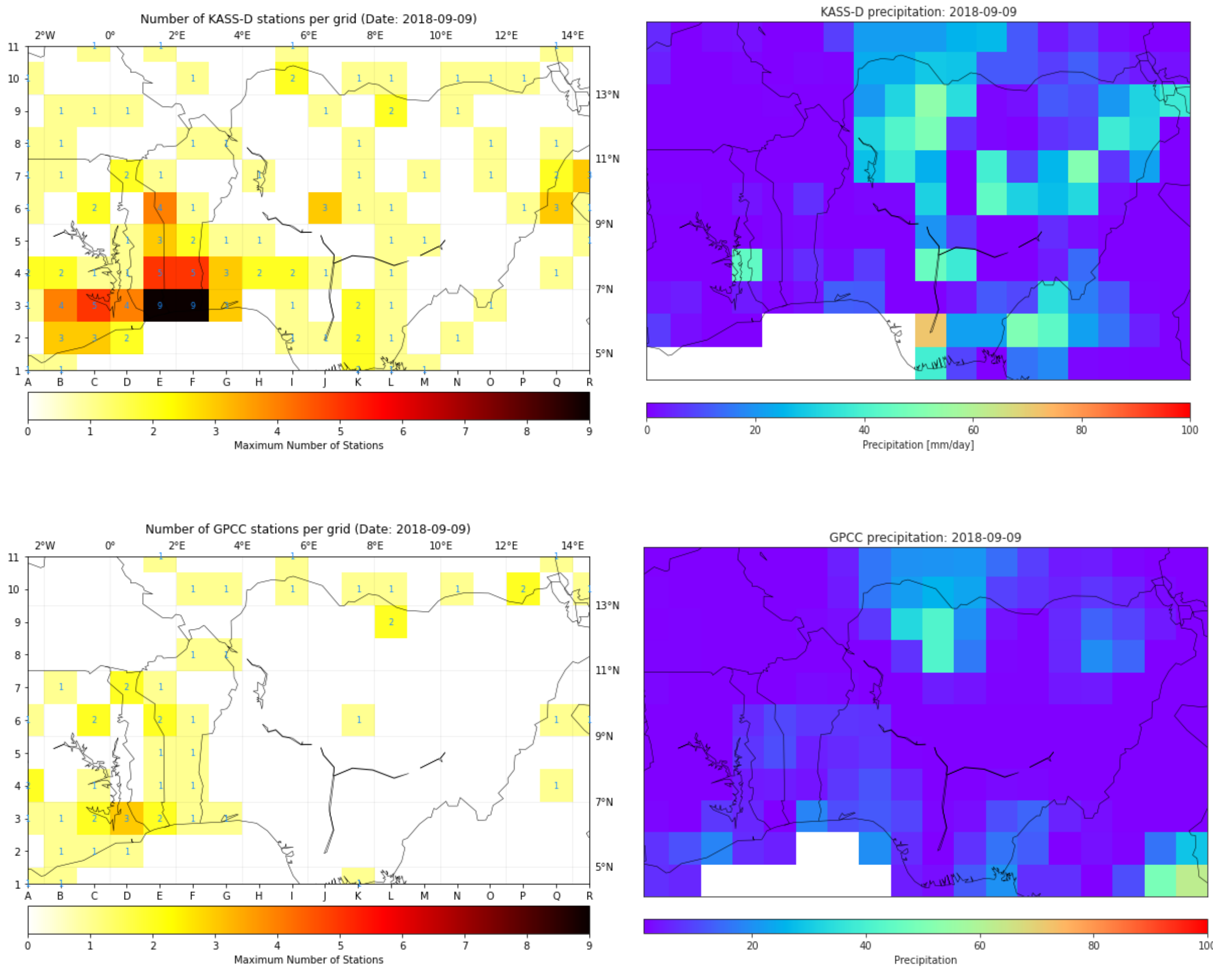

Figure 4.3: Number of gauging stations used per 1° grid cells (left panels) and spatial daily rainfall amount (right panels) for KASS-D (top panels) and GPCC (bottom panels) for 2018-09-09.

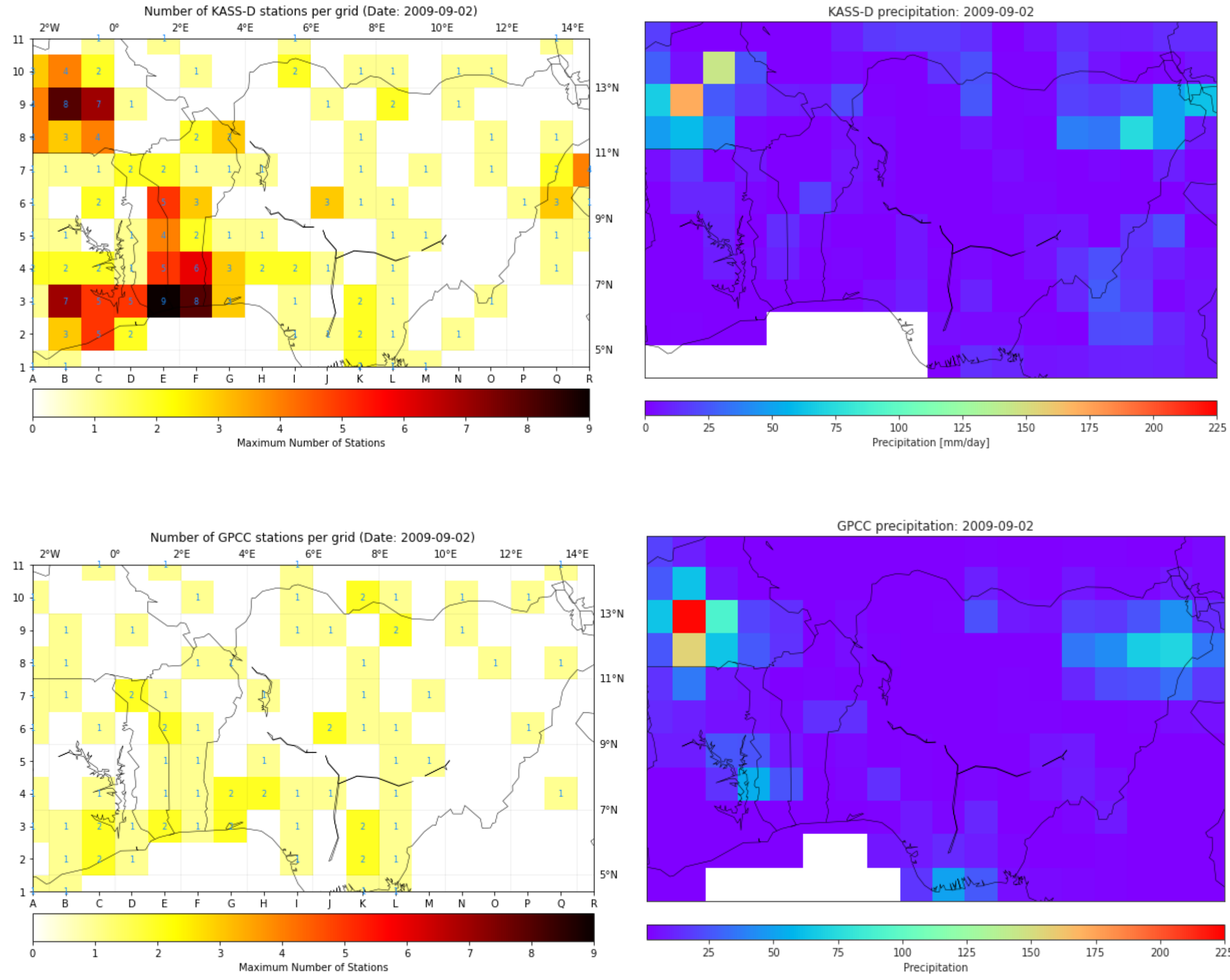

Figure 4.4: Number of gauging stations used per 1° grid cells (left panels) and spatial daily rainfall amount (right panels) for KASS-D (top panels) and GPCC (bottom panels) on 2009-09-02.

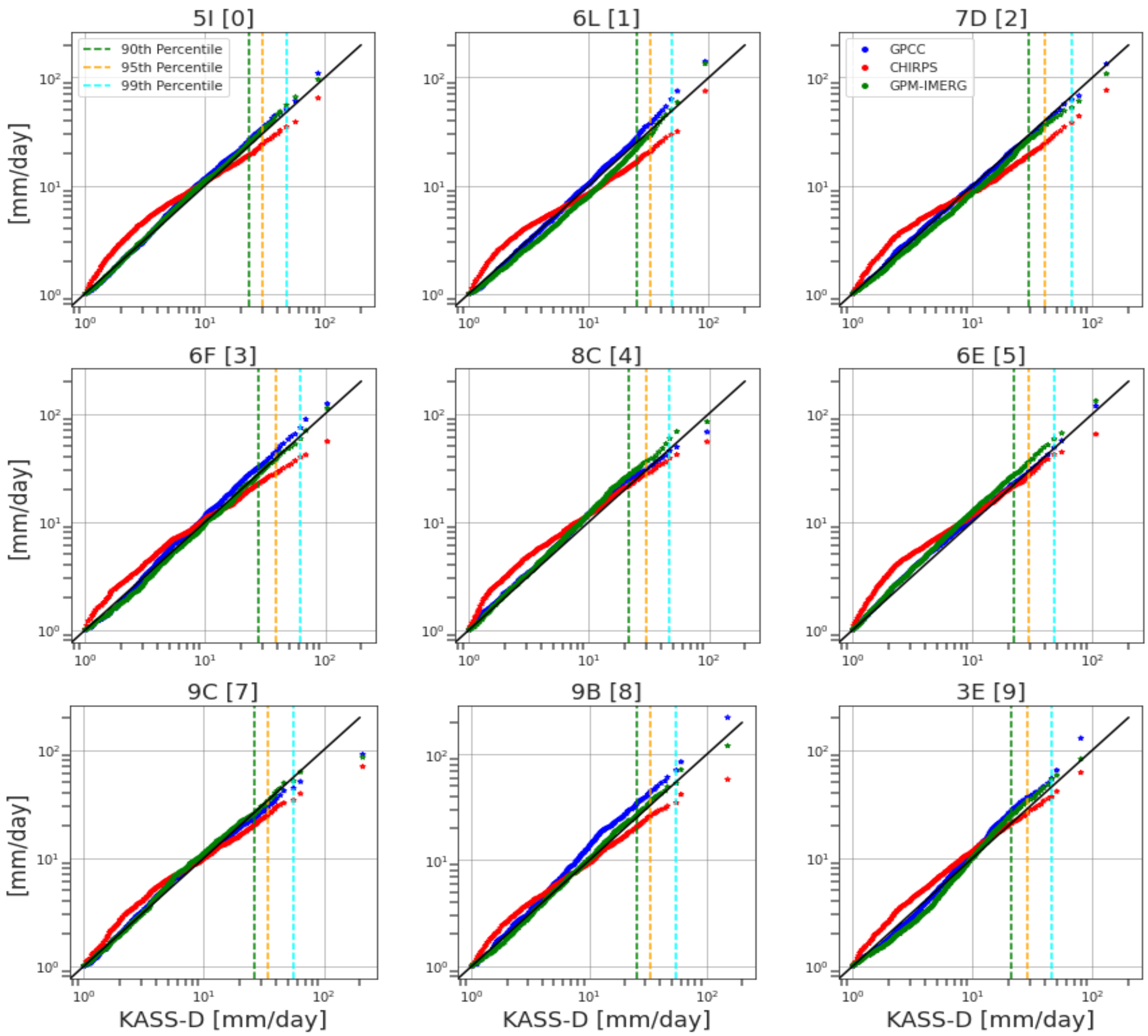

Figure 4.5: Quantile-Quantile plot of wet days only for selected grid cells based on the number of gauging stations within the 1° x 1° grid cell [number in squared bracket].

NOTE: The y-axis corresponds to GPCC, CHIRPS, and IMERG while the x-axis corresponds to the KASS-D (reference) dataset using a logarithmic scale that makes the differences appear less dramatic in the upper quantiles than they are. Vertical green, orange, and cyan broken lines depict KASS-D 90th, 95th, and 99th, percentile locations. The black solid diagonal line depicts the ideal fit line (1:1)

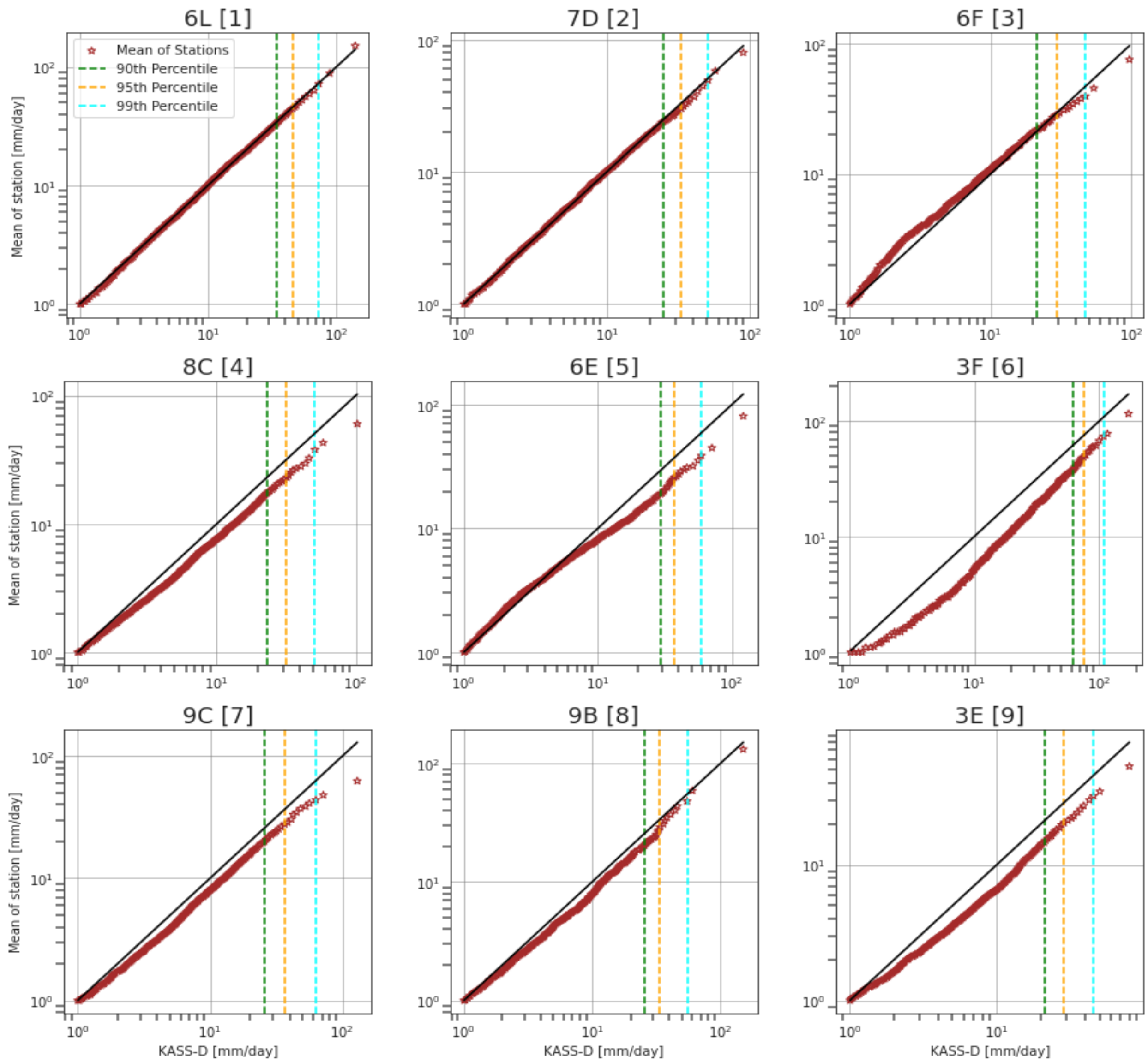

Figure 4.6: Quantile-Quantile plot of wet days only for selected grid cells and number of gauging stations within the 1° x 1° grid cell [number in squared bracket].

NOTE: The y-axis corresponds to the arithmetic mean of stations within the selected grid cells while the x-axis corresponds to the KASS-D (reference) dataset using a logarithmic scale that makes the differences appear less dramatic in the upper quantiles than they are. Vertical green, orange, and cyan broken lines depict KASS-D 90th, 95th, and 99th, percentile locations. The black solid diagonal line depicts the ideal fit line (1:1)

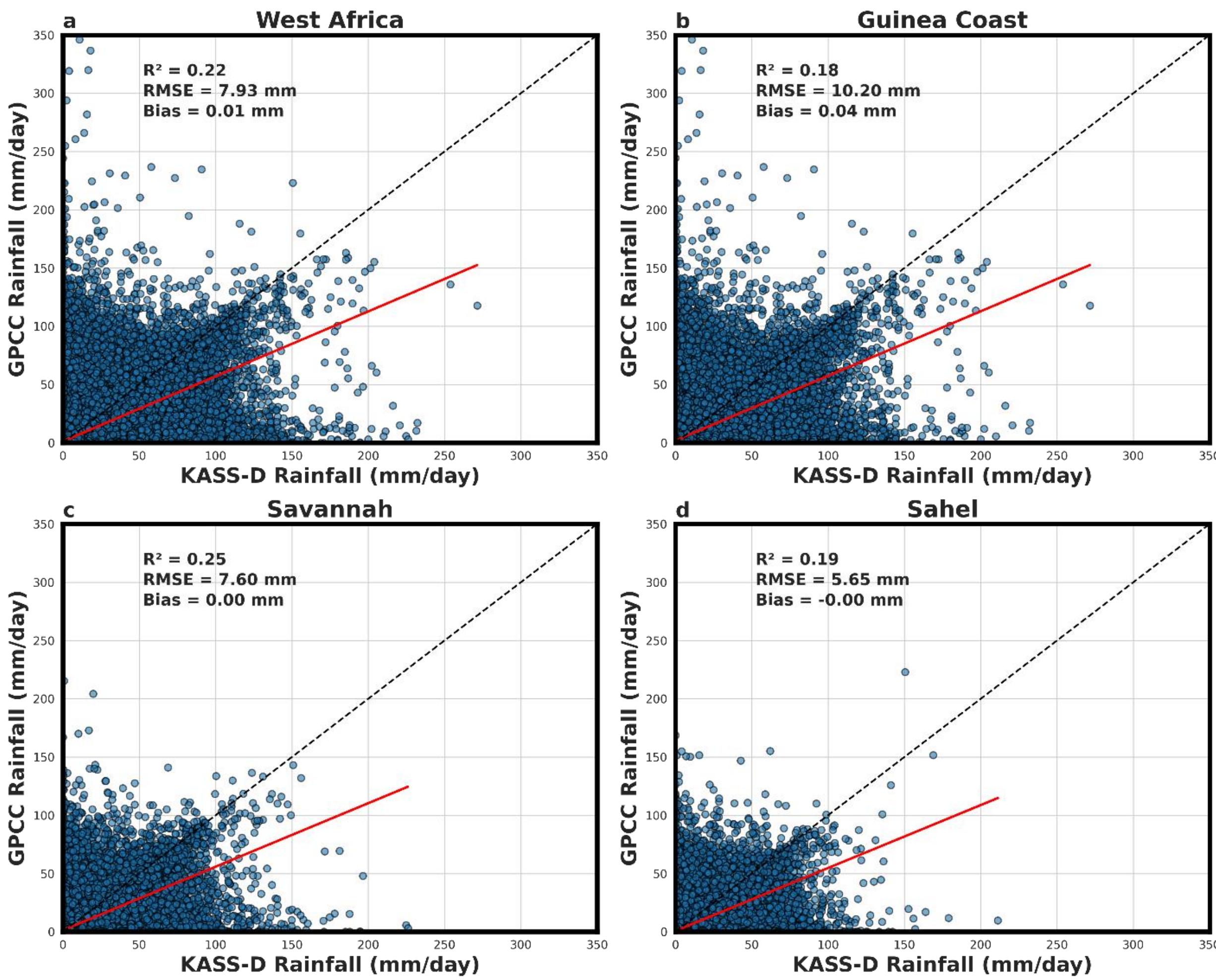

Figure 4.7: Scatter plot between KASS-D and gauge-based GPCC for wet days only averaged over the whole blue area (a), Guinea Coast (b), Savannah (c) and Sahel (d) for the period 1982-2020.

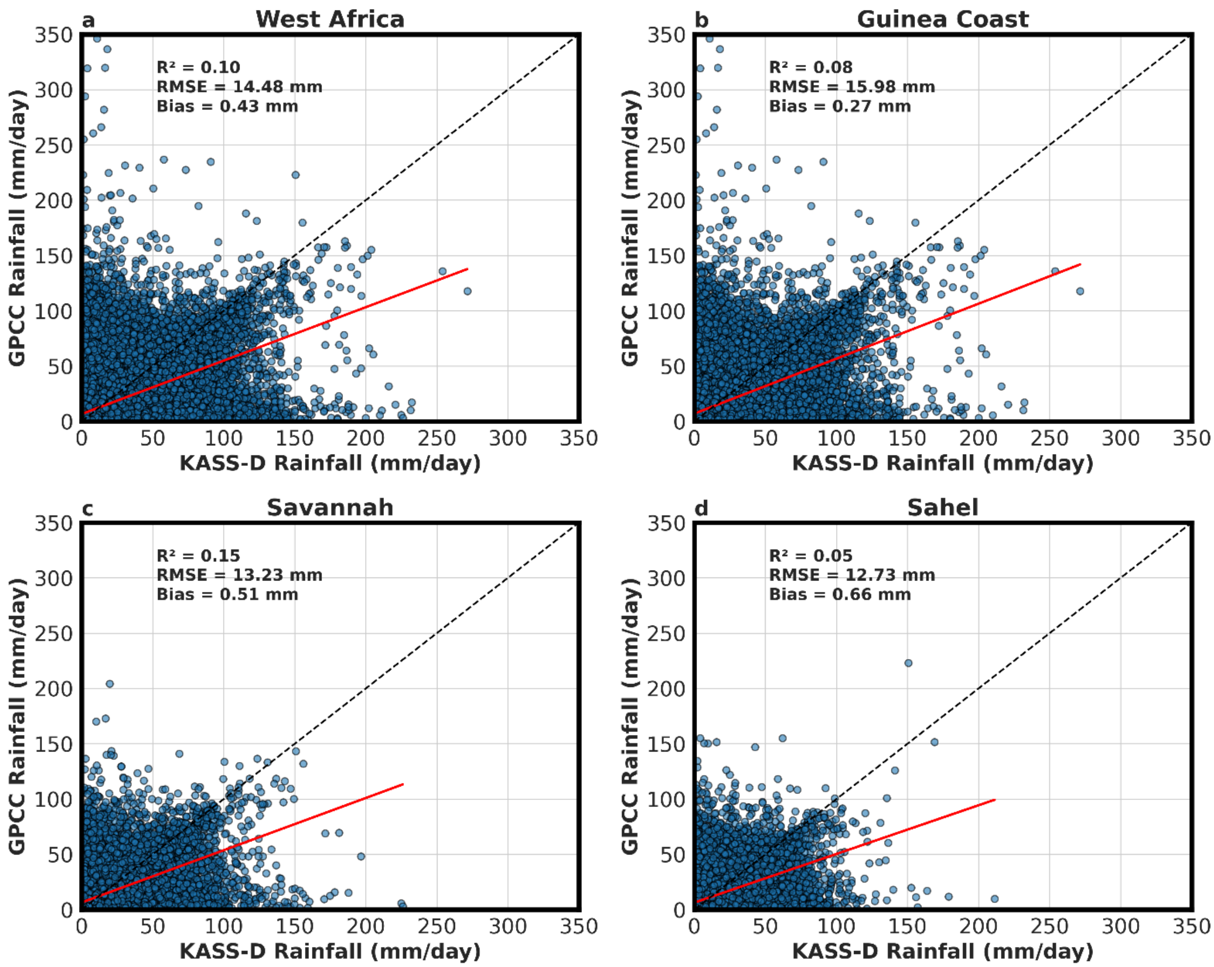

Figure 4.8: Scatter plot between KASS-D and gauge-based GPCC for both wet and dry days only averaged over the entire area of study (a), Guinea Coast (b), Savannah (c) and Sahel (d) from 1982-2020.

Table 4.1: Daily summary of the skill scores obtained from the dichotomous metrics between in-situ measurements and KASS-D, GPCC and CHIRPS averaged over the three climatic zones. The bold number denotes the best scores among the final products, whereas r, ME, PB, MAE, RMSE and E are computed from the subset of wet days only. IMERG was excluded because of its shorter data period

DATASETS	**CLIMATIC ZONE**	**POD**	**POFA**	**BID**	**HSS**	***r***	**ME**	**PB**	**MAE**	**RMSE**
	Guinea Coast	0.59	0.28	2.12	0.29	0.08	-1.76	-9.38	14.51	20.09
KASS-D	Savannah	0.58	0.21	1.56	0.27	0.08	-3.07	-12.34	12.93	19.13
	Sahel	0.42	0.13	0.98	0.21	0.06	-4.64	-16.01	12.45	19.59
	Guinea Coast	0.58	0.31	2.21	0.19	0.04	-2.37	-13.38	15.18	22.64
GPCC	Savannah	0.52	0.22	1.66	0.24	0.04	-3.96	-23.04	14.39	21.35
	Sahel	0.35	0.13	0.99	0.21	0.03	-5.81	-34.52	14.05	21.16
	Guinea Coast	0.52	0.37	2.44	0.11	0.03	-1.14	-4.88	13.83	20.08
CHIRPS	Savannah	0.51	0.28	1.94	0.18	0.03	-4.65	-27.87	12.79	19.13
	Sahel	0.36	0.15	1.14	0.19	0.03	-7.25	-43.72	12.99	19.95

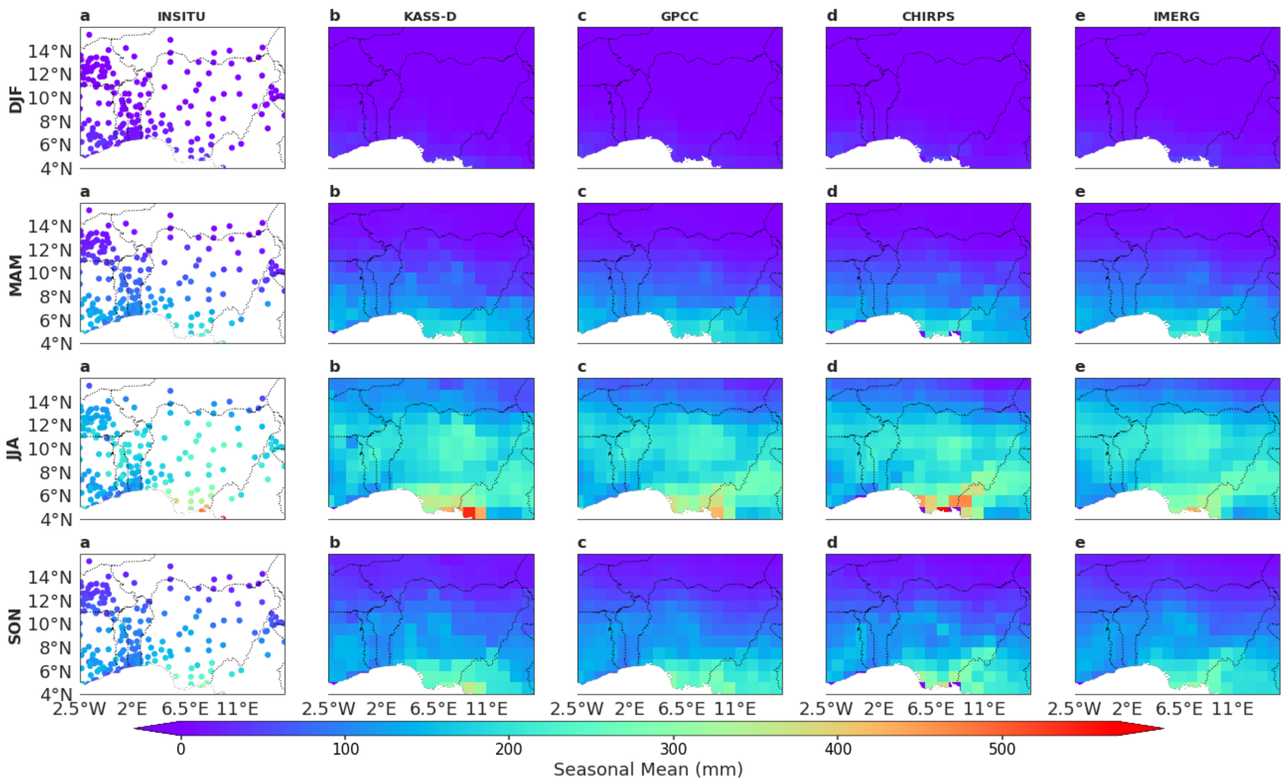

Figure 4.9: Comparing mean seasonal rainfall spatial distribution over the domain used for the interpolation for the period 1982-2020 for DJF, MAM, JJA, SON seasons for the different datasets indicated on top of each column.

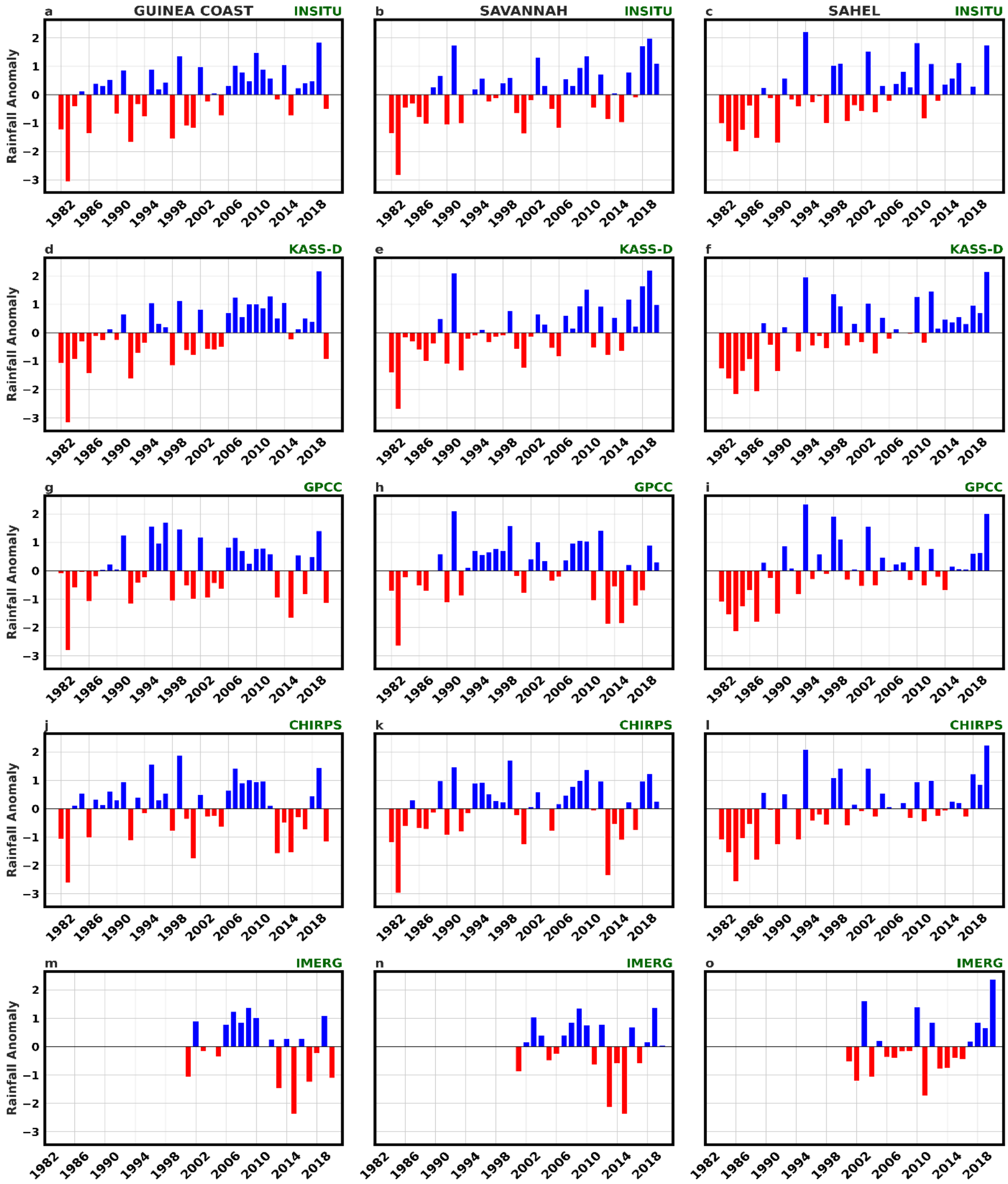

Figure 4.10: Inter-annual variation of SRAI over Guinea Coast (first column), Savannah (second column) and Sahel (third column) used for the interpolation for 1982-2020 for in-situ (a-c), KASS-D (d-f), GPCC (g-i), CHIRPS (j-l) and 2001-2020 for IMERG (m-o)

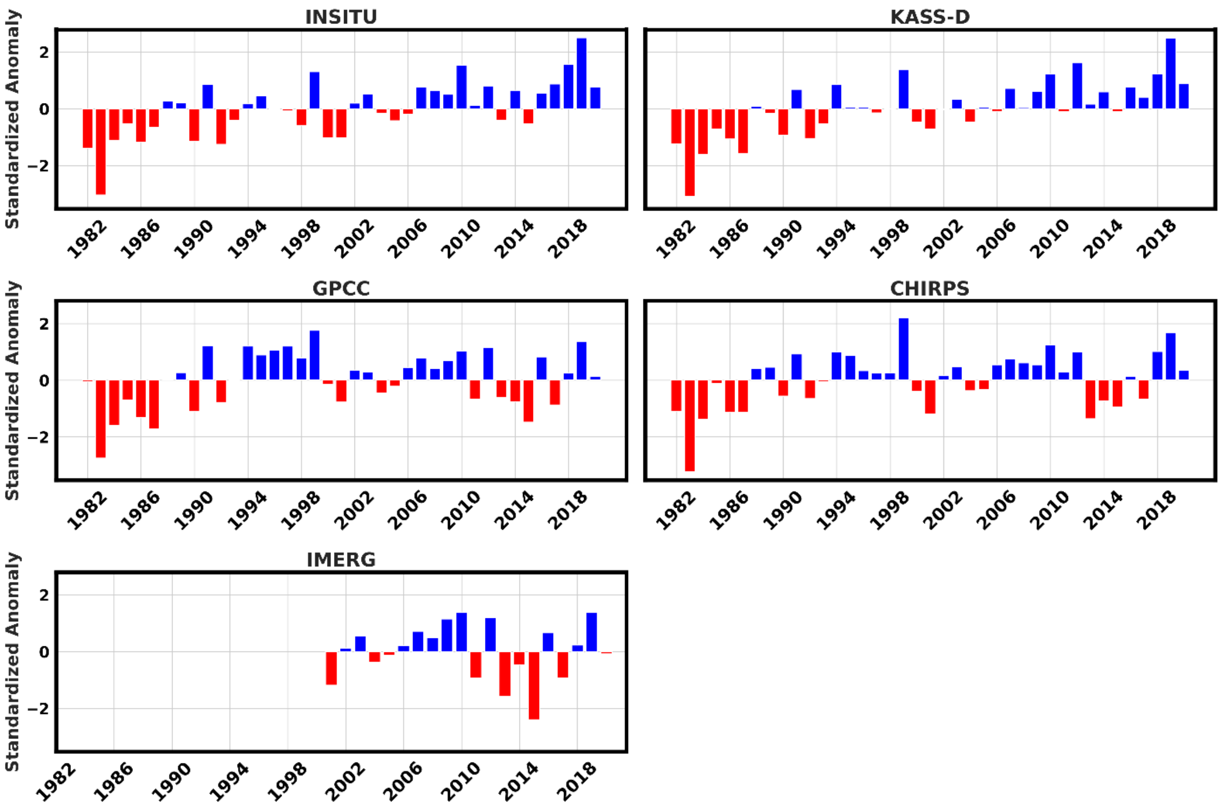

Figure 4.11: Inter-annual variation of SRAI over the entire domain used for the interpolation between 1982 and 2020 for in-situ, KASS-D, GPCC, CHIRPS and 2001-2020 for IMERG as indicated on the plots.

4.2 OCCURRENCE AND CHARACTERISTICS OF INTENSE MULTI-DAY WET SPELLS

This section aims to enhance the robustness of the analysis by incorporating interpolated KASS-D data alongside GPCC, CHIRPS, and IMERG datasets to identify and characterise intense multi-day wet spells. The objective is to assess how the results vary across and depend on different precipitation data sources. Rather than making direct comparisons, the focus here, is on highlighting key similarities and differences among the datasets. It is important to note that IMERG, due to its shorter data coverage (2001–2020) compared to the other datasets (1982–2020), was excluded from all temporal and trend analyses.

4.2.1 Description of the Climatological 3-day and 5-day 90th Percentile Value and Frequency of Occurrence

The spatial distribution of the 90th percentile value for 3-day and 5-day accumulation rainfall amounts is shown in Figure 4.12 for each dataset from 1982-2020 (KASS-D, GPCC, CHIRPS) and 2001-2020 (IMERG). Also, Figure 4.13 depicts the difference in 90th percentile values between other rainfall products and KASS-D. The 90th percentile values for the 3-day and 5-day accumulation display a largely meridional variation over the domain in all the datasets with the coastal and Niger Delta regions of Nigeria having the highest 90th percentile accumulation values.

For KASS-D, the 3-day and 5-day 90th percentile have a maximum value of 90 mm and 140 mm, respectively, that extends from the coastal region of Nigeria to the Cameroon highland area that then relatively decrease to the far north (Figure 4.12). The latitudinal variation of 3-day and 5-day 90th percentile amounts in KASS-D can be seen in all other datasets irrespective of the data period.

In the inland area, the 3- and 5-day 90th percentile amount depicted by KSS-D and GPCC are higher than the amount shown by satellite products (CHIRPS and IMERG). This is similar to the spatial variation of mean annual rainfall over West Africa that is defined by the north - south oscillation of the rain-belt (Nicholson 2013). However, the latitudinal variation in satellite-based products (CHIRPS and IMERG) is smoother and relatively low compared to rain gauge-based products (KASS-D and GPCC). This artifact can be associated with the algorithm adopted by these satellite-based datasets that estimate daily rainfall amount at equal distances (grid points) using different means like TIR CCD in addition to long and smooth decorrelations length in CHIRPS or PMW-based approaches in IMERG compared to direct rainfall measurements by rain-gauge that are not equidistant from each other.

Using the 90th percentile value of 3-day and 5-day accumulation amounts at each grid point as a threshold, an intense multi-day wet spells are defined as 3-day or 5-day rainfall accumulations exceeding the 90th percentile threshold at each grid point, with minimum of 2 wet days ($\geq$ 1 mm) for 3-day spells and minimum of 3 wet days with no consecutive dry days for 5-day spells. Counting the number of intense multi-day wet spell events in each year, Figure 4.14 depicts the spatial distribution of the annual mean number of intense 3- and 5-day wet spells and the mean annual number of wet days. Climatologically, the spatial distribution of 3-day intense wet spell frequency of occurrence follows the spatial pattern of the 90th percentile value in Figure 4.12. KASS-D annual mean frequency of occurrence of 3-day intense wet spell in Figure 4.14a ranges between 13 and 20 events over the coastal region and Niger Delta area of Nigeria to events less than 5 events per year north of 11°N. Compared to its surroundings, the mean annual number of intense 3-day wet spells is low over the Ghana-Benin dry zone (Dahomey region; Vollmert *et al.*, 2003) due to the observed relative dryness of the area resulting from the combination of frictional divergence oriented along SW-NE coastlines and coastal upwelling of cold waters (Nicholson, 2011; Vollmert *et al*., 2003; William 2001). However, the frequency of occurrence varies from one grid cell to the other between 7.5°N and 11°N in the range of 5 to 12 events per year. All these features are also observed in GPCC, CHIRPS, and IMERG but with a slight variation in the mean annual number and spatial pattern of the 3-day intense wet spell. Additionally, differences in rainfall representation over mountain and coastal areas ranges, particularly the Jos Plateau and the Niger Delta region, between station- and satellite-based products become evident due to the number of stations in the area. This highlights the importance of high station density for accurately representing rainfall spatially, which is a significant challenge in West Africa. The mean annual number of wet days (daily rainfall amount greater than 1 mm) decreases from the coastal region to the far north. At the Coast and Niger Delta particular, KASS-D and GPCC have an average number of about 180 wet days (contour lines) in a year but lower than satellite-based datasets (CHIRPS and IMERG) average number of wet days. The mean annual number of wet days decreases with an increase in latitude to less than 40 days in the far north (north of 14°N). Similarly, the spatial distribution of the occurrence of 5-day intense wet spells is highly similar to 3-day but lower in magnitude.

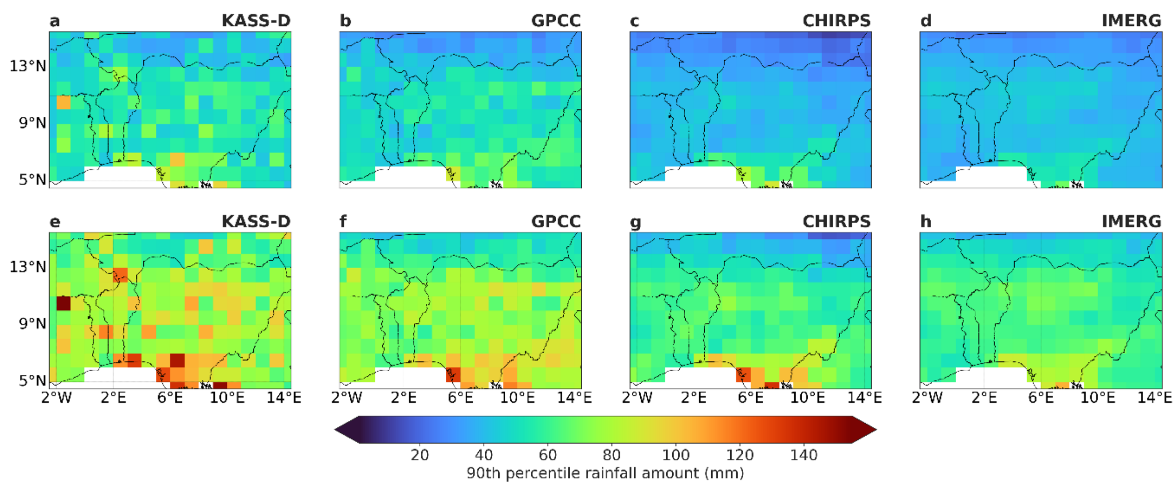

Figure 4.12: Spatial distribution of 90th percentile 3-day (first row) and 5-day (second row) accumulation rainfall amount over the domain. KASS-D, GPCC, and CHIRPS 90th percentile values are computed from 1982 through 2020 while IMERG is from 2001 to 2020.

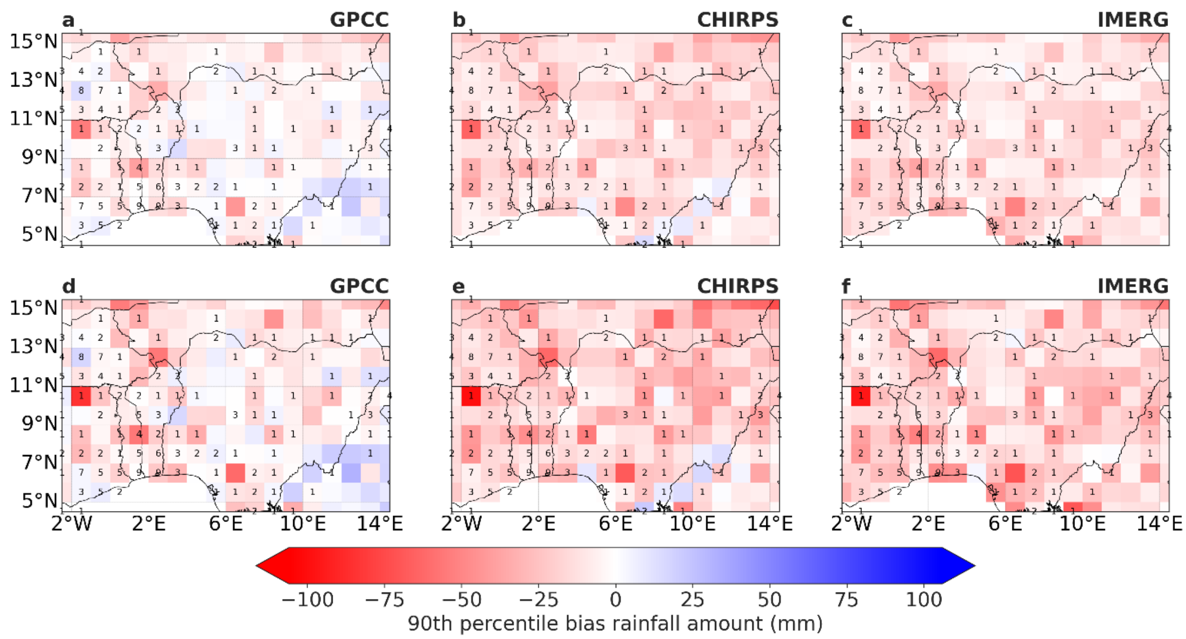

Figure 4.13: Difference in 90th percentage values between KASS-D and GPCC (a, d), CHIRPS (b, e) and IMERG (c, f) for 3-day (a-c) and 5-day (d-f). The number on the plot represents the underlying maximum number of gauging stations used in KASS-D 1° grid cell.

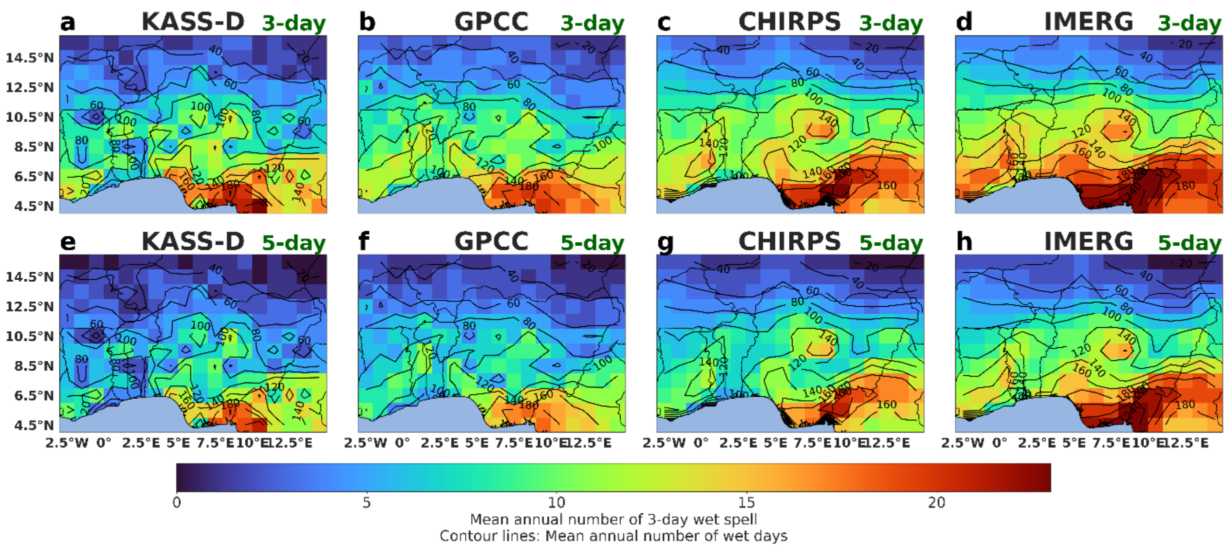

Figure 4.14: Spatial distribution of mean annual frequency of occurrence of intense 3-day (first row) and 5-day (second row) wet spells (color fill) and mean annual number of wet days (contour line) for 1982-2020 (KASS-D, GPCC, and CHIRPS) and 2001-2020 (IMERG)

4.2.2 Seasonal and Annual Variation of 3-Day and 5-Day Wet Spells

Figure 4.15 illustrates the seasonal variability of 3- and 5-day intense wet spells across the Guinea Coast, Savannah, and Sahel. In all months and zones, 3-day wet spells occur more frequently than 5-day wet spells. The Guinea Coast shows smaller differences between 3-day and 5-day spells compared to the Savannah and Sahel, likely due to fewer rainy days in the latter regions and the Guinea Coast's proximity to the Atlantic Ocean and frequent convective activities. Over the Guinea Coast, the number of 3-day and 5-day intense wet spells exhibits a bimodal pattern, peaking in June and September with fewer than 15 (KASS-D) and 12 (GPCC) events per grid cell in these months. The first peak in June is higher in satellite-based CHIRPS data than the second peak in September, a pattern also observed in IMERG data despite its shorter period. In the Savannah and Sahel, a unimodal pattern appears with a peak in August. The Savannah experiences about 19 3-day events per grid cell in August, higher than the Sahel's fewer than 14 events. Most intense 3-day and 5-day wet spells in the Sahel occur from July to September (Figure 4.15c, f, i, l), driven by Mesoscale Convective Systems (MCSs) and squall lines, which deliver over 90% of its rainfall (Omotosho and Abiodun, 2007; Fink *et al*., 2006; Fink *et al*., 2017).

Figure 4.16 displays the inter-annual variation in the number of 3- and 5-day intense wet spells per grid cell across the interpolated domain. The occurrence of 5-day wet spells is closely linked to 3-day events, indicating that intense 5-day wet spells are often extensions of 3-day intense wet spells. The mean annual number of intense 3-day (5-day) wet spells over the study domain ranges from 7.5 (5.5) to 9 (7) events across all datasets. The lowest mean annual number is in KASS-D, while the highest is in CHIRPS. From 1982 to 1999 (Figure 4.16a), KASS-D shows an increasing trend in the annual number of 3-day and 5-day intense wet spells, reaching 10 and 8 events per grid cell, respectively. However, periods like 1992-1993 and 1995-1998 experienced decreases in frequency, with events per grid cell below the long-term means of 7.9 (3-day) and 4.9 (5-day). Post-2001, there was a significant decline in frequency, followed by an increase until 2012, with many events exceeding the long-term mean. The frequency reduced again after 2012 but showed an upward trend towards 2020. GPCC and CHIRPS exhibit similar inter-annual variation patterns (Figure 4.16b & c), with slight differences in the years when the frequency of 3- and 5-day wet spells remained above average. The highest frequency of 3-day and 5-day events occurred in 2019 (KASS-D), 1999 and 2007 (GPCC), and 1999 (CHIRPS). Despite the differences in rainfall products and with the correlation coefficient higher than 0.60 (Figure 4.17), there is a noticeable level of agreement among the datasets in the patterns of increase or decrease in the annual number of intense wet spells.

The increasing trend in the annual frequency of multi-day wet spells shown by KASS-D in Figure 4.15 is confirmed by a statistically significant rate of 0.07 events per year for 3-day wet spells and 0.06 events per year for 5-day wet spells (text on Figure 4.16). GPCC and CHIRPS reported no trend, with trend lines almost parallel to the long-term mean. The significant trend in KASS-D is further explained in Figure 4.18 by averaging effects of high positive Sen's slope values over Nigeria, Burkina Faso, and Niger, and low negative values over Ghana, Togo, Benin, and Cameroon Highlands. GPCC and CHIRPS show low positive and high negative Sen's slope values over the same countries compared to KASS-D. This difference is likely due to the higher underlying number of stations in KASS-D compared to GPCC (Figure 3.2). The increase in the frequency of intense wet spells post-1990 across all datasets may be attributed to the partial recovery of rainfall from the dry years of the 1980s (Sanogo *et al*. 2015; Nicholson 2013).

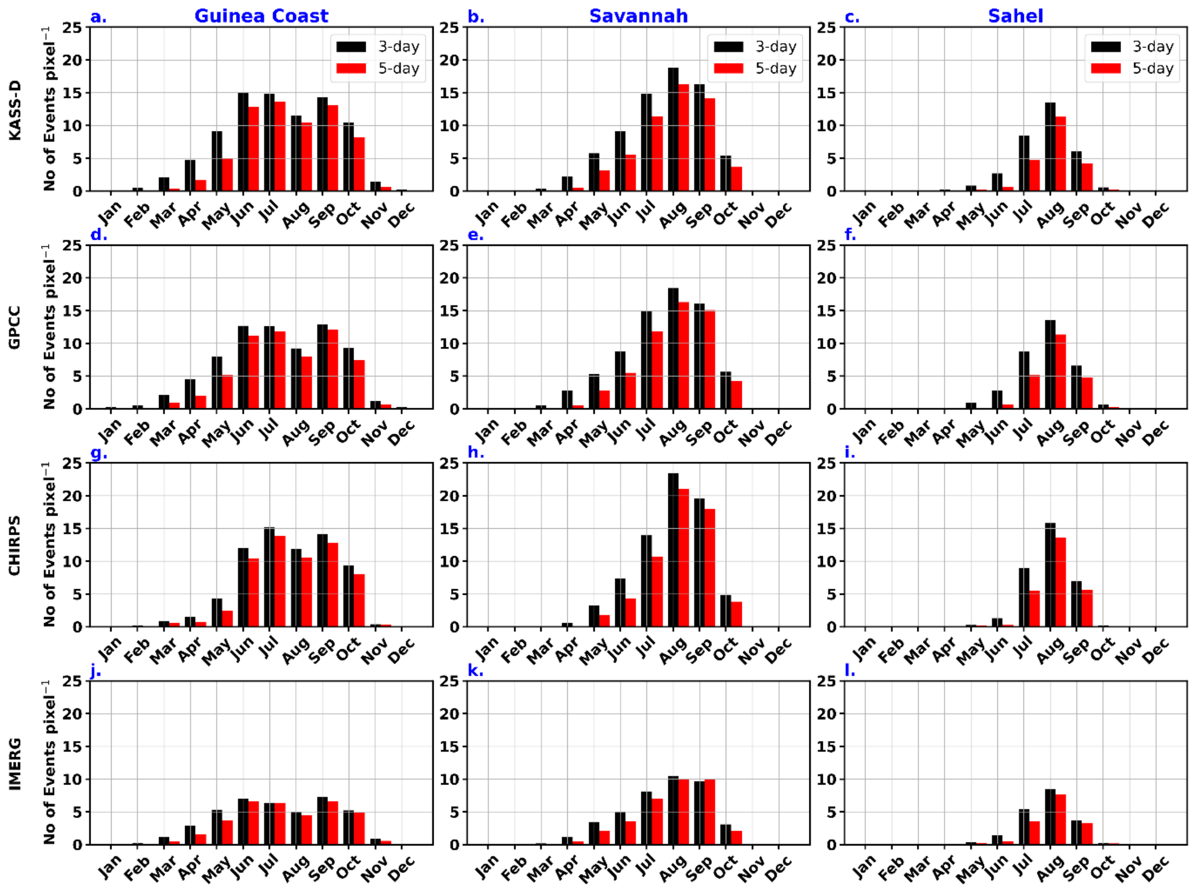

Figure 4.15: Seasonal frequency of occurrence of intense 3-day and 5-day wet spells per grid cell (pixel) from 1982-2020 (KASS-D, GPCC, and CHIRPS) and 2001-2020 (IMERG) averaged over the Guinea Coast, Savannah, and Sahel climatic zones of the study domain.

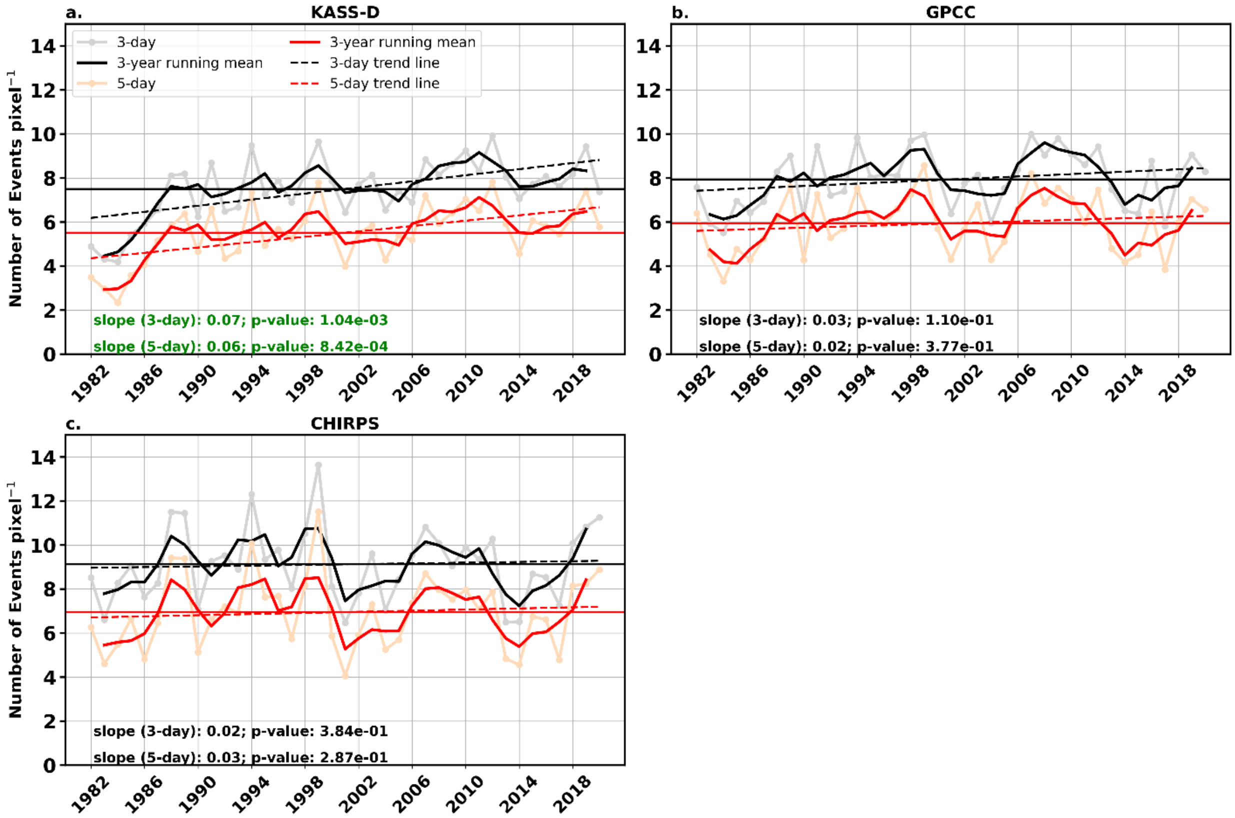

Figure 4.16: Inter-annual variation of frequency of occurrence of intense 3-day and 5-day wet spells per grid cell (pixel) from 1982-2020 (KASS-D, GPCC, and CHIRPS) averaged over the study domain.

NOTE: Black and red thick (dashed) lines represent the climatological mean (trend line) of intense 3- and 5-day frequency of occurrence, green colored text indicates significant trend at 0.05 significance level.

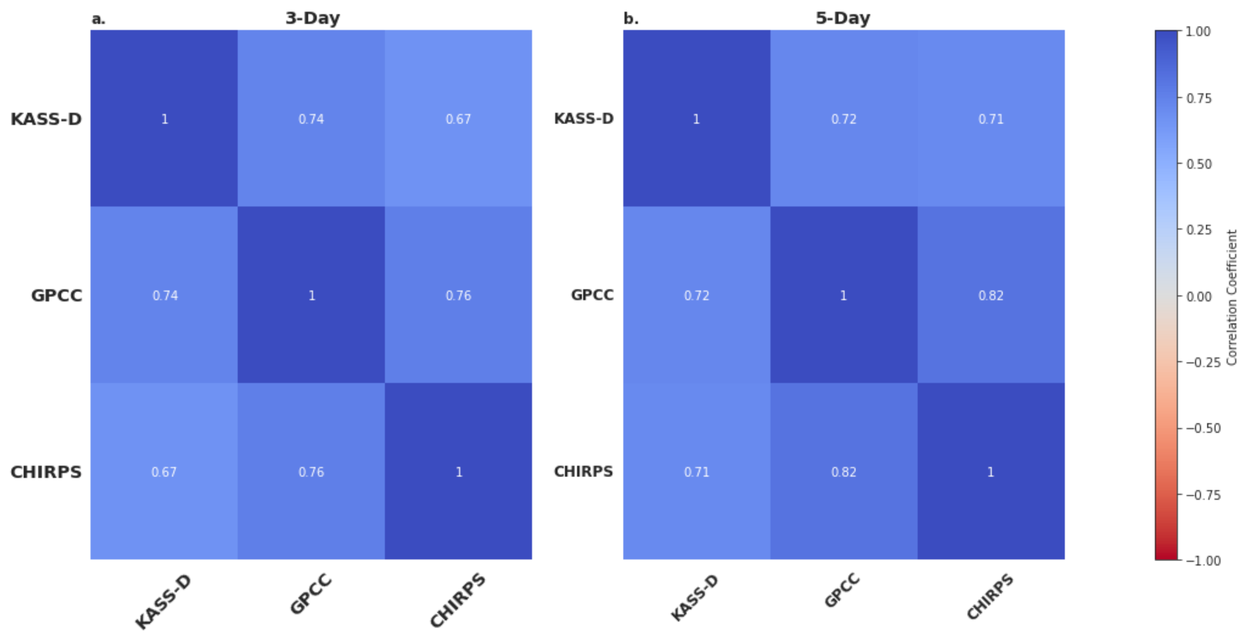

Figure 4.17: Pattern correlation of annual frequency of 3-day and 5-day intense wet spells among the three datasets (KASS-D, GPCC and CHIRPS) over whole domain.

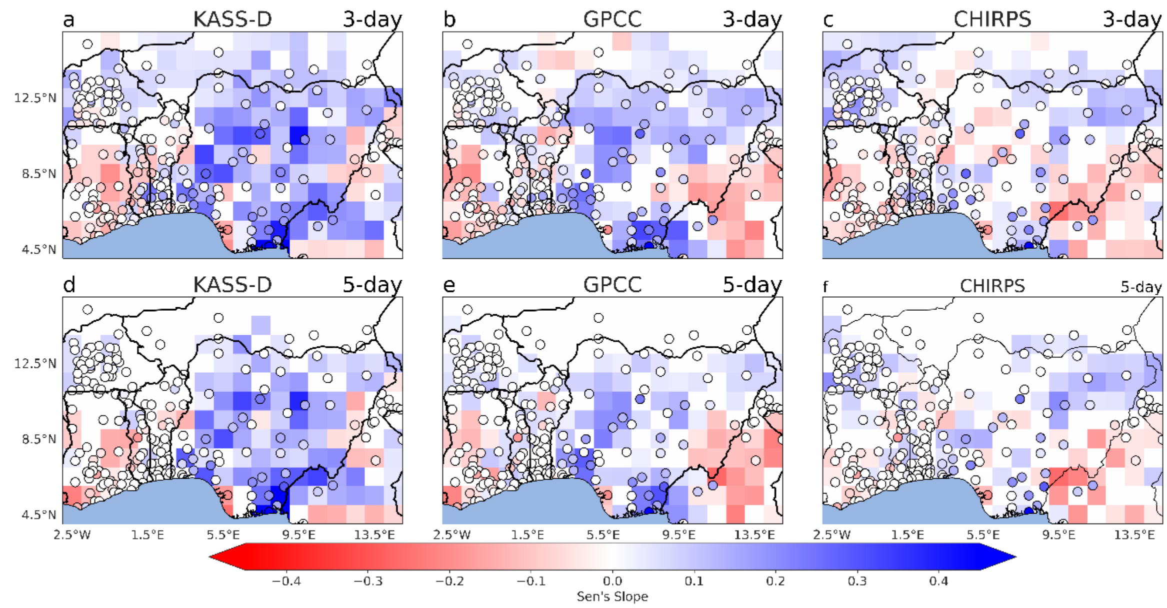

Figure 4.18: Spatial distribution of Sen's slope value (color fill) at each grid cell for KASS-D, GPCC, and CHIRPS as indicated on the plot for 3-day (a-c) and 5-day (d-e).

NOTE: Filled scatter plots on each plot represent Sen's slope values computed for each station used in the interpolation of KASS-D

The effects of climate change, particularly in the frequency and intensity of extreme weather events, are more pronounced at the local level than globally (IPCC 2021). This study further examines the frequency of intense multi-day wet spells across three climatic zones in the interpolated domain. The inter-annual variation of 3-day and 5-day intense wet spells per grid cell for KASS-D, GPCC, and CHIRPS averaged over Guinea Coast, Savannah, and Sahel is shown in Figure 4.19. At the Guinea Coast (first column in Figure 4.19), the mean annual occurrence of 3-day wet spells ranges from 11 to 12.5 events per pixel, and 5-day wet spells from 9 to 10 events per pixel across all datasets. The long-term annual mean for 3-day intense wet spells is 11 events/year for KASS-D, 12 for GPCC, and 12.5 for CHIRPS. For 5-day intense wet spells, it is 9 events/year for KASS-D, 9.5 for GPCC, and 10 for CHIRPS. KASS-D (Figure 4.19a) shows an increasing pattern of 3-day and 5-day intense events from 1982 to 2020, despite significant lows in the early 1980s and between 2012 and 2018. GPCC and CHIRPS also show an increase from 1982 to 1999, followed by low frequencies from 2000 to 2006 (Figure 4.19d & g). Both datasets show a decrease towards the end of the study period after sharp increases in 2007 (GPCC) and 2009 (CHIRPS). The low frequency of 3-day and 5-day intense wet spells before 1988 extends to the Savannah and Sahel (Figure 4.19). The long-term mean frequency of these events in the Savannah and Sahel is lower than in the Guinea Coast, with the Sahel having the lowest. In the Savannah, the first peak of about 10 events/year (KASS-D and GPCC) and more than 16 events/year (CHIRPS) in 1989 was followed by a significant decrease in 1990 across all datasets. For the Sahel, a higher number of occurrences in 1994 was shown by all datasets, but GPCC and CHIRPS showed reduced numbers from the early 2000s until 2017.

In all datasets, only KASS-D shows consistent upward trends for 3- and 5-day intense wet spells per pixel across all climatic zones, with all datasets agreeing on an upward trend in the Sahel. The level of agreement among the datasets in the patterns of increase or decrease in the annual number of intense wet spells is highest in the Sahel with *r* higher than 0.87 compared to other zones (figure 4.20). The MK t-test (Table 4.2) confirms this with significant increasing trend in 3-day/5-day intense wet spells in the Sahel, highest in KASS-D (0.094/0.063) and lowest in GPCC (0.054/0.042). Only KASS-D revealed a statistically significant increasing trend across all climatic zones.

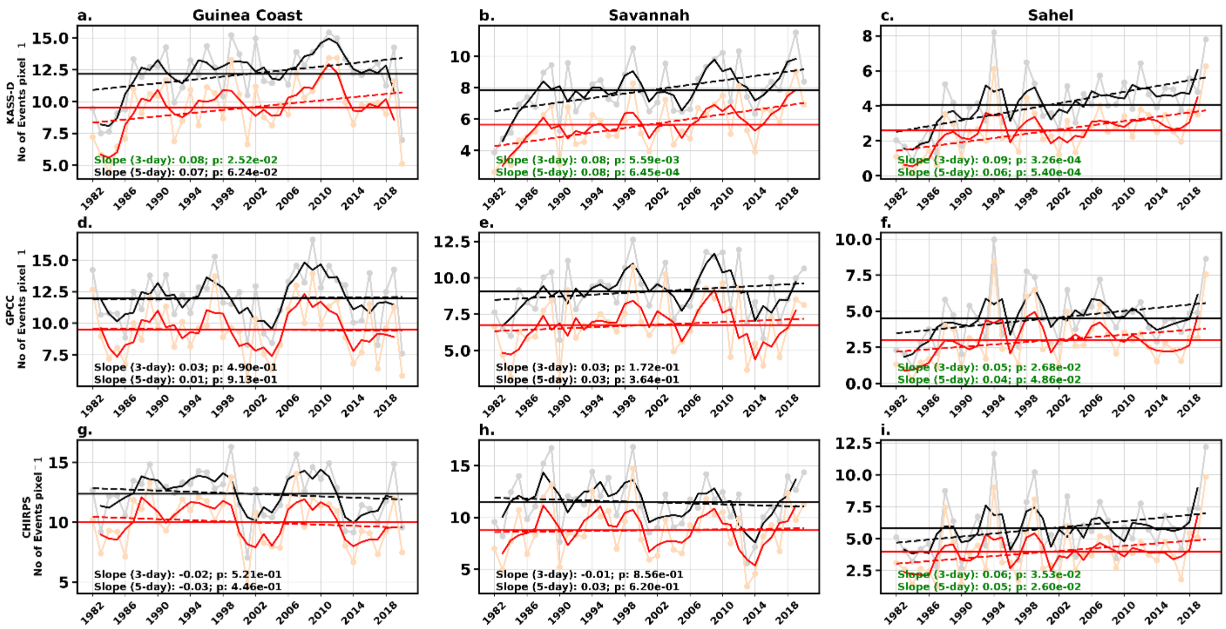

Figure 4.19: Inter-annual variation of frequency of occurrence of intense 3-day and 5-day wet spells per grid cell (pixel) from 1982-2020 (KASS-D, GPCC, and CHIRPS) averaged over Guinea Coast, Savannah, and Sahel.

NOTE: Black and red thick (dashed) lines represent the climatological mean (trend line) of intense 3- and 5-day frequency of occurrence while green colored text indicates significant trend at 0.05 significance level.

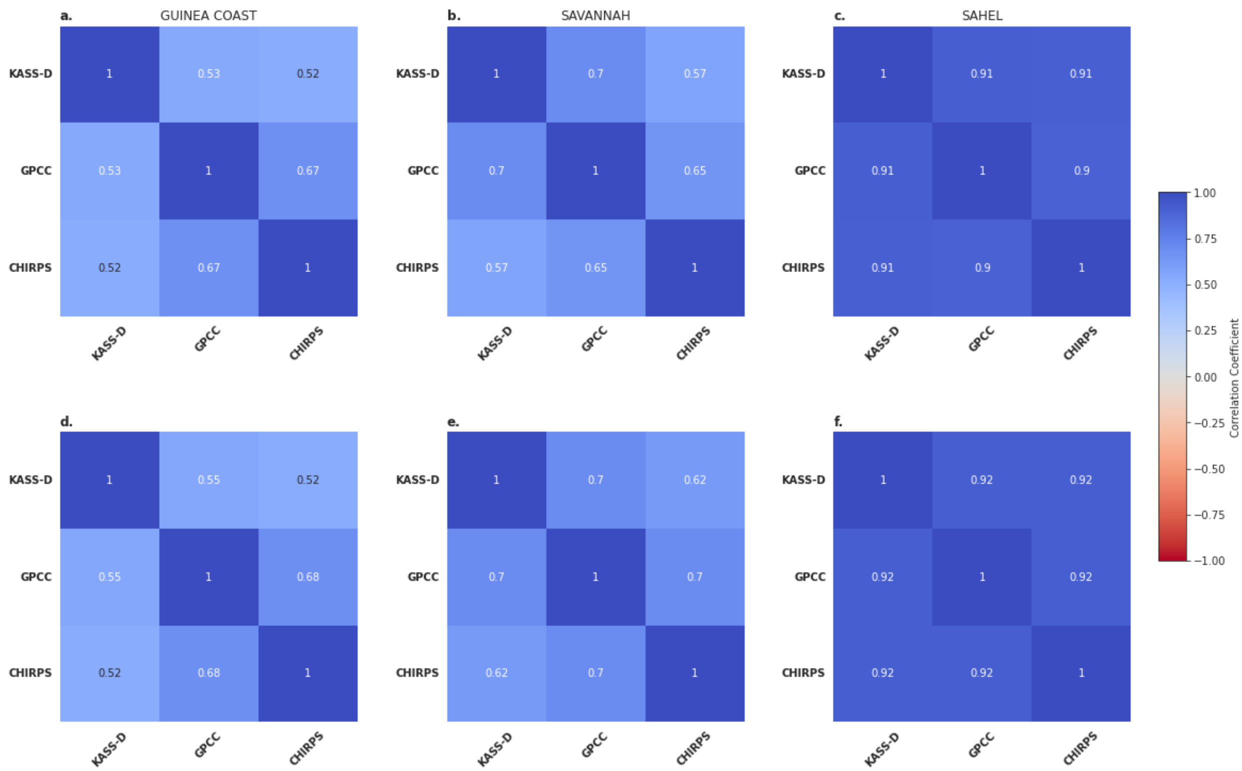

Figure 4.20: Pattern correlation of annual frequency of 3-day (a-c) and 5-day (d-f) intense wet spells among the three datasets (KASS-D, GPCC and CHIRPS) over Guinea Coast, Savannah and Sahel as indicated on the plot.

Table 4.1: Mann-Kendall trend test result for the frequency of occurrence of 3-day and 5-day intense multi-day wet spells over the three climatic zones in the study domain. The bold p-value indicates a statistically significant trend at a 0.05 significant level.

		3-day			5-day		
Dataset	Region	Trend	Sen's Slope	p-Value	Trend	Sen's Slope	p-Value
KASS-D	Guinea Coast	increasing	0.080	***0.0086***	increasing	0.069	***0.0145***
	Savannah	increasing	0.089	***0.0002***	increasing	0.088	***0.0003***
	Sahel	increasing	0.094	***0.0001***	increasing	0.063	***0.0004***
GPCC	Guinea Coast	no trend	0.020	0.4904	no trend	0.006	0.8845
	Savannah	no trend	0.030	***0.0171***	no trend	0.025	0.377
	Sahel	increasing	0.054	***0.0268***	increasing	0.042	***0.0459***
CHIRPS	Guinea Coast	no trend	-0.025	0.5214	no trend	-0.025	0.4459
	Savannah	no trend	-0.007	0.8559	no trend	0.026	0.6113
	Sahel	increasing	0.062	***0.0353***	increasing	0.051	***0.0276***

4.2.3 Size Classification of Intense 3-Day and 5-Day Events

The classification of 3-day and 5-day intense wet spells by size, based on grid cells exceeding the 90th percentile amount, reveals that small-size events occurred more frequently than mid-size and large-size events at annual scale (Figure 4.21). Small-size events decreased between 1982 and 1990, with CHIRPS showing the lowest and KASS-D the highest occurrences, followed by a brief increase in these events before a general decrease. From 1982 to 2020, mid-size events increased overall (Figure 4.21b & e), despite declines from 2000-2005 and 2010-2015. CHIRPS reported the highest number of 5-day mid-size events before 1995. Large-size events showed an early increase, with CHIRPS and GPCC above their long-term mean until 2002, followed by two low-occurrence periods (2000-2005 and 2010-2015). CHIRPS focus on large-scale events might be due to its design since it relies on TIR-CCD, covering a wider area on the average. CHIRPS and GPCC displayed a decreasing trend that is significant and non-significant, respectively, in small-size events (Table 4.3), while KASS-D showed no trend. KASS-D alone showed a significant increasing trend for mid-size and large-size 3-day and 5-day intense wet spells.

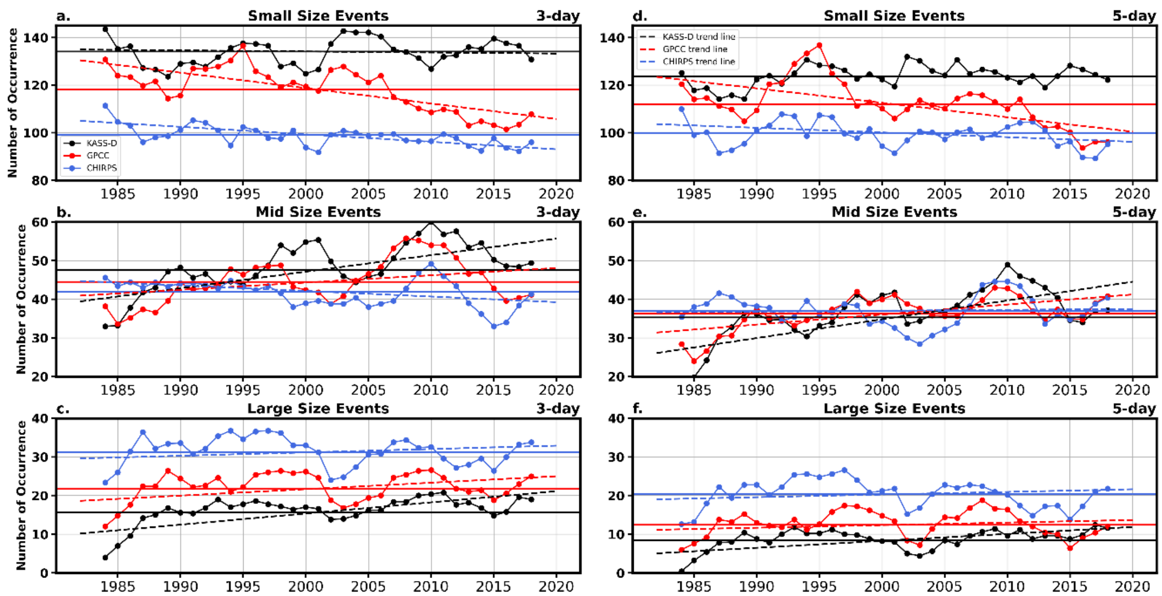

Figure 4.21: The 5-year running mean of an annual mean of small-size (1-9 grid cells), mid-size (10-20 grid cells), and large-size (greater than 20 grid cells) events of 3-day (a-c) and 5-day (d-f) intense wet spells over the interpolation domain.

NOTE: Color thick horizontal lines and broken lines depict long-term mean and trend lines, respectively, from 1982 to 2020.

Table 4.2: Mann-Kendall trend test result for different sizes of 3-day and 5-day intense multi-day wet spells over the study domain. The bold p-value indicates a statistically significant trend at a 0.05 significant level.

		3-day			5-day		
Data	Size Classification	Trend	Sen's Slope	p-Value	Trend	Sen's Slope	p-Value
KASS-D	Small Size	no trend	0.00	0.932	no trend	0.00	1.000
	Mid-Size	increasing	0.421	**0.008**	increasing	0.461	**0.011**
	Large Size	increasing	0.333	**0.004**	increasing	0.210	**0.020**
GPCC	Small Size	decreasing	-0.629	**0.007**	no trend	-0.583	**0.004**
	Mid-Size	increasing	0.228	0.135	no trend	0.227	0.051
	Large Size	no trend	0.187	0.123	no trend	0.060	0.593
CHIRPS	Small Size	decreasing	-0.375	0.089	no trend	-0.25	0.389
	Mid-Size	no trend	-0.166	0.111	no trend	0.00	0.980
	Large Size	no trend	0.161	0.194	no trend	0.1333	0.383

4.2.4 Average Size and Maximum Size

The average and maximum size of intense events in a year indicate the mean and largest size of all such events within that year. This helps determine whether extreme events are becoming larger and affecting larger areas over time. Figure 4.22 shows the annual average and maximum size of both 3- and 5-day intense wet spells for all the datasets. The average size of 3-day and 5-day intense wet spells by KASS-D, GPCC, and CHIRPS over the years are similar. Long-term average size of 3-day and 5-day intense wet spells by KASS-D are 8.5 and 7 grid cells while GPCC are 9.5 and 8 grid cells and CHIRPS are 11.5 and 10 grid cells, respectively, making CHIRPS with the highest long-term average size among the datasets due to its TIR-CCD information. Before 1990, the average size of 3-day (5-day) intense events increased from 5 (4) grid cells in 1984 to 9 (8) grid cells depicted by KASS-D (Figure 4.22a). From 2004, average size of both intense events continues to increase in KASS-D until the end of the study period. However, 1991, 1994, 2009, and 2019 are the noticeable years with an average size of both intense events exceeding 9 grid cells. Also, there are periods like 1995-1998 and 2000-2006 (Figure 4.22a) when 3-day and 5-day average sizes were observed below the long-term mean despite the increase that occurred in the average size of the intense events over the years. GPCC in Figure 4.22b shows an upward trend in the average size of intense wet spells similar to what is displayed by KASS-D. With correlation coefficient equal or greater than 0.7 (Figure 4.23), there is fair agreement among all the datasets when there is an increase or reduction in the average size of the two intense wet spells that signal a strong correlation between the time series.

For KASS-D in Figure 4.22d, the maximum size of 3-day and 5-day intense events increased from 19 and 24 to 53 and 47 grid cells, respectively, between 1982 and 1998, despite the occurrence of years with a decrease in maximum size. After this period, a pronounced decrease in maximum size occurred when the maximum size of 3-day and 5-day wet spells were far below the long-term mean. Comparing this observed pattern to GPCC and CHIRPS (Figure 4.22e-f), they are similar with differences in the number of grid cells. For example, KASS-D's highest number of grid cells for a maximum size of 3-day and 5-day events occurred in 2019 (Figure 4.22d) with over 50 grid cells but in GPCC (Figure 4.22e), it occurred in 2007 with 78 grid cells for 3-day events and 1991 with 62 grid cells for 5-day intense events. This is also true for CHIRPS (Figure 4.22f) in 1999 and 2007 with higher number of grid cells. As shown in Table 4.4, only KASS-D and GPCC exhibit statistical significance increasing trend with respect to the average and maximum size of 3-day and 5-day intense events while CHIRPS has no trend.

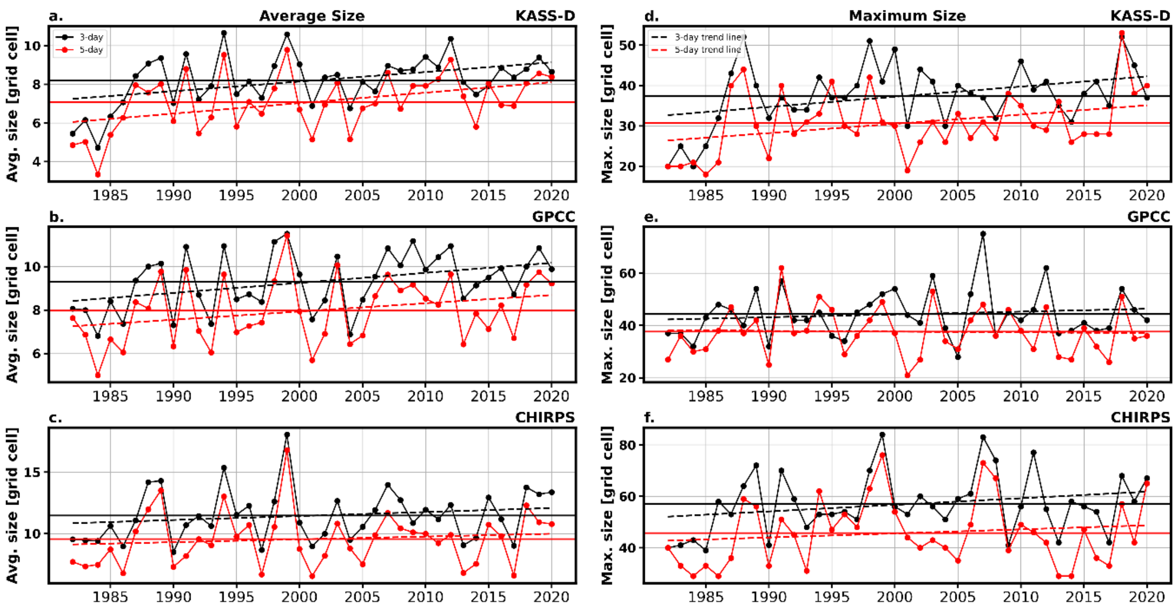

Figure 4.22: Average and maximum size annual time series of 3- (left panels) and 5-day (right panels) intense wet spells over the domain. Black and red thick (dashed) lines represent the climatological mean (trend line) of intense 3- and 5-day frequency of occurrence.

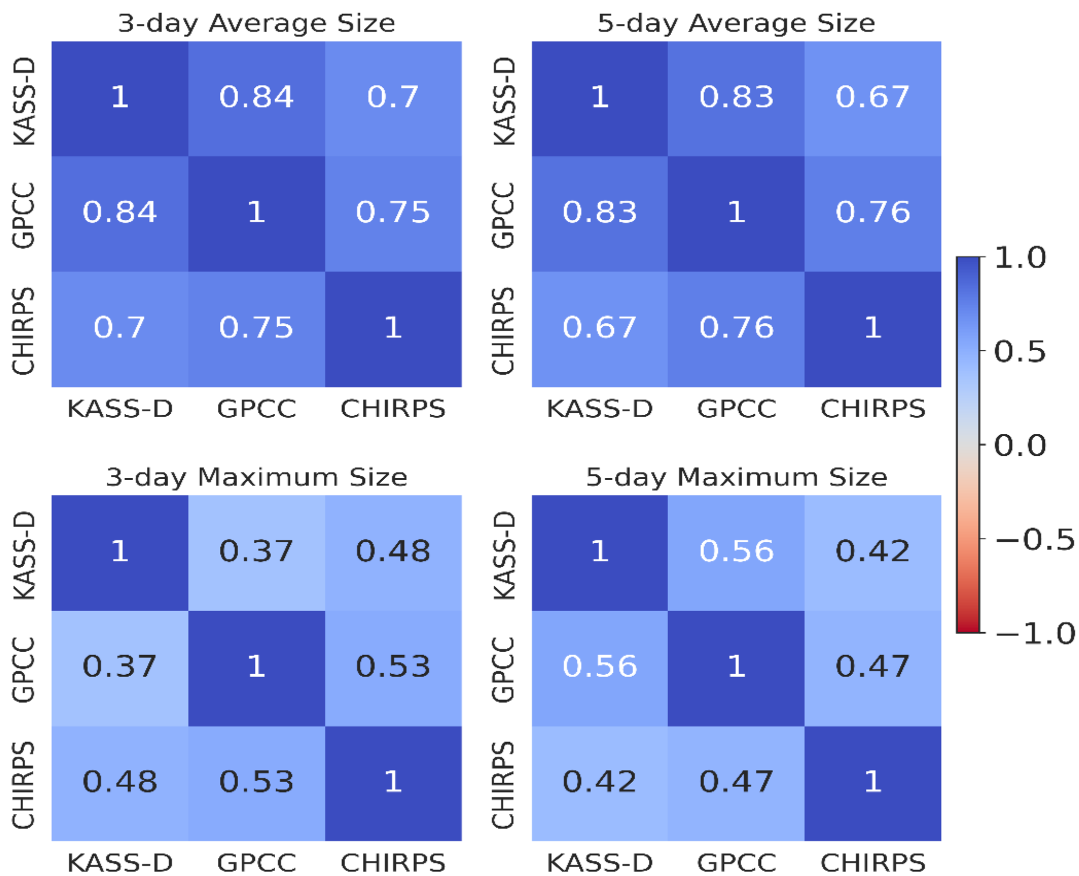

Figure 4.23: Correlation of average size and maximum size of 3- and 5-day intense events among the three datasets (KASS-D, GPCC and CHIRPS)

Table 4.3: Mann-Kendall trend test result for the annual average size of 3-day and 5-day intense multi-day wet spells over the study domain. The bold p-value indicates a statistically significant trend at a 0.05 significant level.

Data	Intense Event Duration	Trend	Sen's Slope	p-Value
KASS-D	3-day	increasing	0.071	**0.001**
	5-day	increasing	0.064	**0.008**
GPCC	3-day	increasing	0.048	0.014
	5-day	no trend	0.040	0.090
CHIRPS	3-day	no trend	0.050	0.090
	5-day	no trend	0.040	0.191

Table 4.4: Mann-Kendall trend test result for the annual maximum size of 3-day and 5-day intense multi-day wet spells over the study domain. The bold p-value indicates a statistically significant trend at a 0.05 significant level.

Dataset	Intense Event Duration	Trend	Sen's Slope	p-Value
KASS-D	3-day	increasing	0.250	**0.049**
	5-day	increasing	0.217	**0.047**
GPCC	3-day	no trend	0.090	0.459
	5-day	no trend	0.0	0.903
CHIRPS	3-day	no trend	0.272	0.067
	5-day	no trend	0.133	0.489

4.2.5 Contribution of Extreme Intense Wet Spells to Annual Rainfall

Figure 4.24 displays the 3-year running mean of the percentage contribution of 3- and 5-day intense wet spells to annual rainfall across the Guinea Coast, Savannah, and Sahel. The Guinea Coast shows the highest long-term mean proportion of annual rainfall from these intense events, while the Sahel has the lowest. KASS-D indicates an increasing trend in the contribution of intense wet spells across all climatic zones, with the most significant rise in the Sahel (Figure 4.24a-c). For KASS-D, the contribution of 3-day (5-day) intense wet spells rose from 27% (24%) in the 1980s to 36% (33%) by the end of the study period in the Guinea Coast (Figure 4.24a). Over the Savannah, the contribution increased from 22% (16%) to 38% (30%) (Figure 4.24b), and in the Sahel, it rose from 15% (6%) to around 35% (26%) (Figure 4.24c). GPCC and CHIRPS reveal a lesser visible increase in the contribution to annual rainfall over Guinea Coast and Savannah, while GPCC reflects a similar increase in the Sahel from 15% (8%) to about 30% (24%) (Fig 14f). Panthou *et al*. (2014) also reported an increase in the percentage of annual rainfall from extreme events in the central Sahel over different decades but more from daily extreme.

Despite variations in the contribution patterns, datasets generally agree on the trends of intense wet spells during dry and wet periods. In the 1980s, a drought period (Nicholson 2012), the contribution of 3- and 5-day intense wet spells was below the long-term mean, particularly in the Savannah and Sahel. This trend persisted in the Guinea Coast and Savannah into the late 1980s and mid-1990s, respectively, before surpassing the long-term mean. The same pattern occurred during the dry periods of 2000-2005 and 2012-2015, with significant decreases over the Guinea Coast and lesser impacts in the Savannah and Sahel. Notably, from 2006 to 2010, all datasets consistently show an increase in the percentage contribution of intense wet spells above the long-term mean during the wet period when annual rainfall was higher than long-term mean.

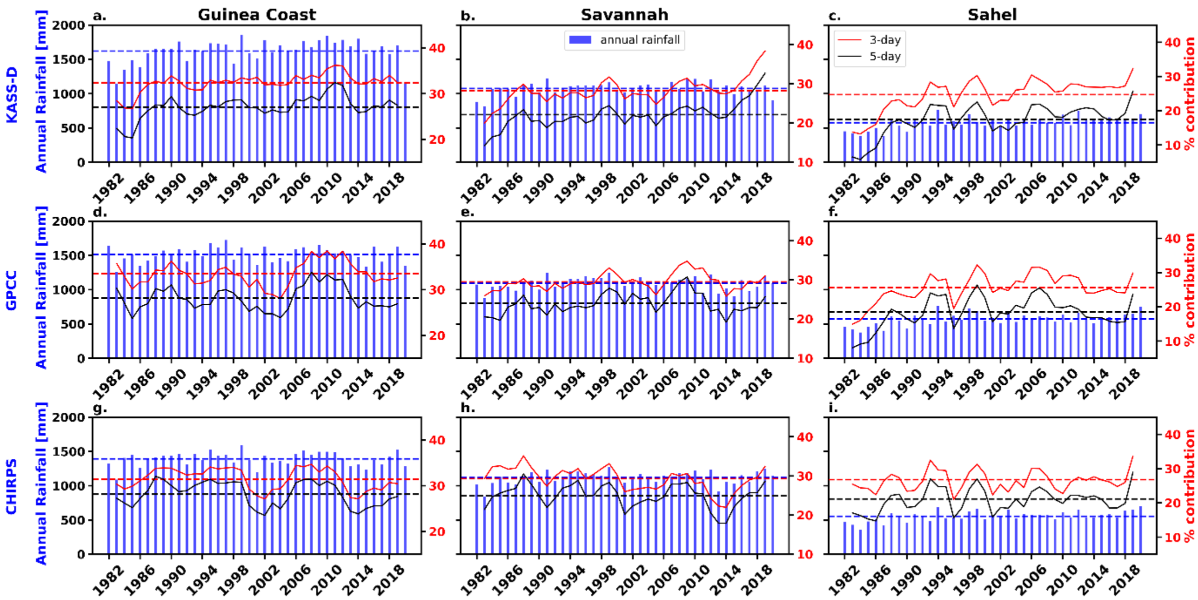

Figure 4.24: Three-year running mean of the percentage contribution of 3- and 5-day intense wet spells to annual rainfall (right axis) and total annual rainfall (left axis) over Guinea Coast Savannah, and Sahel from for KASS-D (a–c), GPCC (d–f), and CHIRPS (g–i).

NOTE: Broken red and black lines represent the annual long-term mean of the percentage contribution of intense 3- and 5-day wet spells to annual rainfall from 1982-2020 while the broken blue line depicts the climatological mean of annual rainfall.

4.3 DYNAMICS OF INTENSE MULTI-DAY WET SPELLS

This section presents the climatological descriptions of all the variables used, the dynamics associated with wet and intense multi-day wet spells as highlighted under methodology section. Composite analysis was employed to systematically identified environmental factors contributing to the development and sustenance of multi-day wet spells and intense multi-day wet spells. First, the distinct differences between environmental factors associated with a typical wet and dry spells were identified, then, followed by intense multi-day wet spells over West Africa.

Subsections 4.3.1, 4.4.1, 4.4.2, 4.4.3 and 4.4.4 discuss some key environmental factors responsible for the evolution and sustenance of intense multiday wet spells. The parameters used are the Convective Available Potential Energy (CAPE), Convective Inhibition (CIN), Column Vertically-Integral Water Vapor (TCWV), Vertical Integral of Divergence of Moisture Flux (VIDMF), Vertical Integral of Eastward Water Vapor (VIEWV) and Vertical Integral of Northward Water Vapor (VINWV).

4.3.1 Climatological Description of Vertically Integrated Fluxes and Upper-Level Variables

Figure 4.25 depicts the daily climatological mean of rainfall, convective indices (CAPE and CIN) and moisture fluxes (VIMVD, VIEWV and VINWV) integrated vertically from the surface of the earth to the top of the atmosphere. Climatological mean of daily rainfall shows that western coastal and the Guinea coastal regions received the highest amount of rainfall more than 80 mm/day owing to higher amount of TCWV that both decrease latitudinally. Convective activities measured by high CAPE value (600 - 3000 J/kg) and CIN values that ranges between 200 J/kg and 900 J/kg dominate the region south of 15°N and the coast. Within the Guinea Coast, CAPE values observed to be less than 1000 J/kg revealed the less influence of this convective indices on rainfall within this climatic zone. For the VIMVD, a negative value indicates moisture flux convergence (hereafter, MFC) while positive value depicts moisture flux divergence (MFD). Over the West

Africa, area of MFC coincide with area of high daily rainfall amounts (Figure 4.25a & e) while the climatology of VIEWV and VINWV together with their vector plot show that water vapor flux traveled from southeasterly (east) to the west of West Africa. At 1000, 850, 650 and 200 hPa levels, Figure 4.26 shows the spatial daily mean climatology of zonal and meridional winds overlay with wind vectors and specific humidity over West Africa. At 1000 hPa (surface) level, continental southwesterly monsoon winds penetrated West Africa up to 19°N with maximum wind speed along the coast and within the norther Sahel. At 850 hPa level, southwesterly winds that dominate west Africa is restricted to the south of 15°N with observed easterly winds in the north of this latitude. Also, noted at this level is the strong wind in the Bodelé depression. However, strong easterly winds dominate West Africa at 650hPa and 200 hPa levels. Occurred at 650 hPa level, is a strong easterly wind known as AEJ with core speed of about 14 m/s around 15°N closer to the West Coast. AEJ formed due to the thermal contrast between the hot, dry Sahara air mass to the north of 15°N and the cooler, moist monsoon flow to the south. (Fink *et al*. 2004). Daily, this jet speed can exceed 20 m/s as reported by Thorncroft *et al*. (2003). Likewise, TEJ is seen at 200 hPa with it core around 8°N (Figure 4.26h). This TEJ unlike the one formed from the Indian Monsoon region located at higher altitude and around 15°N, suspected to formed because of the geopotential height gradient within the south of the upper-level Saharan anticyclone and outflow from the upper-level convection over the Sahel and central equatorial Africa. Over the south of 15°N and at 1000hPa level, specific humidity is greater than 13 kg/kg and this decrease with height (Figure 4.26).

The daily climatological cross-sections averaged over the monsoon season (June–September) from 1982–2020 shown in Figure 4.27 reveal the classical features of a dynamically coupled monsoon system, consistent with earlier findings (e.g., Cook, 1999; Nicholson, 2013) over West Africa. The zonal wind field (Figure 4.27a) exhibits strong low-level westerlies (positive values) below 800 hPa that extend between 2° and 18°N. This is a characteristic of the West African southwesterlies monsoon flux that transport humidity into inland during monsoon season (Diallo *et al*., 2010). Also, a distinct mid-tropospheric easterly maximum around 600 hPa near 15°N that represent the core of the AEJ that serves as a dynamical driver for synoptic-scale disturbances. Upper-tropospheric easterlies centered around 7°N at 200 hPa mark the occurrence of TEJ associated with upper-level divergence. The meridional wind in Figure 4.27b depicts southerly flow in the lower levels, especially south of 10°N that support poleward moisture transport from the Gulf of

Guinea. Vertical velocity (Figure 4.27c) reveals negative values (upward motion) between 5°–15°N, concentrated below 800 hPa and between 850–400 hPa show the persistent deep convective activity in the monsoon trough. This is supported by negative divergence (Figure 4.27d) in the lower troposphere. This reflects horizontal convergence and upward motion coupled with weak upper-level divergence that suggests gradual mass evacuation. Specific humidity (Figure 4.27e) peaks in the lower troposphere between 5°–10°N, showing a well-moistened monsoon layer that is conducive for convection activities. However, positive relative vorticity in Figure 4.27 dominates the mid-troposphere over the same latitudinal band, signifying enhanced cyclonic shear and atmospheric instability that dynamical support ascent of airmass. Collectively, these features depict the canonical monsoon structure over the Guinea Coast and Sahel of West Africa characterized by moist low-level inflow. This is convectively favourable for vertical motion, and dynamical jet interactions that sustain rainfall delivery during WAM season (Thorncroft *et al.*, 2003, Sultan & Janicot, 2003; Parker *et al*., 2005).

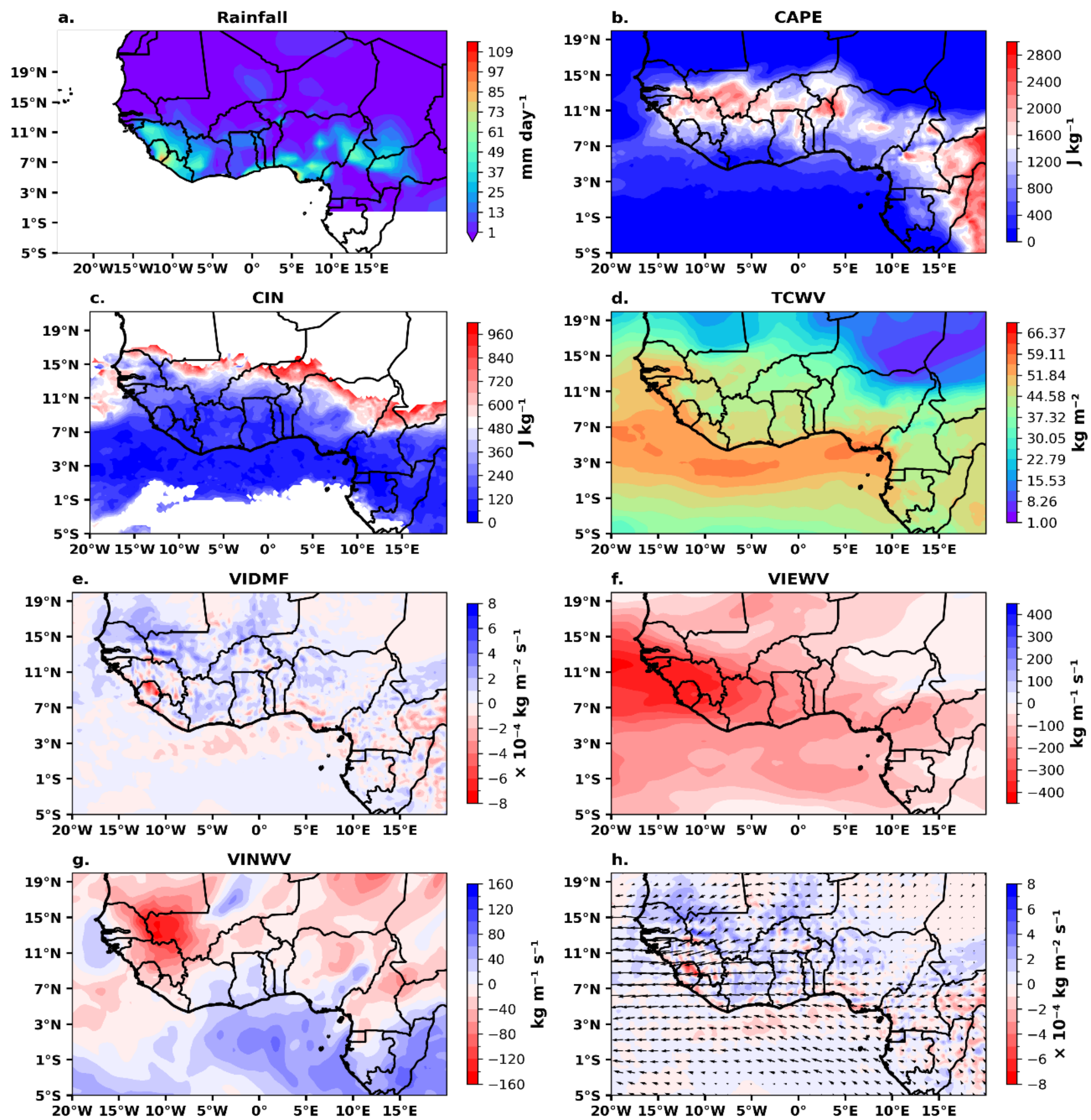

Figure 4.25: Daily climatological mean of rainfall (a), CAPE (b), CIN (c), TCWV (d), VIDMF (e), VIEWV (f), VINWV (g) and VIDMF overlay with vector from VIEWV and VINWV (h).

NOTE: Negative and positive values of VIMVD indicate moisture convergence and divergence, respectively.

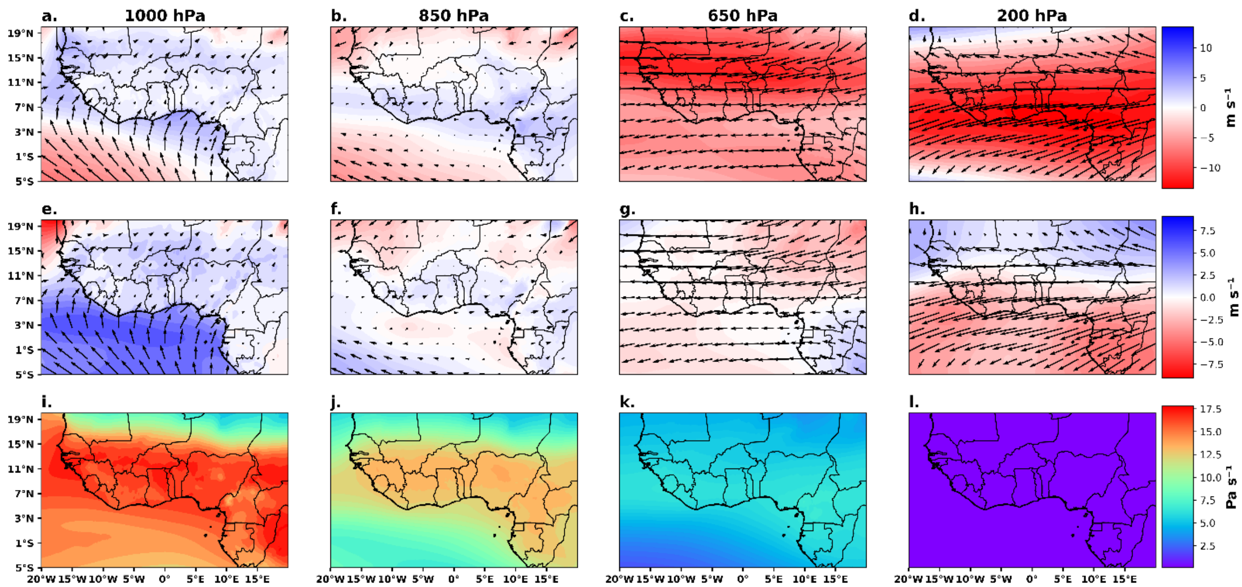

Figure 4.26: Daily climatology of zonal wind (first row), meridional wind (second row) and specific humidity (third row) at 1000 hPa (a, e, i), 850 hPa (b, f, j), 650 hPa (c, g, k) and 200 hPa (d, h, i) levels.

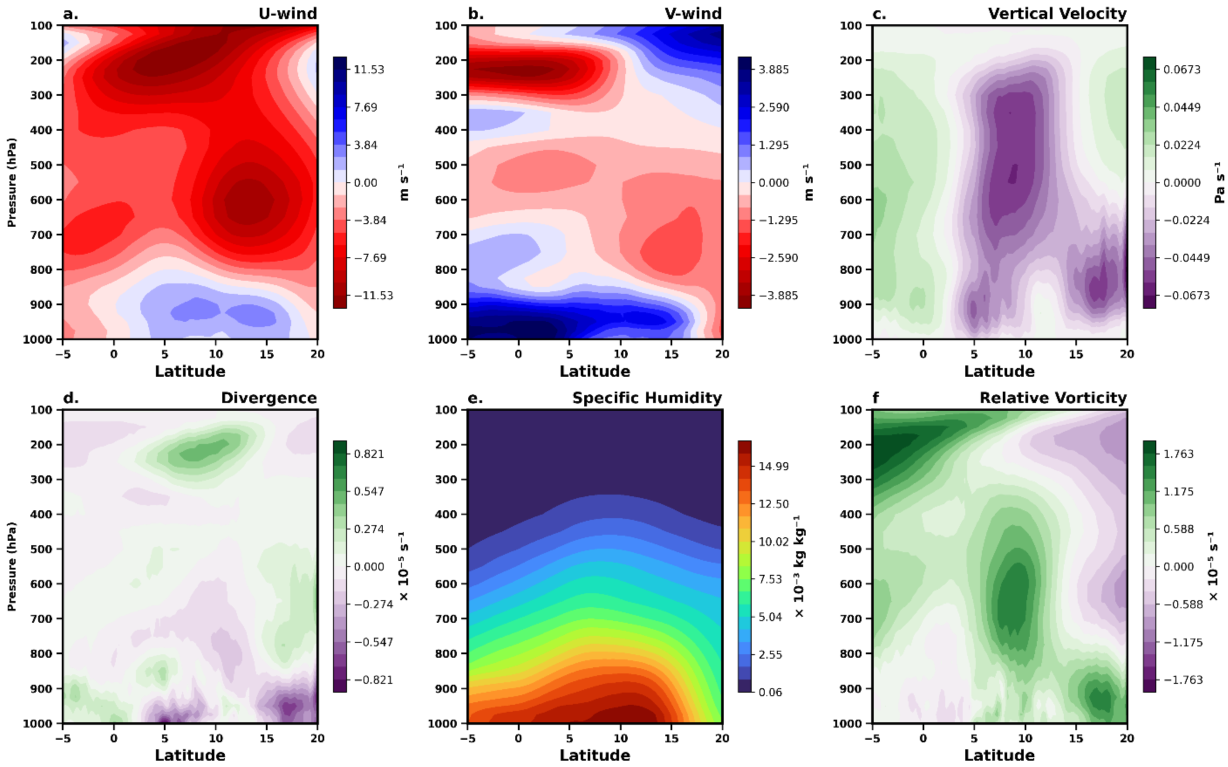

Figure 4.27: Climatological daily mean meridional cross-sections of key atmospheric variables averaged over the monsoon season (June–September) from 1982–2020 over the West African region.

NOTE: Panel (a) Zonal wind (m s^{-1}); (b) Meridional wind (m s^{-1}); (c) Vertical velocity (Pa s^{-1}); (d) Divergence ($\times 10^{-5}$ s^{-1}); (e) Specific humidity ($\times 10^{-3}$ kg kg) and (f) Relative vorticity ($\times 10^{-5}$ s^{-1}).

4.3.2 Large-scale Atmospheric Conditions Associated with a Typical Wet and Dry Spell

Using a typical wet and dry spells identification criterion specified under methodology section, a total of 242 wet spell days and 968 dry spell days were identified during the summer monsoon season over the period 1982–2020 based on KASS-D. The composite rainfall and atmospheric circulation analysis (Figure 4.28) highlights distinct and contrasting patterns associated with these wet and dry spells. During wet spells, the larger part of Guinea Coast of West Africa (south of 8°N) exhibits significantly enhanced rainfall anomalies exceeding 1.6 mm/day, with this anomaly spatially decreasing northward. In contrast during the same wet spells, regions north of 8°N and prominent orographic areas such as the Cameroon Mountains, Adamawa Highlands, Jos Plateau and Fouta Djallon experience suppressed rainfall anomalies during these episodes (Top left panel in Figure 4.28). Conversely, the pattern reverses during dry spell phases with a marked reduction in rainfall (anomalies < –1.6 mm/day) observed over the Guinea Coast and accompanied by enhanced rainfall anomalies over the north of 8°N and highland regions (Top right panel in Figure. 4.28).

The low-level wind patterns at 850 hPa illustrate the characteristic behavior of the Low-Level Jet (LLJ) during both wet and dry spells over west Africa (Figure 4.28b, f). During wet spell phases, there is a notable anomalous intensification of westerly winds (> 0.15 m/s) across the Guinea Coast region (south of 8°N), accompanied by a weakening of westerlies to the north of 8°N (< –0.15 m/s) in the Savannah and intensification of westerlies in the most part of the Sahel. This wind configuration signals a strengthening of moisture transport into the Guinea Coast. In contrast and during dry spells (Figure 4.28f), the anomalous weakening of westerlies over the same coastal region along with a strengthening of westerlies north of 8°N is an indicative of moisture export from the coastal regions. Hence, these circulation changes modulate moisture transport (export) that leads to enhanced (reduced) fluxes towards (from) the Guinea Coast during wet (dry) spells.

This moisture transport pattern is corroborated by anomalies in specific humidity at 850 hPa that exhibit positive (negative) deviations across latitudes south (north) of 12°N with the strongest enhancement concentrated along the coastal area during wet spells (Figure 2.28c). However, during dry spells (Figure 4.28g), specific humidity anomalies are negative across the same latitudinal band with the most pronounced reductions near the coast but positive in the north of 12°N. Furthermore, these circulation and humidity patterns are closely tied to anomalies in Outgoing Longwave Radiation (OLR). Wet spell events coincide with reduced OLR values (Figure 4.28d) over the coastal region that highlight increased cloud cover and convective activity. Dry spell periods exhibit positive OLR anomalies (Figure 4.28h), signaling reduced cloudiness and suppressed rainfall. The negative OLR anomalies reflect widespread cloud formation that is conducive for rainfall while the positive anomalies observed during dry phases highlight a drier and clearer atmosphere.

This dipole-like structure in rainfall, circulation, specific humidity and OLR bears resemblance to patterns documented over the Pra River catchment in Ghana, where moisture convergence and elevated column water vapor were found to enhance wet spells (Osei *et al*., 2021). The concurrent low-level westerlies and inland moisture transport, along with a ridge formation at 850 hPa, appear to support the development of wet spells during the June–July–August (JJA) monsoon season. Also, this spatial shift in rainfall anomalies between wet and dry spells is an indicative of the break phase of the WAM system that reflects the fundamental dynamics of monsoonal variability and its associated circulation features. A similar dipole circulation in rainfall pattern has also been reported in South Asian monsoon regions, particularly over India (Resmi *et al*., 2023; Prathipati *et al*., 2021) that further reinforce the broader applicability of these findings to global monsoon systems.

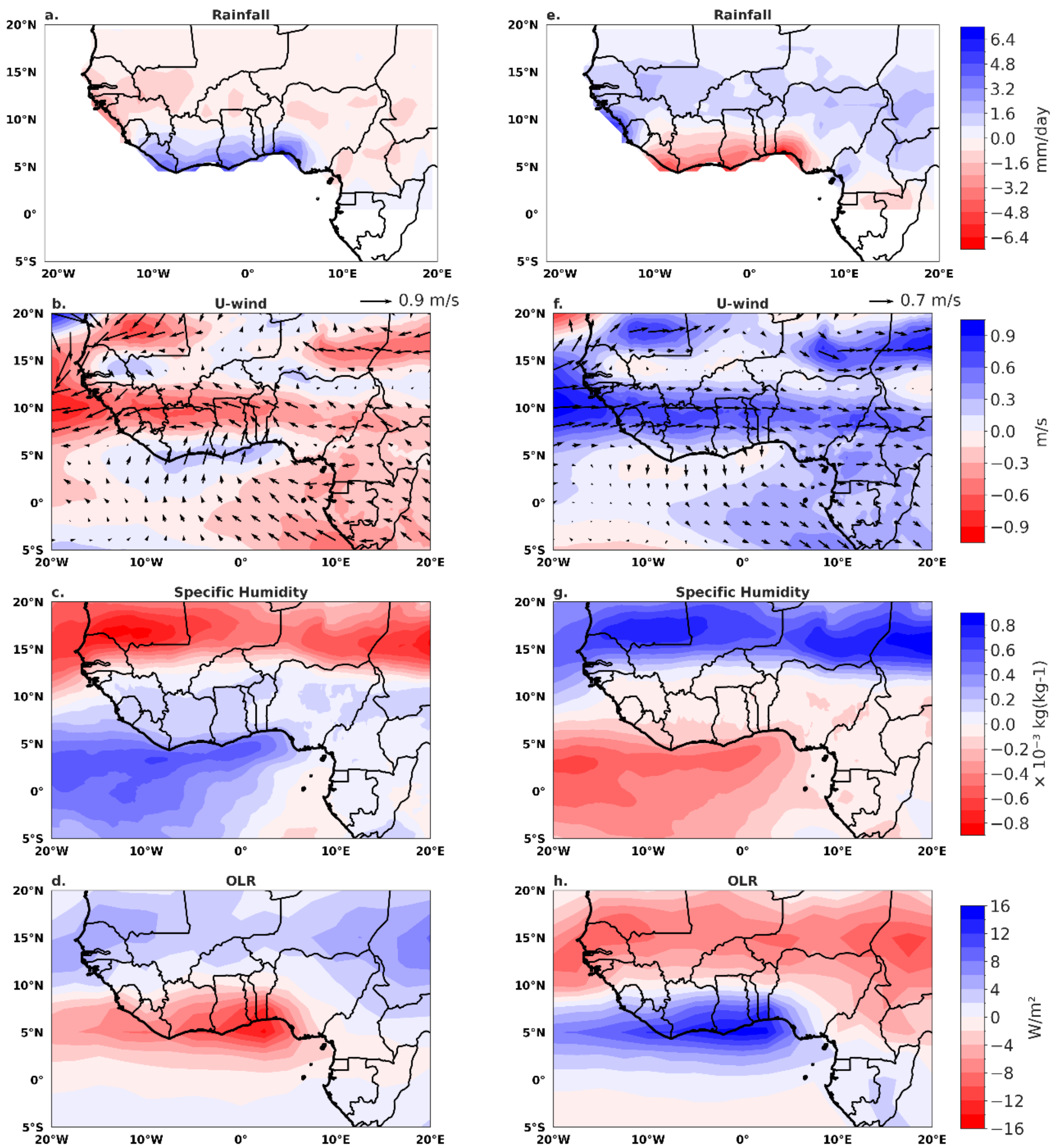

Figure 4.28: Composite anomaly of different variables calculated by subtracting daily climatological mean for 1981–2020 during wet (left panel) and dry (right panel) spells.

NOTE: Rainfall from GPCC gridded data (a, e), zonal winds overlay with wind streamlines (b, f), specific humidity (c, g) at 850 hPa from ERA5, and NOAA interpolated outgoing longwave radiation (d, h). The anomaly is calculated by subtracting the daily climatological mean for 1981–2020.

4.3.3 Evolution of large-scale atmospheric conditions and vertical profile of wind circulation during wet and dry spells

To show the potential precursors of a typical wet and dry spell events, a composite analysis of large-scale circulation patterns was conducted for the period spanning five days prior (Day –5) to six days after (Day +6) each spell onset with 'Day' representing the initiation/start of the event. Over the study period, 342 wet spell days were identified from which 107 independent wet spell events were selected using the first day of each spell for lead–lag analysis. A similar approach was applied to dry spells yielding 212 distinct cases based on their onset day.

Five days before the onset of wet spells (Day –5), easterly wind anomalies become dominant over West Africa and adjacent oceanic regions at 850 hPa that suggests a weakened cross-equatorial moisture flux (Figure 4.29a). By Day –1 (a day before the start of wet spells), a weakened low-level westerly curtails moisture transport into the coastal region of Nigeria, Benin, Togo and Ghana while northeasterly flow intensifies over other area of West Africa (Figure 4.29e). At the beginning of wet spells (Day), a marked intensification of southwesterly winds emerges over the coastal zone that coincides with the development of an anomalous cyclonic circulation off the Ivory Coast (Figure 4.29f). This system facilitates moisture advection from Central Africa, merging with strengthened southwesterlies from the Atlantic Ocean that further collectively steer moisture northeastward into the Guinea Coast. By Day +1, the cyclonic anomaly strengthens and shifts westward and continue sustaining inland moisture transport (Figure 4.29g). However, by Day +2, the westerly anomalies weaken that diminish moisture inflow while northeasterly winds begin to migrate southward. From Day +3 up to Day +5, easterly anomalies originating from Central Africa essentially dominate the region limiting moisture convergence and thus rainfall (Figure 4.29i–l).

In contrast, dry spell events are preceded by positive westerly anomalies over larger part of West Africa starting at Day –5 that progress with intensification through Day –1 (Figure 4.30a–e). However, by Day –3, enhanced low-level westerlies over land and ocean introduce excessive moisture into the Guinea Coast that potentially disrupting convection initiation. At the onset ('Day'), this regime transitions into enhanced easterly anomalies that persist through Day +1 (a day after the onset) by redirecting moisture away from the southern and western part of West Africa (Figure 4.30f–g). Although these easterlies weaken by Day +2 and Day +3, westerly anomalies over the ocean persist and likely to have suppress convection. This was confirmed in by the anomalous increase in the CIN from the onset ('Day') of the dry spell up to Day +4 in Figure 4.31. This anomalous increase in CIN suspected to hinder the formation of moist and deep convection in parts of West Africa like the Guinea Coast.

Climatologically, the LLJ is a southwesterly monsoon flux extending between 2° and 20°N from 1000 to 850 hPa and is instrumental in transporting humidity inland during boreal summer (Diallo *et al*., 2010). At mid-troposphere, the African Easterly Jet (AEJ) operates between 500–700 hPa, peaking at around 15 m/s near 15°N, while the Tropical Easterly Jet (TEJ) forms aloft near 7°N at 200 hPa during summer. The vertical structure of zonal winds along the study area within the Guinea Coast during wet spells (Figure 4.32) reveals a pronounced easterly anomaly in the lower troposphere (1000–800 hPa) prior to onset (Figure 4.32a–e) that signal a reduction in monsoon depth. At mid-levels (700–500 hPa), the AEJ weakens and decreasing dry air entrainment. Simultaneously, the TEJ strengthens and promote upper-level divergence and deep convection. These anomalies persist post-onset (Figure 4.32f–l) with sustained low-level easterlies, continued

AEJ weakening and persistent TEJ enhancement. These collectively foster a convectively favorable environment.

Conversely, during dry spells (Figure 4.33), positive zonal wind anomalies in the lower troposphere suggest strengthened westerlies that paradoxically suppress rainfall by diminishing low-level convergence. The AEJ that intensifies promote mid-level subsidence while the TEJ weakens and limiting upper-level divergence. These unfavorable conditions continue after onset with persistent low-level westerlies, enhanced AEJ-induced subsidence, and suppressed TEJ activity. All these contribute to reduce the potential for convective processes. Enhanced westerly anomalies in the mid-troposphere can induce subsidence warming and disrupt vertical ascent, thereby suppressing convective development. Such disruptions alter the meridional thermal and moisture gradients that drive the West African monsoon, weakening low-level convergence and the convective triggers necessary for rainfall (Hsieh & Cook, 2007; Pu & Cook, 2012). This anomalous circulation regime appears to inhibit both dynamical uplift and thermodynamic instability that ultimately play a pivotal role in the onset and maintenance of dry spells. This mechanism is further substantiated by the positive anomalies in OLR over the Guinea Coast during dry spells (Figure 4.31). Elevated OLR indicates reduced deep convection and a stabilized atmospheric column (Liebmann & Smith, 1996; Janowiak et al., 2001). Although moisture is a necessary condition for convection, an oversaturation in the mid-to-upper troposphere can paradoxically suppress it. Excess moisture can weaken the vertical lapse rate, reduce buoyancy and lower CAPE that are critical for deep convection (Emanuel, 1994; Sherwood *et al.*, 2010). Additionally, the formation of extensive stratiform clouds under such moist conditions can limit surface solar heating which further reducing atmospheric instability and suppressing convection (Houze, 2004; Posselt *et al.*, 2008).

The temporal evolution of key atmospheric parameters that include rainfall, relative humidity at 700 hPa and 850 hPa zonal winds is shown in Figure 4.34. During wet spell episodes, zonal wind anomalies exhibit a marked increase in wind speed post-onset until Day +3, after which a gradual decline is observed. In contrast, dry spells show a reversal with decreasing wind speeds initially and followed by a sustained increase. Relative humidity anomalies display a lead time of one day and a lag time of five days combined with elevated humidity levels from Day –1 to Day +4 during wet spells. This underscores their critical role in preconditioning the atmosphere for rainfall events. The coupling between low-level zonal wind anomalies and rainfall variability underscores the potential of LLJ diagnostics as early predictors for the onset of wet and dry spells. Such precursors are particularly valuable in the context of intensifying monsoon variability and extremes.

While adequate moisture is necessary for convection, excessively strong low-level westerlies can paradoxically suppress rainfall by weakening vertical ascent and reducing convergence (Holton, 2004; Cook, 1999). These westerlies can overshoot inland and disrupting the balance between the LLJ and AEJ, thereby impeding the uplift of moist air (Sultan & Janicot, 2003; Houze, 2004). Furthermore, excessive moisture in the mid-to-upper troposphere may lead to atmospheric stabilization, diminishing the surface-to-upper-level temperature gradient and at the same time reducing convective buoyancy (Emanuel, 1994). Additionally, this can foster the development of stratiform clouds which reduces surface heating and available convective energy (Houze Jr, 2014).

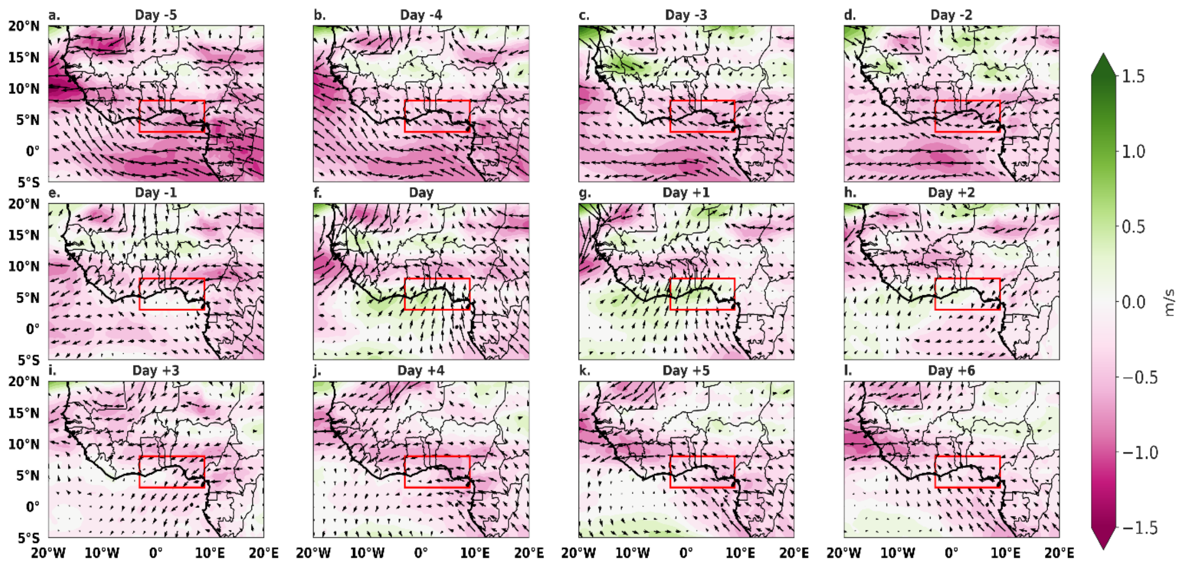

Figure 4.29: Composite anomaly of zonal wind in m/s overlaid with wind vector at 850 hPa from Day-5 before to Day + 6 days after the start of wet spells. 'Day' in the plot depicts the first date/day of the wet spells. NOTE: Anomalies were computed by subtracting the climatological daily mean from 1982-2020.

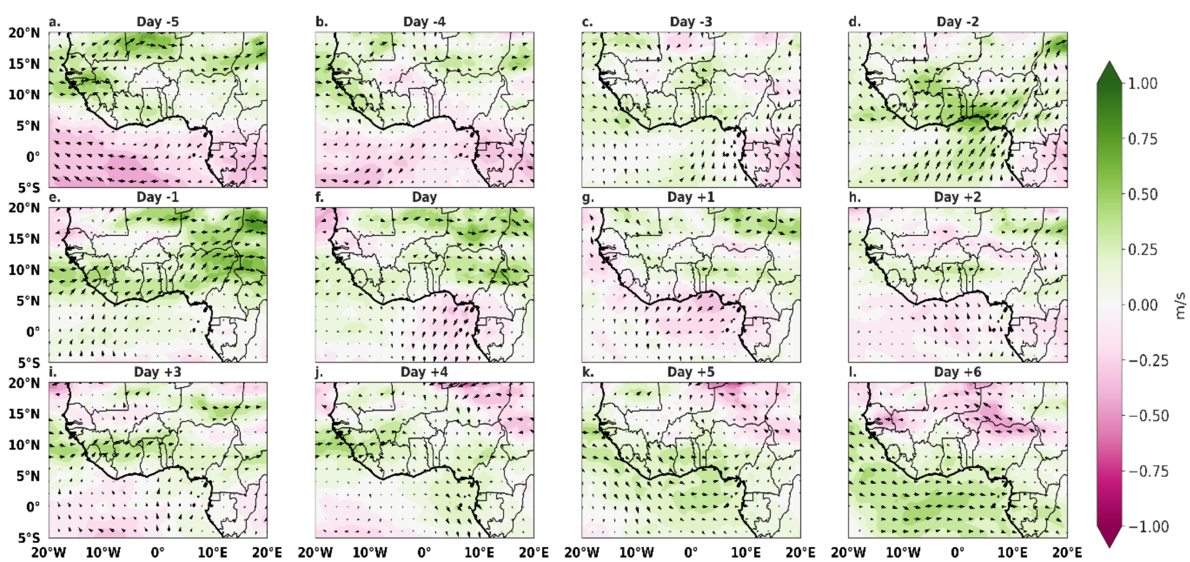

Figure 4.30: Composite anomaly of zonal wind in m/s overlaid with wind vector at 850 hPa from Day-5 before to Day + 6 days after the start of dry spells. 'Day' in the plot depicts the first date/day of the wet spells. NOTE: Anomalies were computed by subtracting the climatological daily mean from 1982-2020.

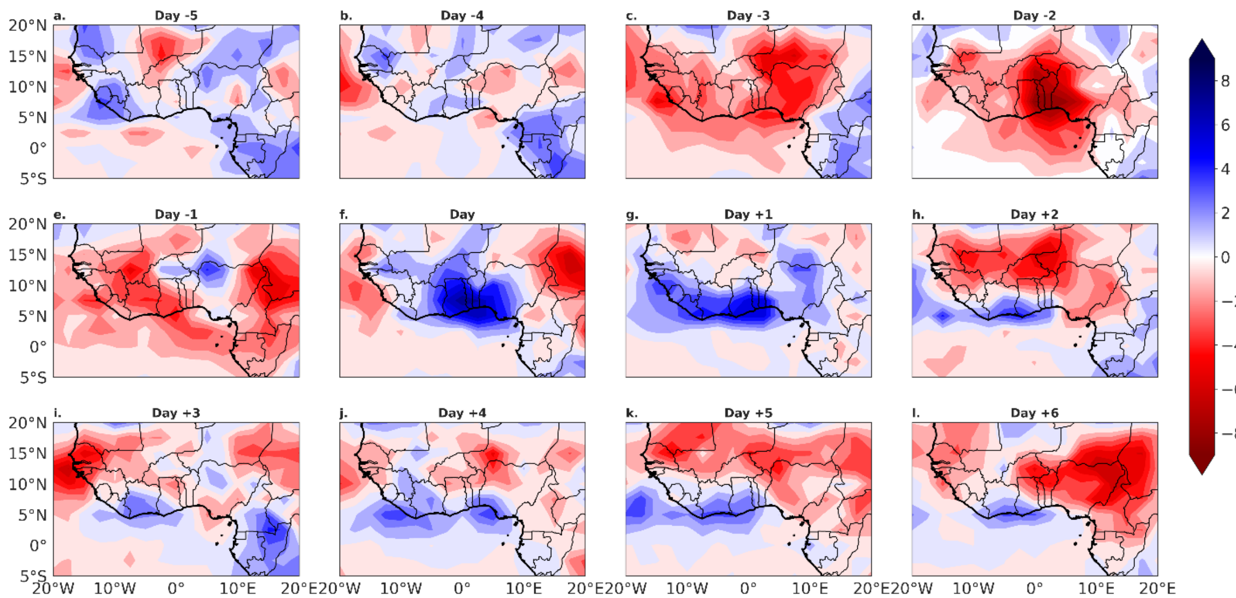

Figure 4.31: Composite anomaly of OLR in Wm^{-2} from Day-5 before to Day + 6 days after the start of dry spells. 'Day' in the plot depicts the first date/day of the wet spells.

NOTE: Anomalies were computed by subtracting the climatological daily mean from 1982-2020.

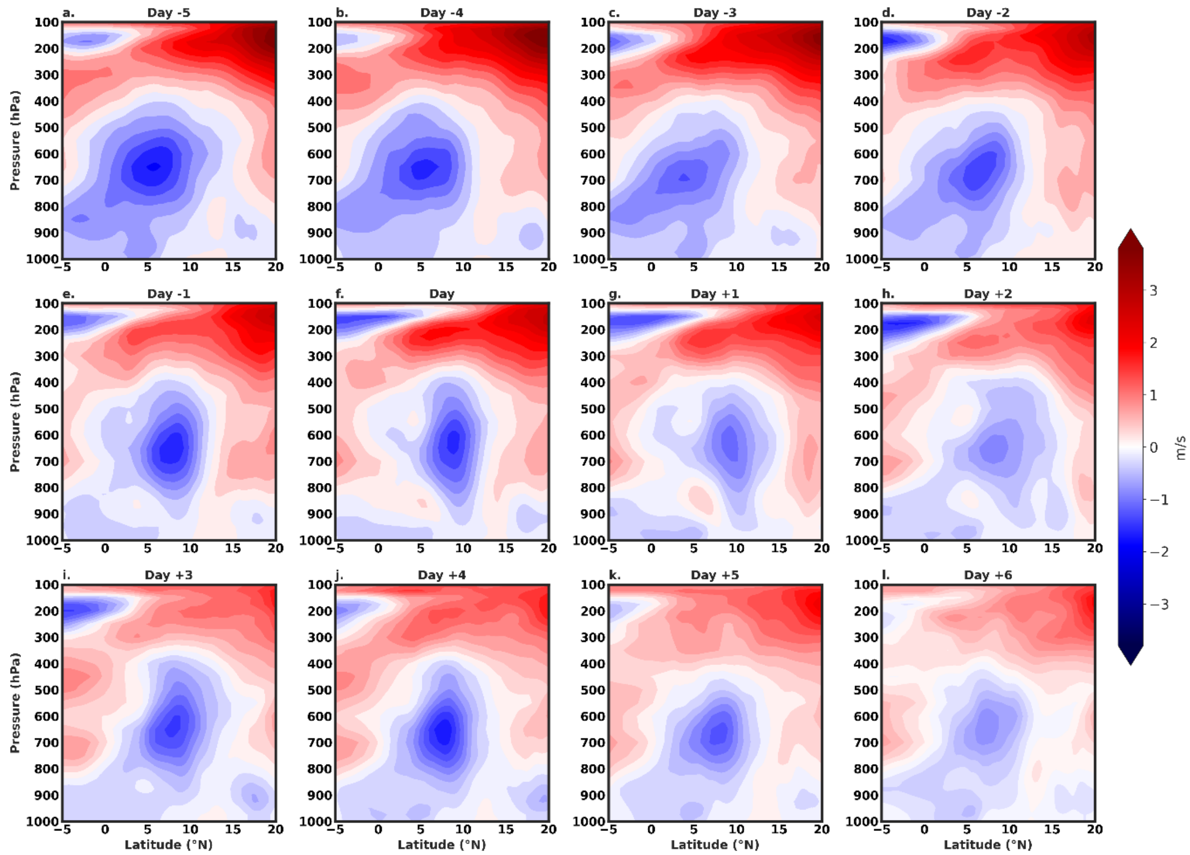

Figure 4.32: Meridional cross-section of zonal wind anomaly in m/s from 1000 hPa to 100hPa from Day-5 before to Day + 6 days after the start of wet spells and averaged between 3°W and 9°E. 'Day' in the plot depicts the first date/day of wet spells.

NOTE: Anomalies were computed by subtracting the climatological daily mean from 1982-2020.

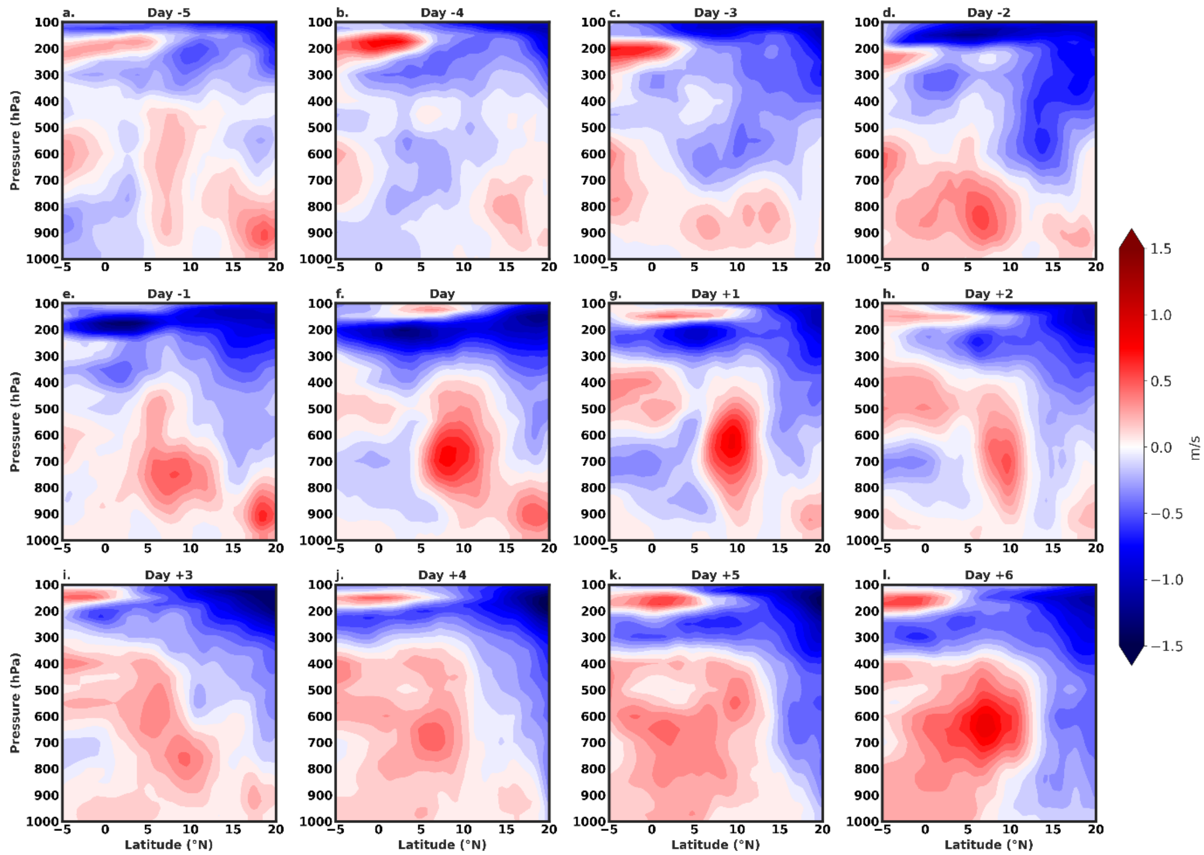

Figure 4.33: Meridional cross-section of zonal wind anomaly in m/s from 1000 hPa to 100hPa from Day- Day-5 before to Day + 6 days after the start of dry spells and averaged between 3°W and 9°E. 'Day' on the plot depicts the first date/day of dry spells.

NOTE: Anomalies were computed by subtracting the climatological daily mean from 1982-2020.

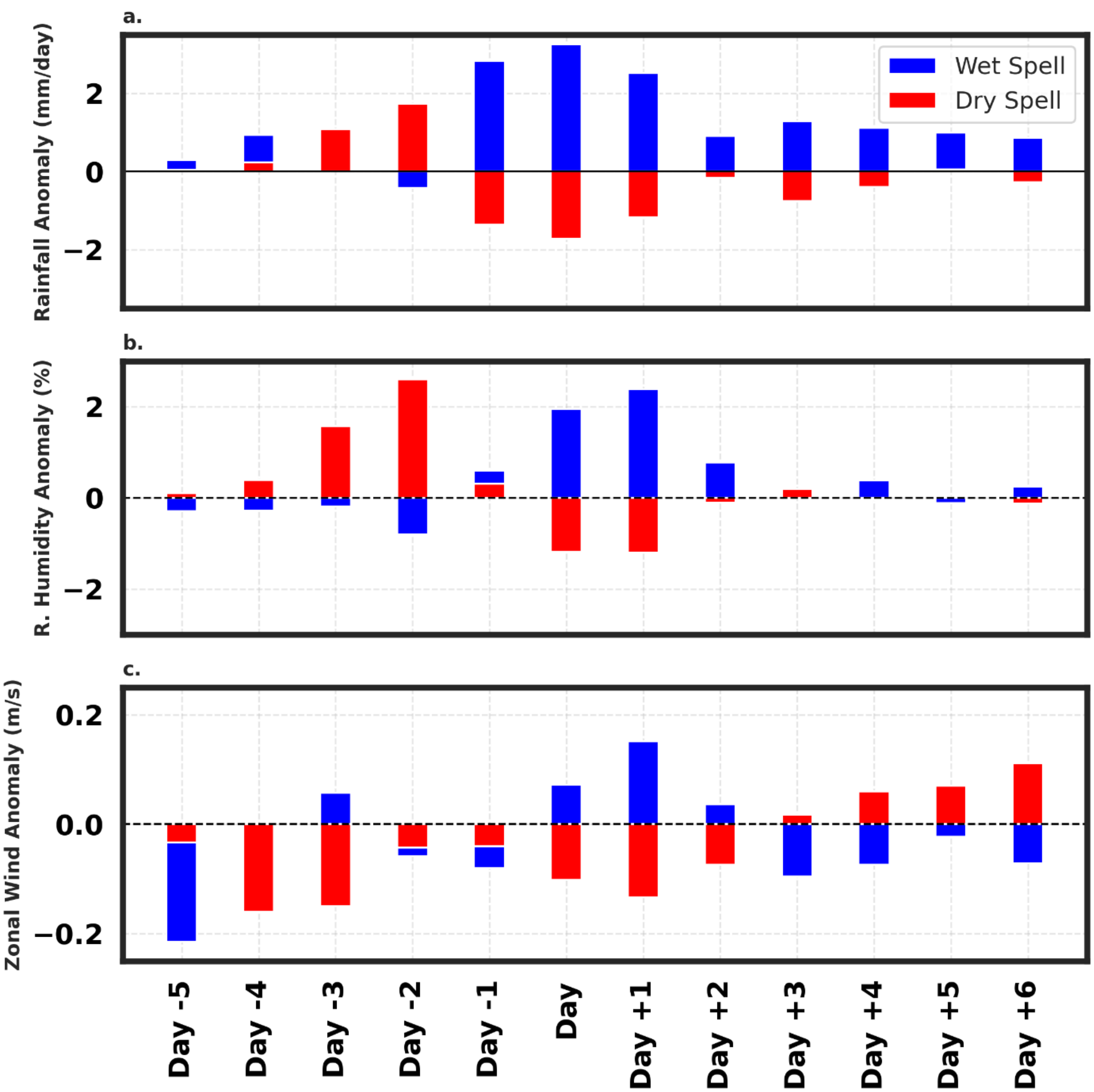

Figure 4.34: Composite temporal evolution of rainfall anomalies in mm/day (a), relative humidity (%) at 700 hPa (b) and zonal winds (m/s) anomaly at 850 hPa (c), and relative humidity (%) at 700 hPa in wet and dry spells (c).

4.4 INTENSE MULTI-DAY WET SPELLS

Using KASS-D and the intense multi-day wet spells identification criterion highlighted under section 3.3.3 and 3.3.5, a total of 403 intense 3-day wet spells and 237 intense 5-day wet spells were identified and subjected to composite analysis. These makes up of 1209 and 1185 intense 3-day and 5-day wet spell days. Figures 4.35 and 4.36 show the sample of the identified intense 3-day and 5-day wet spells using KASS-D with a comparable spatial pattern of rainfall accumulation over the area that experienced intense multi-day wet spells.

4.4.1 Composite Analysis of Intense Multi-Day Wet Spells

For all the intense 3-day and 5-day multi-day wet spell days identified, the composite analysis of CAPE, CIN TCWV, VIDMF, VIEWV and VINWV is depicted in Figure 4.37 and Figure 4.38. This was done to identify the possible drivers of these multi-day wet spells, one objectives of this study. A negative value of VIDMF indicate moisture concentrating over an area (convergence and hereafter MFC) and a negative value indicate moisture spreading out from an area (divergence and hereafter MFD). The composite anomalies associated with intense 3-day wet spells across West Africa (1982–2020) reveal a coherent pattern of decrease convective and moisture related processes, supporting the onset and intensification of rainfall over these intense events. As shown in the Figure 4.37a, anomalous increase in rainfall amount dominates larger area within the south of 15°N with higher anomalous high rainfall amount concentrated over the area between 11°N and 15°N. However, parts of Ghana, Ivory Coast, and entire Liberia and Sierra Leone experienced a decrease in rainfall amount over these 3-day intense events. This observed spatial pattern of intense 3-day rainfall can be seen in 5-day intense events that highlights the spatial extent and influence of intense multi-day wet spells.

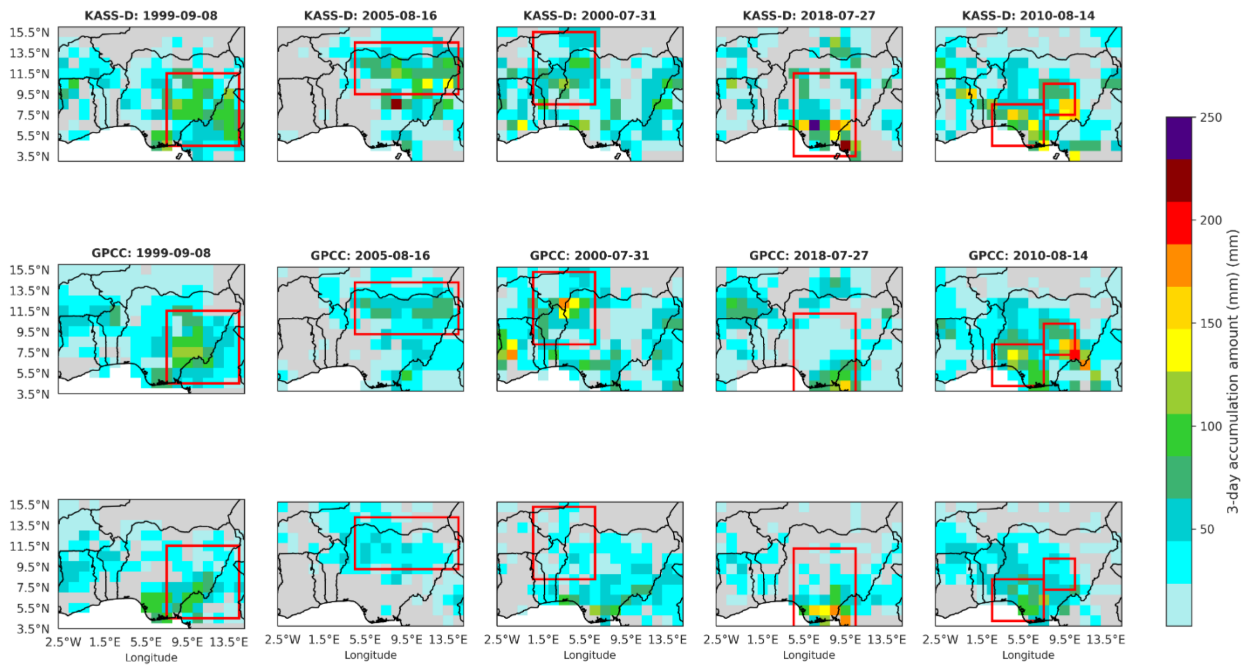

Figure 4.35: Sample plot of 3-day intense event dates identified and selected using KASS-D (first row) and the pattern of the grid cells were then compared to GPCC (second row), and CHIRPS (third row).

NOTE: Color shade depicts accumulation amount and the red box in each panel represent the area experiencing extreme events on the date identified by KASS-D.

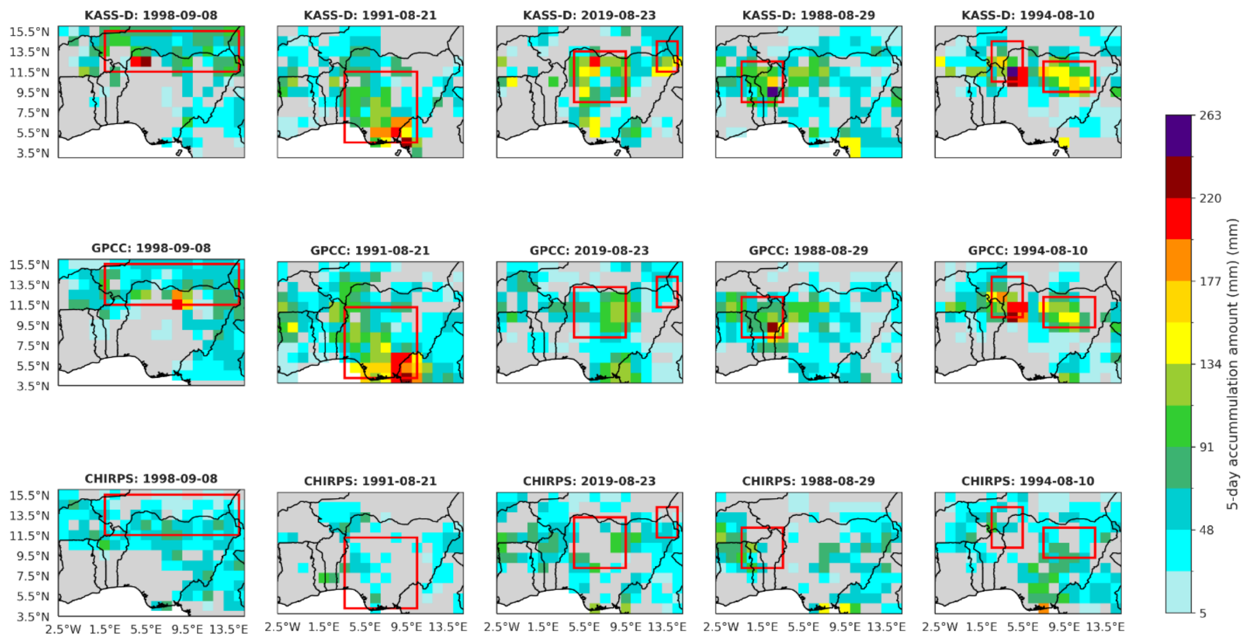

Figure 4.36: Sample plot of 3-day intense event dates identified and selected using KASS-D (first row) and the pattern of the grid cells were then compared to GPCC (second row), and CHIRPS (third row).

NOTE: Color shade depicts accumulation amount and the red box in each panel represent the area experiencing extreme events on the date identified by KASS-D.

The associated atmospheric environment during these events is marked by significant positive and (negative) anomalies in CAPE over the north (south) of 15°N as shown by both 3-day (Figure 4.37b) and 5-day (Figure 4.38b) intense multi-day wet spells. This suggests elevated atmospheric instability north of 15°N and reduced instability south of 15°N that are not be necessarily conducive for deep convection and intense rainfall (Emanuel, 1994; Houze 2004; Sherwood *et al*., 2010). Concurrently, CIN is reduced across most areas (Figure 4.37c and Figure 4.38c) over larger parts of West Africa except part of Ghana, Ivory Coast and Guinea.

The increase in TCWV (Figure 4.37d and 4.38d) depicts an anomalously moist troposphere, extending across coastal and larger inland regions during 3-day and 5-day events. This moisture availability is a critical precondition for sustained convective activity that further reinforces the rainfall anomalies observed during the multi-day intense wet spells (Figure 4.37a and 4.38a). The presence of this moisture is further supported by the VIDMF (Figure 4.37e and 4.38e), which indicates anomalous widespread MFC. Moisture transport pathways were further characterized by the zonal VIEWV and meridional VINWV components of the vertically integrated water vapor flux for both 3-day and 5-day events. The VIEWV (Figures 4.37f and 4.38f) shows a strong west-to-east transport anomaly over the Atlantic Ocean and the Gulf of Guinea and into south of 15°N West Africa and consistent with enhanced Atlantic monsoonal inflow. In parallel, the VINWV (Figure 4.37g and 4.38g) shows strengthened meridional transport from the ocean toward the continent, particularly from 3°E to 10°E, signifying intensified moisture advection. These two components together indicate a robust monsoonal circulation that favours inland propagation of moist air masses from the ocean.

The anomaly in the VIDMF overlaid with streamlines derived from the VIEWV and VINWV (Figure 4.37h and 4.38h) offer a comprehensive depiction of moisture transport dynamics during intense wet spell events. The spatial structure reveals a well-defined region of MFC centered over central West Africa between latitude 11°N and 15°N. This indicate an area where moisture is accumulating in the atmospheric column which is a critical precursor for sustained deep convection. The overlayed streamlines trace coherent and anomalous moisture transport from the Atlantic Ocean into inland of West Africa that converge over the rainfall maxima zone (Figure 4.37 and 4.38). This pattern suggests that both enhanced westerly monsoonal inflow and strengthened southerly moisture transport from the Gulf of Guinea synergistically contribute to a focused zone of low-level convergence. This configuration is likely instrumental in sustaining deep convection by continuously supplying moist static energy to the boundary layer and mid-troposphere (Sherwood *et al*., 2010; Holloway & Neelin, 2009) that may intensify and sustain the observed intense rainfall during these intense multi-day wet spells. Furthermore, the alignment between MFC and streamline convergence confirms the crucial role of dynamically forced moisture accumulation in modulating prolong and heavy rainfall events across the study area.

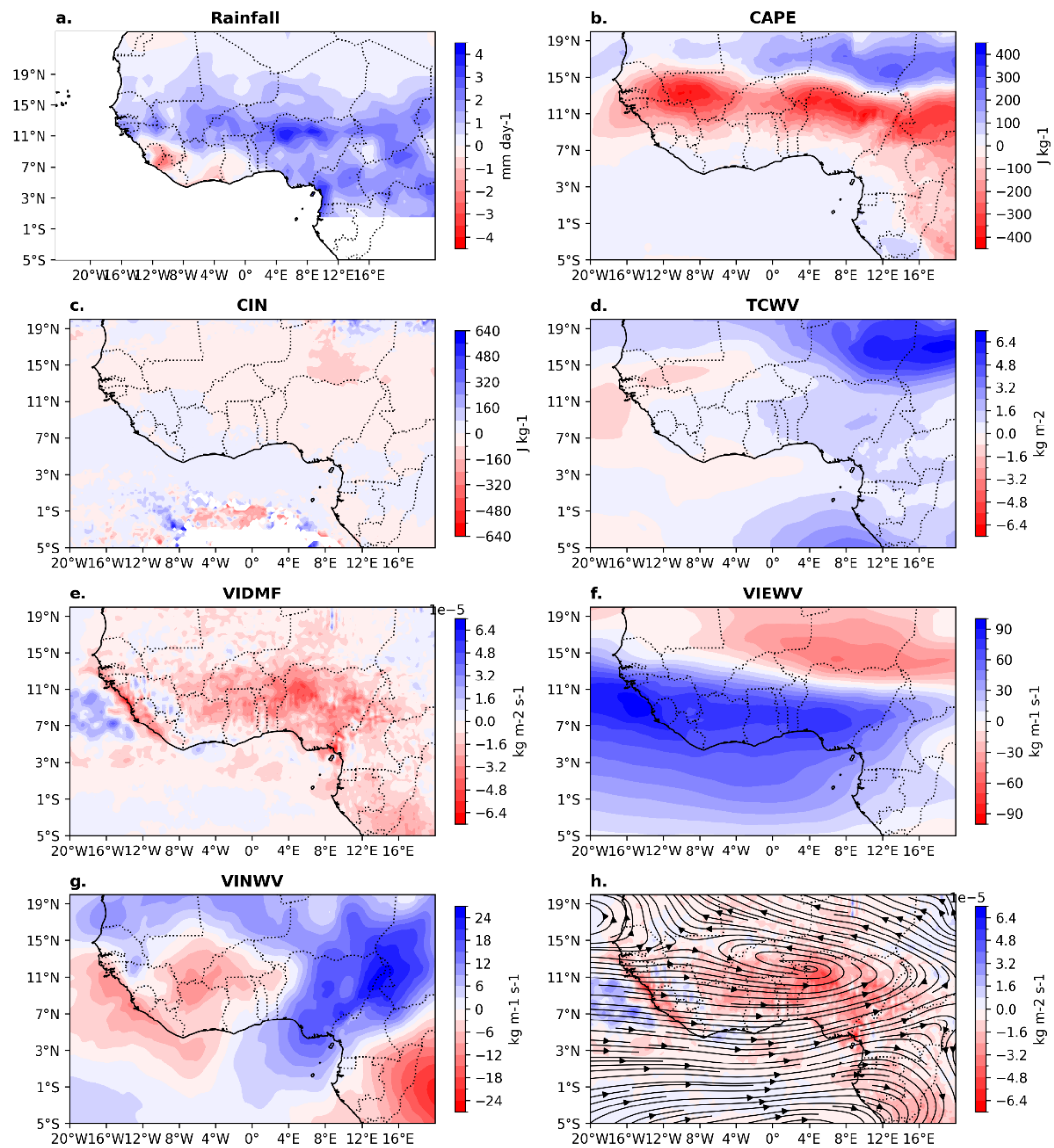

Figure 4.37: Composite anomalies of key variables during 3-day intense wet spells over West Africa for the period 1982–2020.

NOTE: Panels show spatial anomalies of (a) Rainfall from GPCC, (b) CAP), (c) CIN, (d) TCWV), (e) VIDMF, (f) VIEWV, (g) VIEWN and (h) VIDMF overlaid with streamlines of VIEWV and VINWV. Anomalies are computed relative to the seasonal climatology (June–September)

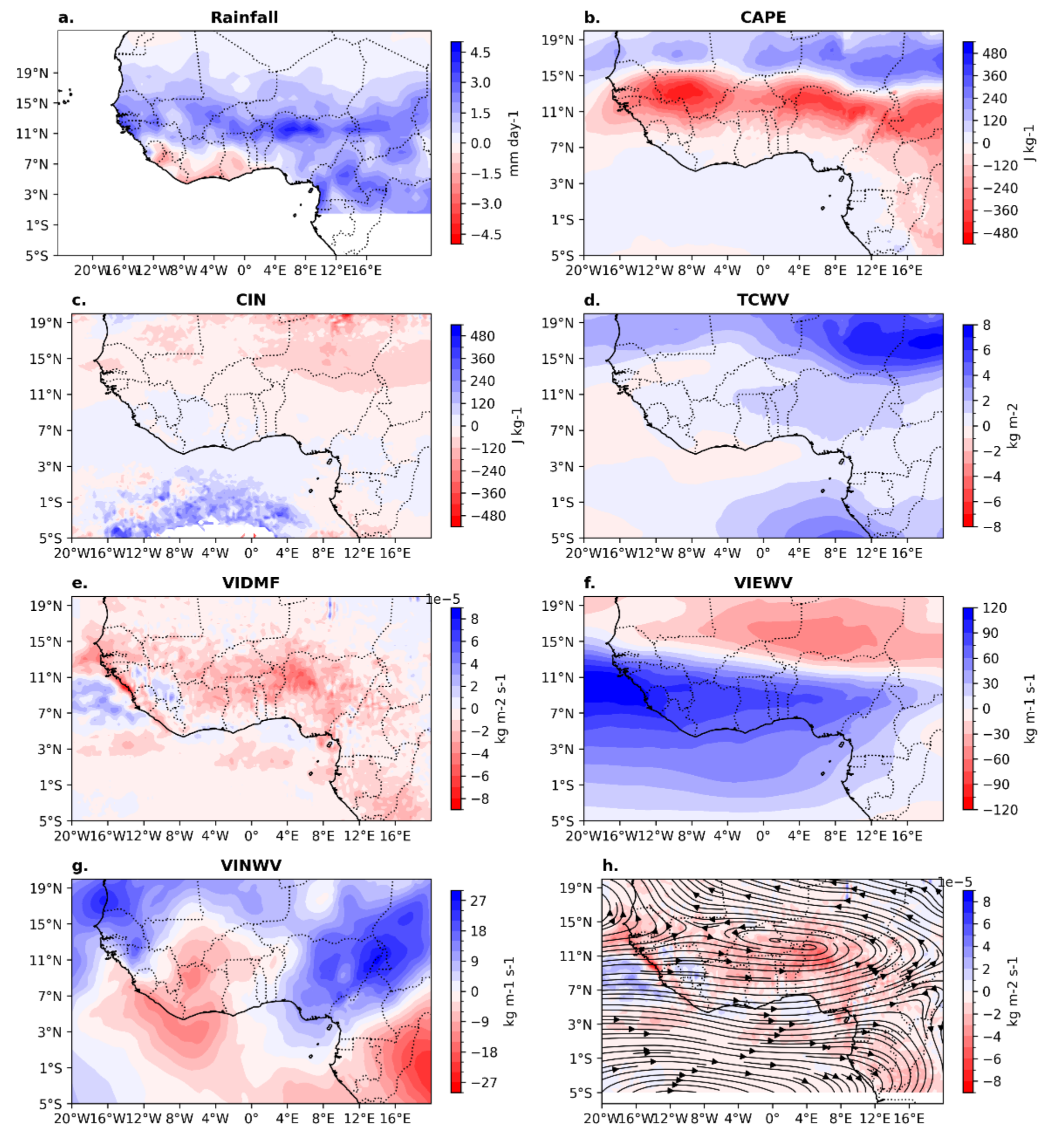

Figure 4.38: Composite anomalies of key variables during 5-day intense wet spells over West Africa for the period 1982–2020.

NOTE: Panels show spatial anomalies of Rainfall from GPCC (a), CAPE (b), CIN (c), TCWV (d), VIDMF (e), VIEWV (f), VIEWN (g) and VIDMF overlaid with streamlines of VIEWV and VINWV (h). Anomalies are computed relative to the seasonal climatology (June–September)

4.4.2 Evolution of Rainfall, CAPE, CIN, TCWV and VIDMF at Different Stages of Intense Multi-Day Wet Spells

Figure 4.39 illustrate the longitudinal evolution of rainfall, CAPE, CIN, TCWV and VIDMF averaged between 3°N and 20°N at different stages of 3-day intense wet spells, from a day before onset of the events (3T–1), through the event days (3T1, 3T2, 3T3) and two days after (3T+1, 3T+2). These offer crucial insight into the spatiotemporal dynamics that precede, accompany, and follow intense 3-day rainfall over West Africa.

During the 3-day intense wet spells (3T1 to 3T3), a pronounced positive rainfall anomaly emerges between ~4°E and 15°E that peaks around 5°–10°. This region of maximum increased rainfall coincides with an area of climatological maxima in convective activity. This rainfall anomaly is preceded by a marked decrease in CIN and a simultaneous increase in CAPE, that create a favourable preconditioning for deep convection. The essential suppression and enhancement of CIN and CAPE coincide with the onset of the intense rainfall event, suggesting a direct modulation of convective potential during the buildup phase of the event. TCWV anomalies show a coherent eastward intensification beginning at 3T–1 and peaking during 3T2–3T3 between ~4°E and 15°E that highlight the progressive accumulation of column-integrated moisture which supports sustained convective activity. Notably, anomalous increased TCWV after 3-day (3T+1) indicate a delayed decay in atmospheric moisture after the peak of the events. The VIDMF anomalies reveals a strong MFC concentrated around 4°E to 15°E during the peak of 3-day intense events (3T2). This aligned closely with rainfall maxima and underscore the dynamic contribution of low-level convergence to convective sustenance. However, before the event, convergence anomalies begin to develop and intensify eastward that indicate the role of moisture accumulation and dynamical forcing in preconditioning the environment for the occurrence and sustenance of this intense wet spells.

Similar results were also obtained for 5-day intense wet spells in Figure 4.40 but with increase in longitudinal band of area with high rainfall amount that coincide with enhanced TCW and MFC. Collectively, the longitudinal progression captured in these anomalies shows a multivariate and spatially coherent build-up phase characterized by destabilization, moisture enrichment, and convergence. These culminate into intense rainfall for multiple days. However, decay stage of these multi-day intense wet spells are marked by decrease MFC (i.e., divergence) and diminishing convective potential.

To elucidate the mechanisms underpinning moisture flux convergence (MFC) during intense multi-day wet spells over West Africa, the relationship between rainfall, vertically integrated moisture flux divergence (VIDMF), and total column water vapor (TCWV) observed in Figures 4.39 and 4.40 is further analysed in Figure 4.41 and Figure 4.42 for 3-day and 5-day intense wet spells, respectively. This Figure 4.41 presents the evolution of the VIDMF field (shaded) and associated moisture flux vectors (streamlines) before, during, and after intense 3-day wet spell events. During these events, the moisture flux pattern reveals the presence of two distinct and persistent cyclonic circulations. The first is located over the tropical Atlantic Ocean, while the second is centered over the continental interior between 10°N and 15°N, coinciding with the core region of anomalous moisture convergence (negative VIDMF). These two circulations are consistently separated by a col region, characterized by weak flow and positive VIDMF anomalies (indicating moisture divergence), suggesting a structural boundary between the influence zones of the two systems.

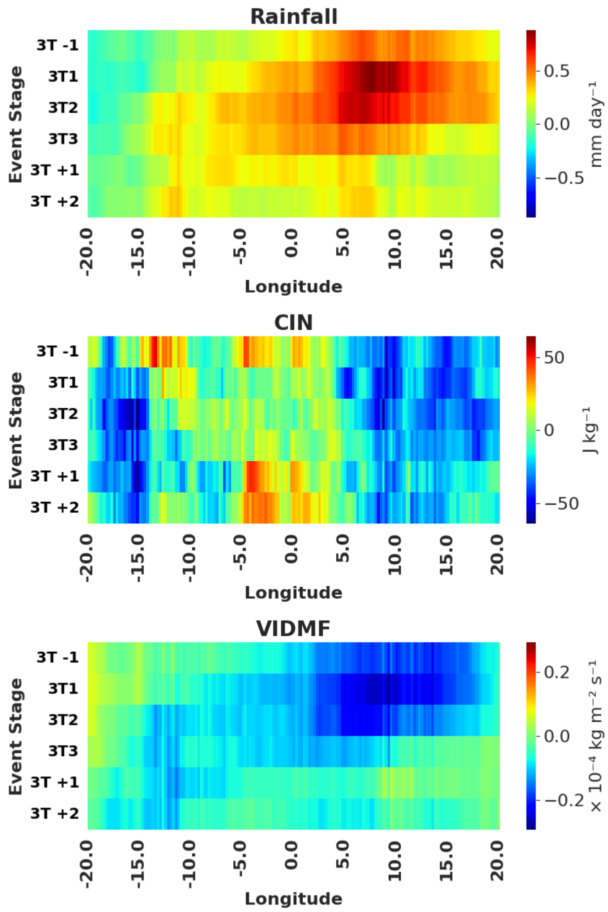

Figure 4.39: Longitudinal evolution of composite anomalies of key variables during 3-day intense wet spells average between 3° N and 20° N for the period 1982–2020.

NOTE: Shown are anomalies of (a) Rainfall from GPCC, (b) CAP), (c) CIN, (d) TCWV, (e) VIDMF, (f) VIEWV, (g) VIEWN and (h) VIDMF overlaid with streamlines of VIEWV and VINWV. Anomalies are computed relative to the seasonal climatology (June–September)

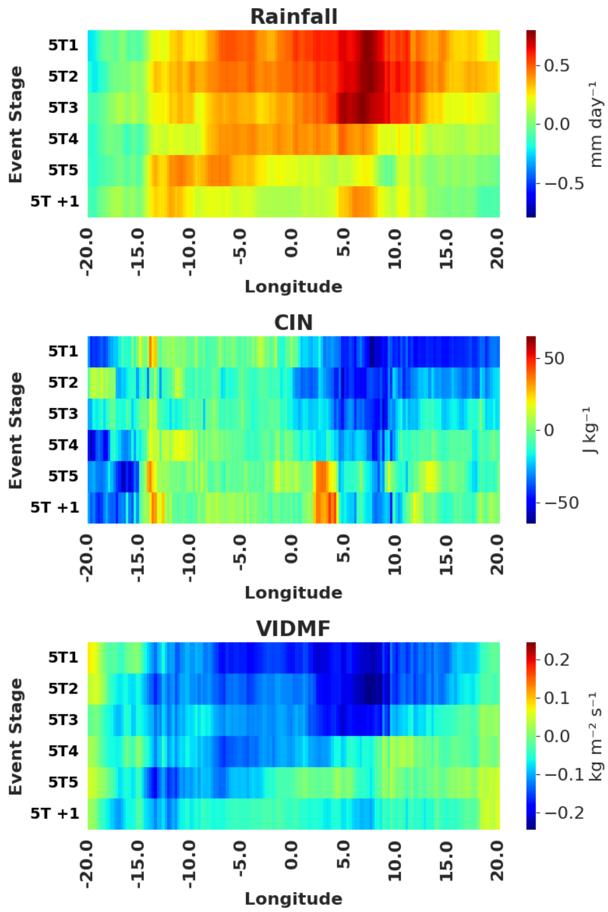

Figure 4.40: Longitudinal evolution of composite anomalies of key variables during 5-day intense wet spells average between 3° N and 20° N for the period 1982–2020.

NOTE: Shown are anomalies of (a) Rainfall from GPCC, (b) CAP), (c) CIN, (d) TCWV, (e) VIDMF, (f) VIEWV, (g) VIEWN and (h) VIDMF overlaid with streamlines of VIEWV and VINWV. Anomalies are computed relative to the seasonal climatology (June–September).

As the events progress, the inland cyclonic circulation appears to propagate westward and potentially merges with the Atlantic cyclone by the end of 3-day events (3T3), forming an elongated ridge extending eastward toward northeastern Nigeria. This typically brings fair, dry, and stable weather over the inland of West Africa where the core of the cyclone is located during the events. The Atlantic cyclone serves as a critical source of moist air, continuously channelling moisture inland from the Gulf of Guinea through regions dominated by divergence (positive VIDMF) toward the inland convergence zones. Additionally, a prominent anticyclonic circulation in the Southern Hemisphere contributes to moisture transport by reinforcing cross-equatorial flow, supporting the low-level monsoonal southwesterlies. This system also exhibits westward migration, working in tandem with the northern cyclones to funnel moisture into West Africa. Following the termination of the wet spell events (3T +1), divergence dominates the eastern and northern flanks of the now-elongated ridge, signalling weakening moisture convergence and the eventual dissipation of the convective systems. This shift reflects the breakdown of the favourable dynamical configuration necessary for sustaining organized deep convection, thus marking the cessation of the intense wet spells. The westward migration of cyclonic circulation is similar to what was reported by Engel *et al.*, (2017) in their study of extreme rainfall events in the city of Dakar and Ouagadougou.

A similar dynamical configuration is observed for the 5-day intense wet spell events, as illustrated in Figure 4.42. The moisture flux and VIDMF fields show persistent and spatially coherent patterns of anomalous convergence, resembling those identified during the 3-day events. Notably, by Day 5T3 (the third day of the 5-day composite), a pronounced merging of the two cyclonic circulations is evident. This merger occurs over a broad region characterized by strong negative VIDMF anomalies. The persistence of this MFC particularly during and after the cyclonic merger, appears to play a pivotal role in reformation and sustaining the convective environment necessary for prolonged rainfall. The formation of a new, consolidated cyclonic system over the core convergence zone likely enhances dynamical lifting and reinforces the inland transport of moist air, thereby prolonging the convective activity. This sustained anomalous MFC acts as a key dynamical mechanism in extending the duration of the wet spell beyond three days, highlighting the importance of cyclonic interactions and the evolution of low-level convergence structures in the formation of multi-day extreme rainfall events over West Africa.

4.4.3 Upper Level

Figure 4.43 illustrates composite anomalies of zonal wind (m s^{-1}) associated with all 3-day intense rainfall events over West Africa, displayed at four pressure levels (1000 hPa, 850 hPa, 650 hPa, and 200 hPa) overlaid with streamlines derived from the horizontal wind components (u and v). At 1000 hPa (Figure 4.43a), a pronounced westerly anomaly (blue shading) dominates over the equatorial to the south of 12°N that is an indicative of enhanced low-level monsoonal flow from the Atlantic Ocean inland. North of 12°N at the same level, reveal the enhancement of easterly anomaly. This low-level monsoonal flow at 1000 hPa coincides with the convergence accentuated at 850 hPa (Figure 4.43b) where an intensified low-level westerly monsoonal flow is evident south of the convergence core located around 15°N. This is a domicile region of convective rainfall maxima and contrasting with anomalous easterlies to the north. The 650 hPa level (Figure 4.43c) reveals a marked core of weaker AEJ and easterlies extending broadly across south of 15°N. This weakening of the AEJ is important for the increased monsoonal flow into the Sahel (Akinsanola and Zhou, 2020). Notably, the 200 hPa (Figure 4.43d) exhibits strong easterly anomalies south of 10°N and westerly anomalies to the north. This convergence-divergence dipole reflects the classic structure of deep convection sustained by ventilation from both ends of the troposphere, a characteristic of organized MCSs in the region (Houze, 2004; Fink & Reiner, 2003; Laing & Fritsch, 2000). The vertical alignment of these anomalies also corresponds with the dynamical

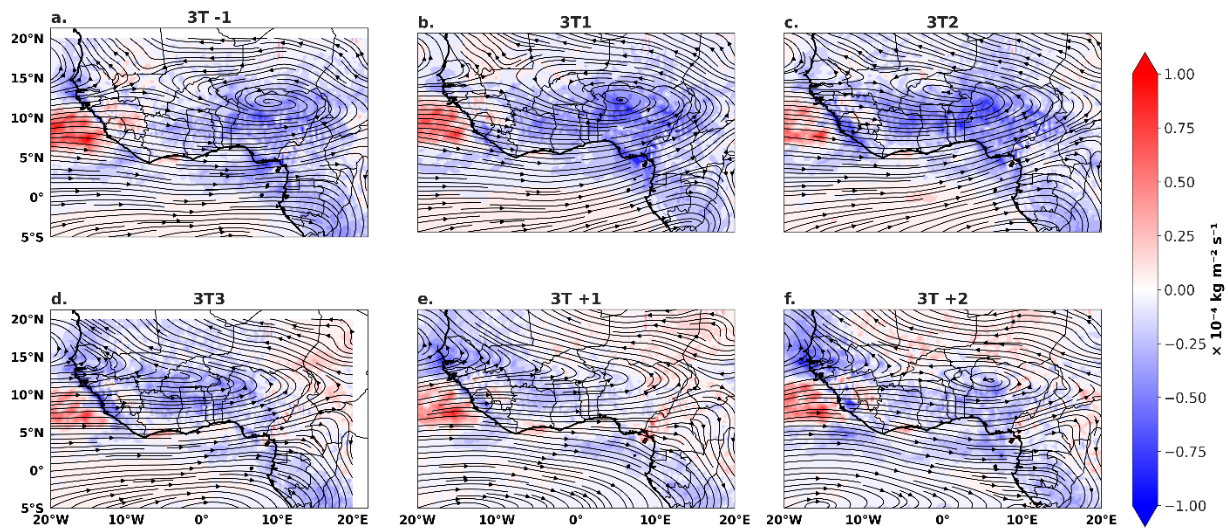

Figure 4.41: Composite anomaly of VIDMF (shades) overlay with streamlines of VIEWV and VINWV before (3T-1), during (3T1, 3T2, 3T3) and after (3T+1, 3T+2) 3-day intense events. Anomaly is computed by subtracting the daily value for 1982-2020 climatological mean.

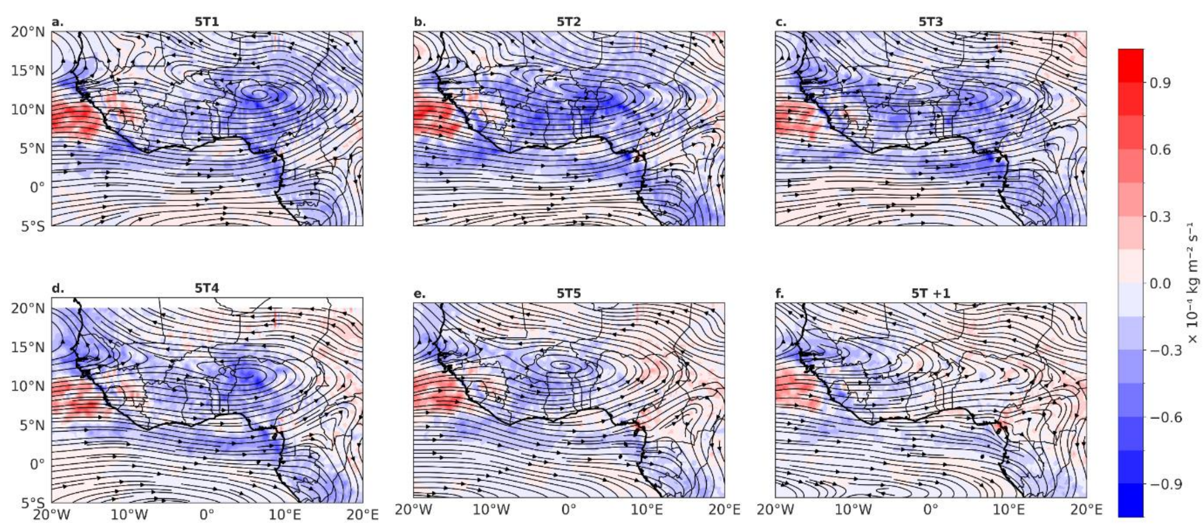

Figure 4.42: Composite anomaly of VIDMF (shades) overlay with streamlines of VIEWV and VINWV before (5T-1), during (5T1, 5T2, 5T3, 5T4) and after (5T+1) 5-day intense events. Anomaly is computed by subtracting the daily value for 1982-2020 climatological mean.

signature of tropical wave activity, particularly AEWs that modulate convection and rainfall variability through amplification of upward motion and moisture convergence (Kiladis *et al*., 2006; Janicot *et al*., 2009). This finding is also valid for 5-day intense multi-day wet spells in Figure 4.44

Furthermore, Figure 4.45 (a) to (f) represent the evolution from one day before the event (3T–1) through the event core (3T1–3T3) to two days after (3T+1 and 3T+2) zonal cross-section of vertical velocity anomalies of 3-day intense events. The observed pattern in 3-day is highly similar to 5-day events in Figure 4.46. A pronounced deep-layer anomalous ascent (negative vertical velocity anomaly) is observed from mid- to upper troposphere (~600–200 hPa) centered around 5 -10°E during the core event days, particularly 3T1 and 3T2 indicating vigorous upward motion associated with MCSs. This ascent is preceded by weaker anomalies and followed by a transition into subsidence (positive anomalies) notably at low and mid-levels (~900–400 hPa) after the cessation (3T+1 and 3T+2) that suggests convective decay and atmospheric stabilization. The longitudinal asymmetry, with enhanced upward motion east of 5°E depicts the influence of regional orographic and dynamical controls such as the AEJ and monsoon surge (e.g., Nicholson, 2013; Vogel *et al*., 2020). These underscore the transient but vertically coherent nature of intense rainfall events over West Africa and the potential utility of vertical velocity anomalies as a diagnostic for convection-related dynamical processes during multi-day intense events.

Also, for the cross-section of divergence anomaly shown in Fig 4.47 from the onset day (3T1) through the event peak (3T2–3T3) and post-event (3T+1 and 3T+2), all referenced against the composite mean of 3-day events. The result for 5-day is shown is Figure 4.48 A coherent dipole structure is evident throughout the event evolution, characterized by anomalous divergence in the upper troposphere (~250–100 hPa) and corresponding convergence in the mid-to-lower troposphere (~700–850 hPa), most prominently between 5° and 15°E. This pattern intensifies from

5T1 through 5T3, suggesting sustained deep convection with robust upward mass flux and efficient vertical coupling that is consistent with MCS development. The persistence of upper-level divergence and lower-level convergence into 5T4 and 5T5 points to the longevity and maturity of the convective systems. By 5T+1, the upper-level divergence anomalies shift eastward and weaken that reveal the decaying phase of convection. These features align with established frameworks of tropical convection dynamics (e.g., Mapes, 2001; Janiga and Thorncroft, 2016) that show the role of divergence fields in diagnosing the vertical structure and life cycle of deep convection over the West African monsoon domain.

For the specific humidity, Figure 4.49 and 4.50 represent the progression from one day prior to two days following the 3-day and 5-day intense events that are very similar. For the 3-day events, a consistent positive anomaly in specific humidity emerges prominently across the lower and mid-troposphere (~ surface–500 hPa) east of 5°E during the event peak (3T1–3T3), peaking near 10°–15°E that depict moistening associated with deep convection and enhanced monsoonal inflow. The moist layer deepens vertically during 3T1 and 3T2 showing the contribution of moisture availability in sustaining convective systems during these intense events. Even on 3T–1, preconditioning is evident with anomalous enhancement of low-level moisture east of the 5°, suspecting the presence of a favorable thermodynamic environment ahead of convection. After the event (3T+1 and 3T+2), specific humidity anomalies gradually weaken and retreat, particularly at mid-levels, implying drying of the atmospheric column as convective activity decreases. The spatiotemporal distribution of these anomalies is consistent with Peyrillé and Lafore (2007) conceptual model of convectively coupled systems over West Africa that highlights moisture buildup, peak, and dissipation as critical phases in convective event evolution.

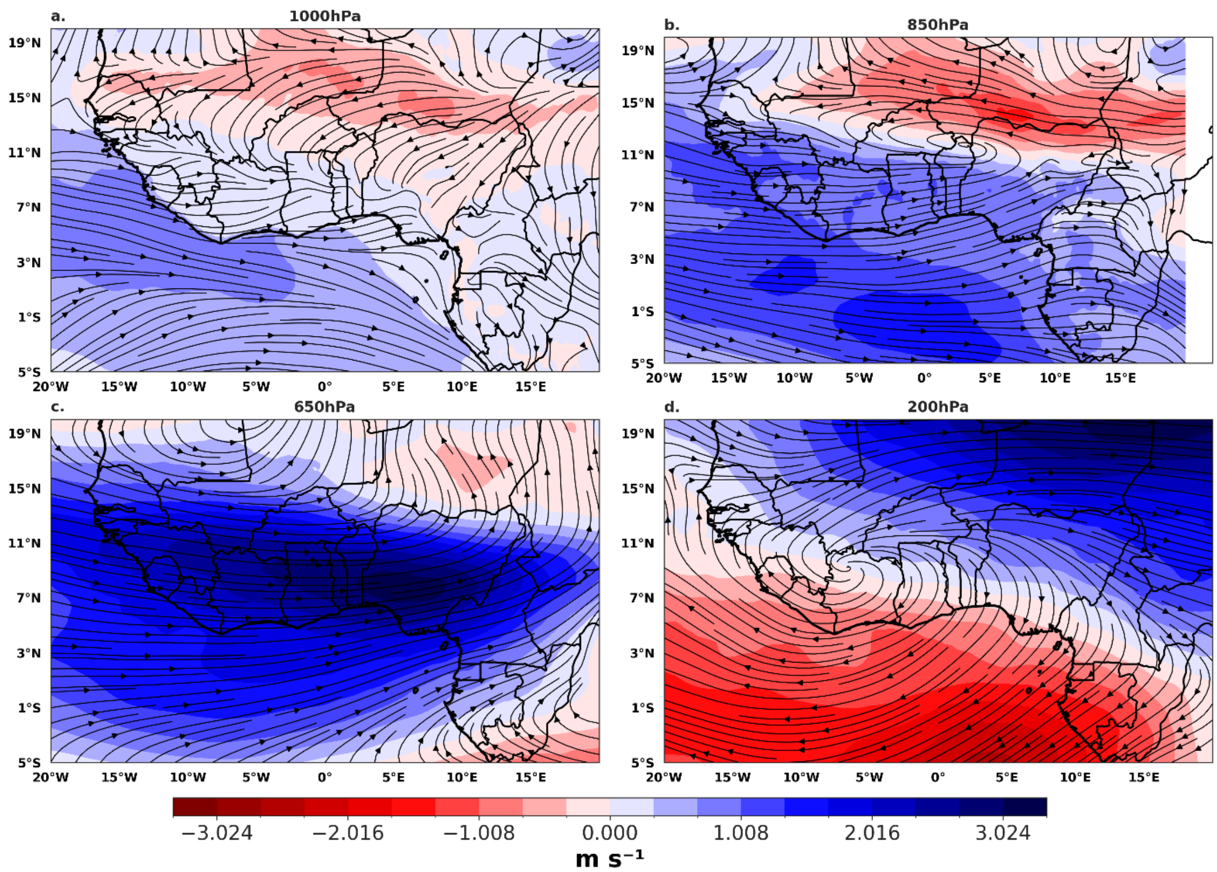

Figure 4.43: Composite anomalies of zonal wind (m s^{-1}) associated with all 3-day intense rainfall events, displayed at (a) 1000 hPa, (b) 850 hPa, (c) 650 hPa, and (d) 200 hPa pressure level and overlaid with streamlines derived from u and v wind components.

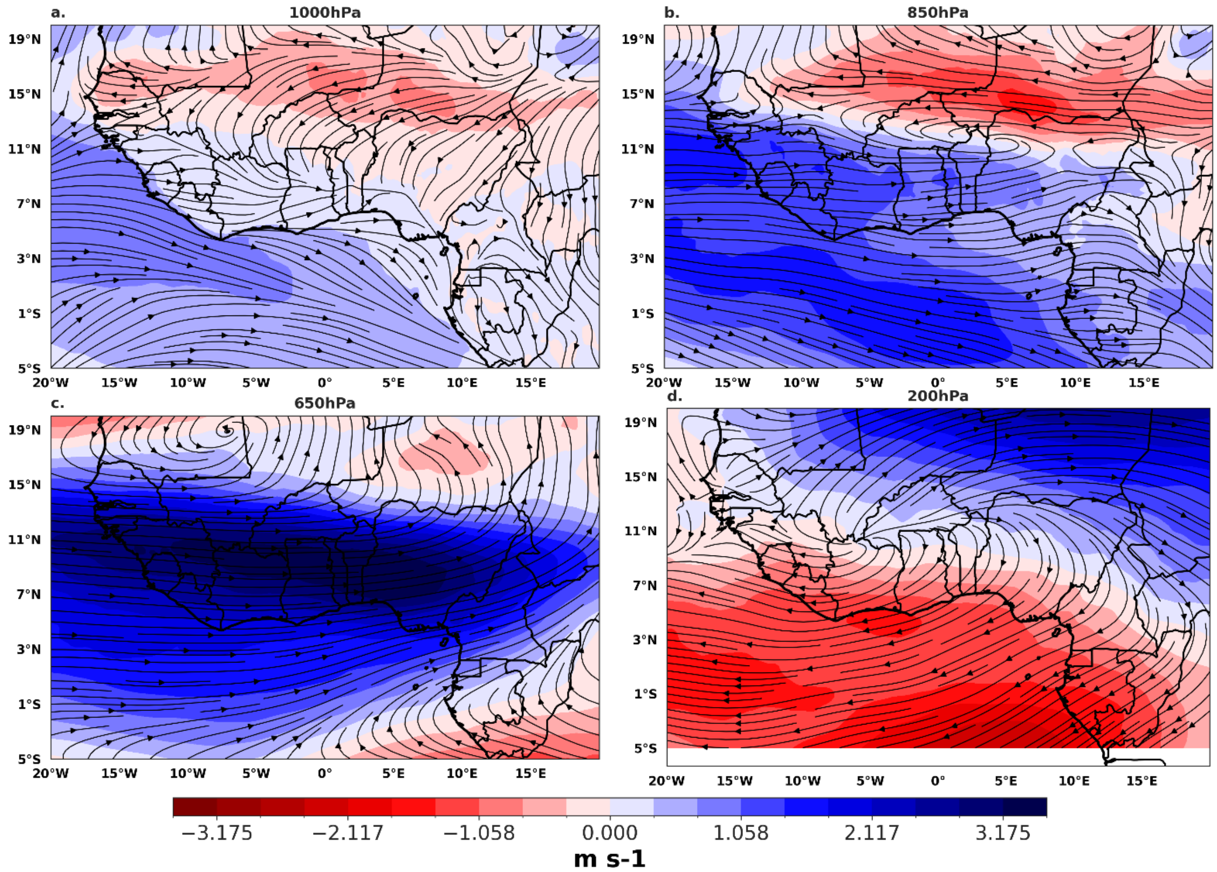

Figure 4.44: Composite anomalies of zonal wind (m s^{-1}) associated with all 5-day intense rainfall events, displayed at (a) 1000 hPa, (b) 850 hPa, (c) 650 hPa, and (d) 200 hPa pressure level and overlaid with streamlines derived from u and v wind components.

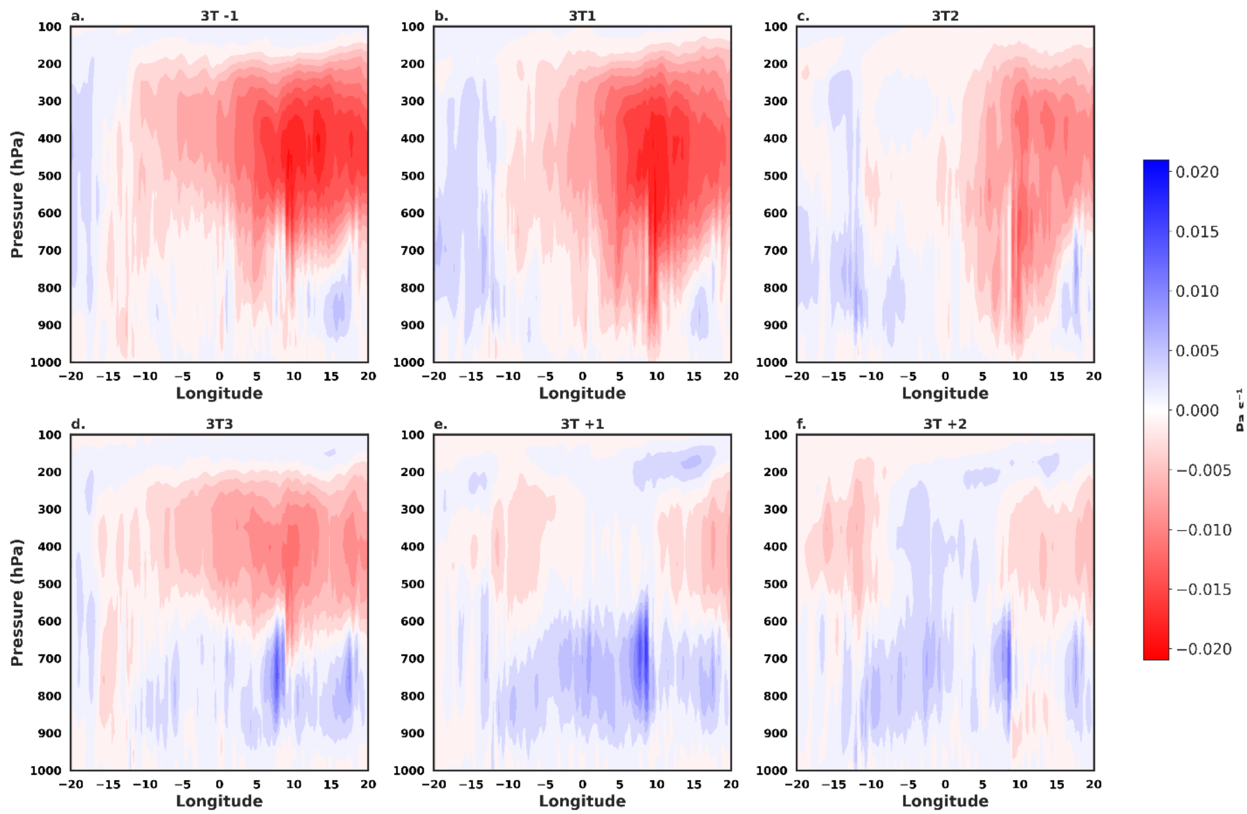

Figure 4.45: Zonal cross-section of vertical velocity anomalies (Pa/s) averaged over the latitudinal belt of West Africa 3-day intense events.

NOTE: this period spanned different phases of composite 3-day intense wet events from one day before the event (3T–1) through the event core (3T1–3T3) to two days after (3T+1 and 3T+2) zonal cross-section of vertical velocity anomalies of 3-day intense events. The anomalies are calculated relative to the climatological mean derived from all the 3-day intense events identified.

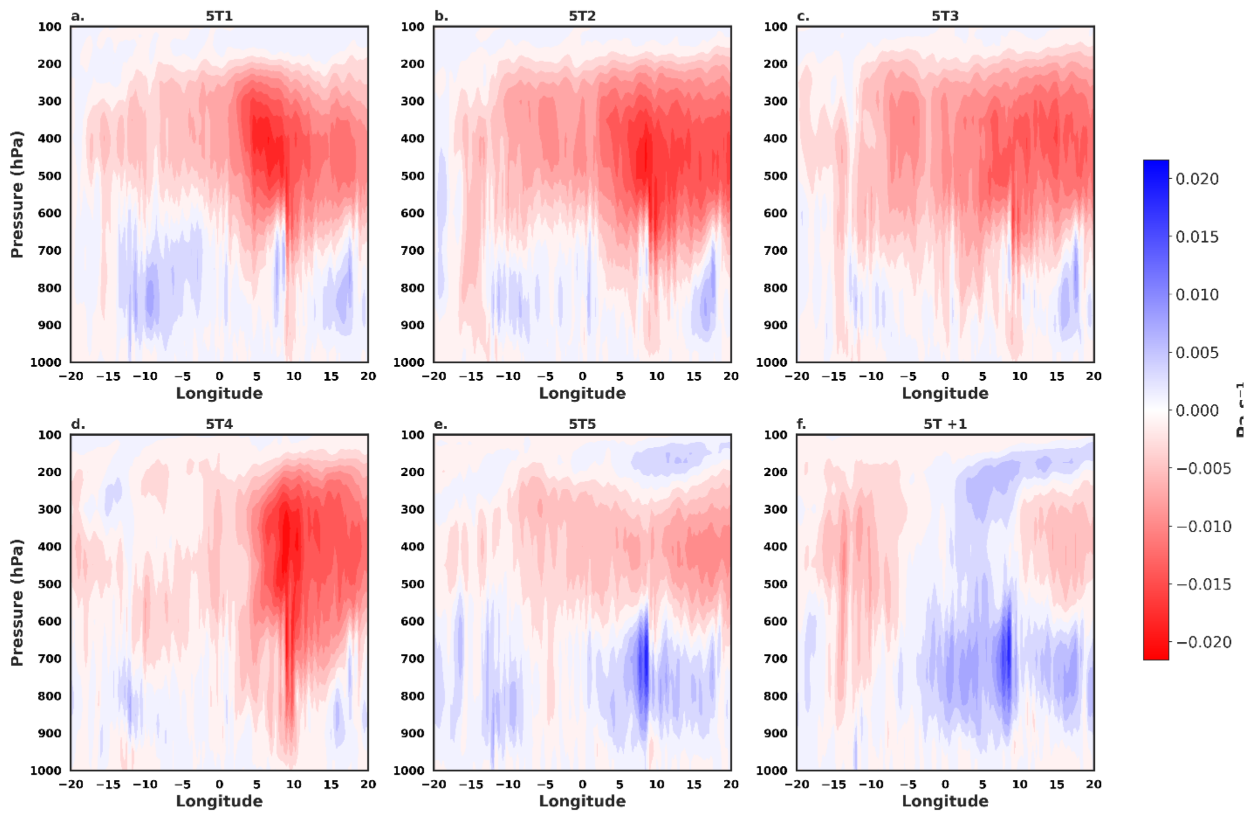

Figure 4.46: Zonal cross-section of vertical velocity anomalies (Pa/s) averaged over the latitudinal belt of West Africa for 5-day intense events.

NOTE: this period spanned different phases of composite 5-day intense convective events from one day before the event (5T–1) through the event core (5T1–5T5) to two days after (5T+1) zonal cross-section of vertical velocity anomalies of 3-day intense events. The anomalies are calculated relative to the climatological mean derived from all the 5-day intense events identified.

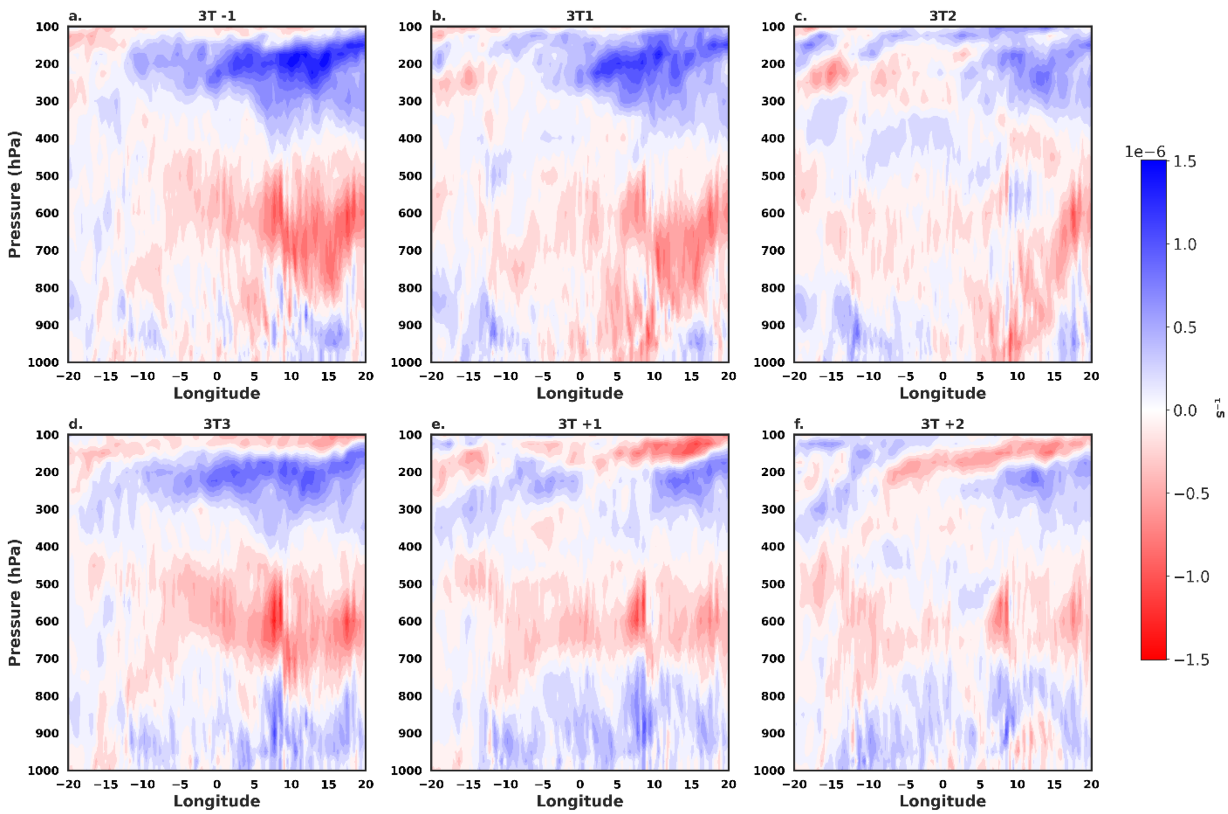

Figure 4.47: Zonal cross-section of divergence anomalies (S^{-1}) averaged over the latitudinal belt of West Africa for 3-day intense events.

NOTE: this period spanned different phases of composite 3-day intense convective events from one day before the event (3T–1) through the event core (3T1–3T3) to two days after (3T+1 and 3T+2) zonal cross-section of vertical velocity anomalies of 3-day intense events. The anomalies are calculated relative to the climatological mean derived from all the 3-day intense events identified.

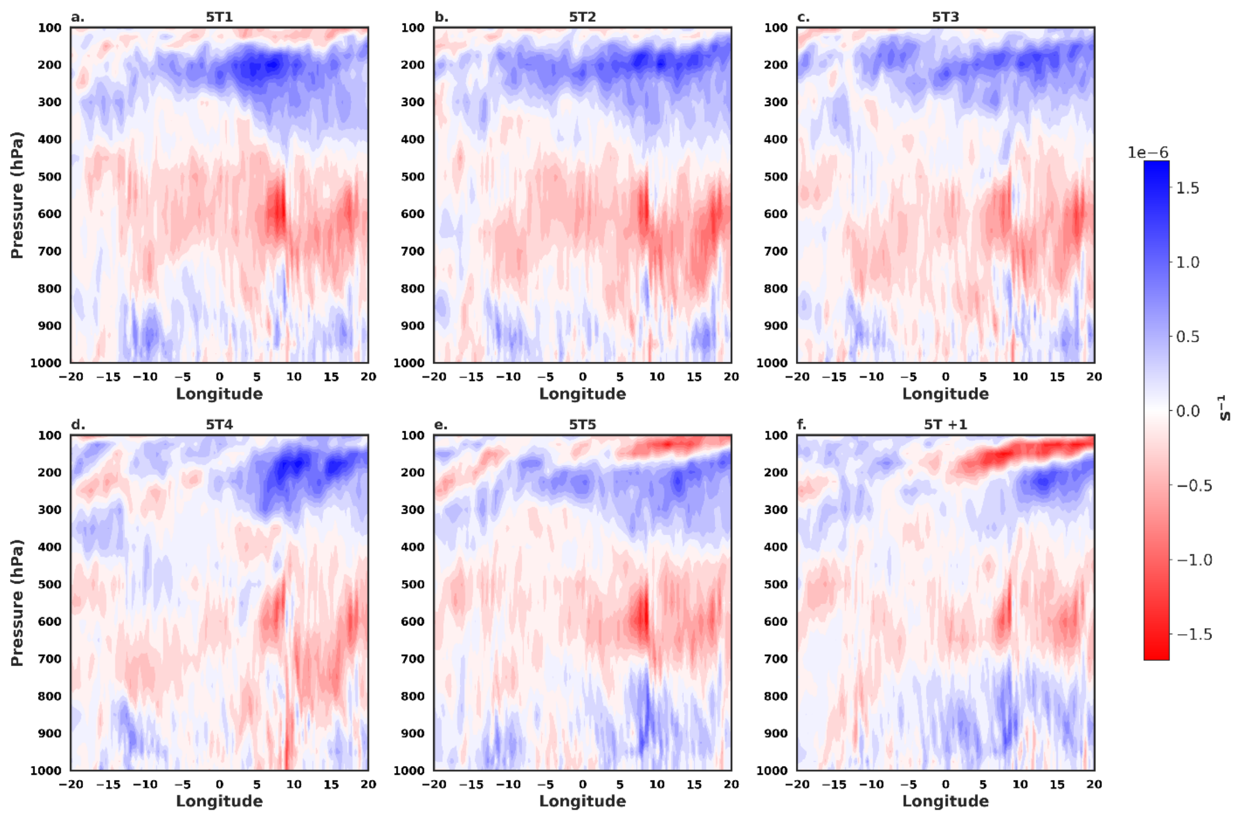

Figure 4.48: Zonal cross-section of divergence anomalies (S^{-1}) averaged over the latitudinal belt of West Africa for 5-day intense events.

NOTE: this period spanned different phases of composite 5-day intense convective events from one day before the event (5T–1) through the event core (5T1–5T5) to two days after (5T+1) zonal cross-section of vertical velocity anomalies of 3-day intense events. The anomalies are calculated relative to the climatological mean derived from all the 5-day intense events identified.

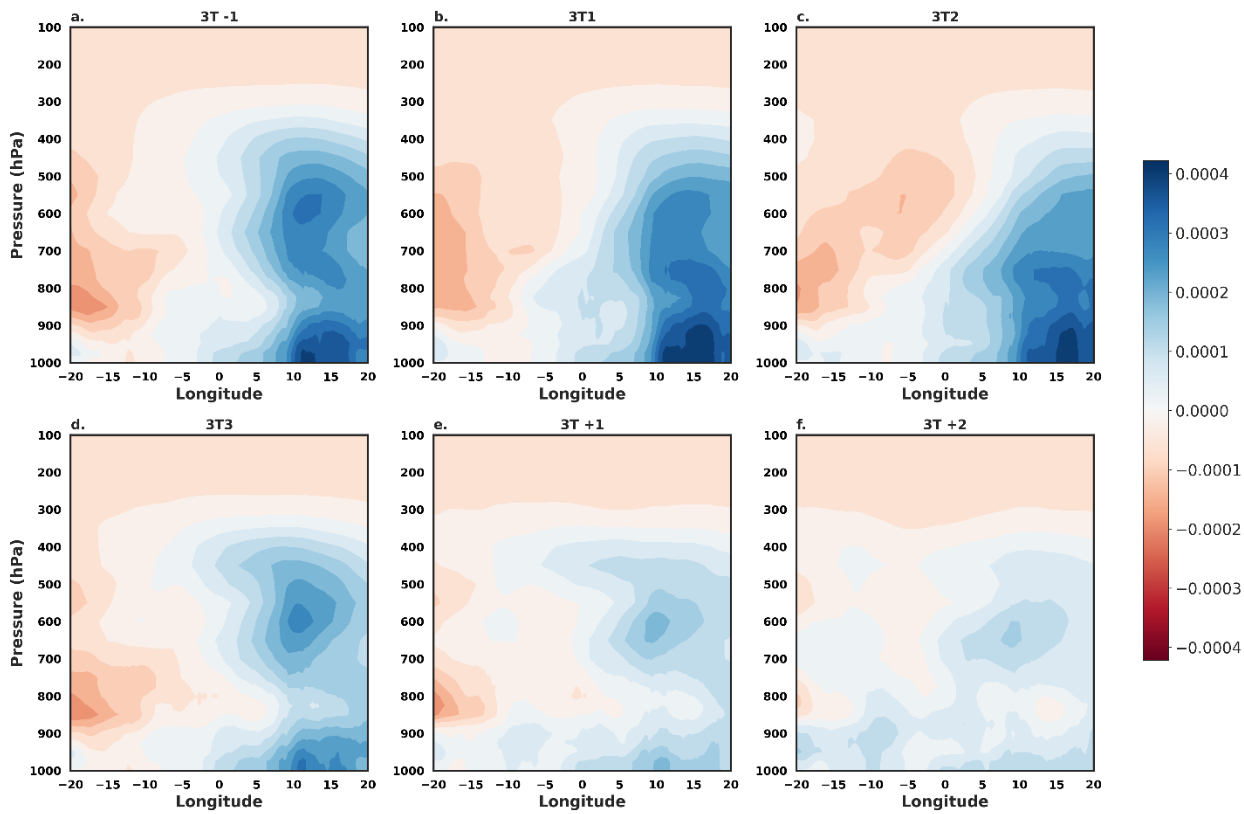

Figure 4.49: Zonal cross-section of specific humidity anomalies (kg m^{-2}) of 3-day wet spells averaged over the latitudinal belt of West Africa.

NOTE: this period spanned different phases of composite 3-day intense convective events from one day before the event (3T–1) through the event core (3T1–3T3) to two days after (3T+1 and 3T+2) zonal cross-section of vertical velocity anomalies of 3-day intense events. The anomalies are calculated relative to the climatological mean derived from all the 3-day intense events identified.

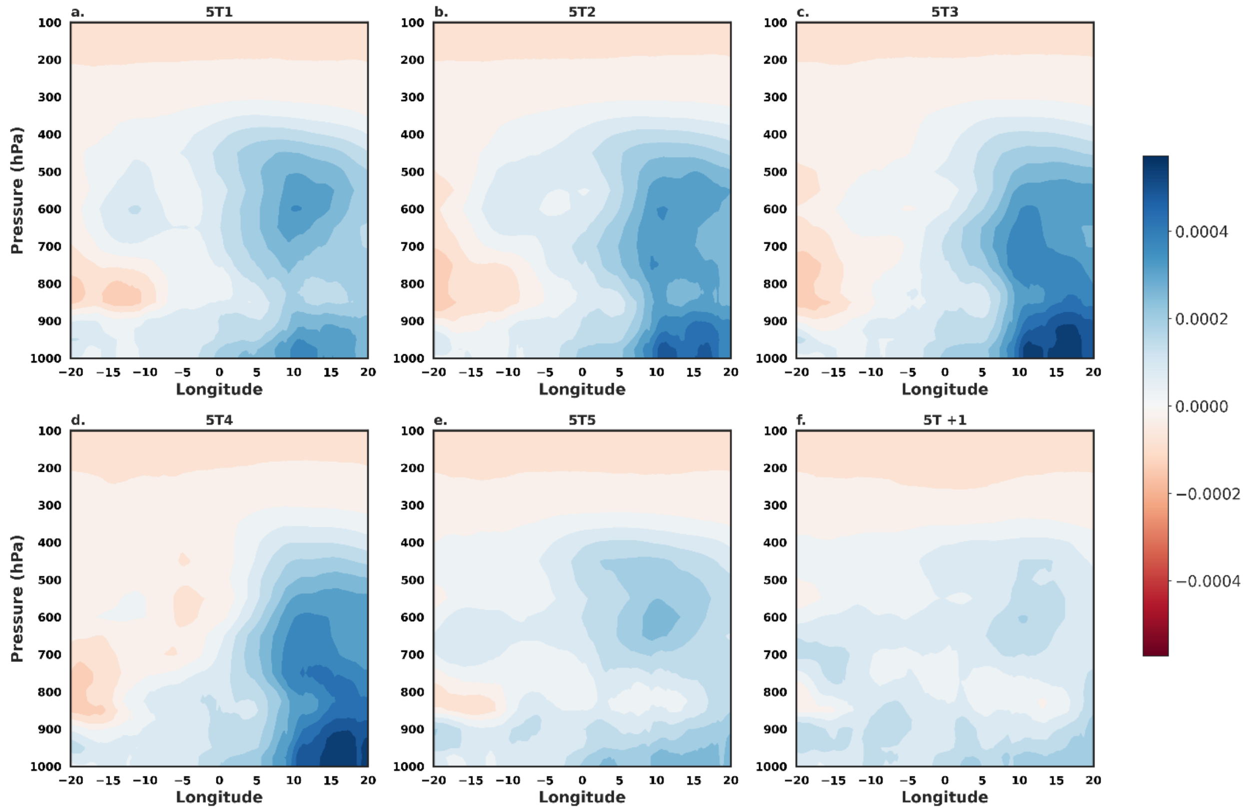

Figure 4.50: Zonal cross-section of specific humidity anomalies (kg.m^{-2}) of 5-day wet spells averaged over the latitudinal belt of West Africa

NOTE: this period spanned different phases of composite 5-day intense convective events from one day before the event (5T–1) through the event core (5T1–5T5) to two days after (5T+1) zonal cross-section of vertical velocity anomalies of 3-day intense events. The anomalies are calculated relative to the climatological mean derived from all the 3-day intense events identified.

The evolution of intense 3-day and 5-day intense wet spell events over West Africa examined by the dynamically coupled system involving zonal wind anomalies, vertical motion, divergence fields, and moisture availability depicts the environmental configuration at different phase of these events. During the onset and peak phases (3T1–3T3 and 5T1-5T5), lower-tropospheric zonal wind anomalies (1000–850 hPa) show an intensification of southwesterly monsoon flow, leading to enhanced low-level convergence particularly around 5°–15°E. This anomalous monsoon surge facilitates the transport of moist air from the tropical Atlantic inland and corroborated by positive specific humidity anomalies extending from the surface up to mid-troposphere (Figure 4.43, 4.44, and 4.49, 4.50). Concurrently, the upper troposphere (200 hPa) displays enhanced easterly anomalies south of 15°N and divergence that balance the convergence (cyclonic circulation) at 850 hPa, which create an efficient exhaust pathway for rising air, thereby sustaining deep convection. This vertical coupling of convergence at low levels and divergence aloft aligns with the classic structure of a typical organized MCSs (Houze, 2004; Laing & Fritsch, 2000). The zonal cross-sections of vertical velocity (Figure 4.45 and Figure 4.46) further confirm the presence of deep upward motion peaking between 400–200 hPa during 3T1-3T2 and 5T1-5T3, indicative of intense convective activity facilitated by favourable dynamical and thermodynamical conditions (Fink & Reiner, 2003).

As the events progress toward their decaying phase (3T+1-3T+2 and 5T+1), the anomalous monsoon inflow weakens that reflected in the gradual dissipation of low-level westerly anomalies and a reduction in specific humidity (Figure 4.49 and 4.50), particularly at mid-levels. This transition is accompanied by the collapse of deep upward motion and the onset of anomalous subsidence as seen in the reversal of vertical velocity anomalies ((Figure 4.49 and 4.50) and the emergence of mid-level convergence in the divergence field (Figure 4.47 and 4.48). The weakening of upper-level divergence at 200 hPa further signifies the loss of upper-tropospheric support for convection, completing the convective life cycle. These patterns are consistent with convectively coupled equatorial wave dynamics, such as AEWs and the Madden–Julian Oscillation, which modulate the timing and intensity of rainfall by altering wind shear, vertical motion, and column moisture (Kiladis *et al*., 2006; Janicot *et al*., 2009; Thorncroft *et al*., 2011). Overall, the interplay between zonal wind anomalies, vertical velocity, divergence, and specific humidity across the different phases of the intense multi-day wet spells highlights the crucial role of multiscale atmospheric interactions in driving high-impact rainfall episodes over the West African.

4.5 EXAMINATION OF THE 2005-08-16 3-DAY AND 1991-08-21 5-DAY INTENSE MULTI-DAY WET SPELLS

This section investigates atmospheric preconditioning and environmental factors that favoured the initiation and sustenance of these two identified multi-day intense wet spells. A 3-day intense rainfall event of 2005-08-16 started on 2005-08-14 with centroid area that covered latitude 9.5°N-14.5°N and longitude 4.5°E-14.5°E centered over the Sahelian region of Nigeria. Likewise, 1991-08-21 5-day intense wet spells centroid area covered the latitude between 4.5°N-11.5°N and longitude within 3.5°E-10.5°E that extend from coastal region to the Sahel part of Nigeria. Figure 4.51 illustrates the evolution of VIDMF (shaded) and associated moisture transport (streamlines of VIEWV and VINWV) over West Africa surrounding a representative 3-day intense wet spell event from 14–16 August 2005. The red-outlined box highlights the centroid of the rainfall event that indicate the core region experiencing the intense 3-day event.

On the day prior to onset (13 August; Figure 4.51a), the region around the red box exhibits weak convergence, with cyclonic circulations ahead of it centered over Ivory Coast and another anticyclonic circulation over Gabon and Congo. However, by the onset date (14 August; Figure 4.51b), a clear intensification of moisture convergence appears within the box transported from the Central Africa and a well-defined inland cyclonic circulation centered at the western coast of West Africa. This coincides with the establishment of an efficient moisture pathway from the Atlantic Ocean into the Sahel, driven by the dual action of a southern cyclonic system offshore and the southern hemispheric anticyclone.

During the peak of the event on 15–16 August (Figure 4.51c–d), the inland cyclonic center remains anchored within the red box, marking persistent and deep convergence favorable for sustained convective activity. Concurrently, the offshore cyclonic system continues to funnel moisture inland, enhancing vertical moisture flux into the centroid area. The juxtaposition of these two circulations maintains a high-gradient moisture transport corridor converging into the centroid zone, with a transient col-like structure in between, suggesting mesoscale modulation of convergence. However, the cyclonic circulation over the centroid area was constantly being maintained by the southern hemispheric anticyclonic system around the Gabon

Post-event evolution on 17–18 August (Figure 4.51e–f) shows the cyclonic systems beginning to merge and shift westward, forming an elongated cyclonic arc extending into the Atlantic with divergence dominating over the centroid region. By 18 August, divergence emerges around the red-box region particularly over its northern and western flanks, marking the dissipation of the convergent moisture core and signalling the termination of the wet spell. The persistent alignment of moisture convergence within the red box (centroid) area and moisture transport to it highlights how mesoscale to synoptic-scale circulations interact to maintain rainfall extremes while their decay marks a transition toward drier conditions.

Figure 4.51 also, presents the VIDMF and streamlines during an intense 5-day wet spell over West Africa spanning August 18–21, 1991. Like the 3-day case, the red box highlights the centroid region of maximum rainfall and convergence. On the day preceding the event (August 17), a coherent cyclonic moisture flux circulation emerges inland, overlapping with a region of intense MFC. As the event unfolds, a pronounced strengthening of this cyclonic core is observed, particularly between August 18 and 20, when the MFC intensifies and the cyclonic pattern expands vertically and zonally across the centroid region.

By August 21 (Figure 4.52e), the convergence center is at the western side of the centroid, coinciding with a deepened inland cyclonic system and stronger inflow from the Atlantic via the southwesterly flux. Notably, a merger of inland and coastal cyclonic features occurs during this stage, resulting in an extended zone of enhanced moisture convergence with its ridge over the centroid box. The post-event panel (August 22, Figure 4.52f) shows the presence of a col, indicative of event decay and termination. Throughout the episode, the consistent southward displacement of the anticyclonic ridge in the Southern Hemisphere within the Gabon vicinity aids the meridional advection of moisture, supporting the persistence of the multi-day rainfall event.

A comparison between these 3-day and 5-day intense wet spells highlights several common dynamical features and key differences that shape event persistence. In both cases, the onset of intense rainfall is preceded by the formation of a well-organized inland cyclonic circulation that draws moisture from the Atlantic via a low-level southwesterly jet, feeding into a localized zone of MFC (negative VIDMF known as convergence) within the core region. The red box in both figures marks this consistent area of enhanced convergence and rainfall. However, the 5-day event exhibits a more prolonged and structurally coherent convergence zone, with signs of system merging and regeneration during the event's core days. Unlike the 3-day event where the inland cyclone migrates westward and weakens after day 3, the 5-day event sustains its cyclonic core through the five days, with stronger zonal moisture advection and interaction between adjacent synoptic systems. This prolonged convergence and system reinforcement, particularly around the third and fourth day, appears critical for extending the lifetime of the intense 5-day wet spell. Additionally, the anticyclonic support in the Southern Hemisphere is more persistent in the 5-day case and it promote continuous equatorward moisture transport. These differences underscore the importance of sustained MFC mechanisms and cyclonic merging in the development and longevity of multi-day extreme rainfall events over West Africa.

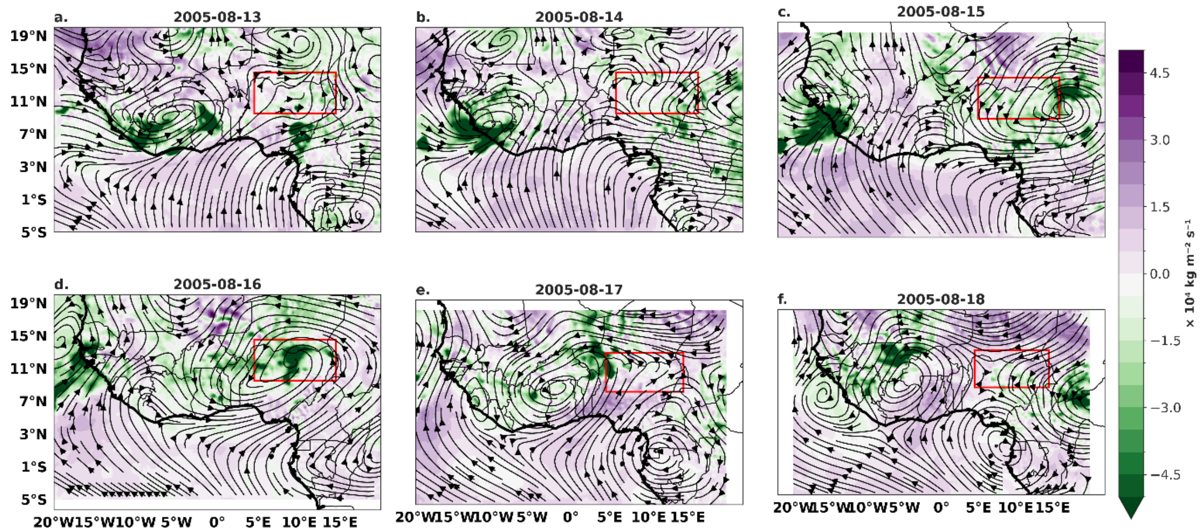

Figure 4.51: Daily evolution of VIDMF; shaded, in ×10-5 kg m-2 s-1 overlaid with streamlines derived from VIEWV and VINWV during 2005-08-16 3-day intense wet spell over from August 14 to 16, 2005.

NOTE: The red box denotes the centroid region of extreme rainfall (9.5-14.5°N, 4.5-14.5°E).

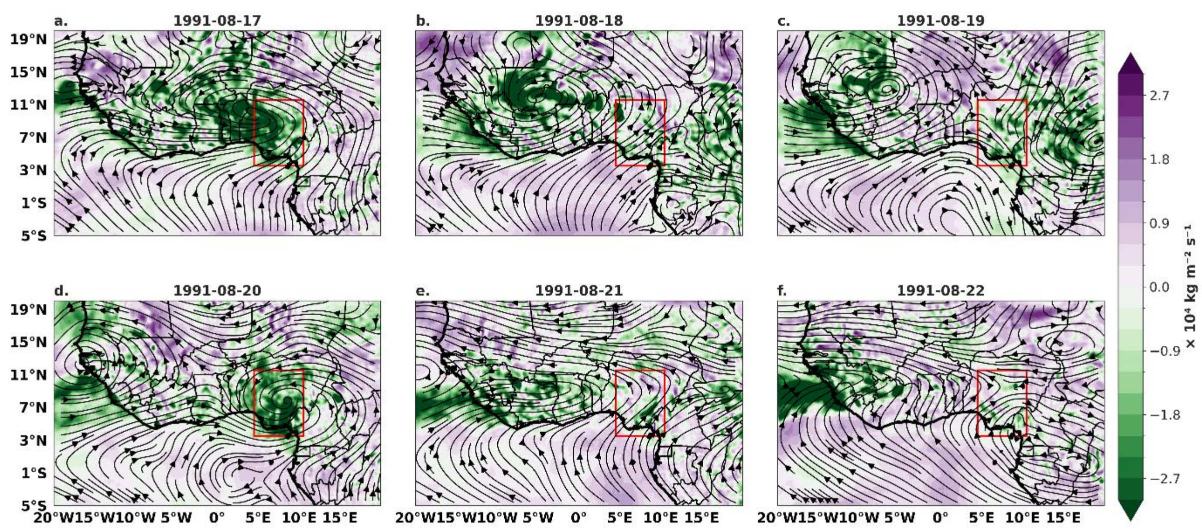

Figure 4.52: Daily evolution of VIDMF; shaded, in ×10-5 kg m-2 s-1 overlaid with streamlines derived from VIEWV and VINWV during 1991-08-21 5-day intense wet spell over from August 14 to 16, 2005.

NOTE: The red box denotes the centroid region of extreme rainfall (9.5-14.5°N, 4.5-14.5°E).

4.6 IMPACT OF CLIMATE CHANGE

This section assesses the impact of warming climate on the occurrence and characteristics of multi-day wet spells under SSP2-4.5 and SSP5-8.5 using the ensemble mean (EnsMean) of 23 high-resolution NEX-GDDP-CMIP6 models that outperform its individual models in replicating daily rainfall. SSP2-4.5 and SSP5-8.5 were selected to represent moderate (current policy-aligned) and high-emission (fossil fuel-intensive) scenarios, respectively, for robust climate impact assessment. see Chapter 2 (Section 2.7) for SSP details. This was done to answer the hypothesis question "what will change in the characteristics of intense multi-day wet spells in time if the rainfall distribution of current times would attain the distribution of a future state?" It is important to state that due to the shorter period of IMERG rainfall dataset compared to KASS-D, GPCC and CHIRPS, it was excluded from the analysis in this section because IMERG climate change signal is not comparable with other datasets.

4.6.1 Climate Model Evaluation

Rainfall over West Africa in space and time is highly heterogeneous, while the network of rain gauges used to quantify it is very poor. Hence, different alternatives, such as reanalysis and satellite rainfall estimates, have been chosen by different researchers to investigate different aspects of rainfall and its extremes. The ability of the NEX-GDDP-CMIP6 models to reproduce the annual daily mean rainfall amount and wet day rainfall amount over West Africa and its three climatic zones was evaluated using Taylor's diagram, as shown in Figure 4.53, and the skill scores are shown in Tables 4.5 – 48. Across West Africa, all the NEX-GDDP-CMIP6 models have correlation values between 0.6 and 0.7 and standard deviations that ranges between 2.8 and 4.2 mm. EnsMean has a correlation value greater than 0.8 with a standard deviation and an RMSE value lower than those of the individual models. This pattern of results is also observed over

Guinea Coast, Savannah, and Sahel in Figure 4.53. EnsMean consistently outperforms individual model across all the climatic zones in West Africa with the lowest standard deviation and RMSE values. This shows that daily mean rainfall is better replicated in EnsMean by efficiently reducing the systematic biases incurred from each model (Bobde *et al*., 2024; Ilori and Balogun, 2021; Mekonnen et al., 2023).

Furthermore, the ability of EnsMean to accurately reproduce rainy days as observed with KASS-D is better than that of the individual NEX-GDDP-CMIP6 models. This is evident by the high POD values between 0.78 and 0.95, with the lowest POFA values reported over West Africa and its three climatic zones (Tables 4.5 – 4.8). This further agreed with the results obtained in Figure 4.53, where EnsMean displayed high correlation values. The HSS is negatively influenced by false alarms (i.e., POFA), EnsMean with the lowest values of POFA is associated with the highest HSS and vice versa for individual models with higher POFA values. The POD of EnsMean and the individual model's ability to identify rainy days are higher than those of the HSS relative random chance. Considering daily rainfall amounts, low r values indicate a low level of agreement between the CHIRPS data and the model data. Across West Africa and its climatic zones, EnsMean consistently has r values greater than or equal to 0.22 compared to individual models with r values less than 0.12. All the models and EnsMean underestimate the rainfall amount, and the underestimation confirmed by the RMSE is mostly for higher rainfall amounts in the order of 10–12 mm day-1. However, EnsMean consistently performed better than the individual NEX-GDDP-CMIP6 models in replicating rainfall amounts and detecting rainy days over West Africa and its climatic zones, as measured by different evaluation metrics. Hence, guided by this result, EnsMean was used in to examine the impact of climate change over West Africa to minimize the effects of systematic biases shown by individual models. Kouakou *et al*., 2023, Bobde *et al*. 2024 and Ilori and Ajayi (2021) used this approach in their studies.

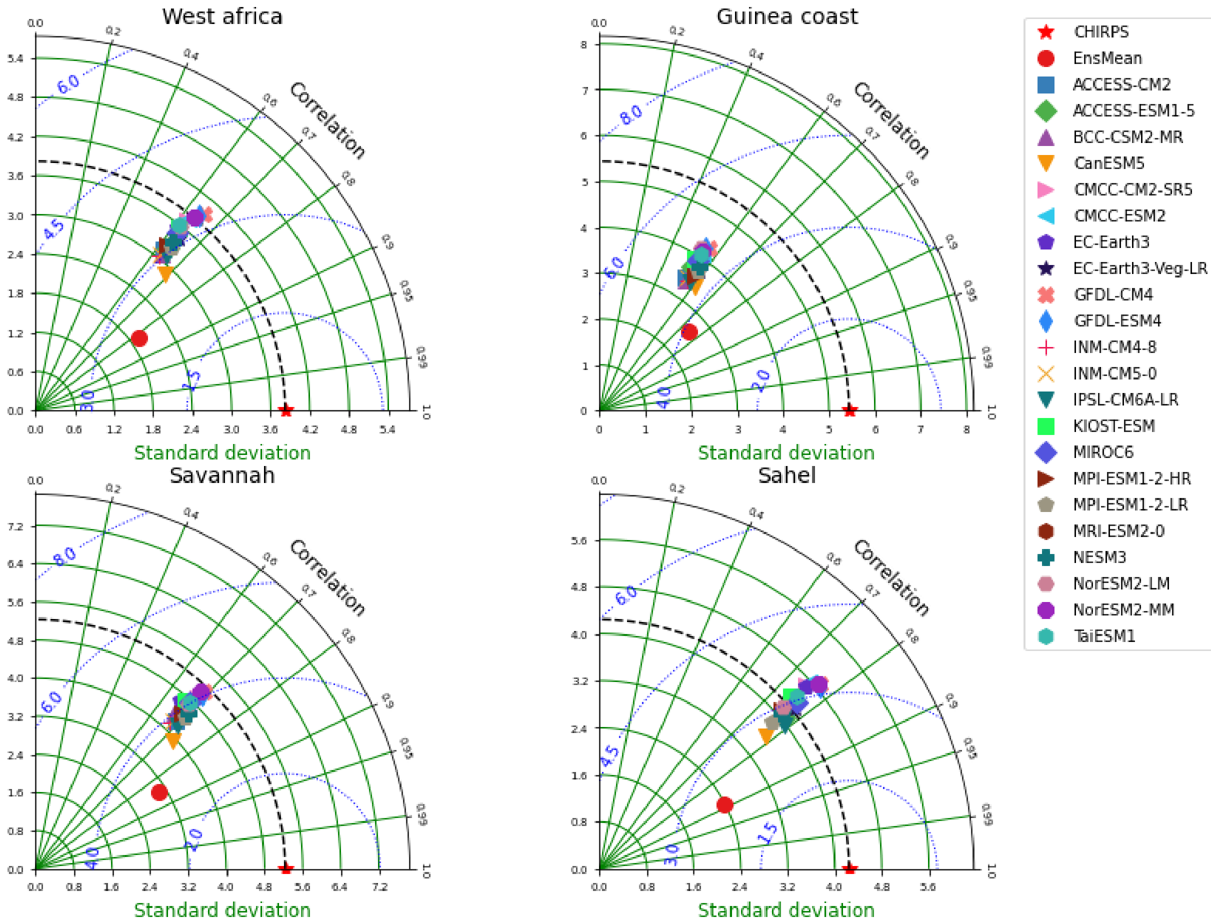

Figure 4.53: Taylor diagrams over West Africa, Guinea Coast, Savannah, and Sahel.

NOTE: The plot shows the correlation coefficient, standard deviation (green arc), and centered RMSE (blue arc) between the NEX-GDDP-CMIP6 models (see the legend), their EnsMean (red circle marker) and CHIRPS reference (red star marker) for both dry and wet days rainfall amount.

Table 4.5: Daily summary of the skill scores obtained from the dichotomous metrics over West Africa. The bold number denotes the best scores among the final products, whereas r, ME, PB, MAE, RMSE and E are computed from the subset of wet days only.

Model	POD	POFA	BID	HSS	r	ME	PB	MAE	RMSE
EnsMean	**0.85**	**0.14**	1.01	0.37	**0.22**	-4.14	-45.31	**5.69**	**8.63**
ACCESS-CM2	0.52	0.22	1.16	0.28	0.07	-1.24	-5.01	7.44	10.79
ACCESS-ESM1-5	0.52	0.22	1.20	0.29	0.07	-1.39	-8.16	7.30	10.68
BCC-CSM2-MR	0.49	0.21	1.13	0.27	0.06	-0.94	-2.33	7.58	11.15
CanESM5	0.61	0.25	1.38	0.32	0.08	-2.50	-21.64	6.88	10.09
CMCC-CM2-SR5	0.45	0.19	1.01	0.26	0.06	-0.44	2.91	7.65	11.11
CMCC-ESM2	0.44	0.19	1.02	0.26	0.06	-0.33	4.53	7.74	11.29
EC-Earth3	0.48	0.20	1.09	0.28	0.05	-0.42	3.49	7.76	11.30
EC-Earth3-Veg-LR	0.51	0.21	1.17	0.29	0.06	-0.93	-1.72	7.54	10.98
GFDL-CM4	0.46	0.19	1.04	0.27	0.05	-0.18	6.24	7.89	11.58
GFDL-ESM4	0.45	0.19	1.03	0.26	0.06	-0.35	4.24	7.72	11.26
INM-CM4-8	0.53	0.23	1.22	0.29	0.07	-1.67	-11.32	7.29	10.69
INM-CM5-0	0.53	0.23	1.22	0.29	0.06	-1.62	-10.60	7.29	10.67
IPSL-CM6A-LR	0.53	0.23	1.16	0.29	0.07	-1.58	-9.51	7.21	10.43
KIOST-ESM	0.52	0.22	1.17	0.29	0.06	-1.44	-9.38	7.38	10.78
MIROC6	0.49	0.21	1.13	0.28	0.06	-0.93	-3.11	7.59	11.18
MPI-ESM1-2-HR	0.51	0.21	1.16	0.29	0.05	-1.18	-6.50	7.36	10.60
MPI-ESM1-2-LR	0.55	0.23	1.25	0.30	0.07	-1.81	-13.73	7.21	10.45
MRI-ESM2-0	0.48	0.20	1.09	0.27	0.05	-0.84	-2.64	7.53	10.91
NESM3	0.55	0.23	1.27	0.30	0.07	-1.65	-12.78	7.20	10.39
NorESM2-LM	0.53	0.22	1.23	0.30	0.07	-1.47	-9.88	7.34	10.68
NorESM2-MM	0.45	0.19	1.02	0.26	0.06	-0.12	6.64	7.88	11.43
TaiESM1	0.48	0.20	1.10	0.27	0.07	-0.63	0.26	7.64	11.18

Table 4.6: Daily summary of the skill scores obtained from the dichotomous metrics over Guinea Coast. The bold number denotes the best scores among the final products, whereas r, ME, PB, MAE, RMSE and E are computed from the subset of wet days only.

Model	POD	POFA	BID	HSS	r	ME	PB	MAE	RMSE
EnsMean	**0.95**	**0.35**	**1.07**	**0.26**	**0.27**	-5.08	-44.46	**7.01**	**11.15**
ACCESS-CM2	0.69	0.45	1.31	0.23	0.08	-3.42	-27.20	8.24	12.19
ACCESS-ESM1-5	0.67	0.44	1.27	0.22	0.09	-3.15	-25.02	8.24	12.11
BCC-CSM2-MR	0.66	0.44	1.26	0.22	0.08	-3.12	-24.67	8.34	12.28
CanESM5	0.76	0.50	1.44	0.25	0.11	-4.14	-33.97	8.01	12.07
CMCC-CM2-SR5	0.59	0.39	1.12	0.20	0.08	-2.48	-18.56	8.45	12.30
CMCC-ESM2	0.59	0.39	1.12	0.20	0.07	-2.43	-18.15	8.51	12.37
EC-Earth3	0.64	0.41	1.20	0.22	0.07	-2.67	-20.50	8.48	12.35
EC-Earth3-Veg-LR	0.65	0.42	1.23	0.23	0.08	-3.08	-24.00	8.38	12.27
GFDL-CM4	0.60	0.39	1.13	0.21	0.07	-2.45	-18.61	8.49	12.33
GFDL-ESM4	0.60	0.39	1.13	0.21	0.07	-2.44	-18.41	8.51	12.38
INM-CM4-8	0.71	0.47	1.34	0.23	0.09	-3.68	-29.61	8.20	12.17
INM-CM5-0	0.70	0.47	1.34	0.22	0.09	-3.60	-28.90	8.24	12.22
IPSL-CM6A-LR	0.71	0.46	1.34	0.24	0.09	-3.77	-30.32	8.16	12.14
KIOST-ESM	0.68	0.45	1.29	0.23	0.08	-3.38	-26.96	8.36	12.33
MIROC6	0.64	0.42	1.20	0.22	0.07	-2.90	-22.53	8.48	12.40
MPI-ESM1-2-HR	0.65	0.42	1.21	0.22	0.08	-3.00	-23.32	8.36	12.27
MPI-ESM1-2-LR	0.70	0.45	1.31	0.24	0.08	-3.56	-28.56	8.23	12.21
MRI-ESM2-0	0.65	0.41	1.21	0.23	0.07	-2.86	-22.20	8.37	12.25
NESM3	0.68	0.45	1.30	0.23	0.09	-3.31	-26.16	8.29	12.22
NorESM2-LM	0.67	0.44	1.27	0.23	0.08	-3.19	-25.09	8.37	12.34
NorESM2-MM	0.60	0.39	1.13	0.21	0.08	-2.30	-17.19	8.53	12.37
TaiESM1	0.61	0.40	1.15	0.20	0.08	-2.37	-17.97	8.44	12.28

Table 4.7: Daily summary of skill score obtained from the dichotomous metrics over Savannah. The bold number denotes the best scores among the final products while r, ME, PB, MAE, RMSE and E are computed from the subset of wet days only.

Model	POD	POFA	BID	HSS	r	ME	PB	MAE	RMSE
EnsMean	0.93	0.18	1.05	0.46	0.31	-1.32	-6.52	6.24	9.51
ACCESS-CM2	0.61	0.28	1.12	0.33	0.08	-2.16	-17.86	7.95	11.26
ACCESS-ESM1-5	0.61	0.28	1.12	0.33	0.09	-1.95	-16.46	7.86	11.12
BCC-CSM2-MR	0.58	0.26	1.06	0.32	0.08	-1.66	-13.34	8.07	11.40
CanESM5	0.71	0.32	1.30	0.37	0.11	-3.17	-28.30	7.49	10.83
CMCC-CM2-SR5	0.53	0.23	0.95	0.30	0.07	-1.11	-7.85	8.16	11.42
CMCC-ESM2	0.53	0.23	0.95	0.30	0.07	-0.93	-6.28	8.20	11.50
EC-Earth3	0.57	0.25	1.02	0.32	0.06	-1.26	-9.62	8.23	11.52
EC-Earth3-Veg-LR	0.59	0.26	1.06	0.33	0.07	-1.70	-13.72	8.09	11.38
GFDL-CM4	0.54	0.24	0.97	0.31	0.06	-1.04	-7.55	8.22	11.53
GFDL-ESM4	0.54	0.24	0.98	0.30	0.07	-1.03	-7.49	8.20	11.49
INM-CM4-8	0.64	0.29	1.16	0.34	0.09	-2.35	-20.08	7.82	11.15
INM-CM5-0	0.63	0.29	1.16	0.34	0.09	-2.34	-19.95	7.87	11.20
IPSL-CM6A-LR	0.64	0.28	1.16	0.35	0.08	-2.38	-20.30	7.73	10.99
KIOST-ESM	0.61	0.27	1.11	0.33	0.07	-2.07	-17.38	7.97	11.30
MIROC6	0.58	0.26	1.04	0.32	0.08	-1.54	-12.28	8.08	11.41
MPI-ESM1-2-HR	0.59	0.26	1.07	0.33	0.08	-1.70	-13.74	7.98	11.22
MPI-ESM1-2-LR	0.63	0.28	1.14	0.34	0.09	-2.23	-18.84	7.85	11.11
MRI-ESM2-0	0.57	0.25	1.02	0.32	0.07	-1.27	-9.58	8.11	11.39
NESM3	0.63	0.28	1.14	0.34	0.09	-1.94	-16.37	7.90	11.16
NorESM2-LM	0.62	0.27	1.12	0.34	0.07	-1.92	-15.98	7.98	11.27
NorESM2-MM	0.54	0.23	0.97	0.31	0.06	-0.88	-5.93	8.33	11.64
TaiESM1	0.56	0.25	1.01	0.31	0.07	-1.24	-9.50	8.09	11.38

Table 4.8: Daily summary of the skill scores obtained from the dichotomous metrics over Sahel. The bold number denotes the best scores among the final products, whereas r, ME, PB, MAE, RMSE and E are computed from the subset of wet days only.

Model	POD	POFA	BID	HSS	r	ME	PB	MAE	RMSE
EnsMean	0.86	0.11	1.07	0.44	0.23	1.15	3.36	5.29	7.89
ACCESS-CM2	0.48	0.14	1.10	0.34	0.07	-0.36	1.70	7.37	10.56
ACCESS-ESM1-5	0.50	0.14	1.15	0.34	0.06	-0.74	-3.69	7.24	10.49
BCC-CSM2-MR	0.46	0.13	1.07	0.32	0.06	0.00	5.59	7.57	11.14
CanESM5	0.58	0.16	1.32	0.37	0.07	-1.77	-15.73	6.79	9.88
CMCC-CM2-SR5	0.42	0.11	0.94	0.31	0.06	0.49	10.86	7.64	11.11
CMCC-ESM2	0.42	0.12	0.97	0.31	0.07	0.64	13.50	7.76	11.28
EC-Earth3	0.45	0.12	1.03	0.33	0.04	0.58	12.34	7.76	11.33
EC-Earth3-Veg-LR	0.50	0.13	1.13	0.35	0.06	-0.09	4.75	7.46	10.79
GFDL-CM4	0.43	0.12	0.98	0.31	0.06	0.87	16.16	7.94	11.60
GFDL-ESM4	0.42	0.12	0.98	0.31	0.07	0.58	12.13	7.66	11.08
INM-CM4-8	0.50	0.14	1.16	0.34	0.07	-0.85	-4.98	7.24	10.58
INM-CM5-0	0.50	0.14	1.15	0.34	0.06	-0.84	-4.65	7.21	10.49
IPSL-CM6A-LR	0.50	0.14	1.13	0.34	0.08	-0.84	-5.00	7.01	9.97
KIOST-ESM	0.49	0.14	1.11	0.34	0.07	-0.58	-2.08	7.32	10.73
MIROC6	0.47	0.13	1.07	0.33	0.07	-0.10	3.75	7.50	11.00
MPI-ESM1-2-HR	0.49	0.13	1.12	0.34	0.05	-0.57	-1.87	7.21	10.30
MPI-ESM1-2-LR	0.53	0.15	1.22	0.36	0.07	-1.19	-9.21	7.09	10.19
MRI-ESM2-0	0.45	0.13	1.04	0.32	0.05	-0.01	4.47	7.41	10.66
NESM3	0.54	0.15	1.24	0.36	0.07	-0.96	-7.38	7.08	10.15
NorESM2-LM	0.52	0.15	1.20	0.35	0.07	-0.78	-4.53	7.24	10.48
NorESM2-MM	0.43	0.12	0.97	0.32	0.06	0.80	14.52	7.87	11.35
TaiESM1	0.46	0.13	1.06	0.32	0.07	0.07	6.22	7.63	11.18

4.6.2 Adjusted Daily Rainfall Amount, Description of the 3-Day and 5-Day 90th Percentile Value and Frequency of Occurrence

Figure 4.54 illustrates the adjusted daily rainfall amounts derived from three observational datasets (KASS-D, GPCC, and CHIRPS), incorporating projected climate change signals from the ensemble mean (EnsMean) of the NEX-GDDP global climate models under the SSP2-4.5 and SSP5-8.5 scenarios. The assessment focuses on four representative locations namely: Ouagadougou, Jos, Parakou, and Port Harcourt for the calendar year 2009.

Across all stations and observational datasets, the adjusted daily rainfall values consistently exceed the corresponding observed (gauged) rainfall, suggesting a robust intensification signal in future climate projections. Despite the overall increase in magnitude, the temporal characteristics, specifically, the onset and intra-seasonal progression of rainfall are well preserved in the adjusted datasets. This maintained alignment with the historical rainfall pattern. This upward shift in rainfall intensity is further validated through the quantile-quantile (Q-Q) analysis presented in Figure 4.55, which reveals enhanced adjusted rainfall values across all quantile levels under both SSP scenarios. These results underscore the implication that, should historical rainfall distributions adopt the characteristics of projected future climates, the frequency and magnitude of daily rainfall events would be substantially higher. Moreover, the adjusted datasets exhibit a significant elevation in the 90th percentile of 3-day and 5-day accumulated rainfall amount over the study region (Figures 4.56 and 4.57). However, the increase is more pronounced under SSP5-8.5 compared to SSP2-4.5, with enhancements exceeding 15% in the coastal and Niger Delta regions and narrowing to below 10% north of 12°N. This spatial gradient is particularly well captured in the CHIRPS dataset, which exhibits a coherent latitudinal variation with smoother transitions (Figure 4.56d, h).

Using these percentile-adjusted datasets and applying the methodology outlined for multi-day wet spell identification, Figure 4.58 presents the projected spatial distribution of the mean annual frequency of intense 3-day and 5-day wet spells and overlaid with the contour of number of wet days, under SSP2-4.5. The distribution shows the highest wet-day counts in the southern coastal zone and the lowest in the northern Sahel region. The frequency of 3-day intense wet spells exhibits a marked latitudinal gradient, with adjusted KASS-D (Figure 4.58b) indicating between 20 and 45 annual events in the south and fewer than 10 events north of 12°N. A region of lower wet spell frequency is evident over the Ghana-Benin dry zone (Dahomey Gap) that is consistent with documented climatic features of this area (Vollmert *et al*., 2003; Nicholson, 2011; Weber *et al*., 2001). This anomaly is attributable to coastal upwelling and SW-NE-oriented frictional divergence, which collectively contribute to the relative aridity of the region. Within the latitudinal band of 7°N to 12°N, a high spatial variability is observed with intense wet spell counts ranging from 12 to 40 events per year. Comparable patterns are detected in the adjusted GPCC and CHIRPS datasets, albeit with minor variations in magnitude and spatial coherence. CHIRPS, for instance, tends to simulate a higher frequency of events south of 8°N compared to GPCC and KASS-D.

Over orographic and coastal regions, such as the Jos Plateau and the Niger Delta, inter-dataset discrepancies in rainfall representation persist that emphasize the influence of topography and coastal dynamics on precipitation processes over West Africa. The relatively subdued and smoothed signal observed in EnsMean projections (Figure 4.58a, f) could be linked to both the lower 90th percentile values and the inherent averaging effect of ensemble methodologies.

The spatial pattern of 5-day intense wet spells (Figure 4.59) mirrors that of the 3-day events but at reduced magnitudes, reflecting the influence of event duration on extreme precipitation characteristics across the domain.

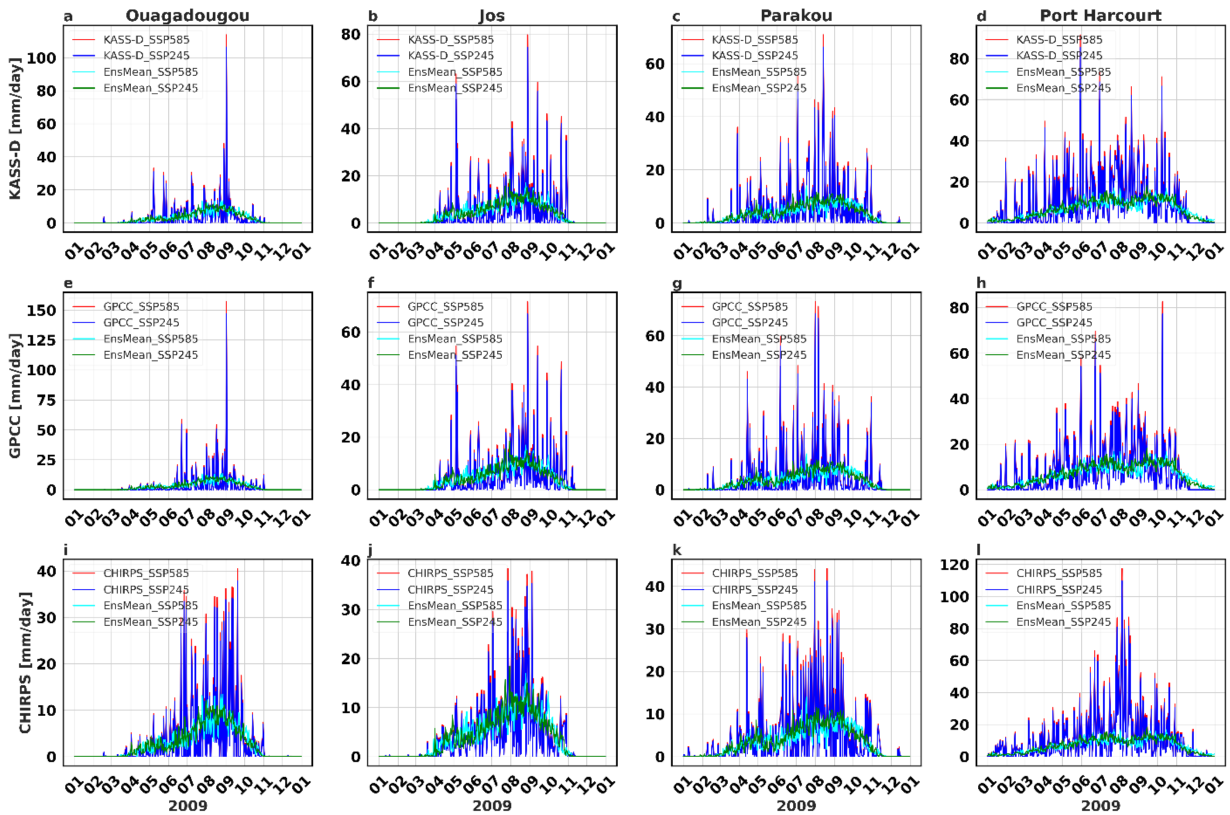

Figure 4.54: Comparing adjusted KASS-D (a-d), GPCC (e-h) and CHIRPS (i-l) daily rainfall amount under SSP2-4.5 (purple line) and SSP5-8.5 (red line) with historical EnsMean daily rainfall (cyan line) over four selected stations.

NOTE: These selected stations include Ouagadougou (first column), Jos (second column), Parakou (third column) and Port Harcourt (fourth column).

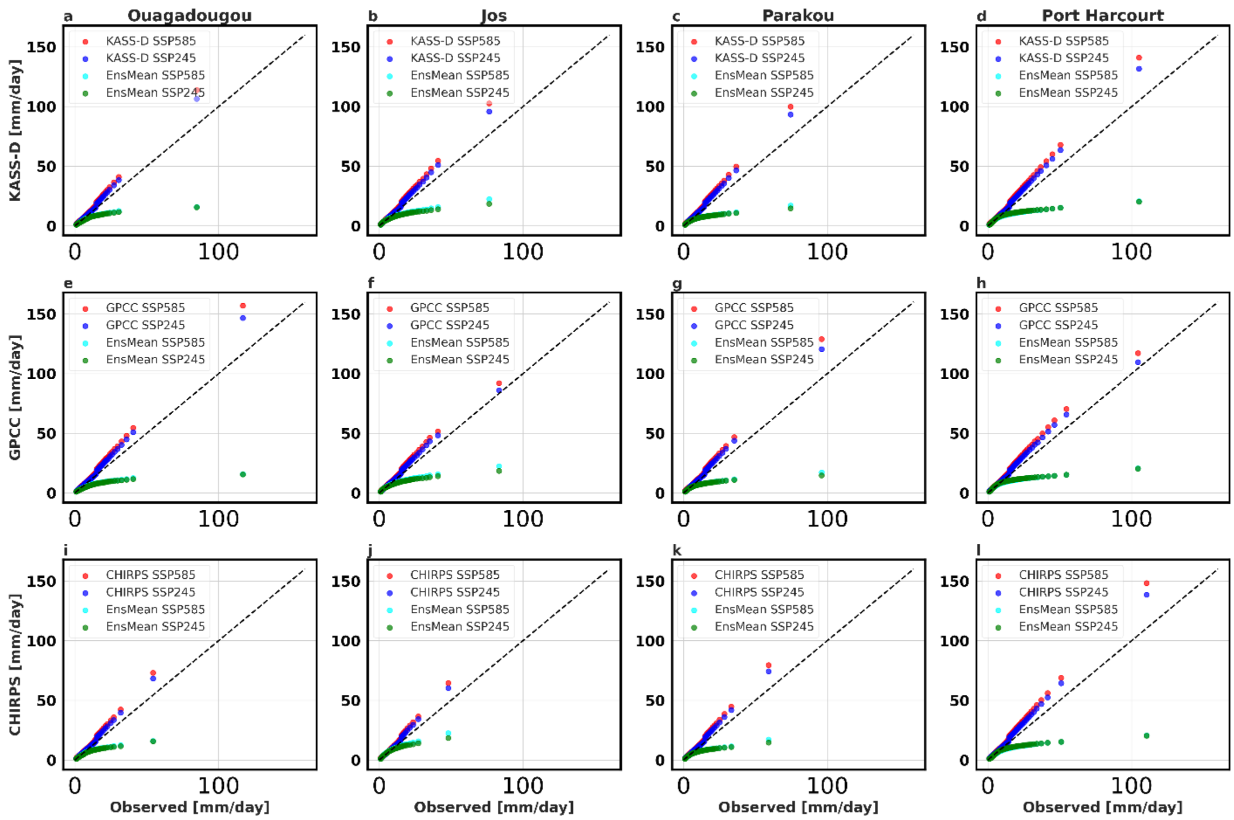

Figure 4.55: Quantile-Quantile plot of wet days only for Ouagadougou (first column), Jos (second column), Parakou (third column) and Port Harcourt (fourth column).

NOTE: The y-axis corresponds to the adjusted daily rainfall of KASS-D (a-d), GPCC (e-h) and CHIRPS (i-l) daily rainfall amount under SSP2-4.5 (purple line) and SSP5-8.5 (red line) while the x-axis corresponds to the observation dataset (reference) dataset. The cyan and green circle-colored markers depict projected EnsMean daily rainfall under SSP2-4.5 and SSP5-8.5, respectively. The black dash diagonal line depicts the ideal fit line (1:1)

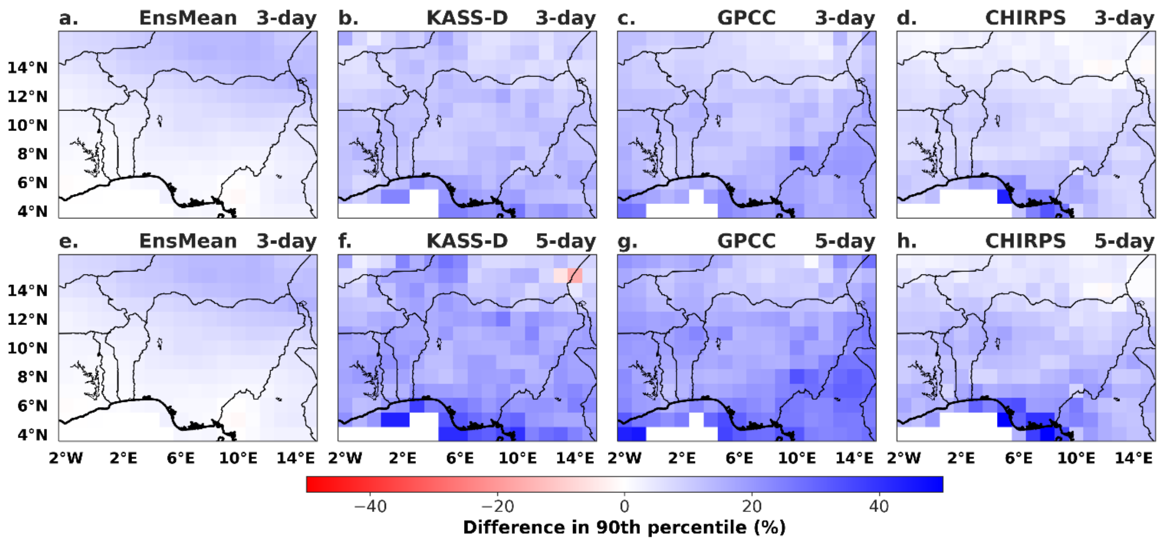

Figure 4.56: Difference in 3-day and 5-day accumulation 90th percentile value computed between adjusted observed KASS-D, GPCC and CHIRPS relative to unadjusted observation in percentage under SSP2-4.5. The same was done for EnsMean.

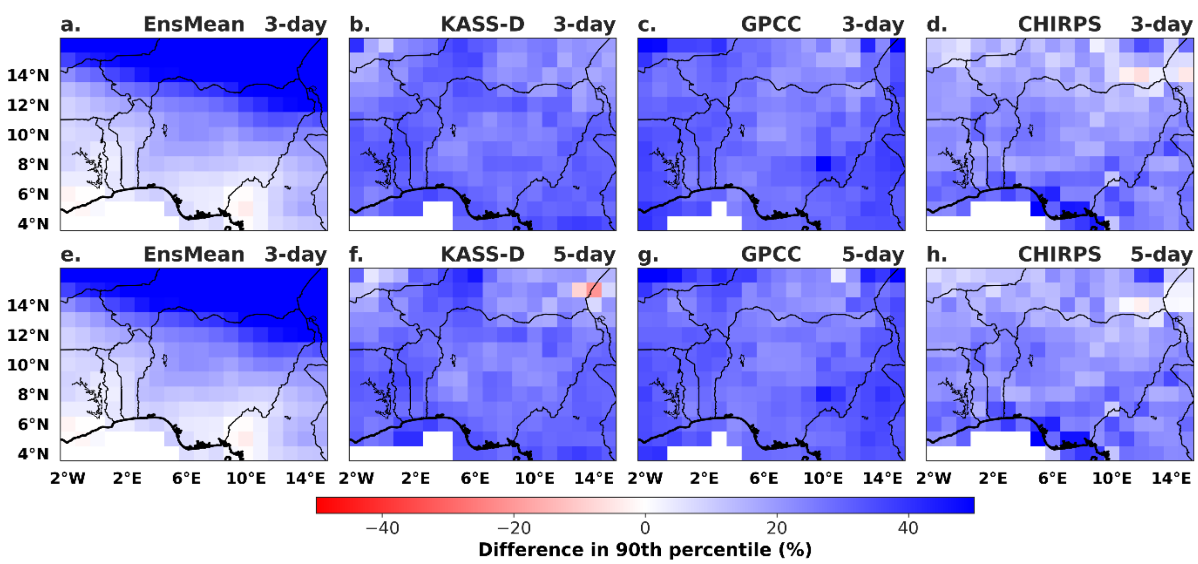

Figure 4.57: Difference in 3-day and 5-day accumulation 90th percentile value computed between adjusted observed KASS-D, GPCC and CHIRPS relative to unadjusted observation in percentage under SSP5-8.5. The same was done for EnsMean.

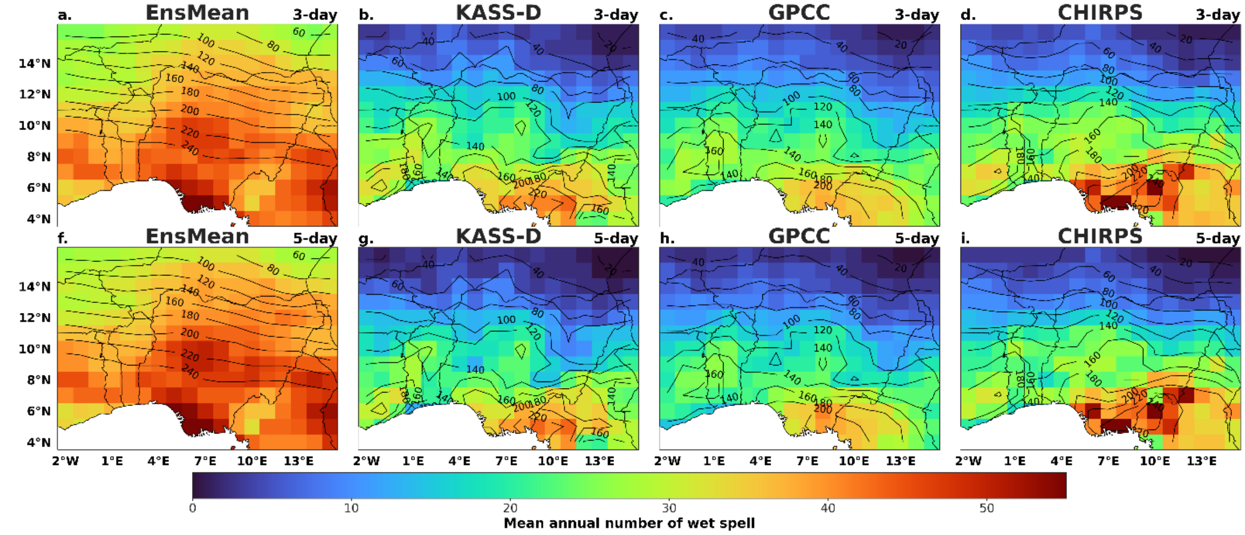

Figure 4.548: Spatial distribution of mean annual frequency of occurrence of intense 3-day (first row) and 5-day (second row) wet spells (color fill) and mean annual number of wet days (contour line) for the adjusted KASS-D, GPCC, CHIRPS and EnsMean under SSP2-4.5.

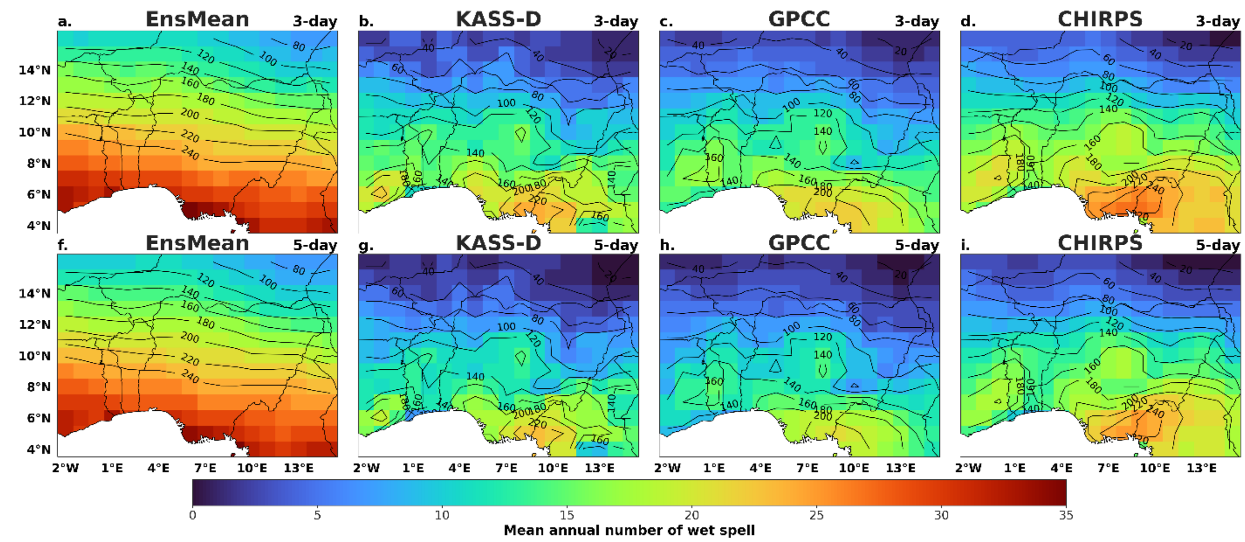

Figure 4.59: Spatial distribution of mean annual frequency of occurrence of intense 3-day (first row) and 5-day (second row) wet spells (color fill) and mean annual number of wet days (contour line) for the adjusted KASS-D, GPCC, CHIRPS and EnsMean under SSP5-8.5.

4.6.3 Seasonal, Inter-Annual Variation and Size Classification of Adjusted 3-day and 5-Day Wet Spells

Figures 4.60 and 4.61 illustrate the seasonal differences in the frequency of occurrence of 3-day and 5-day intense wet spells between observation and adjusted observational datasets (KASS-D, GPCC, and CHIRPS) across the three principal climatic zones of West Africa: the Guinea Coast, the Savannah, and the Sahel. These comparisons were conducted under the SSP2-4.5 and SSP5-8.5 emission pathways. Positive anomalies in the number of events per grid cell noted in both scenarios indicate that if the present rainfall distributions were to reflect the characteristics of projected climates, a significant amplification in the seasonal frequency of intense multi-day wet spells would occur. The projected changes under SSP5-8.5 are consistently more pronounced than those under SSP2-4.5. These increases align with the seasonal progression of rainfall across the region, suggesting a potential intensification of the West African Monsoon (WAM) and its associated moisture delivery mechanisms. In all adjusted datasets, the most substantial increases in event frequency occur during the peak of the rainy season in each climatic zone, with increased rainfall further noted at the onset of the season.

Given that the impacts of climate change on precipitation extremes tend to be more perceptible at regional scales (IPCC, 2021), Figures 4.62 to 4.64 present inter-annual trends in the frequency of intense 3-day and 5-day wet spells across the same climatic zones. These trends reveal an upward trajectory, with annual increases ranging from 0.03 to 0.07 events over the Guinea Coast, 0.02 to 0.29 events over the Savannah, and 0.02 to 0.17 events over the Sahel compared to the unadjusted observational records. A notable inflection point occurs between 1996 and 1998, where the frequency of multi-day wet spells trend lines begins to surpass the historical long-term mean of unadjusted. Over the Guinea Coast (Figure 4.62), only adjusted KASS-D displays statistically significant trends for both the 3-day and 5-day wet spell frequencies under both SSP scenarios (Figure 4.62c-d). In contrast, the adjusted GPCC dataset exhibits statistically insignificant changes, while adjusted CHIRPS shows a significant upward trend for 3-day wet spells only. Within the Savannah region (Figure 4.63), GPCC alone shows statistically significant trends for both spell durations under both scenarios. The CHIRPS dataset remains largely insignificant, whereas KASS-D shows significance only for 5-day spells under SSP5-8.5. For the Sahel (Figure 4.64), both KASS-D and GPCC reflect significant trends in 3-day and 5-day wet spells, while CHIRPS shows a significant increase only for the 5-day category. The EnsMean projections also reveal spatially differentiated responses: statistically significant increasing trends in 3-day and 5-day spells are detected under SSP5-8.5 in the Guinea Coast and under SSP2-4.5 in both the Savannah and Sahel. These variations across datasets reflect the sensitivity of rainfall extremes to methodological differences, including the density of in-situ observations, algorithmic formulations, and quality control processes employed during dataset development.

Figures 4.65 to 4.67 portray the year-to-year differences in the percentage contribution of intense multi-day wet spells to total rainfall over the Guinea Coast, Savannah, and Sahel, respectively. These contributions derived from exceedance-based event identification indicate the magnitude of extreme rainfall inputs to total annual rainfall amount. In the early 1980s, a general decline in contributions is noted, followed by a progressive increase, particularly under SSP5-8.5, which exhibits greater enhancement than SSP2-4.5. CHIRPS reveals a sustained positive trend from the early 1980s to 2011, signaling an elevated role of intense spells in annual rainfall budgets. Inter-annual variability remains apparent, underscoring the influence of climatic oscillations on precipitation patterns.

Finally, results from the Mann-Kendall trend test (Tables 4.9 – 4.10) classify intense wet spells by spatial extent based on grid cells that would have exceed the 90th percentile amount. Small-sized intense events would have decreased and occurred less at annual scale with a statistically significant decreasing trend across all three datasets under both climate scenarios. Conversely, large-sized events show a significant upward trend, suggesting that intense rainfall episodes are not only becoming more frequent but are also expanding in spatial coverage across the domain. This intensification and spatial proliferation of intense multi-day wet spells aligns with broader climate model projections that anticipate an escalation in the severity and reach of extreme weather events under global warming scenarios (IPCC, 2021).

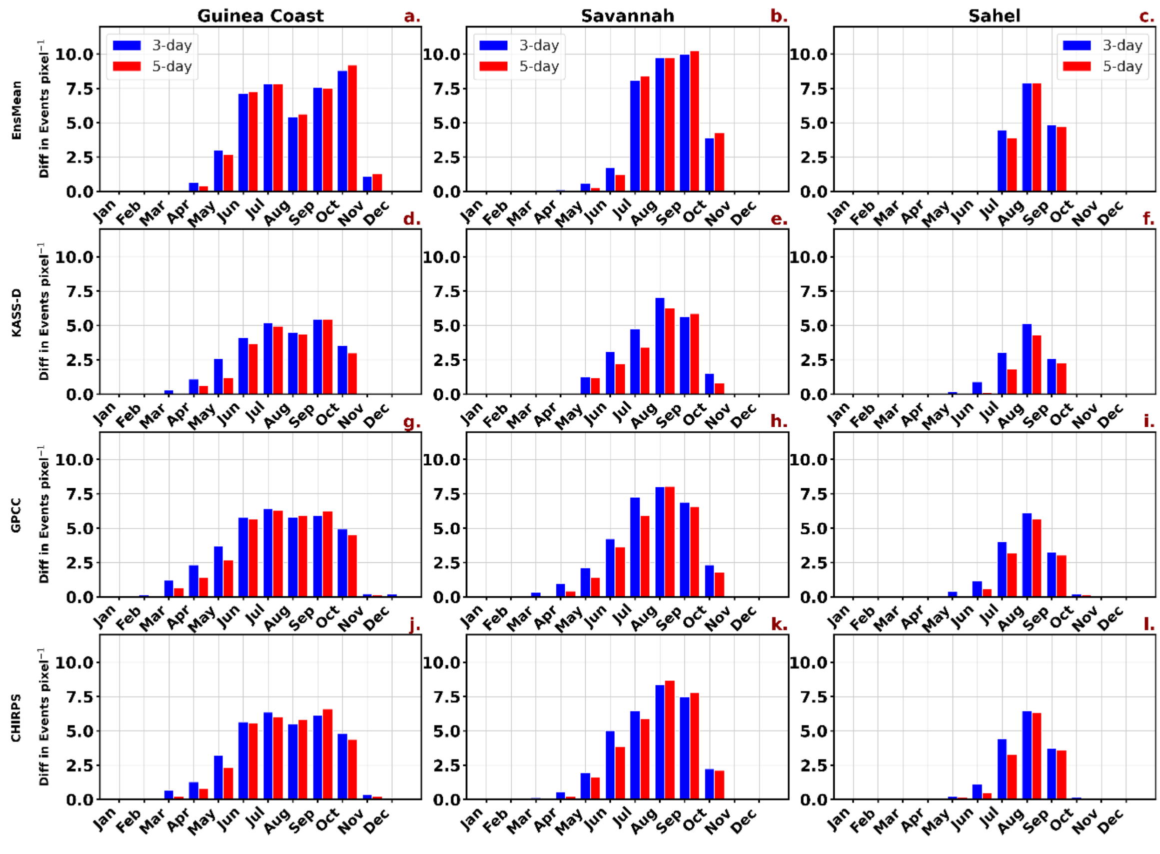

Figure 4.60: Seasonal difference in frequency of occurrence of intense 3- and 5-day wet spells per grid cell for 1982-2011 between observations and its adjusted datasets and EnsMean averaged over the three climatic zones of the interpolation domain under SSP2-4.5.

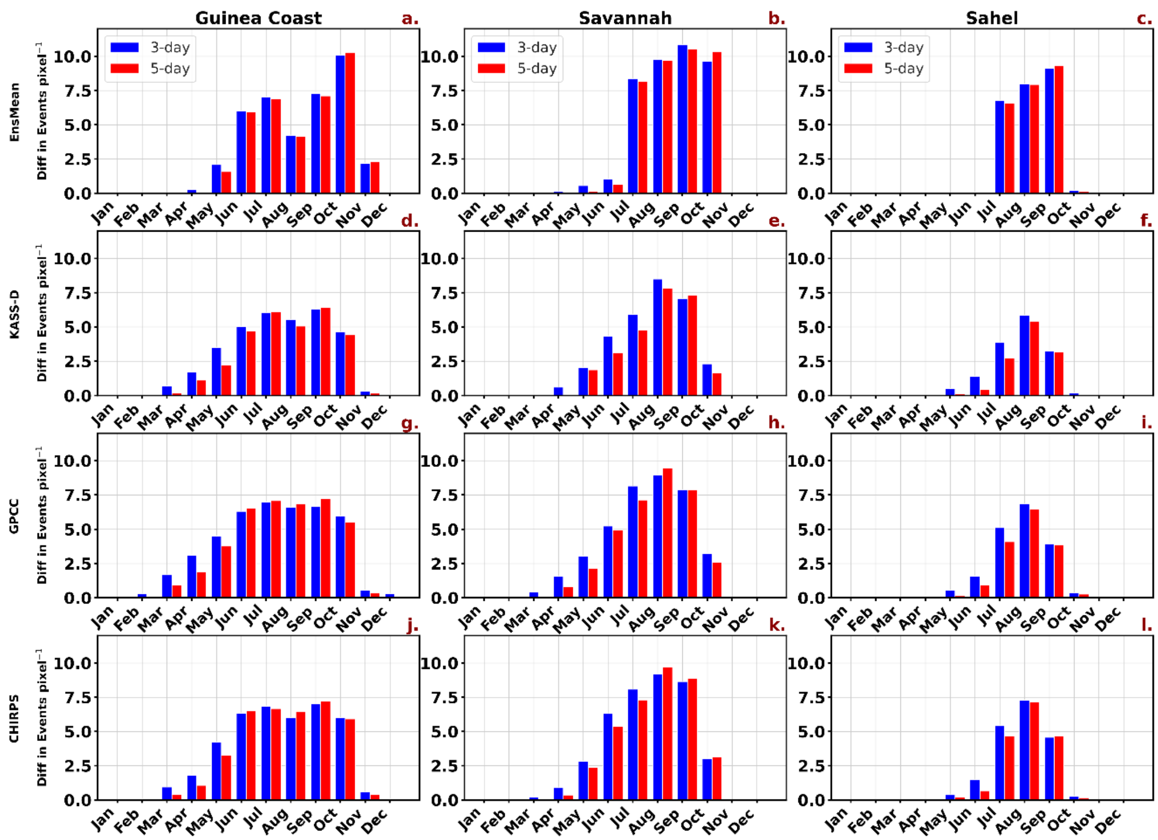

Figure 4.61: Seasonal difference in frequency of occurrence of intense 3- and 5-day wet spells per grid cell for 1982-2011 between observations and its adjusted datasets and EnsMean averaged over the three climatic zones of the interpolation domain under SSP5-8.5

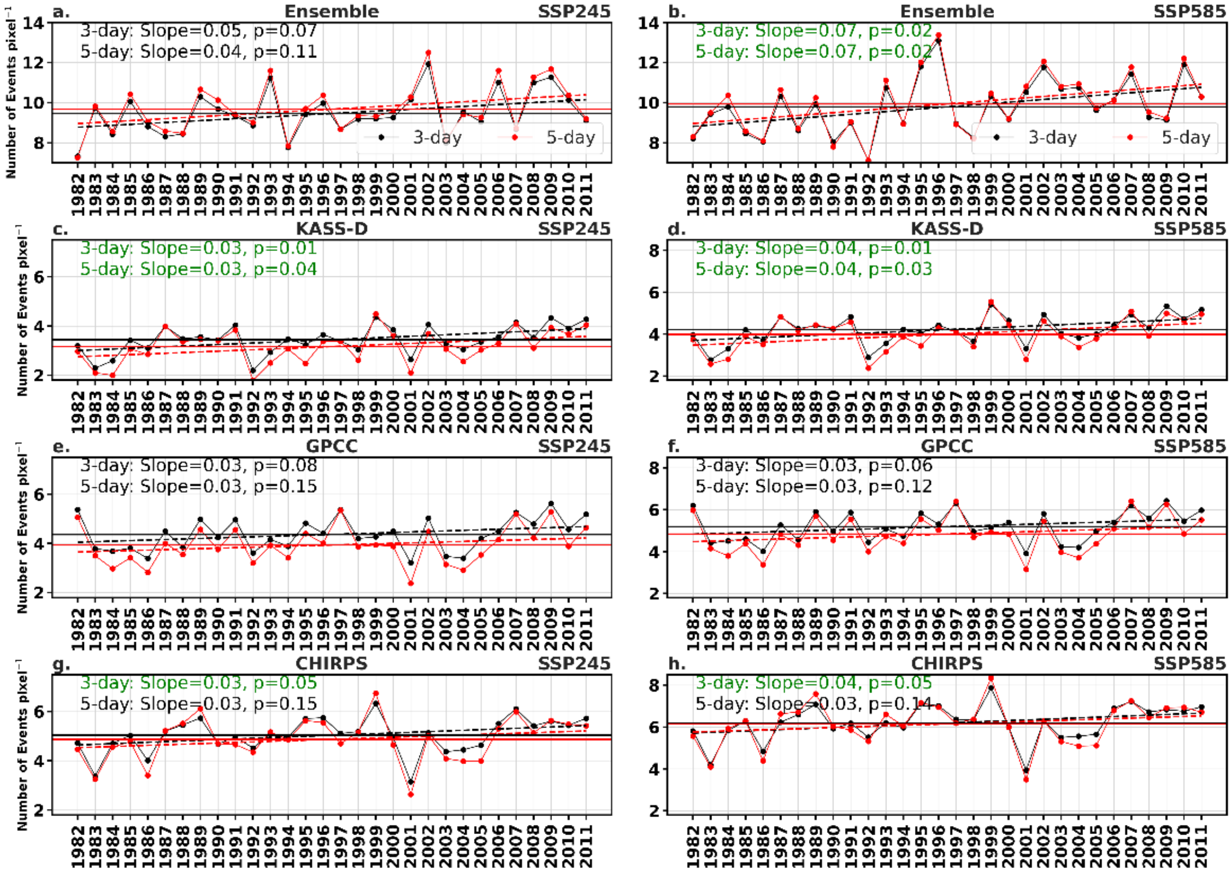

Figure 4.62: Inter-annual variation of frequency of occurrence of intense 3-day and 5-day wet spells per grid cell from 1982-2011 for the adjusted observed KASS-D, GPCC, CHIRPS and EnsMean averaged over Guinea Coast under SSP2-4.5 and SSP5-8.5

NOTE: Black and red thick lines represent the unadjusted climatological mean of intense 3- and 5-day frequency of occurrence while dash lines depict trend lines for the adjusted observation

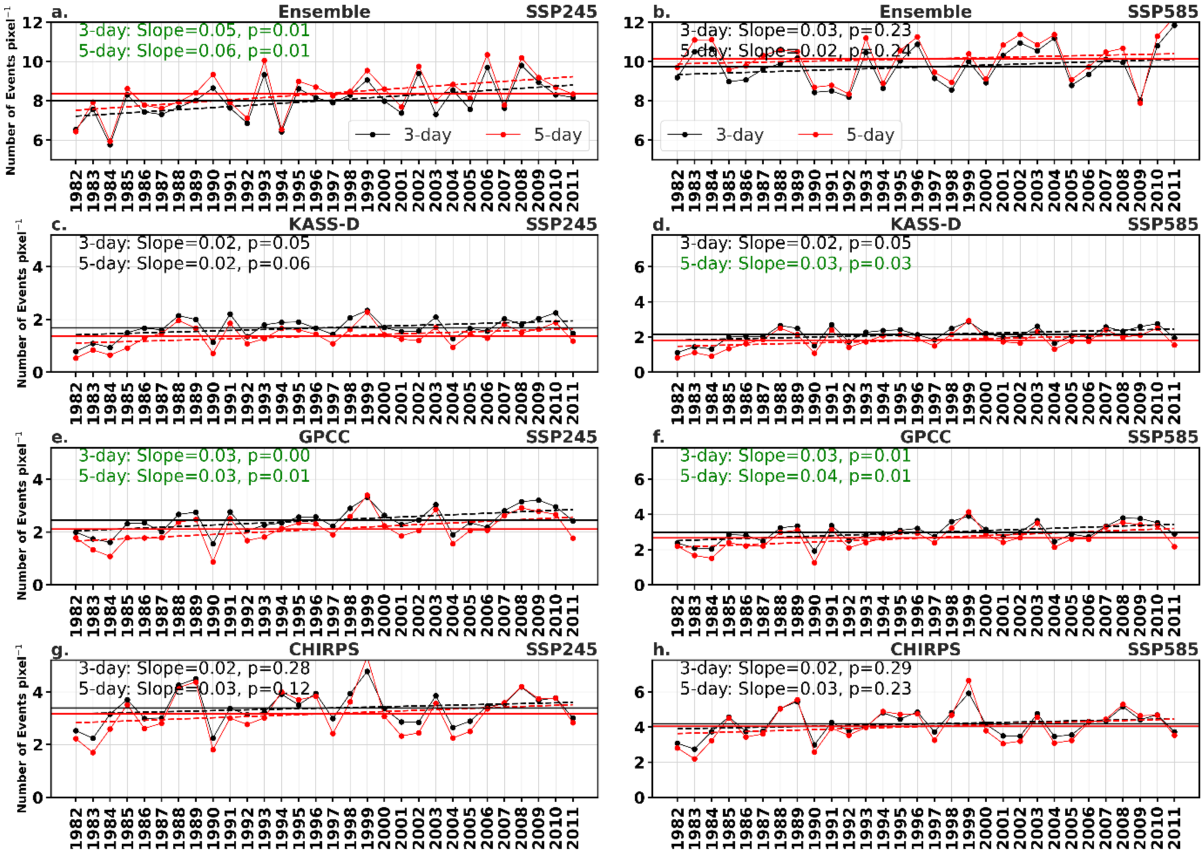

Figure 4.63: Inter-annual variation of frequency of occurrence of intense 3-day and 5-day wet spells per grid cell from 1982-2011 for the adjusted observed KASS-D, GPCC, CHIRPS and EnsMean averaged over Savannah under SSP2-4.5 and SSP5-8.5.

NOTE: Black and red thick lines represent the unadjusted climatological mean of intense 3- and 5-day frequency of occurrence while dash lines depict trend lines for the adjusted observation.

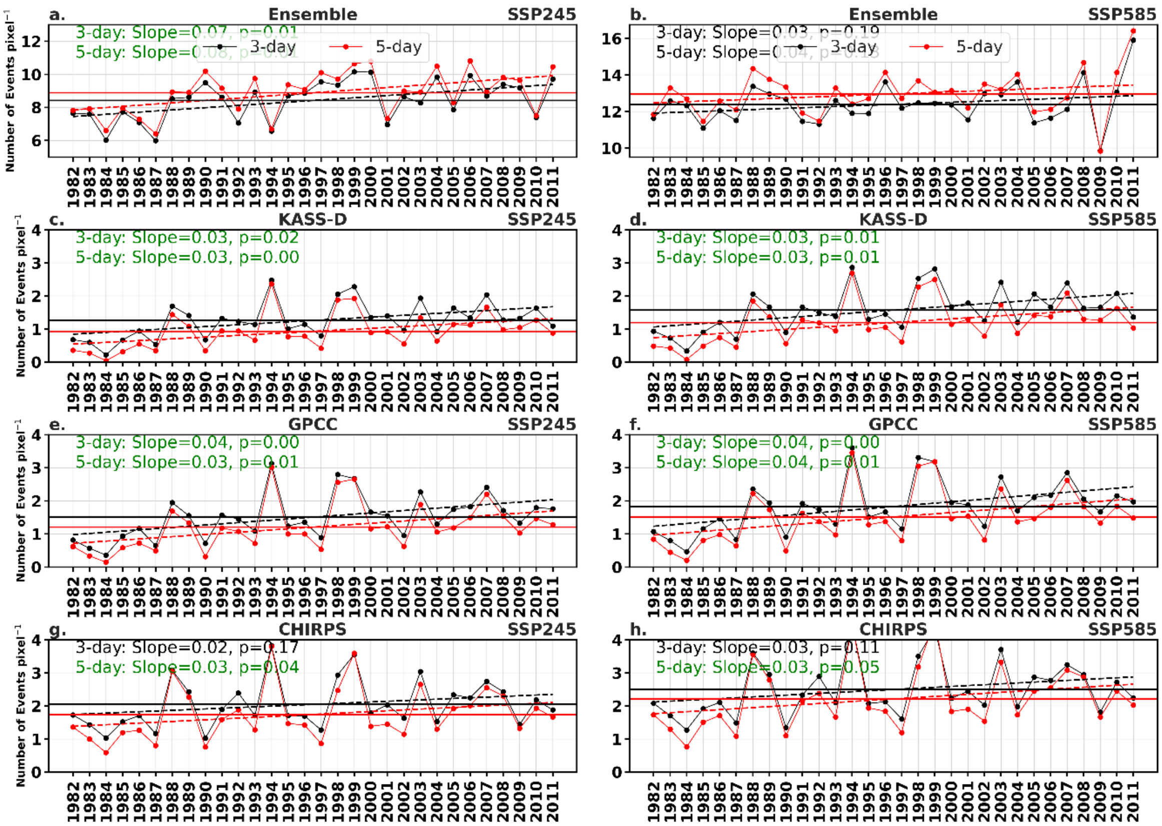

Figure 4.64: Inter-annual variation of frequency of occurrence of intense 3-day and 5-day wet spells per grid cell from 1982-2011 for the adjusted observed KASS-D, GPCC, CHIRPS and EnsMean averaged over Sahel under SSP2-4.5 and SSP5-8.5.

NOTE: Black and red thick lines represent the unadjusted climatological mean of intense 3- and 5-day frequency of occurrence while dash lines depict trend lines for the adjusted observation.

Table 4.9: Mann-Kendall trend test results for 3-day intense multi-day wet spells of different sizes (small: 1–9 grid cells, mid: 10–20, large: >20) over the interpolation domain computed from adjusted observational datasets and EnsMean under SSP2-4.5 and SSP5-8. Note: KASS-D uses SPHEREMAP interpolation (Section 3.3.1); IMERG excluded due to shorter period (2001–2020). The bold p-value indicates a statistically significant trend at a 0.05 significant level.

		SSP2-4.5			SSP5-8.5		
Dataset	Size Classification	Trend	Sen's Slope	p-value	Trend	Sen's Slope	p-value
EnsMean	Small size	Decreasing	-0.33	0.12	**Decreasing**	-0.375	0.018
	Mid size	**Decreasing**	-0.33	0.036	No trend	-0.125	0.37
	Large size	Increasing	0.45	0.12	**Increasing**	0.571	0
KASS-D	Small size	**Decreasing**	-0.33	0.017	Decreasing	-0.107	0.031
	Mid size	**increasing**	0.33	0.04	No trend	0.157	0.361
	Large size	**increasing**	0.71	0.01	**Increasing**	0.727	0
GPCC	Small size	**Decreasing**	-0.54	0.03	**Decreasing**	-0.636	0.018
	Mid size	No trend	0.4	0.11	No trend	0.214	0.209
	Large size	**Increasing**	0.75	0.001	**Increasing**	0.8	0.003
CHIRPS	Small size	**Decreasing**	-0.29	0.11	**Decreasing**	-0.35	0.053
	Mid size	No trend	-0.08	0.34	No trend	0	0.914
	Large size	**Increasing**	0.44	0.11	**Increasing**	0.5	0.041

Table 4.10: KASS-D uses SPHEREMAP interpolation (Section 3.3.1); IMERG excluded due to shorter period (2001–2020). The bold p-value indicates a statistically significant trend at a 0.05 significant level. Note: KASS-D uses SPHEREMAP interpolation (Section 3.3.1); IMERG excluded due to shorter period (2001–2020). The bold p-value indicates a statistically significant trend at a 0.05 significant level.

		SSP2-4.5			SSP5-8.5		
Dataset	Size Classification	Trend	Sen's Slope	p-value	Trend	Sen's Slope	p-value
EnsMean	Small size	**Decreasing**	-0.36	0.18	No trend	0.909	0.734
	Mid size	**Decreasing**	-0.571	0.003	No trend	-0.166	0.267
	Large size	**Increasing**	0.714	0.012	**Increasing**	0.533	0.001
KASS-D	Small size	**Decreasing**	-0.125	0.667	**Decreasing**	-0.125	0.047
	Mid size	No trend	0.178	0.203	No trend	0	0.886
	Large size	**Increasing**	0.8	0.006	**Increasing**	0.888	0.005
GPCC	Small size	**Decreasing**	-0.684	0.02	**Decreasing**	-0.318	0.231
	Mid size	No trend	0.333	0.107	No trend	-0.055	0.928
	Large size	**Increasing**	0.692	0.005	**Increasing**	0.8	0.001
CHIRPS	Small size	**Decreasing**	-0.7	0.041	**Decreasing**	-0.687	0.036
	Mid size	**Increasing**	0.055	0.733	No trend	0	1
	Large size	**Increasing**	0.538	0.047	**Increasing**	0.478	0.076

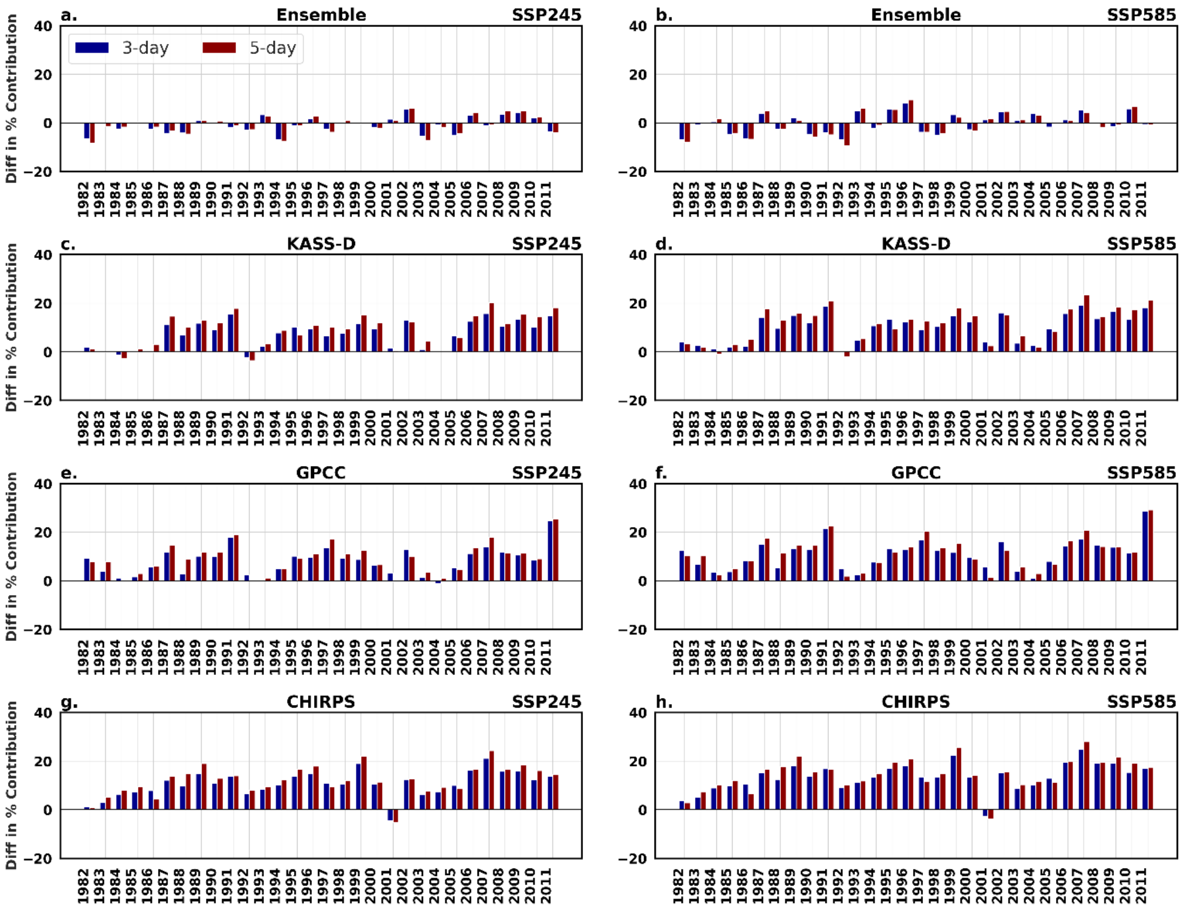

Figure 4.65: Year-to-year difference in percentage contribution of 3- and 5-day intense wet spells to annual rainfall amount between unadjusted and adjusted observations and EnsMean as indicated on the plot under SSP2-4.5 and SSP5-8.5 over the Guinea Coast.

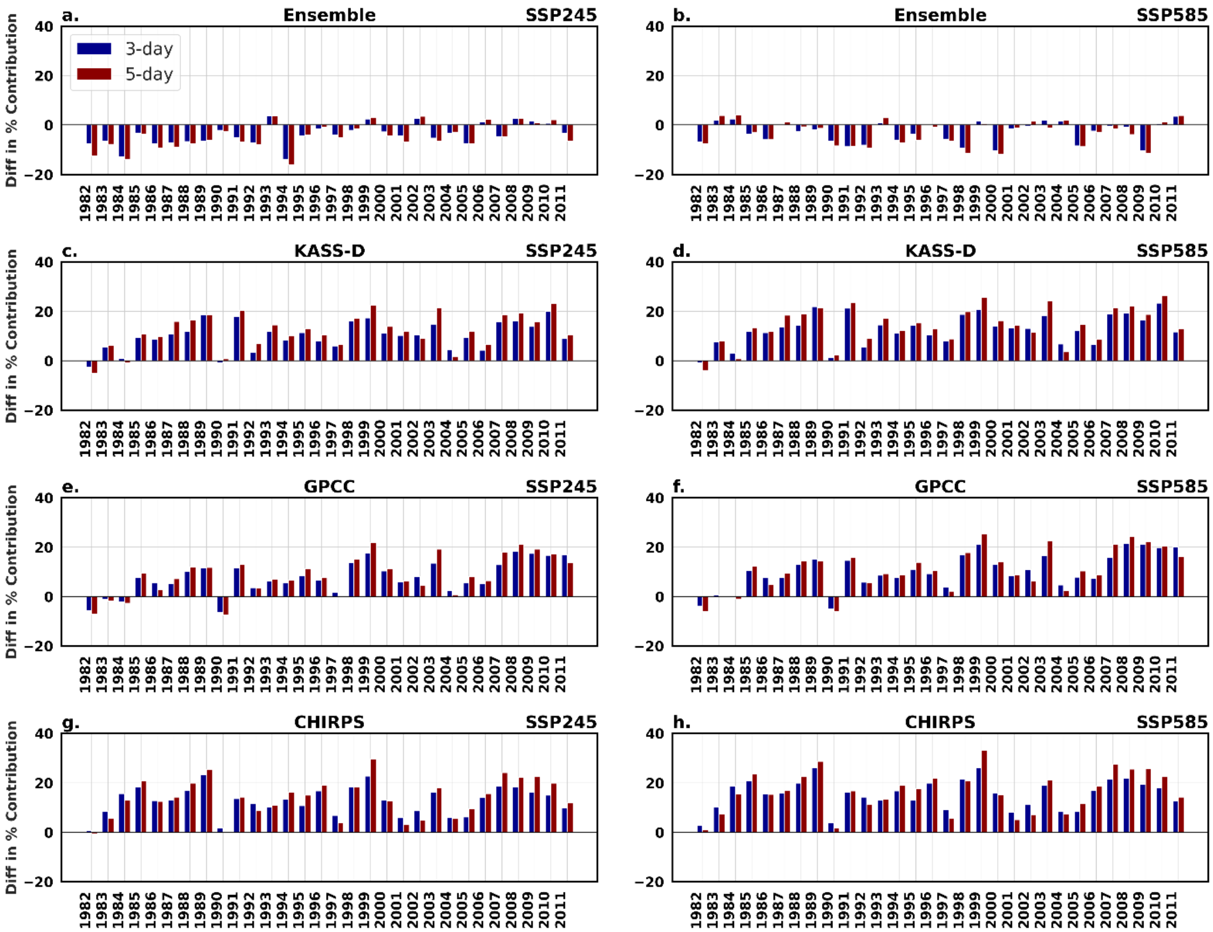

Figure 4.66: Year-to-year difference in percentage contribution of 3- and 5-day intense wet spells to annual rainfall amount between unadjusted and adjusted observations and EnsMean as indicated on the plot under SSP2-4.5 and SSP5-8.5 over the Savannah.

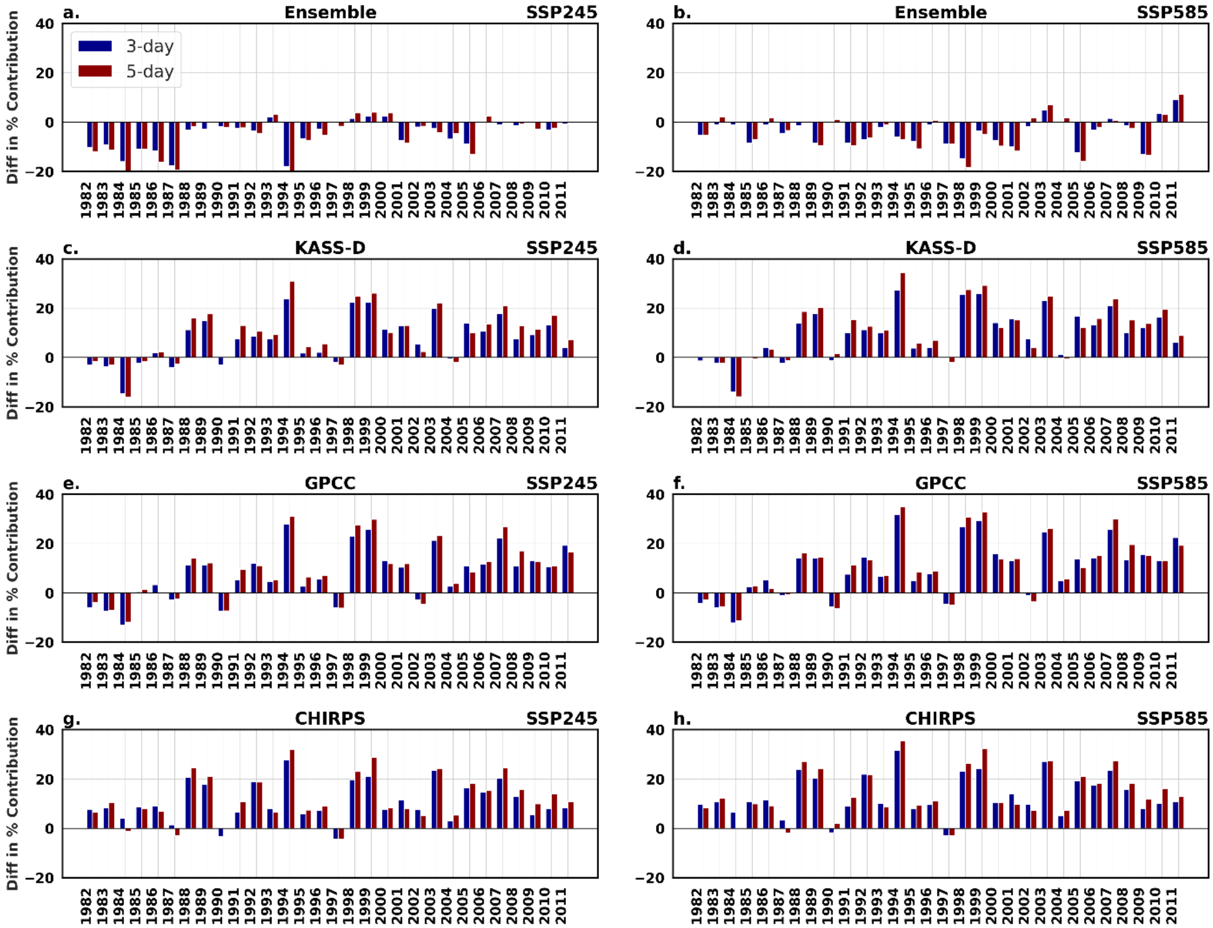

Figure 4.67: Year-to-year difference in percentage contribution of 3- and 5-day intense wet spells to annual rainfall amount between unadjusted and adjusted observations and EnsMean as indicated on the plot under SSP2-4.5 and SSP5-8.5 over the Savannah.

4.7 IMPLICATIONS OF INTENSE MULTI-DAY WET SPELLS FOR FLOOD RISKS AND EARLY WARNING SYSTEMS

This section addresses Objective (v) by examining the implications of intense multi-day wet spells for flood risks and early warning systems, with a view to informing climate resilience and disaster preparedness strategies in West Africa. The analysis draws on the spatial and temporal characteristics of wet spells identified in Section 4.5, their association with large-scale atmospheric dynamics, and their socio-economic impacts, as evidenced by historical flood events.

First, the key findings of the study (see Tables 4.11 and 4.12) are summarized as follows:

(i) **Dataset Performance**: KASS-D outperforms GPCC, CHIRPS, and IMERG in replicating daily rainfall and detecting rainy days, with higher POD (0.42–0.59 vs. 0.35–0.58 for GPCC) and lower POFA (0.13–0.28 vs. 0.15–0.37 for CHIRPS). This is attributed to its dense station network, as supported by Ali and Lebel (2009).

(ii) **Wet Spell Characteristics**: Intense wet spells show a significant increase in frequency (0.06–0.07 events/year for KASS-D) and intensity post-1990, with 13–20 annual 3-day events in coastal areas and fewer in the Sahel. Seasonal peaks occur during the monsoon (June–August), driven by Mesoscale Convective Systems (MCSs).

(iii) **Dynamical Drivers**: Wet spells are associated with enhanced moisture flux convergence, high CAPE, low Convective Inhibition (CIN), and cyclonic circulations, as seen in case studies (e.g., 2005-08-16, 1991-08-21 events). These align with West African Monsoon dynamics (Nicholson, 2013).

(iv) **Climate Change Impacts**: Projections indicate increased wet spell frequency (0.03–0.29 events/year) and intensity (up to 15% in coastal areas under SSP5-8.5), with large events increasing and small events decreasing, consistent with global precipitation trends (IPCC AR6).

(v) **Rainfall Contribution**: The contribution of wet spells to annual rainfall has risen (e.g., 15% to 35% in the Sahel for KASS-D), highlighting their growing significance.

Table 4.11: Summary of Key Findings.

Aspect	Finding	Source
Dataset Accuracy	KASS-D outperforms others (POD: 0.42–0.59, POFA: 0.13–0.28) due to dense stations.	Chapter 4, Section 4.1
Wet Spell Frequency	Increased 0.06–0.07 events/year post-1990, highest in Guinea Coast.	Chapter 4, Section 4.2
Dynamical Drivers	Moisture flux convergence, high CAPE, cyclonic circulations drive wet spells.	Chapter 4, Section 4.3
Climate Projections	Increased intensity and frequency under SSP5-8.5, up to 15% in coastal areas.	Chapter 4, Section 4.4
Rainfall Contribution	Wet spells contribute 15–35% to annual rainfall, increasing over time.	Chapter 4, Section 4.2

Table 4.12: Summary of Intense Wet Spell Trends (1982–2020 and SSP Projections)

Climatic Zone	Frequency Increase (Events/Year, SSP5-8.5)	Rainfall Contribution Increase (%, 1982–2020)	Sources
Guinea Coast	0.03–0.07	9% (3-day, 5-day)	Section 5.1.4, Figures 4.62–4.64, Table 4.11 (frequency); Section 5.1.2, Figure 4.24 (contribution)
Savannah	0.02–0.29	16% (3-day), 14% (5-day)	Section 5.1.4, Figures 4.62–4.64, Table 4.11 (frequency); Section 5.1.2, Figure 4.24 (contribution)
Sahel	0.02–0.17	20% (3-day, 5-day)	Section 5.1.4, Figures 4.62–4.64, Table 4.11 (frequency); Section 5.1.2, Figure 4.24 (contribution)

Notes:

(i) Analyses cover the subregion (2.5°W–15°E, 0°–16°N) due to KASS-D station availability, divided into Guinea Coast (4°–8°N), Savannah (8°–11°N), and Sahel (11°–16°N; Section 3.1).

(ii) Frequency increases are based on Mann-Kendall trend tests (0.05 significance) for 3-day and 5-day intense wet spells under SSP5-8.5, computed from NEX-GDDP-CMIP6 ensemble mean and adjusted datasets (KASS-D, GPCC, CHIRPS), as reported in Section

5.1.4 and visualized in Figures 4.62–4.64 (Section 3.3.4). Table 4.11 provides domain-wide trends.

(iii) Rainfall contribution increases reflect the percentage of annual rainfall from intense 3-day and 5-day wet spells (1982–2020), derived from KASS-D analyses in Section 5.1.2, based on Figure 4.24.

(iv) Intense wet spells exceed the 90th percentile of 3-day/5-day accumulations, with ≥2 wet days (≥1 mm) for 3-day spells and ≥3 wet days with no consecutive dry days for 5-day spells (Section 3.3.3).

The increasing intensity and frequency of multi-day wet spells in West Africa, as revealed through this study, carry far-reaching implications for flood hazards, disaster preparedness, and long-term climate resilience. This subsection therefore explores the hydrological and infrastructural impacts of these events, the limitations of existing early warning systems, and the urgent need for adaptation strategies in the face of evolving rainfall regimes.

4.7.1 Elevated Flood Risks Due to Rainfall Accumulation

Multi-day wet spells (particularly those lasting three to five consecutive days) exert greater hydrological pressure than single-day extremes, as their cumulative rainfall exceeds the absorptive capacity of soil and urban drainage systems. This study confirms that such events are becoming more frequent and intense across all climatic zones in West Africa, particularly the Guinea Coast and Savannah zones. The rising trend in frequency and spatial extent, especially as observed in the KASS-D dataset, suggests a transition toward longer-duration, high-intensity rainfall events that contribute substantially to annual totals (see Figures 4.64–4.67).

These trends align with observed impacts from historical flood disasters. For instance, the devastating flood in Ouagadougou in September 2009, which recorded over 260 mm of rainfall within 24 hours and displaced more than 180,000 people, exemplifies the destructive capacity of such clustered rainfall events (Aich et al., 2016; Sylla et al., 2015). The continued intensification of multi-day rainfall spells under future climate scenarios, particularly SSP5-8.5, poses significant flood risks to urban and peri-urban areas.

4.7.2 Gaps in Early Warning and Forecasting Systems

Current early warning systems across West Africa often rely on daily rainfall thresholds or satellite-based estimates that are insufficiently equipped to capture the complex dynamics of persistent wet spells. Unlike isolated convective storms, multi-day wet spells are driven by mesoscale and synoptic-scale atmospheric anomalies, such as African Easterly Waves (AEWs), monsoon surges, and upper-level divergence fields (see Section 4.5). These drivers create sustained convection over large areas and prolonged periods, which are not adequately represented in most short-term forecast systems.

This study highlights the value of gauge-based high-resolution datasets, particularly KASS-D, which demonstrate superior ability to resolve local rainfall dynamics and extremes compared to reanalysis or satellite-only products (see Tables 4.6–4.9). Integrating such datasets into forecasting platforms and impact-based alert systems could substantially improve the lead time and accuracy of early warnings (Cornforth et al., 2019).

4.7.3 Urban Vulnerability and Infrastructure Deficiencies

Rapid urbanization and poor land-use planning across West African cities exacerbate the impacts of intense wet spells. Informal settlements situated in floodplains or wetlands, coupled with insufficient drainage and solid waste management, heighten exposure and vulnerability to floods. As this study reveals, areas like the Dahomey Gap and interior Nigeria are emerging hotspots of intensified wet spells, requiring immediate policy attention.

The projected increase in wet spell frequency and size implies heightened stress on urban infrastructure – roads, culverts, bridges, and housing. Without proactive interventions, many urban centres will face recurrent flood disasters, public health crises (e.g., cholera outbreaks), and displacement of vulnerable populations (UN-Habitat, 2022; Adelekan et al., 2020).

4.7.4 Strategic Pathways for Climate Resilience and Early Warning

To address these growing threats, this study examines several strategic actions:

(i) **Enhancement of Rain Gauge Networks**: Expand and upgrade in-situ observation infrastructure to fill existing spatial gaps, particularly in underrepresented northern zones and transition belts.

(ii) **Development of Multi-Day Forecast Tools**: Invest in sub-seasonal to seasonal (S2S) forecasting models that integrate moisture flux convergence, CAPE, TCWV, and AEJ/TEJ anomalies for anticipating persistent wet conditions (Thiaw et al., 2011).

(iii) **Risk-Based Urban Planning**: Mainstream hydroclimatic risk into land-use regulations, drainage infrastructure design, and urban development plans, especially in secondary cities where urban sprawl is fastest.

(iv) **Community-Oriented Early Warning Systems**: Design decentralised, locally contextualised early warning systems that translate technical forecasts into actionable messages for at-risk communities (Carr et al., 2020).

4.7.5 Towards Integrated Flood Risk Management

Given the evolving nature of rainfall extremes, this study advocates for an integrated flood risk management framework that links climate diagnostics, hydrological modelling, vulnerability mapping, and policy implementation. By anchoring forecasts on datasets like KASS-D and enhancing understanding of atmospheric precursors, regional stakeholders can develop more anticipatory and adaptive disaster risk reduction mechanisms.

4.7.6 Strategies for Climate Resilience and Disaster Preparedness

To inform climate resilience and disaster preparedness, the findings from this study advocate for a multi-faceted approach that integrates wet spell forecasting, flood risk modelling, and community-based preparedness measures. First, the increasing intensity of wet spells under future climate scenarios (Han et al., 2019; Worou et al., 2022) necessitates the development of robust flood risk models that incorporate wet spell characteristics (e.g., intensity, duration, and spatial extent). These models should be coupled with high-resolution digital elevation models to identify flood-prone areas and prioritize infrastructure investments, such as improved drainage systems in urban centres like Ouagadougou and Lagos (Baldassarre *et al*., 2010).

Second, community-based disaster preparedness strategies should leverage the predictability of wet spells to enhance local resilience. This includes training local stakeholders to interpret EWS outputs and implement contingency plans, such as pre-positioning relief supplies and reinforcing temporary flood barriers (Dos Santos *et al.*, 2019). The findings on the socio-economic impacts of flooding highlight the need for participatory approaches that engage vulnerable communities in flood risk mapping and preparedness planning (Paeth *et al*., 2010).

Finally, regional cooperation is essential to address the transboundary nature of flood risks in West Africa. The Niger River Basin, which spans multiple countries, requires coordinated EWS and disaster response mechanisms to mitigate the impacts of wet spell-induced flooding (Sighomnou et al., 2013). Initiatives such as the African Monsoon Multidisciplinary Analysis (AMMA) provide a framework for sharing meteorological data and forecasting tools across West African nations, enhancing regional resilience (Lafore *et al*., 2017).

CHAPTER FIVE

CONCLUSION AND RECOMMENDATION

5.1 CONCLUSION

This research comprehensively investigates the characteristics, drivers, and likely changes in the characteristics of intense multi-day wet spells in West Africa, addressing critical gaps in understanding regional hydroclimatic extremes and their implications for disaster preparedness and climate resilience. By achieving the five specific objectives outlined, the study provides robust insights into rainfall variability, the dynamics of wet spells, their climatic drivers, and their societal impacts under a warming climate. The findings, derived from high-resolution gauge-based datasets and advanced climate modelling, underscore the increasing intensity and frequency of intense multi-day wet spells and their profound implications for flood risk management and early warning systems in West Africa. In the following sub-sections, the five objectives have been addressed.

5.1.1 Comprehensive Quality Control and Interpolation of In-Situ Rainfall Data

Accurate quantification of rainfall variability remains central to understanding climate dynamics and hydrological extremes in West Africa, a region characterized by complex spatio-temporal rainfall patterns and a sparse observational network. KASS-D data was interpolated from 239 rain gauge stations that have at least 80% data record from 1982-2020 and passed quality control check to a 1°x1° grid using SPHEREMAP and compared with GPCC, CHIRPS, IMERG, and the arithmetic mean of stations within a pixel using Q-Q plots. These rain gauge (in-situ) dataset have at least 80% data record from 1982-2020 and passed quality control check. A comprehensive evaluation reveals that KASS-D reproduces rainfall variability, especially extreme events across the Sahel, Savannah, and Guinea Coast zones. Compared to other datasets, KASS-D captures day-to-day rainfall variability, onset and cessation months, and the distribution of wet-day intensities in a way closer to in-situ (gauge measurements). Q-Q plots highlight that CHIRPS tends to overestimate lower quantiles and underestimate higher quantiles, while GPCC and IMERG show mixed performance. In contrast, KASS-D consistently aligns more closely with in-situ observations, particularly in areas with less than five gauging stations per grid cell.

At seasonal and interannual scales, KASS-D reliably captures the northward shift and intensification of rainfall associated with the West African monsoon, aligning with in-situ rainfall peaks during June–August and accurately reflecting multi-decadal shifts in wet and dry periods. This includes the drought-dominated 1980s and wetter conditions post-2006. The SRAI further demonstrates KASS-D's capacity to track regional rainfall trends and climate teleconnections, including ENSO-related variability. Importantly, KASS-D's enhanced performance stems from its construction: it incorporates a significantly higher density of rain-gauge stations than other products, allowing for more accurate interpolation using the SPHEREMAP method and improved representation of localized rainfall features. This increased number of rain-gauge input provides a key advantage over coarser rain gauge base GPCC or satellite-dominated datasets. With lower RMSE, higher POD and reduced POFA, KASS-D emerges as a highly reliable dataset for rainfall monitoring, extreme event attribution, and climate risk assessment in data-scarce regions like West Africa. Hence, its choice as standard observation dataset in this study to characterized multi-day intense wet spells.

5.1.2 Spatial and Temporal Characteristics of Multi-Day Wet Spells

This study has investigated the spatial and temporal dynamics of intense multi-day wet spells across West Africa from 1982 to 2020, using rain gauge data alongside gauge-corrected satellite products including KASS-D, GPCC, CHIRPS, and IMERG. Wet spells were identified using a 1.0

mm/day threshold, with intense 3-day and 5-day events defined as those exceeding the 90th percentile of accumulated rainfall. Results reveal strong latitudinal gradients, with the Guinea Coast and Cameroon Highlands experiencing the highest frequencies and intensities. While small-size intense wet spells have decreased, large-scale events have grown more frequent and spatially expansive – particularly in the KASS-D dataset, where increased station density enhances reliability. The contribution of these events to annual rainfall increased significantly, by 20% in the Sahel, 16% (3-day) and 14% (5-day) in the Savannah, and 9% in the Guinea Coast, emphasizing their increasing role in regional hydrology.

The evaluation of rainfall products highlights significant methodological biases: GPCC tends to overestimate upper quantiles due to sparse station networks, while CHIRPS underestimates lower quantiles, partly due to its gridded calibration approach. IMERG, though exhibiting higher rainfall intensities in convective regions, benefits from improved resolution. All datasets confirm a consistent meridional structure of wet spell distribution and a clear seasonal modulation linked to the latitudinal migration of the ITD. Notably, the frequency and spatial extent of intense wet spells have increased in recent decades, particularly in wetter years such as 1994, 1999, and 2012. These trends underscore a growing dominance of multi-day rainfall events in shaping annual hydrological budgets in West Africa, with implications for flood risk, agriculture, and water resource management.

5.1.3 Mesoscale, Synoptic, and Thermodynamic Drivers of Intense Wet Spells

Composite analysis of wet and dry spells across West Africa reveals distinct atmospheric patterns behind multi-day rainfall events. Wet spells are characterized by southwesterly wind anomalies, cyclonic circulations, and increased moisture transport, while dry spells exhibit westerly anomalies, moisture divergence, and suppressed convection. Lead-lag and vertical wind structure analyses of show that wet spells are preceded by easterly anomalies and feature a weakening AEJ and strengthening TEJ, fostering deep convection. In contrast, dry spells are marked by inhibited convection and offshore moisture export, with deeper moisture layers suppressing vertical development.

Thermodynamic and dynamic diagnostics of intense 3-day and 5-day wet spells (1982–2020) reveal a coherent atmospheric environment conducive to sustained extreme rainfall. These events are associated with high total column water vapor (TCWV), elevated convective available potential energy (CAPE), and strong low-level moisture flux convergence (MFC), particularly between 11°N and 15°N. Moisture is advected from both the Atlantic Ocean and Gulf of Guinea by intensifying zonal and meridional flows, converging inland to fuel deep convection. This dynamic is reinforced by dual cyclonic systems over the Atlantic and Sahel regions, and supported by anticyclonic flow from the Southern Hemisphere, creating a persistent supply of moist static energy to convective systems. These findings highlight the critical role of coupled thermodynamic-dynamic feedbacks and multiscale atmospheric processes in initiating and sustaining intense wet spells, fully addressing the third objective.

The lifecycle of intense multi-day wet spells is governed by a vertically coupled dynamical framework involving enhanced monsoon surges and mesoscale circulation anomalies. During initiation and peak phases, strong low-level southwesterlies and upper-level easterlies align to promote vertical ascent and deep convection. As the system decays, weakened low-level inflows and depleted mid-level humidity disrupt vertical motion, leading to subsidence and collapse of convective organization. This evolution mirrors convectively coupled equatorial wave behaviour that highlights the role of multiscale interactions in sustaining extreme rainfall events. These insights are vital for advancing predictive capabilities and early warning systems in a region vulnerable to hydrometeorological extremes.

5.1.4 Likely Changes in Characteristics of Intense Multi-Day Wet Spells

Using the ensemble mean (EnsMean) of 23 high-resolution NEX-GDDP-CMIP6 models, this study further evaluates possible changes in the characteristics of intense multi-day wet spells across West Africa under future climate scenarios. The EnsMean, of 23 NEX-GDDP-CMIP6 models operating at a spatial resolution of 0.25° × 0.25° and regridded to 1° × 1°, outperforms individual models in simulating rainfall by minimizing systematic biases stemming from internal variability, parameterization differences, and inconsistencies in land surface representations. When current rainfall distributions are adjusted to mirror future projections under SSP2-4.5 and SSP5-8.5 scenarios, observational datasets (KASS-D, GPCC, CHIRPS) consistently indicate a marked intensification of daily rainfall extremes. The 90th percentile of 3-day and 5-day accumulated rainfall increases significantly, particularly under SSP5-8.5, with local enhancements exceeding 15% in southern coastal zones and around the Niger Delta. These changes suggest an emerging precipitation regime characterized by higher intensity and frequency of extreme rainfall, as further evidenced by Q-Q plot analyses revealing an upward shift in the distribution of daily rainfall extremes.

Seasonal and interannual variability analyses reinforce this shift, showing statistically significant increases in the frequency of intense multi-day wet spells, especially during peak monsoon months. This upward trend aligns with a strengthening of the West African Monsoon, with estimated increases in event frequency ranging from 0.03–0.07/year over the Guinea Coast, 0.02–0.29/year in the Savannah, and 0.02–0.17/year in the Sahel. Larger, more spatially extensive wet spells could have become more prevalent while smaller events could have declined, pointing to a climate-driven transition toward longer-duration and high-impact precipitation episodes. Notably, the contribution of these intense events to annual rainfall totals could have risen since the 1980s, with the steepest gains possible to have occurred under SSP5-8.5 if the current rainfall distribution matches the future projection. The latitudinal gradients and spatial anomalies observed (e.g., suppression over the Dahomey Gap) emphasize the role of coastal dynamics and topography in modulating these trends. Collectively, these findings underscore that if the current rainfall system were to attain the future distribution projected under SSP2-4.5 and SSP5-8.5, West Africa could have been transitioned into a significantly wetter and more extreme hydrological regime with profound implications for water resource management, agriculture, and disaster risk reduction'

5.1.5 Implications of Intense Multi-Day Wet Spells for Flood Risks and Early Warning Systems in West Africa

The analysis of multi-day wet spells in West Africa reveals their critical role in driving flood risks, particularly in the Sahel and Guinea Coast, where high intensity and prolonged duration amplify socio-economic impacts. The predictability of these events, driven by atmospheric precursors such as SHL dynamics and AEWs, offers significant potential for enhancing early warning systems. By integrating wet spell forecasting into flood risk models and promoting community-based preparedness, West African nations can strengthen climate resilience and disaster preparedness. These strategies are essential for mitigating the impacts of intensifying rainfall extremes under a warming climate, ensuring sustainable development and safety for vulnerable populations.

5.2 **RECOMMENDATIONS**

This study, through the development and application of a dense and quality-controlled rain gauge dataset (KASS-D), has advanced the understanding of intense multi-day wet spells across West Africa. In light of the findings and methodological insights, the following recommendations are proposed:

5.2.1 Expansion and Modernisation of Observation Networks

There is an urgent need to expand and modernise the rain gauge observation network across West Africa. Many regions, particularly parts of the Sahel and mountainous or conflict-prone zones, still suffer from sparse or uneven station distribution. A denser and well-maintained network will improve the detection, quantification, and spatial mapping of wet spell events, and enhance regional capabilities for real-time monitoring of hydroclimatic extremes.

5.2.2 Integration of High-Resolution Gauge-Based Data into Early Warning Systems

National meteorological services and hydrological agencies should prioritise the integration of high-resolution datasets like KASS-D into operational early warning and forecasting systems. These datasets have demonstrated superior performance in capturing local rainfall variability and are crucial for accurate flood risk assessments, particularly in urban and vulnerable rural communities.

5.2.3 Investment in Regional Climate Modelling and Forecasting Tools

The study underscores the critical influence of atmospheric drivers such as African Easterly Waves (AEWs), low-level vortices, and the Saharan Heat Low (SHL) in modulating wet spells. Hence, investment in convection-permitting regional climate models and sub-seasonal to seasonal (S2S) prediction frameworks is highly recommended. These should account for multiscale atmospheric interactions and should be calibrated using high-quality observational data.

5.2.4 Improved Risk Communication and Community-Based Preparedness

Effective disaster preparedness requires translating technical forecasts into actionable knowledge for vulnerable communities. This can be achieved through participatory training, flood risk mapping, and integration of local knowledge in contingency planning. Efforts should be made to develop decentralised communication channels that enhance the accessibility and responsiveness of early warning systems.

5.2.5 Strengthening Regional Cooperation and Data Sharing Mechanisms

Transboundary river basins such as the Niger and Volta require harmonised flood forecasting systems and shared meteorological data for coordinated risk management. Regional initiatives like the African Monsoon Multidisciplinary Analysis (AMMA) and ECOWAS climate platforms should be strengthened to facilitate cooperation among West African countries.

5.2.6 Development of Predictive Indicators and Operational Thresholds

Forecast models should incorporate physical indicators such as moisture flux convergence, SHL anomalies, and upper-level divergence that were identified as reliable precursors of wet spells. Additionally, operational thresholds for rainfall accumulation (e.g., 90th percentile over 3 or 5 days) should be updated regularly based on long-term observational data.

5.2.7 Support for Climate Services and Infrastructure Resilience Planning

The increasing dominance of extreme wet spells under future climate scenarios necessitates the establishment of robust climate services that inform infrastructural design, agricultural planning, and public health management. Investments should target drainage systems, flood shelters, and smart water management technologies across flood-prone zones.

5.3 CONTRIBUTION OF THE RESEARCH TO KNOWLEDGE

This section highlights the fact that this research makes several original contributions to knowledge, filling critical gaps in the climatology of West African rainfall and offering applied value for climate resilience and disaster preparedness:

5.4.1 Development of a Novel Gridded Rainfall Dataset (KASS-D)

A high-resolution, gauge-based gridded dataset (KASS-D) was developed and validated against global products (e.g., GPCC, CHIRPS, IMERG). This dataset demonstrates improved accuracy in replicating daily rainfall characteristics and offers a robust tool for hydrometeorological studies in data-scarce regions.

5.4.2 Objective Definition and Detection of Intense Multi-Day Wet Spells

The study introduced clear, reproducible criteria for identifying 3-day and 5-day intense wet spells using percentile-based thresholds. This contributes to the standardisation of extreme event diagnostics, facilitating inter-study comparison and model validation.

5.4.3 Characterisation of Spatio-Temporal Trends in Wet Spells

Through comprehensive spatial and temporal analyses, the study reveals increasing trends in the intensity and frequency of prolonged rainfall events, particularly post-2000. The contribution of intense wet spells to annual rainfall has risen significantly, indicating a hydrological shift toward more extreme regimes.

5.4.4 Identification of Multiscale Atmospheric Drivers

The research provides new insights into the mesoscale and synoptic-scale mechanisms sustaining multi-day wet spells. The roles of AEWs, SHL anomalies, and vertical wind structures were systematically examined using reanalysis and observational data, offering important guidance for predictive modelling.

5.4.5 Assessment of Future Climate Scenarios and Impact Projections

By leveraging high-resolution downscaled CMIP6 simulations (NEX-GDDP), the study quantified likely changes in wet spell characteristics under SSP2-4.5 and SSP5-8.5 scenarios. Results suggest robust increases in wet spell intensity and spatial extent, with implications for food security, urban flooding, and water resource management.

5.4.6 Practical Guidance for Early Warning and Risk Management

The findings inform the design of flood early warning systems by identifying atmospheric precursors that offer lead times of 3–5 days. These can be incorporated into risk models and climate services across sectors such as agriculture, health, and infrastructure.

5.4.7 Advancement of Theoretical and Applied Climate Science in Africa

This research bridges the gap between observational climatology and applied forecasting, thereby contributing to both academic literature and practical policy frameworks. It strengthens regional capacity for science-based decision-making under climate uncertainty.

5.4.8 Policymakers Guide on Effective Climate Adaptation and Disaster Risk Reduction Strategies.

This study offers evidence-based knowledge that can guide policymakers in designing effective climate adaptation and disaster risk reduction strategies. The findings will be particularly valuable in shaping long-term socio-economic planning, infrastructure development, and climate resilience initiatives across vulnerable communities in West Africa – especially in the context of a warming climate and the increasing frequency of extreme weather events.

REFERENCES

Abiodun, B. J., Adegoke, J., Abatan, A. A., Ibe, C. A., Egbebiyi, T. S., Engelbrecht, F., & Pinto, I. (2017). Potential impacts of climate change on extreme precipitation over four African coastal cities. Climatic Change, 143(3–4), 399–413. https://doi.org/10.1007/s10584-017-2001-5

Adelekan, I. O., Leck, H., et al. (2020). Risk and resilience in African cities: Learning from local knowledge. Environment and Urbanization, 32(2), 1–19.

Adeyewa, Z. D. (2005): An Appraisal of Some Satellite Rainfall Products over Africa. Ife Journal of Science. Vol. 7, No. 2, pp. 237 – 245. [http://ajol.info/index.php/ijs/article/view/32182/23763]

Adeyewa, Z. D. and K. Nakamura (2003): Validation of TRMM Radar Rainfall Data over Major Climatic Regions in Africa. Journal of Applied Meteorology, USA. Vol. 42, No. 2, pp. 331 - 347. [http://journals.ametsoc.org/doi/pdf/10.1175/1520-0450%282003%29042%3C0331%3AVOTRRD%3E2.0.CO%3B2]

Afiesimama, E. A., Pal, J. S., Abiodun, B. J., Gutowski, W. J., & Adedoyin, A. (2006). Simulation of West African monsoon using the RegCM3. Part I: Model validation and interannual variability. Theoretical and Applied Climatology, 86(1–4), 23–37. https://doi.org/10.1007/s00704-005-0202-8

Ageet, S., Fink, A. H., Maranan, M., Diem, J. E., Hartter, J., Ssali, A. L., & Ayabagabo, P. (2022). Validation of Satellite Rainfall Estimates over Equatorial East Africa. Journal of Hydrometeorology, 23(2), 129–151. https://doi.org/10.1175/jhm-d-21-0145.1

Aich, V., Liersch, S., Vetter, T., et al. (2016). Flood projections within the Niger River Basin under future land use and climate change. Science of the Total Environment, 562, 666–677.

Ajayi, V. O., & Ilori, O. W. (2020). Projected Drought Events over West Africa Using RCA4 Regional Climate Model. Earth Systems and Environment, 4(2), 329–348. https://doi.org/10.1007/s41748-020-00153-x

Akinsanola, A. A., & Zhou, W. (2018). Projections of West African summer monsoon rainfall extremes from two CORDEX models. Climate Dynamics, 52(3–4), 2017–2028. https://doi.org/10.1007/s00382-018-4238-8

Akinsanola, A. A., & Zhou, W. (2020). Understanding the variability of West African summer monsoon rainfall: Contrasting tropospheric features and monsoon index. Atmosphere, 11(3), 309. https://doi.org/10.3390/atmos11030309

Anagnostopoulou, C., Maheras, P., Karacostas, T., & Vafiadis, M. (2003). Spatial and temporal analysis of dry spells in Greece. Theoretical and Applied Climatology, 74(1–2), 77–91. https://doi.org/10.1007/s00704-002-0713-5

Atiah, W. A., Tsidu, G. M., & Amekudzi, L. K. (2020). Investigating the merits of gauge and satellite rainfall data at local scales in Ghana, West Africa. Weather and Climate Extremes, 30, 100292. https://doi.org/10.1016/j.wace.2020.100292

Berntell E (2023). Understanding West African Monsoon Variability. Academic dissertation for the Degree of Doctor of Philosophy in Physical Geography at Stockholm University. ISBN 978-91-8014-310-3. http://urn.kb.se/resolve?urn=urn:nbn:se:su:diva-216584

Biasutti, M. (2013). Forced Sahel rainfall trends in the CMIP5 archive. Journal of Geophysical Research Atmospheres, 118(4), 1613–1623. https://doi.org/10.1002/jgrd.50206

Bichet, A., & Diedhiou, A. (2018a). Less frequent and more intense rainfall along the coast of the Gulf of Guinea in West and Central Africa (1981-2014). Climate Research, 76(3), 191–201. https://doi.org/10.3354/cr01537

Bobde, V., Akinsanola, A. A., Folorunsho, A. H., Adebiyi, A. A., & Adeyeri, O. E. (2024). Projected regional changes in mean and extreme precipitation over Africa in CMIP6 models. Environmental Research Letters, 19(7), 074009. https://doi.org/10.1088/1748-9326/ad545c

Burpee, R. W. (1972). The origin and structure of easterly waves in the lower troposphere of North Africa. Journal of the Atmospheric Sciences, 29(1), 77–90. https://doi.org/10.1175/1520-0469(1972)029

Calvin, K., Dasgupta, D., Krinner, G., Mukherji, A., Thorne, P. W., Trisos, C., Romero, J., Aldunce, P., Barrett, K., Blanco, G., Cheung, W. W., Connors, S., Denton, F., Diongue-Niang, A., Dodman, D., Garschagen, M., Geden, O., Hayward, B., Jones, C., . . . Ha, M. (2023). IPCC, 2023: Climate Change 2023: Synthesis Report. Contribution of Working Groups I, II and III to the Sixth Assessment Report of the Intergovernmental Panel on Climate Change [Core Writing Team, H. Lee and J. Romero (eds.)]. IPCC, Geneva, Switzerland. https://doi.org/10.59327/ipcc/ar6-9789291691647

Carr, E. R., Mason, S. J., et al. (2020). Climate services for development: The evolution of climate information use in sub-Saharan Africa. Climate Risk Management, 29, 100239.

Cook, K. H. (1999). "Generation of the African Easterly Jet and its Role in Determining West African Precipitation." Journal of Climate, 12(5), 1165-1184.

Cornforth, R. J., Hoskins, B. J., & Thorncroft, C. D. (2009). The impact of moist processes on the African Easterly Jet-African Easterly Wave system. Quarterly Journal of the Royal Meteorological Society, 135(641), 894–913. https://doi.org/10.1002/qj.414

Cornforth, R. J., Petty, C., et al. (2019). Informing climate adaptation with multi-hazard risk analysis: Forecast-based early action in Africa. Environmental Science & Policy, 98, 72–82.

Di Baldassarre, G. D., A. Montanari, H. Lins, D. Koutsoyiannis, L. Brandimarte, and G. Bl¨oschl, 2010: Flood fatalities in Africa: From diagnosis to mitigation. Geophys. Res. Lett., 37, L22402, https://doi.org/10.1029/2010GL045467.

Diallo I, Camara M, Sylla M, Gaye AT (2010) Représentation haute résolution du système de mousson ouest africain avec un modèle climatique régional. Journal Des Sciences Pour L'ingénieur 12:75–85

Diallo I, Giorgi F, Deme A, Tall M, Mariotti L, and Gaye AT (2016). Projected changes of summer monsoon extremes and hydroclimatic regimes over West Africa for the twenty-first century. Clim. Dyn., 47, 3931–3954, doi:10.1007/s00382-016-30524.

Diallo I, Sylla MB, Giorgi F, Gaye AT, and Camara M (2012). Multi-model GCM-RCM ensemble-based projections of temperature and precipitation over West Africa for the early 21st century. International Journal of Geophysics, 2012(Article ID 972896):19.

Diba, I., Diedhiou, A., Famien, A. M., Camara, M., & Fotso-Nguemo, T. C. (2022). Changes in compound extremes of rainfall and temperature over West Africa using CMIP5 simulations. Environmental Research Communications, 4(10), 105003. https://doi.org/10.1088/2515-7620/ac9aa7

Dike, V. N., Lin, Z., & Ibe, C. C. (2020). Intensification of Summer Rainfall Extremes over Nigeria during Recent Decades. Atmosphere, 11(10), 1084. https://doi.org/10.3390/atmos11101084

Dioha, E. C., Chung, E., Ayugi, B. O., Babaousmail, H., & Sian, K. T. C. L. K. (2024). Quantifying the added value in the NEX-GDDP-CMIP6 models as compared to native CMIP6 in simulating Africa's diverse precipitation climatology. Earth Systems and Environment, 8(2), 417–436. https://doi.org/10.1007/s41748-024-00397-x

Dong, B., & Sutton, R. (2015). Dominant role of greenhouse-gas forcing in the recovery of Sahel rainfall. Nature Climate Change, 5(8), 757–760. https://doi.org/10.1038/nclimate2664

Ebert, E. E. (2007). Methods for verifying satellite precipitation estimates. In Springer eBooks (pp. 345–356). https://doi.org/10.1007/978-1-4020-5835-6_27

Elagib, N. A., Zayed, I. S. A., Saad, S. A., Mahmood, M. I., Basheer, M., & Fink, A. H. (2021). Debilitating floods in the Sahel are becoming frequent. Journal of Hydrology, 599, 126362. https://doi.org/10.1016/j.jhydrol.2021.126362

Emanuel, K. A. (1994). Atmospheric convection. Oxford University Press, USA.

Engel, T., Fink, A. H., Knippertz, P., Pante, G., & Bliefernicht, J. (2017). Extreme precipitation in the West African cities of Dakar and Ouagadougou: Atmospheric dynamics and implications for flood risk assessments. Journal of Hydrometeorology, 18(11), 2937–2957. https://doi.org/10.1175/jhm-d-16-0218.1

Eyring, V., Bony, S., Meehl, G. A., A, C., Senior, Stevens, B., Stouffer, R. J., & Taylor, K. E. (2016). Overview of the Coupled Model Intercomparison Project Phase 6 (CMIP6) experimental design and organization. Geoscientific Model Development, 9(5), 1937–1958. https://doi.org/10.5194/gmd-9-1937-2016

Fink, A. H., & Reiner, A. (2003). Spatiotemporal variability of the relation between African Easterly Waves and West African Squall Lines in 1998 and 1999. Journal of Geophysical Research Atmospheres, 108(D11). https://doi.org/10.1029/2002jd002816

Fink, A. H., D. G. Vincent, and V. Ermert, 2006: Rainfall Types in the West African Soudanian Zone during the Summer Monsoon 2002. Mon. Wea. Rev., 134 (8), 2143-2164, http://journals.ametsoc.org/doi/pdf/10.1175/MWR3182.1.

Fink, A. H., T. Engel, V. Ermert, R. van der Linden, M. Schneidewind, R. Redl, E. Afiesimama, W. Thiaw, C. Yorke, and M. Evans, 2017: Mean climate and seasonal cycle. In: “Meteorology of Tropical West Africa: The Forecasters' Handbook”, D. J. Parker and M. Diop-Kane (Eds.), John Wiley & Sons, Ltd, Chichester, UK., pp. 1□39, ISBN: 978-1-118-39130-3, doi: 10.1002/9781118391297.ch1.

Flaounas E, Janicot S, Bastin S, and Roca R (2012). The West African monsoon onset in 2006: Sensitivity to surface albedo, orography, SST and synoptic scale dry-air intrusions using WRF. Climate Dynamics, 38, 685–708.

Fortune, M. “Properties of African squall lines inferred from time-lapse satellite imagery,” Monthly Weather Review, vol. 108, no. 2, pp. 153–168, 1980.

Froidurot, S., & Diedhiou, A. (2017). Characteristics of wet and dry spells in the West African monsoon system. Atmospheric Science Letters, 18(3), 125–131. https://doi.org/10.1002/asl.734

Funk, C., Peterson, P., Landsfeld, M., Pedreros, D., Verdin, J., Shukla, S., Husak, G., Rowland, J., Harrison, L., Hoell, A., & Michaelsen, J. (2015). The climate hazards infrared precipitation with stations—a new environmental record for monitoring extremes. Scientific Data, 2(1). https://doi.org/10.1038/sdata.2015.66

Gong C and Eltahir EAB (1996). Sources of moisture for rainfall in West Africa. Water Resour. Res., 32, 3115 3121.

Griffiths J. 1972. World survey of climatology: Climates of Africa (vol. 10). Climates of Africa Elsevier Publishing Company.

Hagos SM and Cook KH (2007). Dynamics of the West African monsoon jump. Journal of Climate, vol. 20, no. 21, pp. 5264–5284.

Hastings, D. A., and Coauthors. (1999): The Global Land One- Kilometer Base Elevation (GLOBE) digital elevation model, version 1.0. NOAA National Geophysical Data Centre, accessed 23 July 2021, https://www.ngdc.noaa.gov/mgg/topo/globe.html.

Hersbach, H., Bell, B., Berrisford, P., Hirahara, S., Horányi, A., Muñoz-Sabater, J., Nicolas, J., Peubey, C., Radu, R., Schepers, D., Simmons, A., Soci, C., Abdalla, S., Abellan, X., Balsamo, G., Bechtold, P., Biavati, G., Bidlot, J., Bonavita, M., . . . Thépaut, J. (2020). The ERA5 global reanalysis. Quarterly Journal of the Royal Meteorological Society, 146(730), 1999–2049. https://doi.org/10.1002/qj.3803

Houze Jr, R. A. (2014). Cloud dynamics. Academic press.

Houze, R. A. (2004). Mesoscale convective systems. Reviews of Geophysics, 42(4). https://doi.org/10.1029/2004rg000150

Hsieh J. S and Cook KH (2005). Generation of African easterly wave disturbances: Relationship to the African Easterly Jet. Mon. Wea. Rev., 133:1311–1327.

Hsieh, J., & Cook, K. H. (2007). A study of the energetics of African Easterly waves using a regional climate model. Journal of the Atmospheric Sciences, 64(2), 421–440. https://doi.org/10.1175/jas3851.1

Huffman, D. T. Bolvin, D. Bolvin, D. Braithwaite, K. Hsu, and R. Joyce, 2020: NASA Global Precipitation Measurement (GPM) Integrated Multi-satellitE Retrievals for GPM (IMERG) – Algorithm Theoretical Basis Document (ATBD), version 6.3, accessed 11 May 2020, 35 pp., https://gpm.nasa.gov/sites/default/files/2020-05/IMERG_ATBD_V07.pdf

Hulme, M., & Tosdevin, N. (1989). The Tropical easterly Jet and Sudan rainfall: A review. Theoretical and Applied Climatology, 39(4), 179–187. https://doi.org/10.1007/BF00867945

Ibrahim, B., Karambiri, H., Polcher, J., Yacouba, H., & Ribstein, P. (2013). Changes in rainfall regime over Burkina Faso under the climate change conditions simulated by 5 regional climate models. Climate Dynamics, 42(5–6), 1363–1381. https://doi.org/10.1007/s00382-013-1837-2

Ilori, O. W., & Ajayi, V. O. (2020). Change Detection and Trend Analysis of Future Temperature and Rainfall over West Africa. Earth Systems and Environment, 4(3), 493–512. https://doi.org/10.1007/s41748-020-00174-6

Ilori, O. W., & Balogun, I. A. (2021). Evaluating the performance of new CORDEX-Africa regional climate models in simulating West African rainfall. Modeling Earth Systems and Environment, 8(1), 665–688. https://doi.org/10.1007/s40808-021-01084-w

Jenkins GS, Gaye AT, Sylla B (2005) Late 20th Century attribution of drying trends in the Sahel from the Regional Climate Model (RegCM3). Geophys Res Lett 32:L22705-GL024225

Kalapureddy, M. C. R., Lothon, M., Campistron, B., Lohou, F., & Saïd, F. (2009). Wind profiler analysis of the African Easterly Jet in relation with the boundary layer and the Saharan heat-low. Quarterly Journal of the Royal Meteorological Society, 136(S1), 77–91. https://doi.org/10.1002/qj.494

Kalapureddy, M. C. R., Rao, D. N., Jain, A. R., & Ohno, Y. (2007). Wind profiler observations of a monsoon low-level jet over a tropical Indian station. Annales Geophysicae, 25(10), 2125–2137. https://doi.org/10.5194/angeo-25-2125-2007

Klutse, N. a. B., Quagraine, K. A., Nkrumah, F., Quagraine, K. T., Berkoh-Oforiwaa, R., Dzrobi, J. F., & Sylla, M. B. (2021). The Climatic Analysis of Summer Monsoon Extreme Precipitation Events over West Africa in CMIP6 Simulations. Earth Systems and Environment, 5(1), 25–41. https://doi.org/10.1007/s41748-021-00203-y

Knippertz, P., A. H. Fink, A. Deroubaix, E. Morris, F. Tocquer, M. Evans, C. Flamant, M. Gaetani, C. Lavaysse, C. Mari, J. H. Marsham, R. Meynadier, A. Affo-Dogo, T. Bahaga, F. Brosse, K. Deetz, R. Guebsi, I. Latifou, M. Maranan, P. D. Rosenberg, and A. Schlueter, 2017: A meteorological and chemical overview of the DACCIWA field campaign in West Africa in June–July 2016. Atmos. Chem. Phys., 17, 10893–10918, doi: 10.5194/acp-17-10893-2017.

Knippertz, P.; Martin, J. E., 2005: Tropical plumes and extreme precipitation in subtropical and tropical West Africa Quart. J. Roy. Meteorol. Soc., 131, 2337–2365. doi:10.1256/qj.04.148

Kouakou, C., Paturel, J., Satgé, F., Tramblay, Y., Defrance, D., & Rouché, N. (2023). Comparison of gridded precipitation estimates for regional hydrological modeling in West and Central Africa. Journal of Hydrology Regional Studies, 47, 101409. https://doi.org/10.1016/j.ejrh.2023.101409

Lafore, J.-P., and Coauthors, 2017: A multi-scale analysis of the extreme rain event of Ouagadougou in 2009. Quart. J. Roy. Meteor. Soc., 143, 3094–3109, https://doi.org/10.1002/qj.3165.

Lavaysse C., C. Flamant, S. Janicot, and P.Knippertz, 2010: Links between African easterly waves, midlatitude circulation and intraseasonal pulsations of the West African heat low. Quart. J. Roy. Met. Soc., 136(s1), 141–158.

Lebel T, Diedhiou A, and Laurent H (2003). Seasonal cycle and inter-annual variability of the Sahelian rainfall at hydrological scales. J. Geophys. Res., 108(D8), 8389, doi:10.1029/2001JD001580.

Levinson DH, Lawrimore JH. 2008. State of the climate in 2007. Bulletin of the American Meteorological Society **89**: 1–179.

Liu, Y., Chen, J., Pan, T., Liu, Y., Zhang, Y., Ge, Q., Ciais, P., & Penuelas, J. (2020). Global socioeconomic risk of precipitation extremes under climate change. Earth S Future, 8(9). https://doi.org/10.1029/2019ef001331

Long M, Entekhabi D, and Nicholson SE (2000). Interannual Variability in Rainfall, Water Vapor Flux, and Vertical Motion over West Africa. J. Climate13, 3827–3841.

Maidment, R. I., and Coauthors, 2017: A new, long-term daily satellite-based rainfall dataset for operational monitoring in Africa. Sci. Data, 4, 170063, https://doi.org/10.1038/sdata.2017.63.

Maidment, R. I., D. I. F. Grimes, R. P. Allan, H. Greatrex, O. Rojas, and O. Leo, 2013: Evaluation of satellite-based and model re-analysis rainfall estimates for Uganda. Meteor. Appl., 20, 308–317, https://doi.org/10.1002/met.1283.

Maranan, M., Fink, A. H., Knippertz, P., Amekudzi, L. K., Atiah, W. A., & Stengel, M. (2020). A Process-Based validation of GPM IMERG and its sources using a mesoscale rain gauge network in the West African Forest Zone. Journal of Hydrometeorology, 21(4), 729–749. https://doi.org/10.1175/jhm-d-19-0257.1

Meinshausen, M., Nicholls, Z. R. J., Lewis, J., Gidden, M. J., Vogel, E., Freund, M., Beyerle, U., Gessner, C., Nauels, A., Bauer, N., Canadell, J. G., Daniel, J. S., John, A., Krummel, P. B., Luderer, G., Meinshausen, N., Montzka, S. A., Rayner, P. J., Reimann, S., . . . Wang, R. H. J. (2020). The shared socio-economic pathway (SSP) greenhouse gas concentrations and their extensions to 2500. Geoscientific Model Development, 13(8), 3571–3605. https://doi.org/10.5194/gmd-13-3571-2020

Mekonnen, K., Velpuri, N. M., Leh, M., Akpoti, K., Owusu, A., Tinonetsana, P., Hamouda, T., Ghansah, B., Paranamana, T. P., & Munzimi, Y. (2023). Accuracy of satellite and reanalysis rainfall estimates over Africa: A multi-scale assessment of eight products for continental applications. Journal of Hydrology Regional Studies, 49, 101514. https://doi.org/10.1016/j.ejrh.2023.101514

Meynadier R, Bock O, Gervois S, Guichard F, Redelsperger JL, Agustí-Panareda A, and Beljaars A (2010b). West African Monsoon water cycle: 2. Assessment of numerical weather prediction water budgets. Journal of Geophysical Research: Atmospheres (1984–2012), 115.

Meynadier R, Bock O, Guichard F, Boone A, Roucou P, and Redelsperger JL (2010a). West African Monsoon water cycle: 1. A hybrid water budget data set. Journal of Geophysical Research: Atmospheres (1984–2012), 115.

Mohino, E., Janicot, S., & Bader, J. (2011). Sahel rainfall and decadal to multi-decadal sea surface temperature variability. Climate Dynamics, 37(3–4), 419–440. https://doi.org/10.1007/s00382-010-0867-2

Monerie PA, Fontaine B, and Roucou P (2012). Expected future changes in the African monsoon between 2030 and 2070 using some CMIP3 and CMIP5 models under a medium-low RCP scenario. J. Geophys. Res. Atmos. 1984–2012 117D16111.

Monerie, P., Wainwright, C. M., Sidibe, M., & Akinsanola, A. A. (2020). Model uncertainties in climate change impacts on Sahel precipitation in ensembles of CMIP5 and CMIP6 simulations. Climate Dynamics, 55(5–6), 1385–1401. https://doi.org/10.1007/s00382-020-05332-0

Nicholson, S. E. (2008). On the factors modulating the intensity of the tropical rainbelt over West Africa. International Journal of Climatology, 29(5), 673–689. https://doi.org/10.1002/joc.1702

Nicholson, S. E. (2013). The West African Sahel: A review of recent studies on the rainfall regime and its interannual variability. ISRN Meteorology, 2013, 1–32. https://doi.org/10.1155/2013/453521

Nicholson, S. E., & Dezfuli, A. K. (2012). The relationship of rainfall variability in Western Equatorial Africa to the tropical oceans and atmospheric circulation. Part I: The Boreal Spring. Journal of Climate, 26(1), 45–65. https://doi.org/10.1175/jcli-d-11-00653.1

Nicholson, S., & Grist, J. (2001). A conceptual model for understanding rainfall variability in the West African Sahel on interannual and interdecadal timescales. International Journal of Climatology, 21(14), 1733–1757. https://doi.org/10.1002/joc.648

Odekunle TO, Balogun EE, and Ogunkoya OO (2005). On the prediction of rainfall onset and retreat dates in Nigeria. Theoretical and Applied Climatology, 81(1-2), 101-112.

Omotosho, J. B. (2007). Pre-rainy season moisture build-up and storm precipitation delivery in the West African Sahel. International Journal of Climatology, 28(7), 937–946. https://doi.org/10.1002/joc.1548

Omotosho, J. B'., & Abiodun, B. J. (2007). A numerical study of moisture build-up and rainfall over West Africa. Meteorological Applications, 14(3), 209–225. https://doi.org/10.1002/met.11

Osei MA, Amekudzi LK, Quansah E (2022) Characterisation of wet and dry spells and associated atmospheric dynamics at the Pra River catchment of Ghana, West Africa. J Hydrol Reg Stud 34:100801

Paeth H., A. H. Fink, S. Pohle, F. Keis, H. Mächel, and C. Samimi, 2011: Meteorological characteristics and potential causes of the 2007 flood in sub-Saharan Africa. Int. J. Climatol., 31, 1908-1926, DOI: 10.1002/joc.2199.

Palmer, T. N., & Räisänen, J. (2002). Quantifying the risk of extreme seasonal precipitation events in a changing climate. Nature, 415(6871), 512–514. https://doi.org/10.1038/415512a

Panthou, G., Vischel, T., & Lebel, T. (2014). Recent trends in the regime of extreme rainfall in the Central Sahel. International Journal of Climatology, 34(15), 3998–4006. https://doi.org/10.1002/joc.3984

Parker, D. J., Burton, R. R., Diongue-Niang, A., Ellis, R. J., Felton, M., Taylor, C. M., Thorncroft, C. D., Bessemoulin, P., & Tompkins, A. M. (2005). The diurnal cycle of the West African monsoon circulation. Quarterly Journal of the Royal Meteorological Society, 131(611), 2839–2860. https://doi.org/10.1256/qj.04.52

Pattanaik DR and Satyan V (2000). Fluctuations of Tropical Easterly Jet during contrasting monsoons over India: A GCM study. Meteorology and Atmospheric Physics, vol. 75, no. 1-2, pp. 51–60.

Peyrillé P and Lafore JP (2007). An idealized two-dimensional framework to study the West African monsoon. Part II: Largescale advection and the diurnal cycle. J. Atmos. Sci., 64, 2783–2803, doi:10.1175/JAS4052.1.

Peyrillé P, Lafore JP, and Redelsperger JL (2007). An idealized two-dimensional framework to study the West African Monsoon. Part I: Validation and key controlling factors. Journal of the Atmospheric Sciences, vol. 64, no. 8, pp. 2765–2782.

Poli P, Hersbach H, Dee DP, Berrisford P, Simmons AJ, Vitart F, Laloyaux P, Tan DGH, Peubey C, Thépaut JN, Trémolet Y, Hólm EV, Bonavita M, Isaksen L, Fisher M. 2016. ERA-20C : An Atmospheric Reanalysis of the Twentieth Century. Journal of Climate 29:4083–4097. doi:10.1175/JCLI-D-15-0556.1.

Prathipati, V. K., Viswanadhapalli, Y., Chennu, V. N., & Dasari, H. P. (2021). Study of active and break spell phenomena of Indian Summer Monsoon using WRF downscaled data. Pure and Applied Geophysics, 178(10), 4195–4219. https://doi.org/10.1007/s00024-021-02837- 5

Pu, B., & Cook, K. H. (2012). Role of the West African Westerly Jet in Sahel rainfall variations. Journal of Climate, 25(8), 2880–2896. https://doi.org/10.1175/jcli-d-11-00394.1

Ratan, R., & Venugopal, V. (2013). Wet and dry spell characteristics of global tropical rainfall. Water Resources Research, 49(6), 3830–3841. https://doi.org/10.1002/wrcr.20275

Redelsperger J, Diongue A, Diedhiou A, Ceron J, Diop M, Gueremy J, and Lafore J (2002). Multi-scale description of a Sahelian synoptic weather system representative of the West African monsoon. Q. J. R. Meteor. Soc., 128:1229–1257.

Resmi, E. A., Preethi, B., Ajayamohan, R. S., Ray, P., Unnikrishnan, C. K., Nita, S., Sumesh, R. K., & Dharmadas, J. (2023). Analysis of localized features during wet and dry rainfall episodes over southern tip of India. International Journal of Climatology, 43(15), 7326–7345. https://doi.org/10.1002/joc.8267

Robinson, A., Lehmann, J., Barriopedro, D., Rahmstorf, S., & Coumou, D. (2021). Increasing heat and rainfall extremes now far outside the historical climate. Npj Climate and Atmospheric Science, 4(1). https://doi.org/10.1038/s41612-021-00202-w

Rowell DP, Folland CK, Maskell K, Ward MN. 1995. Variability of summer rainfall over tropical north Africa (1906-92): Observations and modelling. Quarterly Journal of the Royal Meteorological Society 121:669–704. doi:10.1002/qj.49712152311.

Sanogo, S., Fink, A. H., Omotosho, J. A., Ba, A., Redl, R., & Ermert, V. (2015). Spatio-temporal characteristics of the recent rainfall recovery in West Africa. International Journal of Climatology, 35(15), 4589–4605. https://doi.org/10.1002/joc.4309

Sawadogo, W., Neya, T., Semde, I., Korahiré, J. A., Combasséré, A., Traoré, D. E., Ouedraogo, P., Diasso, U. J., Abiodun, B. J., Bliefernicht, J., & Kunstmann, H. (2024). Potential Impacts of Climate Change on the Sudan-Sahel Region in West Africa – Insights from Burkina Faso. Environmental Challenges, 100860. https://doi.org/10.1016/j.envc.2024.100860

Sherwood, S. C., Ingram, W., Tsushima, Y., Satoh, M., Roberts, M., Vidale, P. L., & O'Gorman, P. A. (2010). Relative humidity changes in a warmer climate. Journal of Geophysical Research Atmospheres, 115(D9). https://doi.org/10.1029/2009jd012585

Sighomnou D, Descroix L, Genthon P, Mahé G and others (2013) La crue de 2012 a Niamey: un paroxysme du paradoxe du Sahel? Sécheresse 24: 3−13

Simpkins, G. (2017). Progress in climate modelling. Nature Climate Change, 7(10), 684–685. https://doi.org/10.1038/nclimate3398

Srinivasa Rao BR, Bhaskar Rao DV, and Brahmananda Rao V (2004). Decreasing trend in the strength of Tropical Easterly Jet during the Asian summer monsoon season and the number of tropical cyclonic systems over Bay of Bengal. Geophysical Research Letters, vol. 31, no. 14, pp. L141031–L141033, 2004.

Sultan, B., & Janicot, S. (2003). "The West African Monsoon Dynamics. Part I: Documentation of Intraseasonal Variability." Journal of Climate, 16(21), 3389-3406.

Sultan, Benjamin, & Janicot, S. (2003). The West African monsoon dynamics. Part II: The “preonset” and “onset” of the summer monsoon. Journal of Climate, 16(21), 3407–3427. https://doi.org/10.1175/1520-0442(2003)016<3407:TWAMDP>2.0.CO;2

Sylla, M. B., Dell’Aquila, A., Ruti, P. M., & Giorgi, F. (2009). Simulation of the intraseasonal and the interannual variability of rainfall over West Africa with RegCM3 during the monsoon period. International Journal of Climatology, 30(12), 1865–1883. https://doi.org/10.1002/joc.2029

Sylla, M. B., et al. (2015). Multiyear rainfall variability over the Sahel: Detection and attribution of long-term trends. Journal of Geophysical Research: Atmospheres, 120(10), 4944–4963.

Sylla, M. B., Giorgi, F., Coppola, E., & Mariotti, L. (2012). Uncertainties in daily rainfall over Africa: assessment of gridded observation products and evaluation of a regional climate model simulation. International Journal of Climatology, 33(7), 1805–1817. https://doi.org/10.1002/joc.3551

Sylla, M. B., Nikiema, P. M., Gibba, P., Kebe, I., & Klutse, N. a. B. (2016). Climate Change over West Africa: Recent Trends and Future Projections. In Springer eBooks (pp. 25–40). https://doi.org/10.1007/978-3-319-31499-0_3

Taylor, K. E. (2001). Summarizing multiple aspects of model performance in a single diagram. Journal of Geophysical Research Atmospheres, 106(D7), 7183–7192. https://doi.org/10.1029/2000jd900719

Tebaldi, C., Debeire, K., Eyring, V., Fischer, E., Fyfe, J., Friedlingstein, P., Knutti, R., Lowe, J., O'Neill, B., Sanderson, B., Van Vuuren, D., Riahi, K., Meinshausen, M., Nicholls, Z., Tokarska, K. B., Hurtt, G., Kriegler, E., Lamarque, J., Meehl, G., . . . Ziehn, T. (2021). Climate model projections from the Scenario Model Intercomparison Project (ScenarioMIP) of CMIP6. Earth System Dynamics, 12(1), 253–293. https://doi.org/10.5194/esd-12-253-2021

Thiaw, W. M., Janowiak, J. E., et al. (2011). Precipitation variability and outlook for the Sahel in 2011. NOAA/CPC.

Thorncroft, C. D., & Blackburn, M. (1999). Maintenance of the African easterly jet. Quarterly Journal of the Royal Meteorological Society, 125(555), 763–786. https://doi.org/10.1002/qj.49712555502

Thorncroft, C. D., Nguyen, H., Zhang, C., & Peyrillé, P. (2011). Annual cycle of the West African monsoon: regional circulations and associated water vapour transport. Quarterly Journal of the Royal Meteorological Society, 137(654), 129–147. https://doi.org/10.1002/qj.728

Trenberth, K. E. (2018). Climate change caused by human activities is happening and it already has major consequences. Journal of Energy & Natural Resources Law, 36(4), 463–481. https://doi.org/10.1080/02646811.2018.1450895

UN-Habitat. (2022). The State of African Cities 2022: Climate Resilience and Urban Sustainability. Nairobi: UN-Habitat.

Vizy EK (2002). Development and application of a mesoscale climate model for the tropics: Influence of sea surface temperature anomalies on the West African monsoon. Journal of Geophysical Research, 107. doi:10.1029/2001JD000686.

Vollmert, P. and Fink, A.H. (2003) 'Ghana Dry Zone' und 'Dahomey Gap': Ursachen für eine Niederschlagsanomalie im tropischen Westafrika. Die Erde, 134(4), 375–393

Weber, W., White, L. J. T., Naughton-Treves, L., & Vedder, A. (2001). African Rain Forest Ecology and Conservation: An Interdisciplinary Perspective. Yale University Press.

Webster PJ and Fasullo J (2003). Monsoon: Dynamical Theory. Encyclopedia of Atmospheric Sciences. Eds. J. Holton and J. A. Curry. Academic Press, pp. 1370-1385.

Zhang, Chidong, Nolan, D. S., Thorncroft, C. D., & Nguyen, H. (2008). Shallow meridional circulations in the tropical atmosphere. Journal of Climate, 21(14), 3453–3470. https://doi.org/10.1175/2007JCLI1870.1

Zhang, X., Alexander, L., Hegerl, G. C., Jones, P., Tank, A. K., Peterson, T. C., Trewin, B., & Zwiers, F. W. (2011). Indices for monitoring changes in extremes based on daily temperature and precipitation data. Wiley Interdisciplinary Reviews Climate Change, 2(6), 851–870. https://doi.org/10.1002/wcc.147